INFORMATION TO USERS

This manuscript has been reproduced from the microfilm master. UMI films the text directly from the original or copy submitted. Thus, some thesis and dissertation copies are in typewriter face, while others may be from any type of computer printer.

The quality of this reproduction is dependent upon the quality of the copy submitted. Broken or indistinct print, colored or poor quality illustrations and photographs, print bleedthrough, substandard margins, and improper alignment can adversely affect reproduction.

In the unlikely event that the author did not send UMI a complete manuscript and there are missing pages, these will be noted. Also, if unauthorized copyright material had to be removed, a note will indicate the deletion.

Oversize materials (e.g., maps, drawings, charts) are reproduced by sectioning the original, beginning at the upper left-hand corner and continuing from left to right in equal sections with small overlaps.

Photographs included in the original manuscript have been reproduced xerographically in this copy. Higher quality 6" x 9" black and white photographic prints are available for any photographs or illustrations appearing in this copy for an additional charge. Contact UMI directly to order.

Bell & Howell Information and Learning
300 North Zeeb Road, Ann Arbor, MI 48106-1346 USA
800-521-0600

UMI®

THE UNIVERSITY OF OKLAHOMA

GRADUATE COLLEGE

STUDIES OF THE COMPLEXATION REACTIONS OF POLYETHER IONOPHORE ANTIBIOTICS MONENSIN A AND LASALOCID A WITH LEAD(II), ZINC, CALCIUM AND SODIUM CATIONS

A Dissertation

SUBMITTED TO THE GRADUATE FACULTY

in partial fulfillment of the requirements for the

degree of

DOCTOR OF PHILOSOPHY

By

OLGA G. IVANOVA

Norman, Oklahoma
2000

STUDIES OF THE COMPLEXATION REACTIONS OF POLYETHER IONOPHORE ANTIBIOTICS MONENSIN A AND LASALOCID A WITH LEAD(II), ZINC, CALCIUM AND SODIUM CATIONS

A Dissertation APPROVED FOR THE
DEPARTMENT OF CHEMISTRY AND BIOCHEMISTRY

BY

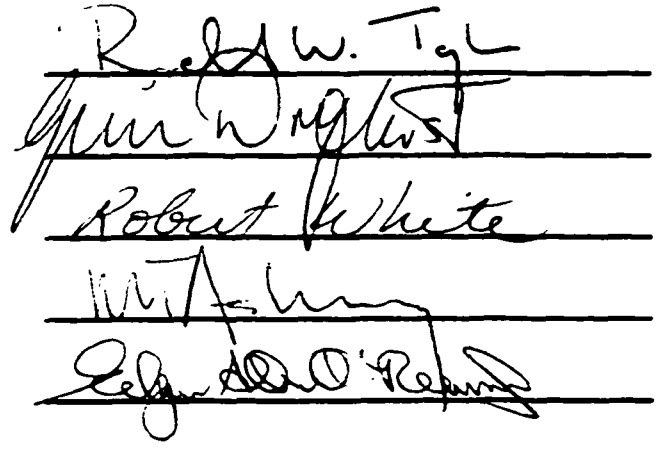

ACKNOWLEDGMENTS

First, I would like to thank the faculty at the Department of Chemistry and Biochemistry who taught me and helped me not only to learn about the science of chemistry but also to understand it in detail. I extend a special gratitude to my advisor, Dr. R.W. Taylor, who encouraged and inspired me on a weekly basis and who's advice kept me focused on my work. I sincerely thank him for all the time that he put into teaching me to write in proper scientific English and to learn chemical methodology. I would like to extend my appreciation to the members of my Advisory Committee, Dr. G. Dryhurst, Dr. R.L. White, Dr. M.T. Ashby, and Dr. E.A. O'Rear for their valuable suggestions, questions that lead me to the better understanding of the subject and cooperation in scheduling meetings.

I also recognize that this work would not be possible without the encouragement and support from my parents, Galina and Gennady Ivanov. Their wisdom and patience helped me to resolve many situations and inspired me enourmously. Most importantly, I would like to thank my fiancé and a good friend for several years, Mr. Sisay Shimelis, who's loving support, confidence and belief in my abilities impelled me to complete this work.

Further, I acknowledge the help of Dr. Larry Russon in obtaining the mass-spectrometry data and in training me to use of the instrumentation. I thank Dr. Eric Enwall for his help with basic NMR training and computer and NMR-system trouble-shouting. I also thank Mrs. John Black and Dean Updegraff for their determination and skill to fix any and all problems with the NMR spectrophotometers. I am indebted to my good friend Dr. Susan Alguindigue for instructing me in the details of the NMR usage and for keeping my spirits up during my studies.

I truly thank all my friends and colleagues among the students and the personnel of the Department of Chemistry and Biochemistry with whom I shared my good and bad moments during these years. Specifically, I thank my lab-mates and co-workers: Drs. Neeraj Khanna, Kay Bjornen, Laura Haley, Dorota Inerowic and Mr. Carlos Rodriguez. They introduced me to the laboratory, showed me the ways to do experiments and helped with the problems that I encountered.

Finally, I acknowledge the Department of Chemistry and Biochemistry for providing the financial support during the period of four years in the form of the graduate teaching assistantship. The work was also funded by the U.S. Department of Energy and the National Institute of Health.

TABLE OF CONTENTS

Page

LIST OF TABLES.....ix

LIST OF FIGURES.....xiii

ABSTRACT.....xviii

CHAPTER I. INTRODUCTION.....1

A. Introduction 1

B. Monensin complexes, literature overview. 16

C. Lasalocid complexes, literature overview 25

D. Summary of studies.....32

References.....34

CHAPTER II. EXPERIMENTAL..... 42

A. Reagents..... 42

B. Preparation of lead-monensin and lead-lasalocid complexes..... 50

C. Preparation of lead-monensin and lead-lasalocid tertiary complexes.....52

D. pH* measurements.....53

E. Determination of CO_2 in the tetramethylammonium hydroxide titrant solutions.....61

F. Measurements of protonation constants and metal complexation constants of monensin and lasalocid.....63

G. Nuclear magnetic resonance studies of monensin-lead and lasalocid-lead complexes.....66

References.....68

Page

CHAPTER III. RESULTS. STUDIES OF MONENSIN-METAL COMPLEXES.....71

A. Preparation and characterization of monensin-lead(II) complexes.....71

B. Potentiometric determination of monensin A protonation constant in 80% methanol-water 81

C. Spectrophotometric studies of lead(II)-monensin A binding.....86

D. Potentiometric studies of metal binding.....93

E. NMR studies of the monensin-lead (2:1) complex.....126

References.....158

CHAPTER IV. RESULTS. STUDIES OF LASALOCID-METAL COMPLEXES.....160

A. Preparation and characterization of lasalocid-lead(II) complexes..... 160

B. Determination of lasalocid A protonation constant in 80% methanol-water.....168

C. Spectrophotometric studies of lasalocid-lead(II) binding..... 175

D. Potentiometric studies of metal binding..... 184

E. NMR studies of the lasalocid-lead (2:1) complex in methanol..... 204

References.....216

CHAPTER V. DISCUSSION..... 218

A. Isolation and characterization of the ionophore antibiotic lasalocid and monensin complexes with lead(II)..... 218

B. Protonation constants of lasalocid A and monensin A..... 224

Page

A. Complex formation constants of ionophores monensin and lasalocid with metal ions..... 228

B. NMR studies of monensin and lasalocid binding in lead complex having 2:1 ionophore lead stoichiometry..... 242

C. Discussion of the lead transport data with respect to the results of the present study..... 249

References.....252

APPENDIX I..... 255

LIST OF TABLES

Page

Table I.1. Stoichiometries reported for complexes of carboxylic acid ionophores with mono- and divalent cations and associated with them modes of transport..... 7

Table I.2. Literature values of the protonation and sodium complex formation constants of monensin in various organic solvents and heterogeneous media..... 20

Table I.3. Literature values of the complex formation constants of monensin with monovalent cations in various organic solvents and heterogeneous media..... 21

Table I.4. Values of formation constants of monensin complexes with divalent cations.....24

Table I.5. Literature values of the overall formation constants for 1:1 lasalocid complexes with monovalent cations..... 29

Table I.6. Literature values of the overall formation constants (β_i) for lasalocid complexes with divalent cations in methanol..... 30

Table II.I. Literature values of acetic acid protonation constant in 80% methanol-water..... 55

Table II.2. Calculated and literature values of solvent autoprotolysis constants in 80% methanol-water..... 60

Table III.1. Experimental and calculated elemental composition of lead-monensin complexes..... 73

Table III.2. Peaks for lead-monensin complexes as obtained from the mass-spectra..... 80

Table III.3 Calculated values of the mixed-mode protonation constant for monensin in 80% methanol..... 85

Table III.4 Apparent and pH-independent complexation constants for lead–monensin derived from UV-Vis titrations..... 91

Table III.5 Log β_x values obtained from potentiometric titrations of monensic acid (HL) and sodium ion (Na^+)..... 96

Table III.6 Log β_x values obtained from potentiometric titrations of monensic acid (HL) and calcium..... 102

Page

Table III.7 Log β_x values obtained from potentiometric titrations of monensic acid (HL) and zinc..... 108

Table III.8 Literature values of the overall stability constants for lead-hydroxide and lead-methoxide complexes..... 114

Table III.9 Log β_x values obtained from potentiometric titrations of monensic acid (HL) and lead (II) ion..... 118

Table III.10 Average logβ_x values of equilibrium constants for various monensin complexes..... 125

Table III.11. ^{1}H and ^{13}C NMR chemical shifts of sodium monensin in methanol and 80% methanol-water..... 130

Table III.12. ^{1}H and ^{13}C NMR peak chemical shifts for sodium monensin in chloroform..... 131

Table III.13. ^{13}C NMR chemical shifts of tetramethylammonium monensin..... 132

Table III.14. ^{1}H NMR chemical shifts of tetramethylammonium monensin..... 133

Table III.15. ^{1}H NMR chemical shifts of free monensic acid..... 134

Table III.16. ^{13}C NMR chemical shifts of free monensic acid..... 135

Table III.17. Experimental ^{1}H NMR chemical shifts of lead-monensin complex..... 147

Table III.18. Experimental ^{13}C NMR chemical shifts of lead-monensin complex..... 148

Table III.19. ^{13}C signal doublets and the values of coupling constants as observed in the ^{13}C NMR spectrum of lead-monensin complex with ^{207}Pb-enriched lead..... 151

Table IV.1. Experimental and theoretically calculated elemental composition of lead-lasalocid complexes..... 162

Table IV.2 Peaks for lead-lasalocid complexes as obtained from the mass spectra..... 167

Table IV.3 Calculated values of the mixed-mode protonation constant for lasalocid in 80% methanol..... 170

Table IV.4. Calculated values for the mixed-mode protonation constants of lasalocid from spectrophotometric titrations..... 174

Page

Table IV.5 Apparent and pH-independent complexation constants for lead –lasalocid derived from UV-Vis titrations..... 181

Table IV.6. Log β_X values obtained from potentiometric titrations of lasalocid and zinc..... 190

Table IV.7 Log β_X values obtained from potentiometric titrations of HLas and lead(II)..... 197

Table IV.8 Average log β_X values of equilibrium constants for various lasalocid complexes.....203

Table IV.9 ^{1}H NMR chemical shifts of lasalocid complexes in methanol..... 208

Table IV.10 ^{13}C chemical shifts in lasalocid complexes in methanol..... 209

Table V.1 Ternary complexes of lead(II) having 1:1:1 lead:L:X stoichiometry that were identified in the present study..... 222

Table V.2 Average values for protonation constants of monensin A and lasalocid A obtained from potentiometric and spectrophotometric titrations and composite values for both methods..... 225

Table V.3 Protonation constants of ionophore antibiotics and simple carboxylic acids in 80% methanol-water and pure water and methanol solvents at 25 °C..... 227

Table V.4. Average values for formation constants of ionophore complexes having 1:1 stoichiometry with lead obtained from both potentiometric and spectrophotometric titrations..... 229

Table V.5. Average experimental and literature values of overall complexation constants of monensin and lasalocid with metal cations..... 232

Table V.6. Comparison between values of equilibrium formation constants of complexes having 1:1 stoichiometry between antibiotics monensin, lasalocid and A23187 and metal cations obtained in 80% methanol-water..... 238

Table V.7. Positions of binding oxygens in monensin, obtained with NMR spectroscopic methods..... 244

LIST OF FIGURES

Page

Figure I.1. Structures of the antibiotics gramicidin S and valinomycin.....3

Figure I.2. Structures of representative polyether carboxylic acid ionophores..... 4

Figure I.3. Schematic illustration of hydrogen bonding scheme in the monohydrate crystal of monensin acid, as inferred from the X-ray structure.....5

Figure I.4. Examples of possible transport modes and reactions involved in cation transport across a lipophilic membrane..... 8

Figure I.5. Selectivity trends for transport of divalent cations by monensin and lasalocid for membrane transport studies using phospholipid vesicles..13

Figure I.6 Bonding in the sodium-monensin complex, as inferred from the X-ray crystallography data. 17

Figure I.7. The X-ray structure of the dimeric lasalocid-barium complex..... 26

Figure II.1. Structure of monensin factors A, B and C..... 43

Figure II.2. FAB mass-spectra of tetraethylammonium monensin (A.), recorded in the negative ion mode, and silver monensin (B.), recorded in the positive ion mode.....45

Figure II.3. ESI mass-spectra of silver lasalocid, recorded in the positive ion mode..... 47

Figure II.4. Plot of the experimentally obtained by Oiwa activity coefficients versus molality for HCl in 80% methanol-water.....58

Figure II.5. Gran plot for a titration of perchloric acid with tetramethyl-ammonium hydroxide. 62

Figure III.1 Part of the positive ion ESI-MS for 2:1 monensin:lead complex..... 76

Figure III.2. Peaks for the 1:1 monensin:lead molecular ion in positive ion ESI-MS..... 77

Figure III.3. Peaks for the 2:1 monensin:lead molecular ion in positive ion ESI-MS..... 77

Figure III.4. Peaks for the 2:2 monensin:lead molecular ion in positive ion ESI-MS. 78

Figure III.5. Peaks for the 1:1:1 monensin A-lead-chloride molecular ion in negative ion ESI-MS..... 79

Page

Figure III.6. Experimental titration curve obtained from the titration of monensic acid solution with Me_4NOH.....81

Figure III.7. UV-Vis spectra from the titration of lead perchlorate with monensin..... 87

Figure III.8. Plot of the absorbance resulting from each aliquot of tetramethylammonium monensin added versus the concentration ratio of total monensin to total lead..... 88

Figure III.9. Change in absorbance at 240 nm as a function of $[HMon]_i$ at pH* 3.25..... 92

Figure III.10. Potentiometric titration curves for various stoichiometric ratios of monensin:sodium in 80% methanol-water at 25.0 °C.....97

Figure III.11. Potentiometric titration curve for 1:1 monensic acid and NaCl..... 98

Figure III.12. Potentiometric titration curve for 2:1 monensin acid and NaCl..... 99

Figure III.13. Species distribution curves for monensin-sodium complexes in solution as a function of p[H]..... 100

Figure III.14. Potentiometric titration curves for various stoichiometric ratios of monensin:calcium in 80% methanol-water solution at 25.0 °C.....103

Figure III.15. Potentiometric titration curve for 1:1 monensic acid and calcium... 104

Figure III.16. Potentiometric titration curve for 2:1 monensic acid and calcium... 105

Figure III.17. Species distribution curves for monensin-calcium complexes in solution as a function of p[H]..... 106

Figure III.18. Potentiometric titration curves for various stoichiometric ratios of monensin:zink in 80% methanol-water at 25.0 °C..... 109

Figure III.19. Potentiometric titration curve for 1:1 monensic acid and zinc..... 110

Figure III.20. Potentiometric titration curve for 2:1 monensic acid and zinc.....111

Figure III.21. Species distribution curves for monensin-zinc complexes in solution as a function of p[H]..... 112

Figure III.22. Plot of thermodynamic solvent autoprotolysis constants as a function of methanol-water solvent composition..... 115

Figure III.23. Potentiometric titration curves for various stoichiometric ratios of monensin:lead in 80% methanol-water at 25.0 °C..... 119

Page

Figure III.24. Potentiometric titration curve for 3:1 monensic acid and lead(II)... 120

Figure III.25. Potentiometric titration curve for 2:1 ratio of monensic acid and lead(II).....121

Figure III.26. Potentiometric titration curve for 1:1 monensic acid and lead(II)... 122

Figure III.27. Species distribution curves for monensin-lead(II) complexes in solution as a function of p[H]..... 123

Figure III.28. Species distribution curves for monensin-lead(II) complexes in solution as a function of p[H]..... 124

Figure III.29. Monensin A molecule with carbon (plain style) and oxygen (in bold) numbering schemes.....127

Figure III.30. Proton NMR spectrum of sodium-monensin complex in 80% deuterated methanol-deuterium oxide.....128

Figure III.31. C-13 NMR spectrum of sodium-monensin complex in 80% deuterated methanol-deuterium oxide.....129

Figure III.32. C-13 NMR spectrum of lead-monensin complex in chloroform, acquired at –40 °C with broadband proton decoupling.....139

Figure III.33. Selected region in the ^{13}C NMR spectrum of lead-monensin complex in chloroform: A. at –40 °C; B. at 25 °C..... 140

Figure III.34. The region in the J-resolved carbon spectrum (APT) of lead-monensin complex in chloroform obtained at –40 °C.....141

Figure III.35. Proton NMR spectrum of the lead-monensin complex in chloroform, acquired at –40 °C.....141

Figure III.36. COSY NMR spectrum for lead-monensin complex in chloroform, acquired at –40 °C.....142

Figure III.37. One-bond heteronuclear ^{1}H – ^{13}C correlation spectrum of lead-monensin complex in $CDCl_3$ acquired using HMQC technique at –40 °C and presented as a contour map..... 145

Figure III.38. Enlarged area of HMQC contour map from Figure III.37 showing the areas or carbon-proton correlations from two different monenin ligands..... 146

Figure III.39. Regions of carbon number 2 resonances in C-13 NMR broadband proton decoupled spectra: a) for lead-monensin complex with regular lead and b) with enriched lead-207..... 150

Page

Figure III.40. Variation of ^{13}C chemical shifts of all the carbons in the monensin molecule from the free monensin anion A^- to the metal complex and free acid in methanol.....154

Figure III.41. Variation of ^{13}C chemical shifts of all the carbons in the monensin molecule from the free monensin anion A^- to the metal complex and free acid in chloroform..... 156

Figure IV.1. Part of the positive ion ESI-MS for 2:1 lasalocid:lead complex..... 165

Figure IV.2. Peaks for the 1:1 lasalocid:lead molecular ion in the positive ion ESI-MS..... 165

Figure IV.3. Peaks for the 2:1 lasalocid:lead molecular ion in the positive ion ESI-MS..... 166

Figure IV.4. Peaks for the 1:1:1 lasalocid-lead-chloride molecular ion in negative ion ESI-MS..... 166

Figure IV.5. Peaks for the 2:1:1 lasalocid-lead-chloride molecular ion in negative ion ESI-MS..... 167

Figure IV.6. Experimental titration curve obtained from the titration of 10.0 mL of 4.50 mM lasalocidic acid solution with 0.02108 M Me_4NOH... 169

Figure IV.7. Representative spectra from the spectrophotometric pH-titration of lasalocid in 80% methanol-water at 25.0 °C.....172

Figure IV.8. Plot of the absorbance at 255 nm as a function of a_H* for the titration of lasalocid shown in fig. IV.7.....173

Figure IV.9. Representative UV-Vis spectra from the titration of lasalocid A with lead perchlorate in 80% methanol-water at 25.0 °C.....176

Figure IV.10. Plot of the absorbance change resulting from each aliquot of lead perchlorate added versus the concentration ratio of total lead to total lasalocid..... 177

Figure IV.11. Representative UV-Vis spectra from the titration of lasalocidic acid with lead perchlorate in 80% methanol-water at 25.0 °C..... 182

Figure IV.12. Change in absorbance at 322 nm as a function of $[Pb^{2+}]_i$ at pH* 3.14 adjusted with 1 mM $HClO_4$.....183

Figure IV.13. Potentiometric titration curves for various stoichiometric ratios of lasalocid:sodium in 80% methanol-water solution at 25.0 °C... 187

Figure IV.14. Potentiometric titration curves for various stoichiometric ratios of lasalocid:calcium in 80% methanol-water solution at 25.0 °C....188

Page

Figure IV.15. Potentiometric titration curves for various stoichiometric ratios of lasalocid:zink in 80% methanol-water at 25.0 °C..... 191

Figure IV.16. Potentiometric titration curve for 1:1 lasalocid free acid and zinc.. 192

Figure IV.17. Potentiometric titration curve for 3:1 lasalocid free acid and zinc.. 193

Figure IV.18. Species distribution curves for lasalocid-zinc complexes in solution as a function of p[H]..... 194

Figure IV.19. Potentiometric titration curves for various stoichiometric ratios of lasalocid-lead.....198

Figure IV.20. Potentiometric titration curve for 2:1 lasalocid free acid and lead.. 199

Figure IV.21. Potentiometric titration curve for 2:1 lasalocid free acid and lead.. 200

Figure IV.22. Potentiometric titration curve for 3:1 lasalocid free acid and lead.. 201

Figure IV.23. Species distribution curves for lasalocid-lead(II) complexes in solution as a function of p[H]..... 202

Figure IV.24. Lasalocid A molecule with carbon (plain style) and oxygen (outlined) numbering schemes..... 205

Figure IV.25. ^{1}H NMR spectrum of the lasalocid-lead complex in methanol at room temperature..... 210

Figure IV.26. ^{13}C broad-band decoupled NMR spectrum of the lasalocid-lead complex in methanol at room temperature.....210

Figure IV.27. COSY spectrum for the lasalocid-lead complex in methanol at room temperature.....211

Figure IV.28. HMQC contour map for the lasalocid-lead complex at room temperature..... 212

Figure IV.29. Variation of ^{13}C chemical shifts of all the carbons in the lasalocid molecule from the free lasalocid anion A^- to the metal complex and free acid in methanol..... 214

Figure V.1. Species distribution curves for monensin-lead(II) complexes in solution as a function of pH..... 235

Figure V.2. Species distribution curves for lasalocid-lead(II) complexes in solution as a function of pH..... 236

Figure V.3. Graph of log K_{ML} plotted versus the effective radius of metal cation..... 239

Figure V.4. Schematic diagram of possible monensin coordination in the lead(II) complex in chlorofom..... 246

Figure V.5. Schematic illustration of possible lasalocid coordination in the lead(II) complex in methanol.....248

ABSTRACT

The reactions of polyether ionophore antibiotics monensin A and lasalocid A with lead(II), sodium, calcium and zinc cations were studied by several methods. The work was undertaken to provide the chemical basis for the effectiveness and selectivity found for the ionophore-mediated lead(II) transport in model membrane studies. Lead complexes that could participate in transport were isolated, and their stoichiometry and composition were determined. The protonation and complex formation equilibria with lead(II) and several biologically important cations were studied in solution. One- and two-dimentional NMR methods were employed to obtain information about the solution structures and cation binding sites in the lead-ionophore complexes.

Lead-ionophore complexes of the form PbLX and PbL_2 (L = monensin A or lasalocid A; X^- = anion) were isolated and characterized by elemental analysis ($X = Cl^-$) and ESI-MS ($X = Cl^-$, NO_3^-, CH_3COO^-). Changes in the UV-Vis spectra indicated that lead(II) also forms stable 1:1 complexes (PbL) with both ionophores in 80% methanol-water (w/w).

The protonation constants and complex formation constants of monensin A and lasalocid A have been determined in 80% methanol-water (w/w) at 25 °C and I = 0.05 M (Et_4NClO_4). Potentiometric titrations for monensin, and both potentiometric and spectrophotometric titrations for lasalocid gave the following values for the concentration protonation constants: log K^c_H* = 6.83 ± 0.05 and log K^c_H* = 4.84 ± 0.01, respectively. Potentiometric titration data was consistent with the presence of PbL, PbL_2, and PbLOH species. The values of the formation constants obtained pointed to the significance of ternary PbLOH species at the physiological pH in solution. The magnitudes of the 1:1 complex formation constants decreased in the following order for lasalocid A: $Pb^{2+} > Zn^{2+} > Ca^{2+}$, Na^+; and for monensin A: $Pb^{2+} > Na^+ > Zn^{2+} > Ca^{2+}$. These trends mirrored those for the rates of lead transport. The results are discussed

with respect to the reaction orders for ionophore-mediated lead(II) transport, transport selectivity, and possible transport modes for monensin and lasalocid.

CHAPTER I.

INTRODUCTION.

Metals play many important roles in biological systems. The compounds that facilitate transport of ions across lipid cellular membranes are called ionophores. The term ionophore (or "ion bearer") describes a large class of compounds that can be divided into two major groups[1] on the basis of the their mechanism of transport. The first group consists of channel forming ionophores that span the membrane to form hydrophilic ion channels that allow a passage of the cations. Interactions of the metal ions with the pore opening or with the interior walls determine the transport selectivity on the basis of ion charge and size. Among the channel-forming ionophores, gramicidins are the most thoroughly investigated[1]. The structure of one representative of this group is shown in Figure I.1. Gramicidin A forms a dimer 25-30 Å long that spans the membrane bilayer. The dimer creates a channel that has a diameter of about 4 Å. It is believed[1] that cations bind to donor oxygen and nitrogen atoms located in hydrophilic interior of the channel. The passage of cations occurs through the channel when its coordination shifts from one set of binding atoms to the next; and it is accompanied by small conformational changes in the gramicidin molecule dimer. In this case, the ionophore structure remains stationary within the membrane throughout the transport cycle. Channel forming ionophores normally have higher rates of transport relative to carrier ionophores[1].

Carrier ionophores belong to the second group. These compounds form a complex of well-defined stoichiometry with the metal cation[2]. The metal ion is located within a cavity formed by the ionophore. The complex has a non-polar surface formed by the ionophore hydrophobic backbone and can travel through the lipophilic membrane, thus transporting the metal ion across. Some carrier ionophores are naturally occuring compounds (e.g., ionophore antibiotics) and others are synthetic (e.g., crown ethers). Further discussion will only involve natural carrier ionophores.

Based on their structure, these compounds can be classified into cyclic and non-cyclic ionophores. An example of a cyclic naturally occurring ionophore, valinomycin, is presented in Figure I.1. It is a neutral dodecadepsipeptide that was found to be selective for the transport of potassium ion. On the other hand, naturally occurring carboxylic acid ionophores are acyclic compounds. This group of ionophores posseses many similar structural features. They are open chain molecules of the polyether type and contain tetrahydropyran rings, tetrahydrofuran rings, or both. There is a carboxylic acid group on one end and, in most cases, the other end is terminated by one or two alcohol groups. The structures of polyether antibiotics monensin, nigericin, lasalocid and A23187 are shown in Figure I.2.

The first representatives of the carboxylic acid antibiotics - X209, lasalocid A (or X537A) and nigericin (or X464) - were isolated in 1951[3,4] from the strains of *Streptomyces* bacteria. These compounds were classified as antibiotics on the basis of their antibacterial activity. When acidic solutions of those compounds in an apolar organic solvent were exposed to the aqueous sodium carbonate, the compounds readily extracted the sodium ion into the organic phase[5] and yielded a sodium salt upon solvent evaporation. In 1967 the antibiotics monensin, X-206 and nigericin were reported to have anticoccidial properties[6]. This biological activity was attributed to the interactions with alkali metal cations and ionophore properties towards potassium transport through mitochondrial membranes[4]. Since then more than forty (excluding homolog derivatives) polyether antibiotics have been discovered and isolated.

The transport properties of ionophore antibiotics towards different metal cations have been extensively studied. Historically, mono- and divalent polyether antibiotic ionophores were distinguished. A large number of ionophores were found to transport alkali metal cations, such as Na^+ and K^+. Monensin and nigericin are the examples of monovalent carboxylic ionophores that until recently were considered to be poor ionophores for divalent cations. Another group of compounds, called divalent

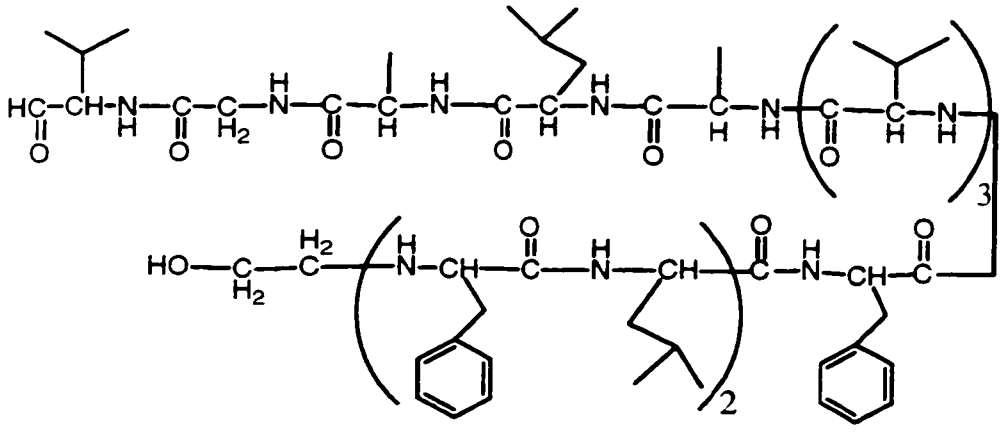

Gramicidin A

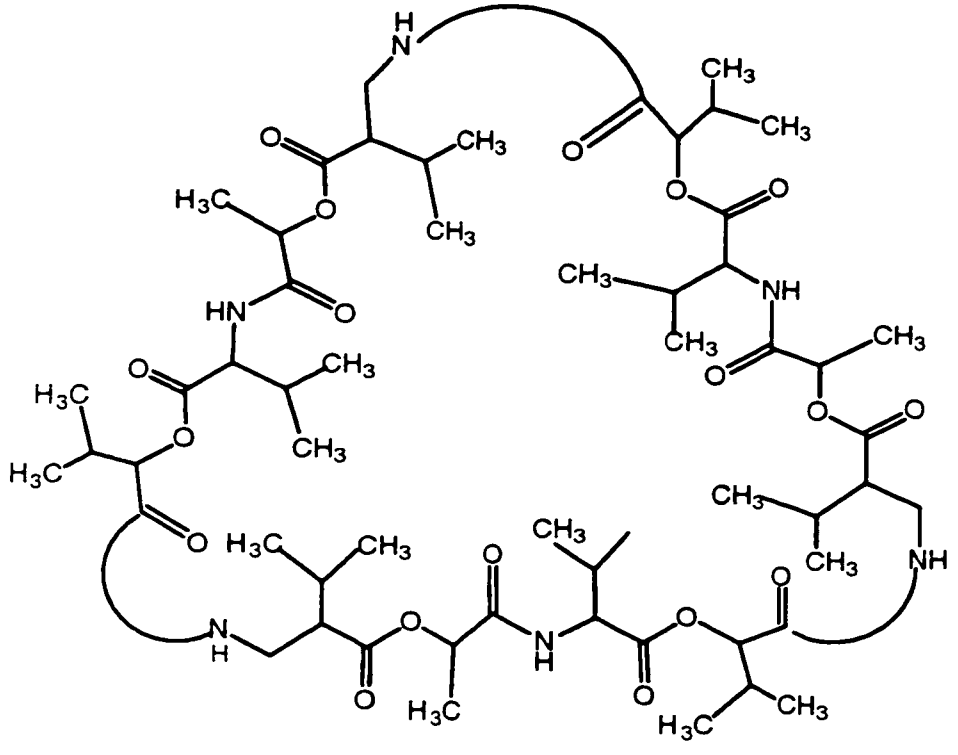

Valinomycin

Figure I.1. Structures of the antibiotics gramicidin S and valinomycin.

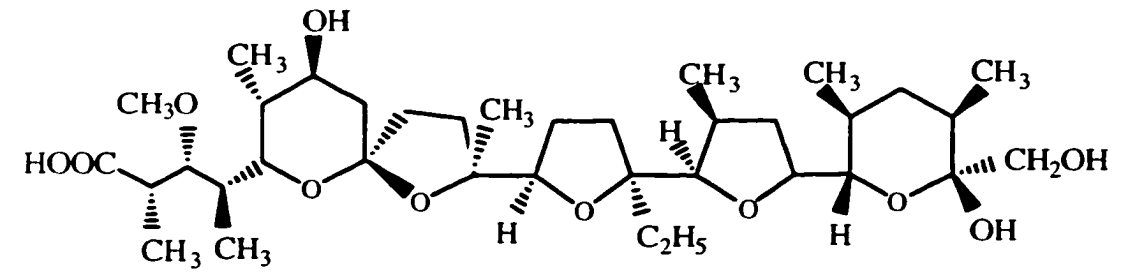

Monensin A

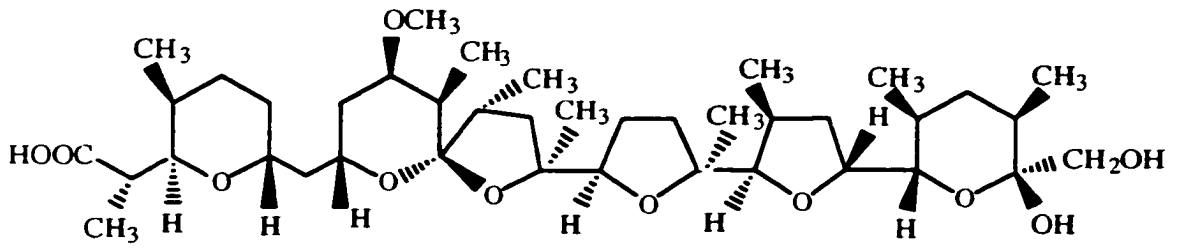

Nigericin

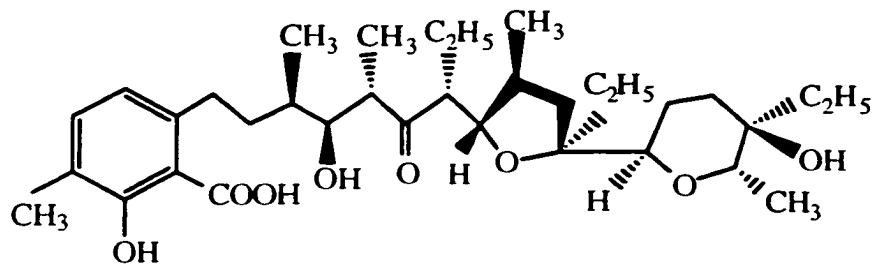

Lasalocid A

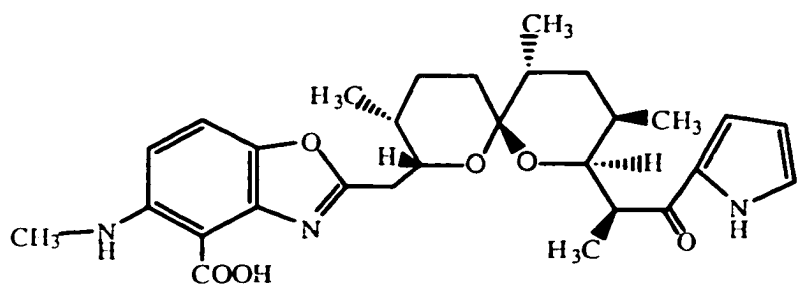

A23187

Figure I.2. Structures of representative polyether carboxylic acid ionophores.

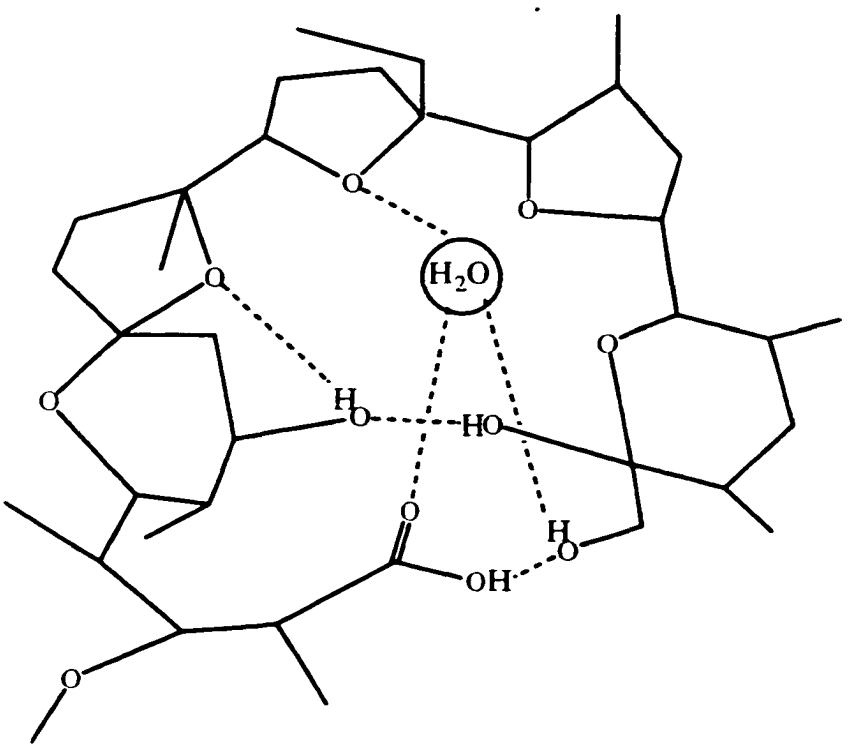

Figure I.3. Schematic illustration of hydrogen bonding scheme in the monohydrate crystal of monensin acid, as inferred from the X-ray structure[7].

ionophores, included the antibiotics A23187 and ionomycin that are well known for their Ca^{2+} and Mg^{2+} transporting properties. The antibiotic lasalocid is included in both groups because it transports both mono- and divalent metal ions.

Although the carboxylic acid polyether antibiotics are acyclic molecules, they can form pseudo-macrocyclic systems by the head-to-tail hydrogen bonding between the carboxylic acid (or carboxylate) function and alcohol groups. This bonding is illustrated in Figure I.3 for monensic acid. Many carboxylic acid antibiotics were found to adopt similar pseudo-cyclic conformation in both free and complexed states. In such a globular structure the oxygen donor atoms are generally oriented toward the center, where they are available for cation complexation. The backbone alkyl groups are located on the

exterior of the complex, thus providing surface hydrophobicity and ensuring the solubility of the complex in the lipophilic membrane interior.

Because of the number of available coordination donor sites in any given carboxylic acid ionophore molecule is limited as well as the possibilities for its pseudo-cyclic conformation in metal ion complexes, complex stoichiometries are well defined. At the biological pH of 7.4 most carboxylic groups in polyether ionophores are ionized and the overall charge on the transporting species depends both on the charge of the metal cation and complex stoichiometry. Ionophore anions can form a neutral complex with a metal cation at the appropriate stoichiometric ratio. Neutral complexes are among the most favorable to travel through the lipophilic membrane, although transport by the charged complexes also occurs. Possible complex stoichiometries and overall charges reported for mono- and divalent ionophore antibiotics[2,8] are summarized in Table I.1. Neutral complexes with 1:1 metal cation-ionophore antibiotic stoichiometry and charged cyclic ionophore complexes having the same stoichiometry were reported for most monovalent cations. Most divalent ionophores, such as lasalocid and A23187, form neutral complexes with 1:2 cation-ionophore stoichiometry[8]. Ionomycin was found to be an exception in this group in that it forms 1:1 neutral complexes with divalent cations[2].

Two transport modes are distinguished depending on the charge of the participating ionophore-metal complex: electrogenic and electroneutral. Both modes belong to the so called "passive" transport processes as they occur through facilitated diffusion and don't require extra energy input[9]. Electroneutral transport is driven by the ion transmembrane concentration gradients and electrogenic transport is driven by a transmembrane potential gradient or a concentration gradient of a different charged species. Because neutral ionophores, such as valinomycin, form charged metal complexes, their transport is electrogenic (Figure I.4A). It is also called uniport because it results in a transport of a single solute ion across the membrane. However, carboxylic

acid ionophores can transport cations by both electroneutral and electrogenic modes because neutral transporting species as well as charged complexes can be formed. Examples of both types are listed in Table I.1. If the transport is electroneutral, but coupled to the secondary transport of other ions (such as protons) in the opposite direction, it is called antiport or countertransport (Figure I.4B). Another type of electroneutral transport occurs when a ternary complex having 1:1:1 metal-ionophore antibiotic-anion stoichiometry, is involved (Figure I.4C). In this case, the transport of hydroxide (or another anion) proceeds in the same direction as the metal ion transport. This is called co-transport or symport. Carboxylic acid ionophores can also induce electrogenic transport if charged complexes having 1:1 ionophore-divalent cation or protonated 1:1 ionophore-monovalent cation stoichiometries are among the transporting species.

Table I.1. Stoichiometries reported for complexes of carboxylic acid ionophores with mono- and divalent cations[a] and the associated modes of transport

Class of carboxylic acid ionophores	Overall reaction of complex formation[b]	Transport mode
Monovalent (L^-)	$M^+ + L^- \rightleftharpoons ML$	Electroneutral
(e.g., monensin, nigericin)	$M^+ + L^- + H^+ \rightleftharpoons MLH^+$	Electrogenic
	$M^+ + 2L^- + H^+ \rightleftharpoons ML_2H$	Electroneutral
Divalent (L^-)	$M^{2+} + L^- \rightleftharpoons ML^+$	Electrogenic
(e.g., A23187)	$M^{2+} + 2L^- \rightleftharpoons ML_2$	Electroneutral
	$M^{2+} + L^- + X^- \rightleftharpoons MLX$	Electroneutral
Divalent (L^{2-})	$M^{2+} + L^{2-} \rightleftharpoons ML$	Electroneutral
ionomycin	$M^{2+} + L^{2-} + H^+ \rightleftharpoons MLH^+$	Electrogenic

[a] Data was obtained from references 2 and 8. [b] M stands for metal, X stands for anion, such as OH^-.

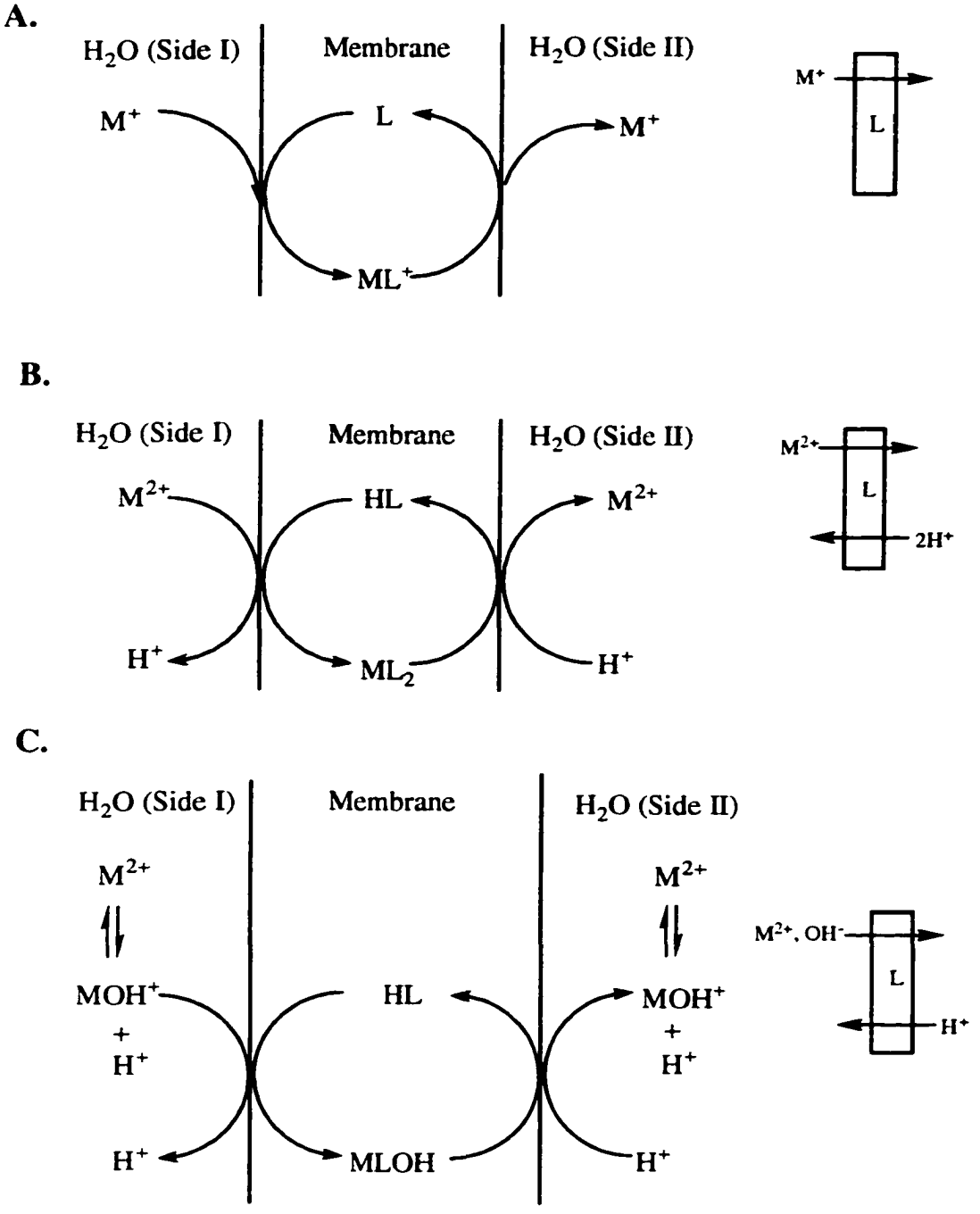

Figure I.4. Examples of possible transport modes and reactions involved in cation transport across a lipophilic membrane. The net results are shown in the smaller diagrams on the right. A. electrogenic transport; L = valinomycin, M = K ; B. electroneutralneutral transport, L = lasalocid, M = Ba; C. electroneutral transport, L = monensin, M = Pb.

Due to concurrent charge transfer, electrogenic transport can interfere with the preexisting cell membrane potentials that are responsible for many biological functions. Therefore, it is important to know the transporting species and transport modes before using ionophore antibiotics in biological systems. Some examples of such studies are discussed below. Both electrogenic and electroneutral modes were reported for the transport of sodium and potassium cations by the monensin[10,11], although the electrogenic component appeared to be of minor importance as compared with the electroneutral pathway. The electrogenic mode was also found to be negligible during calcium transport by A23187 and ionomycin, but associated changes of pH-gradients affected the transport rates and kinetics[12,13].

The following model for metal ion transport by carrier ionophores has been generally accepted[14]. Because of its non-polar nature, the ionophore molecule preferably resides in the lipid membrane of cells or cell components. At the membrane-water interface the ionophore has access to metal cations in solution. When metal binding occurs, the non-polar exterior of the resulting ionophore-metal ion complex reduces its capability to react with the polar environment at the membrane surface. The complex leaves the interface and enters the lipophilic interior of the membrane. After diffusion to the opposite side, the cation is released and the ionophore diffuses back to the original interface, where the whole cycle is repeated.

In general, there are several requirements for a compound to be a "good" ionophore[8,14]. It should have polar donor groups which can replace solvent molecules from a cation solvation sphere in a stepwise manner during complex formation and provide maximum interaction with cation through ion-dipole forces. The conformation of the ligand molecule in the complex should also result in a lipophilic exterior to shield the cation while crossing the apolar membrane interior. The complexation and dissociation reactions should be fast to efficiently pick up the metal on one side of the

membrane and release it on the other side. The complex formation constant (e.g.; β_{ML}) has to be large enough to form appreciable concentrations of transporting species but not so large as to prevent the release of the metal cation following transport. Polyether ionophore antibiotics satisfy most of these conditions and their metal transport properties found a wide range of applications.

In biochemical research, polyether ionophore antibiotics have been employed to study the roles of metal cations in cell functions[15]. Ionophores cause the disruption of transmembrane ion and proton concentration gradients which affect the normal function of biochemical processes, thus allowing their identification and study. The cation transport properties of ionophores were also utilized in the construction of ion-selective membrane electrodes[1]. Valinomycin[15] and nigericin[15] were used to measure the concentration of K^+, monensin[15] was used to measure that of Na^+, and salinomycin and lasalocid were used to measure Ba^{2+} concentration [16]. Calcium selective ionophores found application in medicine as heart stimulants in emergency cases, when their toxicity was of secondary importance[1]. For a number of years the ionophore monensin has been used in agriculture as a growth promoter in cattle feed additives[17]. The increase in weight gain per feed consumed was explained by the interference of the antibiotic with ruminant microorganisms in the animal's gut[18]. Monensin is used as an anticoccidal agent for poultry[5] greatly reducing the number of birds lost to infection, and has had a great economic impact.

Because of the variety of applications and their biological importance, transport selectivity trends for ionophore antibiotics among both mono- and divalent metal cations and trivalent lanthanides was extensively studied. The use of cell[19,20] and subcellular[21] preparations in these studies gave only limited information due to imposed restrictions on experimental conditions, such as pH, temperature and cation concentrations. Also the presence of protein ion channels and pumps in the cell walls and their contribution to the

control of transmembrane ion gradients caused interference with the measurements of interest. Therefore, in many cases ionophore facilitated cation transport was studied using model systems. The simplest of them is a bulk liquid membrane[22]. In this model two aqueous solutions in the arms of a U-shaped tube are separated by a non-aqueous lipophilic layer (usually chloroform). The ionophore is dissolved in the non-aqueous layer and mediates the cation transport from one side of the U-tube to the other. The transport can be monitored by a number of techniques including ion-selective electrodes and spectrophotometry. Because the thickness of non-aqueous layer in this model far exceeds the size of the biological membrane, the model provides only general indications of the transport behavior.

The "planar" bilayer lipid membrane method is used to provide a closer approximation of a biological system[22,23,24]. Two compartments with aqueous solutions are separated by a partition with a pin-hole. A lipid membrane is formed on a pin-hole by dissolving the lipid and the ionophore in decane, placing a drop of a lipid solution into the pin-hole and allowing the decane to slowly evaporate away[22]. The pin-hole is left covered with what is believed to be a single bilayer[24]. The transport can be induced either by applying an electric potential between compartments or by creating a cation concentration gradient across the membrane. The resulting membrane potential or its change are measured and provide information on the transport process. One problem with this method lies in the uncertainty about the nature of the membrane formed: whether it is a true bilayer or a multilamellar structure.

This problem was overcome by the development of methods for the preparation of unilamellar vesicles, or liposomes, in which the phospholipid bilayer separates the inner solution from the outer one[25,26]. The ionophore-catalyzed transport of the metal ion from the external solution to the inside of the vesicles can be monitored spectroscopically by entrapping a fluorescent[27] or UV-Vis absorbance metal indicator[12,13] inside or by monitoring internal and external ions by NMR[22].

The transport of mono-, di- and trivalent cations by polyether antibiotics was studied by the methods described. When monovalent cation transport by monensin was studied in mitohondria and liposomes[2], the following transport selectivity trend was found: $Na^+ >> K^+$, $Li^+ > Rb^+$, Cs^+. In the study of monensin-mediated sodium transport through bilayers of phospholipid vesicles by ^{23}Na NMR spectroscopy, the data was consistent with the model in which one monensin transported one metal ion[28] by forming an electrically neutral complex. The ability of monensin to act as a divalent cation ionophore for Fe(II) was reported in 1977[29] for transport studies using human red cells and liposomes. For lasalocid, the selectivity trends found in the planar bilayer lipid membrane transport studies[23,24] can be presented as $Ba^{2+} > Ca^{2+} > Mn^{2+} > Sr^{2+} >> Mg^{2+}$ for divalent cations and $Cs^+ > Rb^+$, $K^+ > Na^+ > Li^+$ for monovalent cations. The transport of trivalent lanthanide cations by lasalocid was also reported. Eu(III) transport in lipid bilayer vesicles was followed by luminescence spectroscopy[30] and the results implied that both 1:1 and 2:1 lasalocid-Eu(III) complexes can be involved. When P-31 NMR was used to monitor the transport of Pr(III) in the phospholipid vesicles it was also found to be the second order in lasalocid[31]. Studies of Pr(III), Nd(III) and Eu(III) transport kinetics in phospholipid vesicles indicated 2:1 ionophore-cation stoichiometry of the transporting species for lasalocid A and A23187[32]. La^{3+} transport by A23187 and ionomycin was found to be electroneutral[33]. In case of A23187 it was found to occur through complexes having 3:1 ionophore-La stoichiometry at higher ionophore concentrations or 2:1:1 ionophore-La-OH complexes at lower ionophore concentrations. In the case of ionomycin, transport was found to occur through the mixed 1:1:1 Ionophore-La-OH complex in both cases over the entire concentration range studied[33].

Recently, several membrane transport studies of divalent cations with polyether antibiotics were reported[34-36]. These studies showed that ionophores including monensin, ionomycin, lasalocid and salinomycin transport lead(II) cations very effectively. Tsukube et al.[34] reported that monensin transports Pb^{2+} and Ag^+, with Na^+

countertransport, across a bulk chloroform membrane, and that lasalocid transports Pb^{2+}, Cu^{2+}, Zn^{2+}, Ni^{2+} and Co^{2+} with the countertransport of NH_4^+. For monensin, the lead transport rates were larger in comparison with other divalent cations[34]. Similar results were obtained in transport studies using phospholipid vesicles with a number of other ionophores[35,36,37], including ionomycin, salinomycin, A23187 and nigericin. Although ionomycin is generally considered to be a calcium ionophore, the observed transport selectivity trend of $Pb^{2+} > Cd^{2+} > Zn^{2+} > Mn^{2+} > Ca^{2+} > Cu^{2+}$, and about 3000-fold selectivity for lead during competitive transport with calcium suggest that ionomycin should be classified as a lead ionophore[36]. Similar selectivities for lead versus calcium transport were found from relative transport rates for monensin (3,340)[35], lasalocid A (265)[37], salinomycin (3,030) and nigericin (2,890) antibiotics[37]. The presence of sodium ion decreased the rate of monensin-mediated lead transport only slightly. The transport stoichiometric ratios of metal to ionophore were measured for most antibiotics from the initial transport rates. For monensin, ionomycin, salinomycin and nigericin the transport was found to occur through a 1:1 ionophore-lead complex.

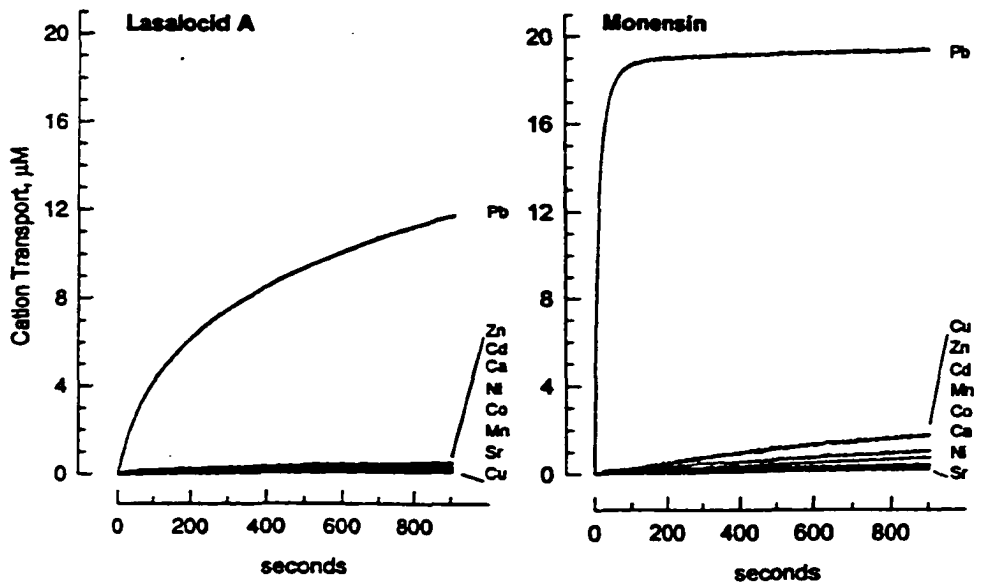

Figure I.5. Selectivity trends for transport of divalent cations by monensin and lasalocid for membrane transport studies using phospholipid vesicles (refs. 35-37).

For lasalocid the data indicated that transport occured through a mixture of 1:1 and 2:1 ionophore-lead complexes. In most cases, the measured transport rates for divalent transition metal cations were very low compared with those for lead(II). The results of transport studies are presented in Figure I.5 for monensin and lasalocid. Transport rates for zinc(II) were among the highest for the divalent metal ions other than lead with the antibiotics tested.

These lead transport activities raise questions about the health effects of antibiotics on the general population. Because monensin and lasalocid are used extensively in agriculture, their residues are present in meat [38,39,40]and related products, such as milk[41] and eggs[42], and digested by people. On the other hand, lead continues to be among the most toxic and high-risk exposure substances not only in the United States[43,44,45] but worldwide[46,47], especially in those countries that did not discontinue the usage of leaded gasoline. Health problems resulting from lead-poisoning can range from hypertension, anemia, hearing loss, infertility and diminished life-span to neuropathy in adults and encephalopathy, developmental abnormalities and diminished IQ in children[48,25]. It was also suggested that lead, in addition to other toxic metals, could be responsible for DNA damage and, thus, has a carcinogenic potential[49]. From the biochemical view, most toxic effects of lead result from the its interference with cellular calcium signaling systems[5,50,51]. It was suggested that inorganic lead can penetrate cell lipid bilayer membranes[52] and even the blood-brain barrier[53] by passive diffusion as the $PbOH^+$ species. In light of recent findings of selective lead(II) transport across lipid bilayer membranes mediated by polyether antibiotic ionophores, the widespread usage of polyether antibiotics may increase the absorption of lead into both animals and humans that live in lead-contaminated areas and increase the lead health hazard. On the other hand, the lead transport behaviour suggests the possibility for application of the polyether antibiotics as chelation agents in the treatment of lead-poisoning if their toxicity can be overcome.

Further application of those transport properties to biological systems requires in-depth knowledge of the structure, stability, stoichiometry and kinetics of transporting complexes and the transport mechanism(s). As mentioned above, the ion transport process across a membrane is governed by both thermodynamics and kinetics. It is related to the structure and the solvation of the participating species. The equilibria at the membrane-aqueous interfaces involve the overall complex formation from an ionophore in the organic phase and the metal in the aqueous phase. This process is the sum of a number of reactions, including deprotonation of the ionophore carboxylic acid group, loss of water molecules from the solvation sphere of the metal cation and, finally, the complex formation. Ion transport across the membrane is then followed by the complex dissociation, solvation of the metal cation and ionophore protonation, as can be seen in Figure I.4. Therefore, knowledge of the solution chemistry of ionophores and their metal complexes that participate in the separate steps of the transport process is important to the understanding the factors that contribute to transport efficiency and specificity. Two representative ionophores were selected for the present study. Monensin, a monovalent ionophore, and lasalocid, which is known to transport both mono- and divalent metal cations, were chosen on the basis of their reported lead(II) transport selectivity among other divalent cations[34,35] and the fact that they are both widely distributed and used as cattle and poultry feed additives and, consequently, can be present in trace amounts in food products.

Previously obtained information on behavior of monensin and lasalocid systems in various solvents, and the results of studies of their metal complexes in both solution and solid states are discussed in the next section.

Monensin complexes, literature overview.

Compounds of the monensin family were discovered and isolated from *Streptomyces cinnomonensis* bacteria in 1967[54]. Those were among the first polyether antibiotics for which molecular structures were determined. Monensin A (Figure I.2) constituted the largest fraction of different monensin factors in the isolated mixture. The structures of other monensins differed by the presence or absence of an extra methylene group among the alkyl side-chains. Monensin factors were easily separated by chromatographic means (see section II.A for details). Any further discussion will refer only to monensin A, if not specified otherwise.

As mentioned above, monensins have been widely used in agriculture to treat chicken coccidiosis and to improve the weight gain/feed ratio in cattle. Its biological activity was attributed to its ionophore properties towards alkali-metal cations. Therefore, properties of monensin complexes with alkali-metals were studied extensively; the results of these studies are described in the following section.

Studies of monensin transport and complexes with monovalent cations.

X-ray crystal structures with and without solvent molecules were obtained for sodium[55,56], potassium[55,57], silver[55,58], thallium[55], sodium bromide[59] complexes of monensin A and a monohydrate for monensin A free acid[6]. Dihydrates of sodium and silver were crystallized in a monoclinic space group, dihydrates of potassium and thallium, hydrate of monensin free acid and anhydrous sodium and sodium bromide complexes crystallized in an orthorombic space group. In all complexes, the ionophore was completely wrapped around the metal ion and the latter was coordinated by a distorted octahedron of six ether and hydroxy oxygen atoms. The carboxylic acid group was deprotonated in all cases except for the mixed sodium-monensin-bromide complex and the free monensic acid. Both carboxylate oxygen atoms participated in head-to-tail hydrogen bonds with terminal hydroxy groups, thus stabilizing the circular ionophore

conformation. The structure for sodium complex is presented in Figure I.6. Comparisons between the structures of metal complexes and that of the free acid revealed differences only in the hydrogen bonding pattern. The ionophore conformation was found to be very similar in all reported structures of metal complexes[60] with the exception of that with potassium. In that case, differences were found in the conformation of the spiro-fused furan ring and were attributed to the necessity to expand the coordination sphere in order to accommodate the larger potassium cation.

In the IR-spectra of monensin free acid in chloroform[61] the absorption band for the carbonyl stretch was observed in the region indicative of a hydrogen-bonded carboxylic acid group. Because no evidence of dimerization was found in the 0.65-65 mM concentration range, the free acid of monensin was proposed to be in the cyclic

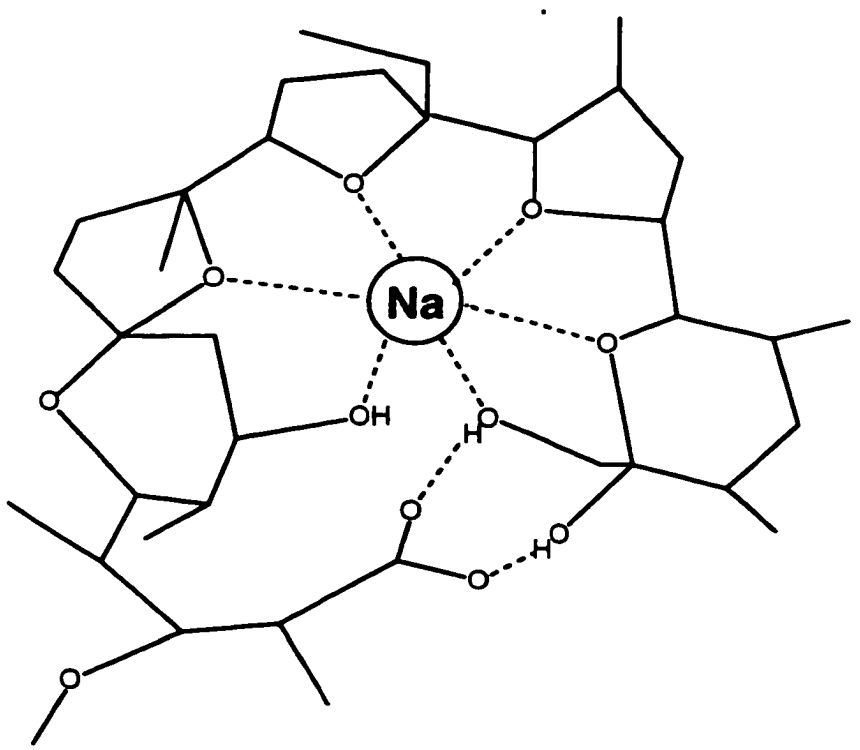

Figure I.6 Bonding in the sodium-monensin complex, as inferred from the X-ray crystallography data (Ref. 56).

conformation similar to that of the silver salt. ^{1}H-NMR studies of monensin free acid[62] and its alkali-metal salts[63] showed their conformations to be identical in chloroform as evidenced by similarity in the values of coupling constants[64]. These solution conformations corresponded to the ones found in the solid state where the antibiotic adopts a pseudo-cyclic form stabilized by intramolecular hydrogen bonding. ^{1}H NMR spectra in methanol, a hydroxylic polar solvent, were also obtained[65]. Analysis of the coupling constant data indicated that in the sodium-monensin complex the ligand kept its cyclic form, whereas the free acid of monensin adopted an open chain conformation.

Major improvements in NMR techniques allowed a systematic study of monensin–monovalent cation systems in solution. Total assignment of ^{13}C and ^{1}H resonance frequencies for the free acid form and free anion forms of monensin and its alkali-metal and silver salts in chloroform was accomplished by Cane et al.[66], Ajaz et al.[67] and Vaufrey-Mary[68], and in methanol by Mimouni et al.[69] It was found that for a series of monovalent cations the values of ^{1}H-^{1}H coupling constants in the two solvents are similar indicating that complexed monensin adopts the same cyclic conformation in both polar and non-polar media. Molecular dynamics simulations were performed for the sodium, potassium and rubidium salts of monensin in chloroform[70] on the basis of interatomic distances obtained from the solution ^{1}H-NMR NOESYexperiments and X-ray crystallographic data. In comparison with the X-ray structures, much shorter distances were found between one of the carboxylate oxygens and the metal ion, implying the existence of coordination between the metal and one of the carboxylate oxygens in solution. The metal cations also appeared to have strong electrostatic interactions with only five oxygen atoms. Size differences for various cations were accommodated by slight conformational changes near the acid group of the ligand. In the rubidium complex, one of the monensin coordination sites was moved from the furan oxygen to a terminal hydroxy group in order to accommodate the larger cation. A model of metal complexation has been suggested[70] where the process starts from binding of the

positive metal ion to the deprotonated carboxylate arm of the ionophore molecule that is extended from the membrane interface into the water. Subsequently, ether and hydroxy oxygens along the ionophore replace the remaining solvent molecules around the metal in a stepwise manner. The computer simulations of the complexation process supported this theory. The latter is opposite to the complex formation model postulated based only on the X-ray data[1], which suggested that metal coordination is started at an ether oxygen atom in the middle of monensin molecule. Consequently, the data acquired for the compound in solution and the associated process of computer simulations provided a more reliable and chemically sound model for the dynamic complexation process in comparison to the X-ray data obtained for the complexes in the fixed state.

The determination of complexation constants and reaction kinetics for monensin and a number of monovalent cations were carried out in different solvents and by a variety of methods. Examples of the equilibria studied and the values obtained for protonation and sodium binding constants are shown in Table I.2. Values of formation constants for monensin complexes with other monovalent cations are presented in Table I.3.

Most of these experiments were designed to identify reasons for the high transport selectivity of monensin for sodium cation. Among alkali metal cations, the sodium complex was found the most stable by all researchers. Solvent dependence of binding constant values indicated that the loss of solvation or the change in monensin conformation occurred upon going from protic to non-polar solvents. However, when the selectivity of monensin for alkali-metal cations was studied in heterogeneous (water-organic phase) systems, the preference of monensin for the extraction of sodium was found to be independent of the solvent used[71]. Measurements of molal volumes in methanol suggested that the ligand cavity size for monensin is optimal for sodium ion, but it is too big or too small for other alkali-metal cations[72]. Solubility measurements for

Table I.2. Literature values of the protonation and sodium complex formation constants of monensin in various organic solvents and heterogeneous media[a]

Reaction[b]	log K_f	method	solvent system	I, M[c]	Ref
$L^- + H^+ \rightleftharpoons HL$	10.3	H^+ potentiometry	methanol	0.15	73
	10.24	calorimetry	methanol	0	74
	22.9	H^+ potentiometry	acetonitrile	0.1	75
	11.45	H^+ potentiometry	ethanol	0	76
$L^- + Na^+ \rightleftharpoons NaL$	6.72	potentiometry	methanol	0.15	73
	6.0	calorimetry	methanol		77
	6.30	calorimetry	methanol	0	74
	6.37	Ag^+potentiometry	methanol		78
	6.30	cyclic voltammetry	DMSO-acetonitrile	0.1	79
	8.82	H^+ potentiometry	ethanol	0	80
	5.4	Na-23 spin-lattice relaxation times	80%methanol-water		81
	1.52	Na-23 NMR, transport studies	phosphatidyl choline vesicles		28
$HL_{(org)} + Na^+_{(aq)} \rightleftharpoons NaL_{(org)} + H^+_{(aq)}$	4.8	extraction	water-chloroform	0.02[d]	71
$HL + Na^+ \rightleftharpoons NaLH^+$	2.5	H^+ potentiometry	methanol	0.15	73
	2.29	calorimetry	methanol	0	74
	3.77	kinetics	ethanol	0	75

[a] 25 °C, molar scale of concentrations. [b] L^- stands for the monoanion of monensin. [c] "I" stands for the ionic strength. [d] Ionic strength control was employed for aqueous phase only

Table I.3. Literature values of the complex formation constants of monensin with monovalent cations in various organic solvents and heterogeneous media[a]

Solvent	Ionic strength, M	Metal cation						Reference
		Li^+	K^+	Rb^+	Cs^+	Tl^+	Ag^+	
methanol	0.15	3.30	5.18	4.58	3.75	5.31	8.20	73
methanol	0	3.90	5.24	4.40	3.70	-	-	74
methanol	0	3.60	4.90	-	-	-	7.86	78
ethanol	0	5.35	7.20	6.20	5.18	-	8.95	80
DMSO-acetonitrile	0.10	4.7	5.7	-	3.6	-	-	79
water-chloroform	0.02 for aq. phase	-6.4	-5.8	-6.8	-8.5	-	-	71
methanol	0	-	-	-	-	4.9	7.4	82

[a] 25 °C; molar concentration scale. The values are presented as log β_1, where β_1 is overall formation constant for the 1:1 monensin-metal cation complex ($M^+ + L^- \rightleftharpoons ML$). In this case the value of β_1 is the same as K_{ML}.

monensin complexes in water revealed that the hydrophobicity trend correlated with transport selectivity for sodium[71]. Protonated complexes of monensin with sodium were also identified[73] (Table I.1). These could be responsible for the transport by an electrogenic mode.

Measurements of kinetic parameters for reactions of formation and dissociation of monensin complexes helped to further understand the transport mechanism and pinpoint the factors responsible for the sodium selectivity against other alkali-metal cations. Measured rate constants for complex formation were lower than those for the diffusion controlled process, suggesting that cation desolvation should be an important rate-limiting step[79]. The formation constants were sufficiently high to indicate that metal coordination proceeds through an efficient stepwise process. Values of rate constants for dissociation of the sodium–monensin complex were determined during transport studies using phospholipid vesicles[83]; the dissociation of the complex was shown to be also an

important rate-limiting step in the transport process. Values of rate constants for the Na^+ - Na-monensin exchange reaction in methanol were consistent with the model when the complex dissociation occurs through a $NaMonH^+$ intermediate[81] The selectivity of monensin for sodium transport was also connected to the interactions within the lipid bilayer and the rates of cross-membrane diffusivities for the neutral complexes of monensin with the monovalent cation[84].

Studies of monensin transport and complexes with divalent cations.

Because monensin was not considered to be a divalent ionophore, studies of divalent cations complexation are rather scarce. The structure and binding in the calcium(II) monensin complexes was studied by NMR spectroscopy[85]. Variations of the ^{13}C chemical shifts were recorded in going from uncomplexed monensin anion to the ligand in the 1:1 calcium-monensin complex or the first monensin ligand in the $CaMon_2$ complex, and from free monensin anion to the second monensin ligand in $CaMon_2$. The data on the broadening of ^{13}C peaks upon addition of paramagnetic manganese(II) to the 1:1 and 2:1 monensin-calcium complexes was also acquired in the same study. This information helped to identify oxygen binding sites on monensin ligand. The results indicated that the first monensin anion interacted with the calcium cation through the carboxylate group on one end, a terminal hydroxy group and a hydroxy-oxygen from the group located on the furan ring of the spiroketal function. Thus, calcium cation was found to be located outside the ionophore cavity in comparison to the structures of alkali-metal complexes. The donor atoms and conformation of the second monensin ligand were different. The carboxylate group did not participate in binding and different ether oxygens were involved in coordination. In general, the cation was insulated by the lipophilic envelope less effectively as compared with the alkali metal complexes. This is consistent with the lower transport efficiency for divalent cations.

Stability constants for 1:1 monensin complexes with alkaline-earth metal cations were obtained by Cox and coworkers[78] in the various protic and polar solvents. In all cases $CaMon^+$ complexes were the least stable. Other researchers reported formation constants in pure methanol for both 1:1 and 2:1 monensin-metal complexes for a number of divalent cations including alkaline-earths[85], first-row transition metals[85] and some heavy metal cations, such as cadmium(II) and lead(II)[82,86]. The values of the complexation constants are presented in Table I.4. Formation of two successive complexes was determined from the analysis of pH-titration curves for all divalent cations studied with the exception of copper(II)[85]. The formation of the $Cu(Mon)_2$ species was found to be negligible because of the strong affinity of copper for the methoxide ion and the formation of a ternary Cu-Mon-OCH_3 complex. In addition, the values of overall extraction constants (defined in eq I.1, where M stands for the metal) for monensin - alkaline-earth cation complexes were obtained[85].

$$2\,HMon_{(CHCl_3)} + M^{2+}_{(aq)} \rightleftharpoons MMon_{2(CHCl_3)} + 2H^+_{(aq)} \quad \beta = \frac{[MMon_{2(CHCl_3)}][H^+_{(aq)}]^2}{[HMon_{(CHCl_3)}]^2[M^{2+}_{(aq)}]} \quad (I.1)$$

The results showed that the formation of magnesium and calcium complexes with 2:1 monensin-metal stoichiometry was the least favorable thermodynamically in comparison with calcium and magnesium complexes of divalent ionophores, such as lasalocid or A23187.

Nevertheless, several transport studies of alkali-earth cations with ionophore monensin were reported; e.g., transport through polyvinyl chloride membranes of ion-selective electrodes[87,88]. The results obtained indicated that monensin transported barium(II) as a monovalent 1:1 ligand-cation complex, but that it also formed a 2:1 ligand-magnesium complex. Electrode responses and membrane ion selectivities indicated the preference for barium among the alkaline-earth cations. These studies pointed to the importance of the carboxylic acid group in the divalent cation transport: electrodes responded weakly if the methyl ester of monensin was employed in the

Table I.4. Values of formation constants of monensin complexes with divalent cations[a]

Cation	log β_1[b]	log β_2	Solvent	Reference
Ca^{2+}	4.4	-	methanol	78
	5.6	-	dimethylsulfoxide	78
	6.0	-	dimethylformamide	78
	5.6	8.9	methanol	86
Ba^{2+}	7.1	-	methanol	78
	5.1	-	dimethylsulfoxide	78
	7.0	-	dimethylformamide	78
	5.0	8.0	methanol	85
Mn^{2+}	6.1	9.8	methanol	85
Fe^{2+}	7.6	13.7	methanol	85
Cu^{2+}	8.0	10.0	methanol	85
		17.1[c]		
Zn^{2+}	6.5	10.6	methanol	85
Pb^{2+}	7.7	12.1	methanol	86
Cd^{2+}	6.7	11.1	methanol	86
Hg^{2+}	9.9	18.9	methanol	82

[a] 25 °C; 0 M ionic strength and molar concentration scale. [b] β_i is the overall complex formation constant for $M(Mon)_i$, M = divalent cation. [c] β_2 is the overall formation constant for the copper(II) mixed complex with monensin and methoxide ions of 1:1:1 stoichiometry as defined in eq 1.

membrane. Modification of monensin by adding a second carboxylate group on the other end of the molecule[89] resulted in an almost three-fold increase of calcium transport in comparison to that of sodium through a $CHCl_3$ liquid membrane.

Lasalocid complexes, literature overview.

Lasalocid was among the first group of polyether ionophores to be discovered in 1951[3,4]. It is different from many other ionophore antibiotics in that it is a smaller molecule which contains an aromatic ring with a hydroxyl group in an ortho-position to the carboxylic acid moiety (Figure I.2). A number of lasalocid factors were isolated from *Streptomyces lasalientis* bacteria, lasalocid A being the predominant one in the mixture. Lasalocids B, C, D and E were found to have an extra methylene group and constituted less than 4% (w/w) of the mixture. Isolasalocid, a structural isomer of lasalocid A, was also identified in miniscule amounts (0.5% w/w). Further discussion will refer only to Lasalocid A, if not specified otherwise.

Lasalocid is one of the ionophores most extensively studied by X-ray crystallography. X-ray structures of the lasalocid silver(I) salts $(LasAg)_2$[90] and $(LasAg)_2 \cdot 2CH_3COCH_3$[91], sodium salts $LasNa \cdot CH_3OH$[92] and $(LasNa \cdot H_2O)_2$[93], cesium salt LasCs[60], barium salt $Las_2Ba \cdot H_2O$[94] and (R)-1-amino-1-(4-bromophenyl) salt $LasC_8H_{11}NBr$[95] were obtained as well as that of the free acid $HLas \cdot CH_3OH$[96] and a bromo-derivative $(HLasBr)_2 \cdot H_2O$[97]. The conformation of the lasalocid molecule was found to be similar in all of them and thought to be stabilized by head-to-tail hydrogen bonds between the carboxyl group and the tertiary terminal hydroxyl on the opposite end. In sodium and silver complexes cations were generally coordinated by ether, ketone and hydroxyl oxygens of a single lasalocid anion. Only in a symmetrical structure of the silver complex dimer[90] the carboxylic group from the second ligand participated in cation coordination. Lasalocid complexes were found to have a tendency to form dimers, possibly due to the conformation and smaller size of the ionophore. The size prevents lasalocid from totally wrapping around the metal cation and in some monomeric sodium complex structures[92] a solvent molecule was bound to the opposite

face of the cation. In the structure of the lasalocid complex with barium an oxygen from the carboxylate group of both anions participated in the cation binding, as shown in Figure I.7. The cation was located closer to one lasalocid, which provided six coordinating oxygens, and was bound to two oxygens of the second lasalocid molecule. The two lasalocid anions were arranged as a head-to-tail dimer with respect to the carboxylate groups. No interactions in the form of hydrogen bonds were found between two ligands.

The structural studies of lasalocid and its complexes in both non-polar and polar bulk solvents contributed to the understanding of both the complexation process and metal transport mechanism. From the early ^{1}H-NMR studies[98] the free acid conformation in chloroform was found to be almost identical to the globular structure found for the sodium salt. Studies of ^{1}H and ^{13}C relaxation times[99] suggested that in chloroform the free acid exists as a monomer, but that the sodium and barium salts

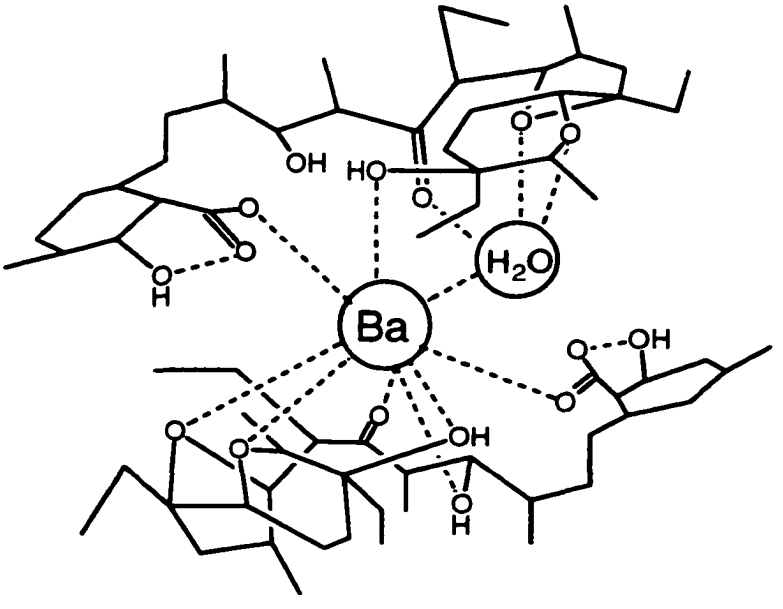

Figure I.7. Cation coordination in the lasalocid-barium complex as inferred from its X-ray structure (ref.96).

are present as $(NaLas)_2$ and $Ba(Las)_2$ complexes, respectively. However, in methanol[100] all the species were found to be monomeric (MLas).

CD spectroscopy measurements showed strong optical activity for lasalocid in aqueous ethanol[13,101] in the presence of both mono- and divalent metal cations, but the free acid form of lasalocid exhibited weak optical activity. However, in a non-polar solvent like heptane, the optical activity was present for free acid form of lasalocid indicating a conformation similar to that in the metal complexes. It was concluded that free lasalocid molecule adopts a cyclic conformation in highly non- polar solvents but has a disordered structure in aqueous ethanol. CD, UV-Vis absorption and fluorescence data in methanol[73] for lasalocid complexes with alkali, alkaline-earth metals, and Mn^{2+} and Ni^{2+} indicated that they are mostly monomeric MLas (or $MLas^+$), while in hexane[102] complexes having MLas, $MLas_2$, and $MLas_2H$ stoichiometries were suggested to exist. Results of Raman spectroscopic measurements of hydroxyl deformation frequencies in the sodium complex of lasalocid at higher concentrations[103] showed that the hydrogen bonding pattern in both methanol and tetrachloromethane was the same and similar to that inferred from the X-ray structure[92]. A computational study of the free lasalocid molecule in vacuo and in aqueous solution[104] indicated that the most energetically favorable conformation in vacuo is a closed one, whereas in polar solvents lasalocid ion has a high flexibility and prefers the unfolded form.

NMR spectroscopy proved to be a useful method to study metal binding in solution. It was concluded from conformational NMR studies of the lasalocid anion, lasalocid free acid, and potassium complex[105], that the lasalocid molecule is rather flexible and can adopt various conformations depending on the cation complexed. However, even in the globular conformation complete cation insulation was not achieved: solvent molecules were found at the metal ion site in protic media and dimerization occured in aprotic solvents. Changes in the ^{13}C NMR chemical shifts of the lasalocid anion caused by potassium complexation allowed identification of the binding

oxygen atoms in the ligand molecule[106]. One of the carboxylate oxygens in each lasalocid ligand in both monomer and dimer complexes, and ketone and two ether oxygens from only one ligand in a dimer were found to participate in coordination.

Changes in the ^{13}C NMR chemical shifts of lasalocid were recorded following the extraction of zinc from an aqueous solution to the chloroform phase using sodium lasalocid[34]. The shift in the aromatic ^{13}C signals of the lasalocid ligand suggested that the salicylic acid moiety played an important role in the complexation of divalent zinc. The effects of paramagnetic Mn^{2+} on the ^{13}C spin-lattice relaxation rates were used to identify the divalent cation binding sites in both chloroform and dimethylformamide[107]. The binding pattern was found to depend upon the solvent polarity. In a polar solvent, such as dimethylformamide, manganese was coordinated by the anionic carboxylate, an ether oxygen from a furan ring and the secondary hydroxyl located in the center of the lasalocid molecule, next to the ketone function; in chloroform an additional coordination bond with the terminal tertiary hydroxyl was shown to be present. Studies of the cation binding sites in calcium(II) and lanthanum(III) complexes were also performed in chloroform using NMR spectroscopy[106]. The complexes were shown to have $CaLas_2$ and $LaLas_3$ stoichiometries. In solution, the calcium binding was similar to that of the manganese. Calcium was bound by the carboxylate group on one end and the hydroxyl on the other end of each lasalocid molecule with ether and secondary hydroxyl oxygens of two ligands taking turns in binding. It was suggested that the ligands were involved in a dynamic intramolecular donor exchange that maintained a constant coordination number for calcium ion. Another study reported assignments of coordinating oxygens for lasalocid complexes with all alkaline-earth cations in chloroform[108]. In the complex having 1:2 calcium-lasalocid stoichiometry a carboxylate, ketone carbonyl, both central and terminal hydroxyls and furan ether oxygens of one ligand served as donor atoms; however, in the second lasalocid oxygen atom from the carboxylate and the terminal hydroxyl were found to participate in cation coordination. When the successive

formation of MLas and $MLas_2$ complexes for the alkali-earth cations was observed in methanol[109], the conformations of the two ligand anions were also found to be different. Six donor atoms from one ligand were involved in metal binding and only two oxygens from the second ligand, one from the carboxylate group and one from either an ether or a hydroxy group, participated in coordination. Slight differences in donor atoms involved were observed as the cation varied from Mg^{2+} to Ba^{2+}. In all studies the salicylate hydroxyl did not participate in cation binding, because it was hydrogen-bonded to one of the carboxylate oxygens.

The reported complex formation constants of lasalocid–alkali-metal cations are presented in Table I.5 and those for lasalocid with alkaline earth cations and transition metal ions complexes are presented in Table I.6. Fe(II) and Cu(II) formed the strongest complexes with lasalocid among the first row transition metals. The comparison of binding parameters to those of salicylic acid suggested that this functional group of the lasalocid anion dominates the binding in the transition metal complexes.

Table I.5. Literature values of the overall formation constants for 1:1 lasalocid complexes with monovalent cations[a]

Solvent	Metal cations							Ref.
	Li	Na^+	K^+	Rb^+	Cs^+	Ag^+	Tl^+	
MeOH	2.15	2.80	3.67	3.62	3.66	4.12		78
MeOH	1.68	2.57	3.58	3.56	3.42			110
MeOH	1.44	2.61	3.45	3.39	3.36			111
MeOH						4.20	4.20	112
EtOH	2.89	4.14	4.73	4.45	4.65	4.87		78

[a] 25 °C and 0 M ionic strength. . The values are presented as log β_1, where β_1 is overall formation constant for the 1:1 monensin-metal cation complex ($M^+ + L^- \rightleftharpoons ML$). In this case the value of β_1 is the same as K_{ML}.

Table I.6. Literature values of the overall formation constants (β_i) for lasalocid complexes with divalent cations in methanol[a]

Cation	log β_1 [b]	log β_2 [b]	Reference
Mg^{2+}	3.90[c]	-	78
	4.20	6.7	111
	3.83		102
Ca^{2+}	4.6[c]	-	78
	5.00	7.5	111
	4.57	-	102
Sr^{2+}	5.60[c]	-	78
	5.71	7.7	111
	5.47		102
Ba^{2+}	6.46[c]	-	78
	6.74	8.8	111
	6.46		102
Mn^{2+}	4.6	7.7	114
	4.4		113
Fe^{2+}	5.0	9.0	114
Co^{2+}	4.8	7.8	114
	4.6		113
Ni^{2+}	5.2	8.5	114
	3.96		113
	3.7		115
	4.50		116
Zn^{2+}	5.4	8.8	113
Cu^{2+}	6.5	10.7	117
		16.1[d]	117
Pb^{2+}	7.7	11.0	86
Cd^{2+}	5.7	9.6	86
Hg^{2+}	8.5	15.7	82

[a] 25 °C and 0 M ionic strength. [b] β_i is the overall complex formation constant for ML_i, where M = metal cation and L = lasalocid. [c] Values in ref. 78 were obtained by silver potentiometry and the formation of 1:2 metal-ligand complexes was not taken into account; [d] Equilibrium constant for the reaction: $Cu^{2+} + Las^- + OCH_3^- \rightleftharpoons CuLasOCH_3$.

The complexation of heavy metal cations Pb(II), Cd(II), and Hg(II) with lasalocid, acetic acid and salicylic acid were also investigated in methanol[86]. Both 1:1 and 2:1 lasalocid-metal complexes were formed and lasalocid was found to be a much better ligand in comparison with the reference compounds.

Several kinetic studies of lasalocid complexation and decomplexation reactions were reported. The value of the rate constant for formation of the barium complex $BaLas^+$ was measured[100] and approached the diffusion controlled rate of association between the charged species. This indicated that fast and effective stepwise substitution of methanol solvent in the barium coordination sphere by the lasalocid donor atoms takes place. The rates of lasalocid exchange between the barium complex and free anion were measured in methanol[100]; the values were characteristic of a rate-determining complex dissociation. In chloroform these exchange rates were found to have a first order dependence on the concentrations of lasalocid free acid and $BaLas_2$, which ruled out dissociation as a rate-determining step in nonpolar solvents.

The values of rate constants were determined for the formation reactions of $NiLas^+$ and $MnLas^+$ complexes in methanol by NMR methods[118]. A conformational change of lasalocid in a transition complex was proposed to be a rate limiting step for the reaction. The formation rate constant of lasalocid reacting with nickel was also found by the stopped-flow method when changes in conductance upon complex formation were monitored[115]. Lifetimes of 1:1 lasalocid complexes with calcium, barium, strontium and nickel were determined in methanol using a dissociation shift reagent and NMR[116]. The lifetime trend found was $CaX^+ < SrX^+ < BaX^+$. A good correlation was found between this trend and the values of stability constants of lasalocid complexes with alkaline-earth metals.

Mechanistic studies of lasalocid-mediated calcium transport were conducted using membranes in the phospholipid vesicles[119]. The results indicated that at low ionophore concentration the overall transport rates were limited by the equilibrium constants for the

formation of $CaLas_n$ complexes. However, the rates of Mn^{2+} transport obtained in the similar system[120] were determined mainly by the rates of $MnLas_2$ diffusion through the membrane.

Summary of studies.

The recently discovered lead transport properties of ionophore antibiotics pointed to a possible danger for public health and posed questions about the mechanism. This study was conducted to discover possible reasons for the lead (II) transport selectivity among divalent cations and to identify the nature of transporting species that are responsible for the observed stoichiometry. Monensin and lasalocid were chosen as representative ionophore antibiotics for the study because of their displayed lead transport activities. In studies of ionophore-mediated metal ion transport [35,37] the lead transport rates were found to be much larger than these found for other divalent cations, such as cadmium, zinc, copper, manganese and calcium. The stoichiometric transport ratios were found to be 1:1 (ionophore-metal) for monensin mediated lead transport, and between 1:1 and 2:1 (ionophore-metal) for lasalocid mediated transport of lead, indicating that complexes with different stoichiometries can be active participants in the latter case. Lasalocid-mediated lead transport rates and selectivity versus calcium were smaller than rates and selectivity of the monensin-mediated lead transport. One approach to better understand the transport behavior consists involves characterization of the individual steps in the transport process.

Figure I.4 illustrated two possibilities for a lead transport mechanism (parts B and C) that involve neutral complexes: through a complex having 2:1 ionophore-lead stoichiometry or a mixed 1:1:1 ionophore-lead-anion complex. Several reactions at the membrane-water interface are associated with the discrete membrane transport steps. These equilibria include ionophore dissociation and protonation (eq I.2); complex formation between a free ionophore anion and the metal cation (eq I.3), and formation of

a neutral species through the reactions illustrated in eqs I.4 and I.5 along with the corresponding dissociation reactions on the other side of the membrane. In equations I.2 – I.5 L^- stands for the mono-anion of ionophore, X^- stands for another anion such as chloride or hydroxide and M stands for a divalent metal ion.

$$H^+ + L^- \rightleftharpoons HL \qquad (I.2)$$

$$M^{2+} + L^- \rightleftharpoons ML^+ \qquad (I.3)$$

$$ML^+ + L^- \rightleftharpoons ML_2 \qquad (I.4)$$

$$ML^+ + X^- \rightleftharpoons MLX \qquad (I.5)$$

Characterization of these equilibria, identification of possible neutral transporting complexes of lead and study of their properties were the focus of this work.

Lead(II) complexes of monensin and lasalocid were prepared, isolated, and their elemental compositions were determined. The results allowed identification of complexes with stoichiometry favorable for transport. Ternary Pb-ionophore-anion complexes were also prepared and characterized by mass-spectrometry, atomic absorption and elemental analysis. The observation of those mixed species pointed to the possibility of their participation in lead transport.

One of the steps in the transport process can include the ligand protonation at the membrane interface, therefore it is important to determine the acid-base properties of the ionophore. The protonation constants of monensin and lasalocid were measured in 80% methanol by potentiometric titration and for lasalocid, by UV-Vis titration as well. Because the extent of complex formation may contribute to the increase in transport selectivity, values of the formation constants for ionophore complexes with a number of metal cations were determined. The stoichiometries and conditional stability constants of lead-ionophore complexes were determined by spectrophotometric titrations in 80% methanol. Stability constants of lead, zinc, calcium and sodium ionophore complexes

were also measured by potentiometric titrations of metal-ligand solutions. Calcium, sodium and zinc were chosen for the study because they participate in important biological functions. Also, calcium and sodium are present at significant concentrations in the living cells and could have a substantial effect on the other cation transport. Lead (II) and Ca(II) cations have similar ionic radii, so it was of interest to compare the strength of their ionophore complexes. Zinc(II) was chosen also as the best transported cation among transition metals and sodium represented monovalent cations. Analysis of the potentiometric titration data and ESI-MS results identified the presence of ternary metal-ionophore-hydroxide complexes with lead and zinc. These species may provide additional pathways for the transport process.

The conformation of the ionophore in complexed form and the metal binding sites define the size of its pseudo-cavity and the degree of cation insulation from the hydrophobic membrane interior. The less shielded cation is less likely to traverse the membrane. In this study an attempt was made to obtain the information about lead binding sites and ligand conformations in solution using nuclear magnetic resonance (NMR) spectroscopy. The ^{13}C and ^{1}H chemical shifts of monensin and lasalocid ligands in lead complexes are reported and compared to those of uncomplexed ligands.

Thus, the influence of several possible factors on the selectivity of lead transport was investigated. The values of equilibrium constants for ligand protonation and complex formation are required to develop a feasible transport model. In turn, a more thorough knowledge of the transport mechanism may be useful in the future for the design of chelating agents for the treatment of lead-poisoning that do not interfere with the biologically important metals. Ionophores with these properties may also be used to make membrane-based electrodes with high selectivity for lead.

References.

1) Dobler, M. *Ionophores and Their Structures* ; Wiley and Sons: New York, 1981.

2) Taylor, R. W.; Kauffman, R. F.; Pfeiffer, D. R. In *Polyether Antibiotics: Naturally Occuring Acid Ionophores, Volume 1: Biology*; Westley, J. W., Ed.; Marcel Dekker, Inc.: New York, 1982; pp. 103-184.

3) Berger, J.; Rachlin, A. I.; Scott, W. E.; Sternbach, L. H.; Goldberg, M. W. *J. Am. Chem. Soc.* **1951**, 73, 5295-5298.

4) Harned, R. L.; Hidy, P. H.; Corum, C. J.; Jones, K. L. *Antibiot. Chemother. I* **1951**, 594-596.

5) Westley, J. W. In *Polyether Antibiotics: Naturally Occuring Acid Ionophores, Volume 1: Biology*; Westley, J. W., Ed. Marcel Dekker, Inc.: New York; 1982, pp. 1-20.

6) Shumard, R. F.; Callender, M. E. *Antimicrob. Agents Chemother.* **1968**, 369-377.

7) Lutz, W. K.; Winkler, F. K.; Dunitz, J. D. *Helv. Chim. Acta*, **1971**, 54, 1103-1108.

8) Hilgenfeld, R.; Saenger, W. In *Host Guest Complex Chemistry II*; Vogtle, F., Ed. Topics in Current Chemistry Series 101; Springer-Verlag: New York; 1982, pp.3-82.

9) Harold, F. M. *The Vital Force: A Study of Bioenergetics.*; W. H. Freeman: New York; 1986, pp. 68-73, 359-369.

10) Sandeux, R.; Seta, P.; Jeminet, G.; Alleaume, M.; Gavach, C. *Biochim. Biophys. Acta*, **1978**, 511, 499-508.

11) Nakazato, K.; Hatano, Y. *Biochim. Biophys. Acta* **1991**, 1064, 103-110.

12) Erdahl, W. L.; Chapman, C. J.; Taylor, R. W.; Pfeiffer, D. R. *Biophys. J.* **1994**, 66, 1678-1693.

13) Erdahl, W. L.; Chapman, C. J.; Taylor, R. W.; Pfeiffer, D. R. *Biophys. J.* **1995**, 69, 2350-2363.

14) Painter, G. R.; Pressman, B. C. In *Host Guest Complex Chemistry II*, Vogtle, F., Ed. Series Topics in Current Chemistry 101; Springer-Verlag: New York, 1982, pp.84-110.

15) Reed, P. W. In *Polyether Antibiotics: Naturally Occuring Acid Ionophores*, Volume 1: Biology, Westley, J. W., Ed.; Marcel Dekker, Inc.: New York; 1982, pp. 185-302.

16) Buhlmann, P.; Pretsch, E.; Bakker, E. *Chem. Rev.* **1998**, 98, 1593-1687.

17) Walker, P. M.; Weichenthal, B. A.; Cmarik, G. F. *J. Anim. Sci.* **1980**, 51, 532-538.

18) Surber, L. M. M.; Bowman, J. G. P. *J. Anim. Sci.* **1998**, 76, 1945-1954.

19) Fasolato, C.; Pozzan, T. *J. Biol. Chem.* **1989**, 264, 19630-19636.

20) Fujise, H.; Lauf, P. K. *Am. J. Physiol.* **1987**, 252, C197-C204.

21) Pressman, B. C.; Harris, E. J.; Jagger, W. S. Johnson, J. H. *Proc. Natl. Acad. Sci. U. S. A.* **1967**, 58, 1949-1956.

22) Riddell, F. G. *Chem. Br.* **1992**, 533-537.

23) Celis, H.; Estrada-O. S.; Montal, M. *J. Membrane Biol.* **1974**, 18, 187-199.

24) Estrada-O. S.; Celis, H.; Calderon, E.; Gallo, G.; Montal, M. *J. Membrane Biol.* **1974**, 18, 201-218.

25) Hope, M. J.; Bally, M. B.; Webb, G.; Cullis, P. R. *Biochim. Biophys. Acta* **1985**, 812, 55-65.

26) Mayer, L. D.; Hope, M. J.; Cullis, P. R. *Biochim. Biophys. Acta* **1986**, 858, 161-168.

27) Puskin, J. S.; Vistness, A. I.; Coene, M. T. *Arch. Biochem. Biophys.* **1981**, 206, 164-172.

28) Riddell, F. G.; Arumugam, S.; Cox, B. G. *Biochim. Biophys. Acta*, **1988**, 944, 279-284.

29) Young, S. P.; Gomperts, B. D. *Biochim. Biophys. Acta* **1977**, 469, 281-291.

30) Cader, B. M.; Horrocks, DeW. W. *Biophys. Chem.* **1989**, 33, 265-275.

31) Grandjean, J.; Laszlo, P. *Biochem. Biophys. Res. Commun.* **1982**, 104, 1293-1297.

32) Shastri, B. P.; Sankaram, M. B.; Easwaran, K. R. K. *Biochemistry*, **1987**, 26, 4625-4930.

33) Wang, E.; Taylor, R. W.; Pfeiffer, D. R. *Biophys. J.* **1998**, 75, 1244-1254.

34) Tsukube, H.; Takagi, K.; Higashiyama, T.; Iwachido, T.; Hayama, N. *J. Am. Chem. Soc.*, **1994**, 33, 2984-2987.

35) Ivanova, O.G.; Erdahl, W.L.; Pfeiffer, D.R.; Taylor, R.W. *Abstracts of papers,* 219th National Meeting of the American Chemical Society, San Francisco, CA, March 25-30, 2000; American Chemical Society: Washington, DC, 2000; INOR 170.

36) Erdahl, W. L.; Chapman, C. J.; Taylor, R. W.; Pfeiffer, D. R. *J. Biol. Chem.*, **2000**, 275, 7071-7079.

37) Pfeiffer, D. R. Ohio State Unversity, Columbus, OH; Taylor, R. W. University of Oklahoma, Norman, OK. Personal Communications, 1997-2000.

38) Salisbury, C. D.; Rigby, C. E.; Chan, W. *J. Agric. Food. Chem.*, **1989**, 37, 105-108.

39) Martinez, E. E.; Shimoda,W. *J. Assoc. Off. Anal. Chem.* **1985**, 68, 1149-1153.

40) Takatsuki, K.; Suzuki, S.; Ushizawa, I. *J. Assoc. Off. Anal. Chem.* **1986**, 69, 443-448.

41) Moran, J. W.; Turner, J. M.; Coleman, M. R. *J. AOAC Int.* **1995**, 78, 668-673.

42) Kennedy, D. G.; Hughes, P. J.; Blanchflower, W. J. *Food Addit. Contamin.* **1998**, 15, 535-541.

43) Moore, P. V.; *AAOHN Journal* **1995**, 43, 428-438.

44) Lanphear, B. P.; *Science* **1998**, 281, 1617-1618.

45) Kessel, I., O'Connor, J. T. Getting the Lead out: the Complete Resource on How to Prevent and Cope with Lead Poisoning, Plenum Press: New York, 1997.

46) Lin, Z.; Harsbo, K.; Ahlgren, M.; Qvarfort, U. *Sci. Total Environment*, **1998**, 209, 47-58.

47) Raghunath, R., Tripathi, R. M.; Khandekar, R. N.; Nambi, K. S. V *Sci. Total Environment* **1997**, 207, 133-139.

48) *Metal Toxicology*; Goyer, R. A.; Klaassen, C. D.; Waalkes, M. P., Eds.; Academic Press, Inc.: San Diego, CA, 1995.

49) Hatwig, A. *Biometals* **1995**, 8, 3-11.

50) Kerper, L. E; Hinkle, P. M. *J. Biol. Chem.* **1997**, 272, 8346-8352.

51) Schanne, F. A. X.; Dowd, T. L.; Gupta, R. K.; Rosen, J. F. *Proc. Natl. Acad. Sci. USA* **1989**, 86, 5133-5135.

52) Diaz, R. S.; Monrel, J. *Molec. Pharmacology* **1995**, 47, 766-771.

53) Bradbury, M. W. B.; Deane, R. *Neurotoxicology* **1993**, 14, 131-136.

54) Haney, M. E.; Hoehn, M. M. *Antimicrob. Agents. Chemother.* **1968**, 349-352.

55) Pinkerton M.; Steinrauf, L. K. *J. Mol. Biol.* **1970**, 49, 533-546

56) Duax, W. L.; Smith, G. D.; Strong, P. D. *J. Am. Chem. Soc.* **1980**, 102, 6725-6729.

57) Pangborn, W.; Duax, W.; Langs, D. *J. Am. Chem. Soc.* **1987**, 109, 2163-2165.

58) Agtarap, A.; Chamberlin, J. W.; Pinkerton, M.; Steinrauf, L. *J. Am Chem. Soc.* **1967**, 89, 5737-5739.

59) Ward, D. L.; Wei. K.-T.; Hoogerheide, J. G.; Popov, A. I. *Acta. Cryst.* **1978**, B34, 110-115.

60) Duesler, E. N. and Paul, I. C. In *Polyether Antibiotics: Naturally Occuring Acid Ionophores, Volume 2: Chemistry*, Westley, J. W., Ed.; Marcel Dekker, Inc.: New York, 1983, pp. 170-178.

61) Lutz, W. K.; Wipf, H.-K.; Simon, W. *Helv. Chim. Acta* **1970**, 53, 1741-1746.

62) Anteunis, M. J. O.; Rodios, N. A. *Bioorg. Chem.* **1978**, 7, 45-55.

63) Anteunis, M. J. O. *Bull. soc. Chim. Belg.* **1977**, 86, 367-379.

64) Anteunis, M. J. O. In: *Polyether Antibiotics: Naturally Occuring Acid Ionophores, Volume 2: Chemistry*, Westley, J. W., Ed.; Marcel Dekker, Inc.: New York, 1983, pp. 245-334.

65) Rodios, N. A.; Anteunis, M. J. O. *Bull. Chem. Soc. Belg.* **1980**, 89, 537-551.

66) Cane, D. E.; Lyang, T.C.; Hasler, H. *J. Am. Chem. Soc.* **1982**, 104, 7274.

67) Ajaz, A. A.; Robinson, J. A.; Turner, D. L. *J. Chem. Soc. Perkin Trans. I* **1987**, 27-36.

68) Vaufrey-Mary, F. Doctorate Thesis, Universite Blaise Pascal, Clermont, France, 1990.

69) Mimouni, M.; Hebrant, M.; Dauphin, G.; Juillard, J. *J. Chem. Res., Miniprint* **1996**, 1416-1433.

70) Martinek, T.; Riddell, F. G.; Wilson, C.; Weller, C. T. *J. Chem. Soc., Perkin Trans. 2*, **2000**, 35-41.

71) Hebrant, M.; Pointud, Y.; Juillard, J. *J. Phys. Chem.* **1991**, 95, 3653-3662.

72) Pointud, Y.; Juillard, J.; Jeminet, G.; David, L. *J. Chem. Soc., Faraday Trans. 1;* **1981**, 77, 1-8.

73) Hoogerheider, J. G.; Popov, A. I. *J. Solution Chem.*. **1979**, 8, 83-95.

74) Pointud, Y.; Pierzo, C.; Tissier, C.; Juillard, J. *J. Chim. Phys.* **1985**, 82, 891-897.

75) Pointud, Y.; Bernard, C.; Touzain, S.; Astier, L.; Sabatier, B.; Juillard, J. *J. Solution Chem.*. **1997**, 26, 479-495.

76) Cox, B. G.; Firman, P.; Schneider, H. *J. Am. Chem. Soc.* **1985**, 107, 4297-4300.

77) Fruh, P. U.; Simon, W. *Proc. Colloq. Protides Biol. Fluids* **1972**, 20, 505-510.

78) Cox, B. G.; Van Truong, N.; Rzeszotarska, J.; Schneider, H. *J. Chem. Soc., Faraday Trans. 1*, **1984**, 80, 3275-3284.

79) Wagner-Czuderna, E.; Rzeszotarska, J.; Orlowska, E.; Kalinowski, M. K. *Ber. Bunsenges. Phys. Chem.* **1997**, 101, 1154-1157.

80) Cox, B. G.; van Truong, Ng.; Rzeszotarska, J.; Schneider, H. *J. Am. Chem. Soc.* **1984**, 106, 5965-5969.

81) Amat, E.; Cox, B. G.; Rzeszotarska, J.; Schneider, H. *J. Am. Chem. Soc.* **1988**, 110, 3368-3372.

82) Mimouni, M.; Perrier, S.; Pointud, Y.; Juillard, J. *J. Solution Chem.*. **1993**, 22, 769-785.

83) Riddell, F. G.; Arumugam, S.; Cox, B. G. *Biochim Biophys. Acta* **1988**, 944, 279-284.

84) Nachliel, E.; Finkelstein, Y.; Gutman, M. *Biochim. Biophys. Acta* **1996**, 1285, 131-145.

85) Hebrant, M.; Mimouni, M.; Tissier, M.; Juillard, J. *New J. Chem.* **1992**, 16, 999-1008.

86) Mimouni, M.; Pointud, Y.; Juillard, J. *Bull. Soc. Chim. Fr.* **1994**, 131, 58-65.

87) Suzuki, K.; Tohda, K.; Aruga, H.; Matsuzoe, M.; Inoue, H.; Shirai, T. *Anal. Chem.* **1988**, 60, 1714-1721.

88) Suzuki, K.; Tohda, K.; Sasakura, H.; Inoue, H.; Tatsuta, K.; Shirai, T. *J. Chem. Soc., Chem. Comm.* **1987**, 932-934.

89) Nagatsu, A.; Tanaka, R.; Hashimoto, M.; Mizukami, H.; Ogihara, Y.; Sakakibara, J. *Tetrahedron Lett.* **2000**, 41, 2629-2632.

90) Maier, C. A.; Paul, I. C. *J. Chem. Soc., Chem. Commun.* **1971**, 181-182.

91) Suh, I.-H.; Aoki, K.; Yamazaki, H. *Inorg. Chem.* **1989**, 28, 358-362.

92) Chiang, C. C.; Paul, I. C. *Science* **1977**, 196, 1441-1443.

93) Smith, G. D.; Duax, W. L.; Fortier, S. *J. Am. Chem. Soc.* **1978**, 100, 6725-6727.

94) Suh, I.-H.; Aoki, K.; Yamazaki, H. *Acta Cryst.* **1989**, C45, 415-418.

95) Westley, J. W.; Blount, J. F.; Evans, R. H. *J. Am. Chem. Soc.* **1977**, 99, 6075-6061.

96) Friedman, J. M.; Rousseau, D. L.; Shen, C.; Chiang, C. C.; Duesler, E. N.; Paul, I. C. *J. Chem. Soc., Perkin Trans. 2* **1979**, 835-838.

97) Bissell, E. C.; Paul, I. C.; *J. Chem. Soc., Chem. Commun.* **1972**, 967-968.

98) Anteunis, M. J. O. *Bioorg. Chem.* **1976**, 5, 327-337.

99) Patel, D. J.; Shen, C. *Proc. Natl. Acad. Sci. USA* **1976**, 73, 1786-1790.

100) Shen, C.; Patel, D. J. *Proc. Natl. Acad. Sci. USA* **1976**, 73, 4277-4281.

101) Alpha, S. R.,; Brady, A. H. *J. Am. Chem. Soc.* **1973**, 95, 7043-7049.

102) Degani, H.; Friedman H. L. *Biochemistry*, **1974**, 13, 5022-5034.

103) Phillies, G. D. J.; Stanley, H. E. *J. Am. Chem. Soc.* **1976**, 98, 3892-3897.

104) Malfreyt, P.; Juillard, J.; Pascal, Y. *New. J. Chem.* **1996**, 20, 1103-1112.

105) Lyazghi, R.; Cuer, A.; Dauphin, G.; Juillard, J. *J. Chem. Soc., Perkin Trans. 2* **1992**, 35-42.

106) Everett, G. W.; Parker, S. B.; Williams, R. J. P. *Biochemistry*, **1983**, 22, 6149-6155.

107) Hanna, D. A.; Yeh, C.; Shaw, J.; Everett, G. W. *Biochemistry*, **1983**, 22, 5619-5626.

108) Lyazghi, R.; Pointud, Y.; Dauphin, G.; Juillard, J. *J. Chem. Soc., Perkin Trans. 2* **1993**, 1681-1686.

109) Mimouni, M.; Malfreyt, P.; Lyazghi, R.; Palma. M.; Pascal, Y.; Dauphin, G.; Juillard, J. *J. Chem. Soc., Perkin Trans. 2* **1995**, 1939-1947.

110) Degani, H.; Friedman, H. L.; Navon, G.; Kosower, E. M. *J. Chem. Soc., Chem. Commun.* **1973**, 431-432.

111) Juillard, J.; Tissier, C.; Jeminet, G. *J. Chem. Soc., Faraday Trans. 1* **1988**, 84, 951-958.

112) Mimouni, M.; Lyazghi, R.; Juillard, J. *New. J. Chem.* **1998**, 367-372.

113) Degani, H.; Hamilton, R. M. D.; Friedman, H. L. *Biophys. Chem.* **1976**, 4, 363-366.

114) Laubry, P.; Tissier, C.; Mousset, G.; Juillard, J. *J. Chem. Soc.; Faraday Trans. 1* **1988**, 84, 969-971.

115) Garcia-Rosas. J.; Schneider, H. *Inorg. Chim. Acta*, **1983**, 70, 183-187.

116) Krishnan, C. V.; Friedman, H. L.; Springer, Jr., C. S. *Biophys. Chem.* **1978**, 9, 23-35.

117) Laubry, P.; Mousset, G.; Martinet, P.; Tissier, M.; Tissier, C.; Juillard, J. *J. Chem. Soc., Faraday Trans. 1* **1988**, 84, 3175-3185.

118) Degani, H.; Friedman, H. L. *Biochemistry*, **1975**, 14, 3755-3761.

119) Haynes, D. H.; Chiu, V. C. K.; Watson, B. *Arch. Biochem. Biophys.* **1980**, 203, 73-89.

120) Degani, H. *Biochim. Biophys. Acta* **1978**, 509, 364-369.

CHAPTER II

EXPERIMENTAL

A. Reagents

Monensin A. Monensin sodium salt was purchased from ACROS. Previous reports identified several monensin factors (A, B and C) that were present in the compound as it was recovered from bacteria *Streptomyces cinnamonensis*[1,2]. Monensin factor B lacks one methylene group at the central pyran ring in comparison to monensin A, and monensin factor C has an additional methylene group in the carboxylic acid arm as shown in Figure II.1. The structural difference between factors A and B resulted in the significant variation (up to 3 times) in the values of sodium and potassium binding constants as reported by Walba and Hermsmeier[3]. Analysis of the commercially available monensin compound using thin layer chromatography (TLC) and fast atom bombardment mass spectrometry (FAB-MS) showed the presence of only two different monensin factors – sodium monensin A ($C_{36}H_{62}O_{11}Na^+$, m/z = 693) and sodium monensin B ($C_{35}H_{59}O_{11}Na^+$, m/z = 679) with the ratio of peak intensities of about 9:1, respectively. The separation of monensin factors was carried out using silica gel column chromatography with ethyl acetate as the eluting solvent[2]. The collected fractions were analyzed by thin-layer chromatography (TLC), using silica gel IB-F plates (Baker-flex) with ethyl acetate solvent. In order to visualize monensin, the plates were sprayed with 5% vanillin solution in concentrated sulfuric acid and heated[2]. The purity of monensin A was confirmed by the TLC and FAB mass-spectrometry. All experiments in this study were performed using purified monensin A, unless indicated otherwise.

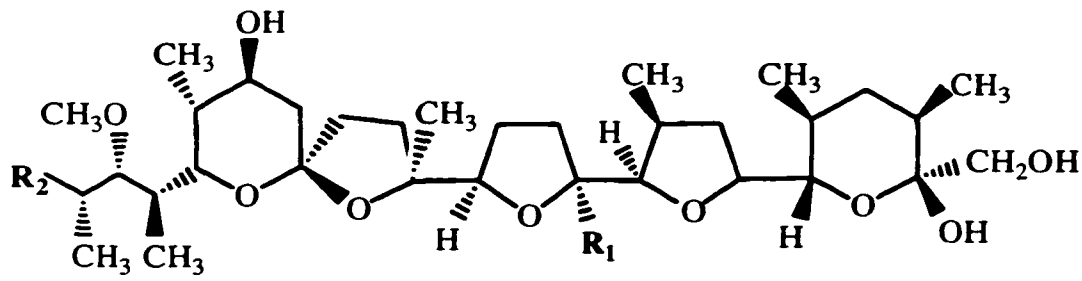

$R_1 = C_2H_5$ in monensin A and C $R_1 = CH_3$ in monensin B

R_2 =COONa in monensin A and B $R_2 = CH_2COONa$ in monensin C

Figure II.1. Structure of monensin factors A, B and C.

Monensic Acid (HMon). The recovered sodium salt of monensin A was converted to the acid form by back extraction with 1M hydrochloric acid[4]. The sodium salt was dissolved in 2-3 mL of chloroform, washed with 3 mL of 1 M HCl three times and then three times with 2-3 mL of double-distilled water. After evaporation of chloroform, the solid was redissolved in acetone and the acetone evaporated to eliminate the traces of water. The resulting acid was dried under vacuum for at least 6 hours and kept in the freezer. The acid was analyzed for the presence of sodium by flame atomic emission and contained not more than 0.05% (w/w) of sodium. NMR spectra of monensic acid in chloroform were obtained and compared to those in literature[4]. ^1H and ^{13}C peak positions were found to be the same as those reported for the free acid form of monensin.

Tetraalkylammonium monensin (Me_4NMon or Et_4NMon). The tetramethyl-ammonium or tetraethylammonium salt of monensin was prepared by reacting monensin acid with a stoichiometric amount (1:1) of the corresponding tetraalkylammonium hydroxide in methanol. The pH of the solution was monitored to confirm the completeness of neutralization. The negative ion FAB mass spectrum of tetraethylammonium monensin did not contain many background peaks. Only one major group of peaks was present in the spectrum at 669 m/z (Figure II.2.A), it corresponded to the monensin anion. A large peak (89% relative intensity) at 131 m/z corresponding to

the tetraethylammonium cation was present in the positive ion FAB-MS. The peaks for the sodium monensin adduct were present in the spectrum at 693 m/z, but were not very prominent (11% for the most intense peak in the cluster). This was not unexpected. Previously, sodium and potassium monensin adducts were reported to be easily formed under conditions of chemical[6] and electrospray[7] ionization from ammoniated monensin and the traces of alkali cations absorbed on the probe material.

Silver monensin A. The silver complex of monensin was prepared from tetramethylammonium monensin by back extraction with silver nitrate. 1 mL of a 0.02 M solution of Me_4NMon in chloroform was washed once with 7 mL of 0.1 M $AgNO_3$ in water. Following this, the chloroform phase was washed three times with 5 mL of double distilled water. The chloroform was evaporated under a stream of nitrogen, the compound redissolved in acetone, and then the acetone evaporated to eliminate any traces of water. The silver monensin compound obtained was dried under vacuum for at least 6 hours. Positive ion FAB-mass spectra of the compound were recorded and showed a peak cluster with the most intense signals at 777 and 779 m/z that corresponded to the molecular ion of 1:1 Ag-monensin stoichiometry. A typical mass spectrum of silver-monensin is illustrated in Figure II.2.B.

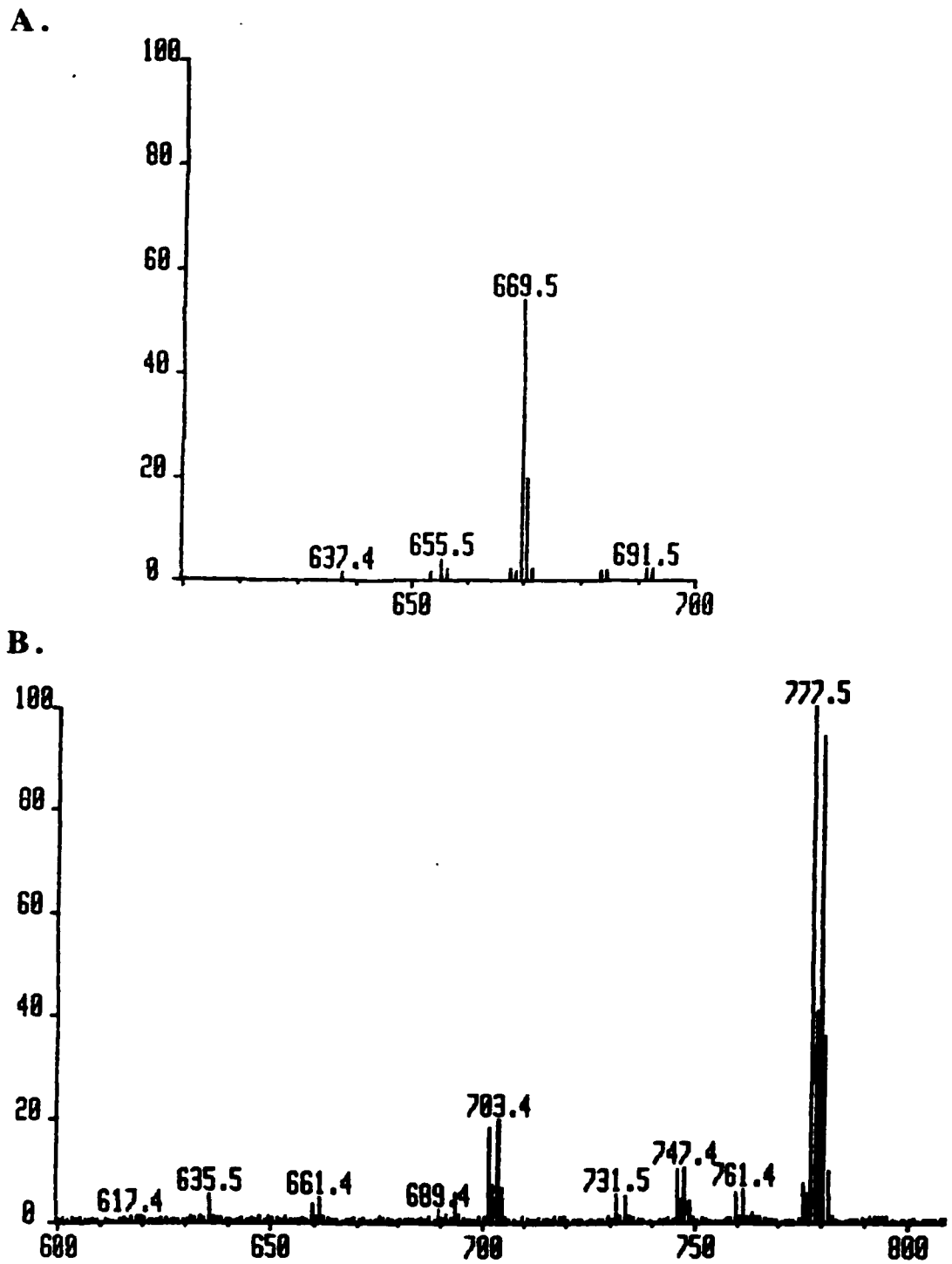

Figure II.2. FAB mass-spectra of tetraethylammonium monensin (A.), recorded in the negative ion mode, and silver monensin (B.), recorded in the positive ion mode. The samples were prepared by dissolving 0.5-1 mg of the compound of interest in methanol.

Lasalocid A. Lasalocid, sodium salt (NaLas), was purchased from Aldrich and its purity was reported to be 95%. Previously, several lasalocid factors were identified[8] in the products, isolated from *Streptomyces lasaliensis* fermentation. Lasalocid B, C, D, and E differ from lasalocid A by having one additional methylene group. Isolasalocid, a structural isomer of lasalocid A, was also reported to be present in the mixture in small amounts. The electrospray ionization (ESI) mass spectrum of the lasalocid sodium salt showed large intensity peaks for $(C_{34}H_{54}O_8Na)^+$ at m/z 613.4 and $(C_{34}H_{53}O_8Na_2)^+$ at m/z 635.4. Because the relative intensity (about 1%) of the highest peaks in the cluster centered at 627.5 m/z in the positive ESI-MS was significantly above the noise level, this indicated that the sample contained small amounts of other lasalocid factors. The absence of significant amounts of isolasalocid in the sample was confirmed by the TLC analysis using silica-gel plates and the mixture of 9:1 benzene methanol[9]. Therefore, lasalocid was found to consist up to 99% of factor A and all experiments in this work were performed using non-purified lasalocid, unless indicated otherwise.

Free acid form of lasalocid(HLas). Lasalocid, sodium salt, was converted to the free acid form as described above for monensic acid. The resulting acid was dried under vacuum for at least 6 hours and kept in the freezer. The acid was analyzed for the presence of sodium and potassium by flame atomic emission and contained not more than 0.09% (w/w) of sodium and not more than 0.03 % (w/w) of potassium.

Tetraalkylammonium lasalocid (Me_4NLas or Et_4NLas). The tetramethyl-ammonium or tetraethylammonium salt of lasalocid A was prepared by reacting lasalocid A free acid with a stoichiometric amount (1:1) of the corresponding tetraalkylammonium hydroxide in methanol. The pH of the solution was monitored to confirm the completeness of neutralization.

Silver lasalocid A. The silver complex of lasalocid was prepared from tetramethylammonium lasalocid by back extraction with silver nitrate. 1 mL of a 0.02 M solution of Me_4NLas in chloroform was washed once with 7 mL of 0.1 M $AgNO_3$ in

water. Following this, the chloroform phase was washed three times with 5 mL of double distilled water. The chloroform was evaporated under a stream of nitrogen, the compound redissolved in acetone, and then the acetone evaporated to eliminate any traces of water. The silver lasalocid compound obtained was dried under vacuum for at least 6 hours. Positive ion ESI-mass spectra of the compound were recorded and showed a peak cluster with the most intense signals at 697 and 699 m/z that corresponded to the molecular ion of 1:1 Ag-lasalocid stoichiometry. A typical mass spectrum of silver-monensin is illustrated on Figure II.3.

Lead Oxide. PbO was obtained from Puratronic (Alfa Aesar) in 99.9995% (metal based) purity. It was used as received.

Lead(Pb^{207}) Oxide. Lead-207 (II) oxide (enriched to 92.2% ^{207}Pb) was purchased from Cambridge Isotope Laboratories, Inc. and used as received.

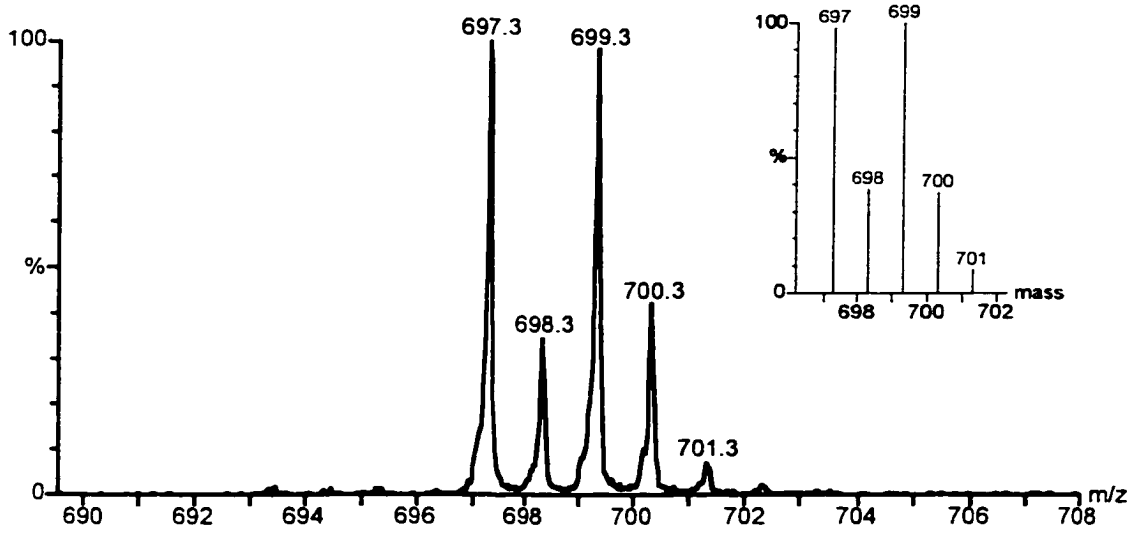

Figure II.3. ESI mass-spectra of silver lasalocid, recorded in the positive ion mode. The sample was prepared by dissolving 0.5-1 mg of the compound of interest in methanol.

Lead Perchlorate. $Pb(ClO_4)_2$ was prepared by reacting PbO (99.9995%, Alfa Aesar) with a slight excess of 70% distilled perchloric acid (GFS Chemicals, Inc.). The resulting solution was diluted to the appropriate concentration and standardized with EDTA using methylthymol blue as indicator and hexamine as a buffer[10].

Lead Chloride. Solutions were prepared by dissolving $PbCl_2$ ('Baker Analyzed' Reagent, 99.95%) in the solvent of choice and standardized with EDTA using the method described for lead perchlorate.

Zinc Perchlorate. $Zn(ClO_4)_2$ was prepared by reacting ZnO (Alfa Aesar, 99.99% (metal based)) with 70% distilled perchloric acid (GFS Chemicals, Inc.). The product was then recrystallized from water and washed with diethyl ether. Stock solutions were standardized with EDTA using Eriochrome Black T (EBT) as the indicator with pH adjusted to 10.0 using ammonia/ammonium chloride buffer[10].

Tetraethylammonium perchlorate (TEAP). $(C_2H_5)_4NClO_4$ was prepared by reacting tetraethylammonium hydroxide (20% in water, Aldrich) with 70% distilled perchloric acid (GFS Chemicals, Inc.). The acid was added to the base dropwise. TEAP was recrystallized three times from double-distilled water, dried under vacuum and stored in a dessicator.

Tetramethylammonium hydroxide. $(CH_3)_4NOH$ was purchased from Fluka in a crystalline form and 97% purity (purum). It was kept in the refrigerator. All solid hydroxides and their solutions were stored under argon gas to minimize absorption of carbon dioxide.

Ethylenediaminetetraacetic acid disodium salt (EDTA). EDTA was purchased from Fisher, Certified A.C.S. grade. Prepared solutions were subsequently standardized with calcium using Eriochrome Black T as the indicator and pH 10 ammonium buffer[10]. Calcium carbonate ($CaCO_3$) of primary standard grade (Mallinckrodt) was used to prepare calcium standard solutions.

Sodium chloride. NaCl was purchased from Aldrich, 99.999% (metal based) purity. It was dried in the oven at 110° C prior to solution preparation.

Calcium chloride. $CaCl_2$ was purchased from Aldrich at 99.999% (metal based) purity (Aldrich). Calcium solutions were standardized with EDTA using Eriochrome Black T indicator and pH 10 ammonium buffer[10].

Acetic acid. Solutions of acetic acid were prepared from concentrated acid (Fisher, glacial, ≥ 99%). They were standardized with tetramethylammonium hydroxide by potentiometric titration.

2-(*N*-Morpholino)ethanesulfonic acid. MES was purchased from Sigma Chemical Co., solutions were prepared by weight.

3-(*N*-Morpholino)propanesulfonic acid). MOPS was purchased from Sigma Chemical Co., solutions were prepared by weight.

N,*N*'-diethyl-*N*,*N*'-bis(sulfopropyl)ethylendiamine. DESPEN was purchased from GFS Chemicals, Inc., solutions were prepared by weight.

Solvents. Studies were performed in 80% (w/w) methanol/water medium. The latter was prepared using double-distilled water obtained from Corning Megapure (model MP-3A) glass distillation apparatus. Methanol (Fisher, reagent grade) was distilled prior to use. Chloroform (Fisher, reagent grade) and ethyl acetate (Mallinckrodt) were used as provided.

The following deuterated solvents were used for NMR: methanol-d_4 (CD_3OD, Cambridge Isotope Laboratories, atom 99.8% D); chloroform-*d* ($CDCl_3$, Cambridge Isotope Laboratories, atom 99.8% D); deuterium oxide (D_2O, Cambridge Isotope Laboratories, atom 99.9% D).

Glassware cleaning. All glassware used to prepare or store solutions of monensin or lasalocid was thoroughly washed in an acid bath (3:1 v/v sulfuric acid-nitric acid), rinsed with distilled water, and dried prior to use.

B. Preparation of lead-monensin A and lead-lasalocid A complexes.

The complexes with the stoichiometry of 2:1 ligand-lead can be obtained by several different methods. The first method involves the reaction between the free acid form of monensin A or lasalocid A and solid lead oxide at the indicated respective molar ratios. For monensin, the process is illustrated by equation II.1.

$$2HMon_{(MeOH)} + PbO_{(s)} \longrightarrow Pb(Mon)_{2\,(MeOH)} + H_2O \qquad (II.1)$$

About 120-200 mg of the acid form of ligand was dissolved in about 30 mL of methanol and solid lead oxide was added (0.020 - 0.030 g). The reaction was performed in polytetrafluororoethylene (PTFE) beakers to avoid the possibility of sodium or potassium contamination from glass. The reaction mixtures were stirred for 24 hours. Any excess of undissolved lead oxide was filtered out through a white sand/pasteur pipette filter and the resultant solution was centrifuged. The supernatant methanol solvent was evaporated, the product was redissolved in acetone and acetone was again evaporated to help eliminate traces of water.

The following two methods were used to produce only monensin-lead complexes. The first consisted of back-extraction of tetramethylammonium monensin in chloroform with an aqueous solution of lead nitrate (equation II.2.). The chloroform was evaporated and the resulting solid redissolved in the acetone and the acetone was evaporated.

$$Et_4NMon_{(CHCl_3)} \xrightarrow{\text{excess } Pb(NO_3)_{2\,(aq)}} Pb(Mon)_{2\,(CHCl_3)} + Et_4NClO_{4\,(aq)} \qquad (II.2)$$

A complex with 2:1 monensin-lead stoichiometry was also obtained by a third method, which involved the reaction of silver monensin with lead chloride in the respective molar ratio of 2:1 monensin-lead (equation II.3). The silver chloride precipitate was removed by filtration using a glass filter with medium to fine pore size. The resulting filtrate was centrifuged to insure the complete precipitate separation and

solvent was evaporated from the supernatant. All lead salts obtained were dried under vacuum for at least 6 hours and stored in the refrigerator.

$$2\ AgMon_{(MeOH)} + PbCl_{2\,(MeOH)} \rightarrow Pb(Mon)_{2\,(MeOH)} + 2AgCl_{(s)} \qquad (II.3)$$

The elemental composition of the lead compounds was determined by combustion analysis and atomic absorption methods. FAB and ESI mass spectra of the products were obtained using Fisons (VG) ZAB and Micromass Q-TOF instruments, respectively. The samples for MS analysis were prepared by dissolving dry solids in methanol and, in the case of mixed complexes (section II.C), in chloroform. The formation of lead complexes was confirmed for all three different methods. Results of the elemental analysis and mass-spectrometry for lead compounds of monensin and lasalocid will be discussed in detail in sections III.A and IV.A.

C. Preparation of lead-monensin and lead-lasalocid ternary complexes.

Mixed lead-ionophore-chloride complexes were prepared by reacting the appropriate silver ionophore salt with lead chloride in a 1:1 stoichiometric ratio. The process is illustrated by equation II.4.

$$AgMon_{(MeOH)} + PbCl_{2\,(MeOH)} \rightarrow PbMonCl_{(MeOH)} + AgCl_{(s)} \qquad (II.4)$$

First, the silver salt of the antibiotic was dissolved in 2-3 mL of methanol. Then the respective amount of 1 mM lead chloride solution in methanol was added to reach the desired stoichiometry. No excess of lead chloride was used. The mixtures were stirred for 2 hours to coagulate some of the precipitated silver chloride. The precipitate formed was removed using a glass filter with medium to fine pore size. The solvent was taken off using a rotary evaporator, and the resulting product was dried under vacuum for at least 6 hours.

Positive ion FAB-MS failed to confirm the presence of chloride in the samples. However, peaks corresponding to the lead-monensin-chloride and lead-lasalocid-chloride molecular ions were present in the negative ion FAB mass-spectra. Formation of the mixed species was also confirmed by the results obtained with negative ion ESI mass spectroscopy and elemental analysis. Detailed discussion of these results will follow in Chapters III and IV.

Mixed lead-monensin-nitrate and lead-monensin-acetate complexes were prepared in solution by dissolving the lead-monensin complex in methanol and adding a ten-fold excess of the desired counter-ion as the tetraethylammonium salt. Peaks resulting from the mixed complexes were observed with negative ion ESI-MS. The detailed discussion of these results will be presented in Chapter III.

D. pH* measurements

The operational pH* scale established by De Ligny et al.[11] and Gelsema et al.[12,13] for methanol-water mixtures was used in the present work for acidity measurements. The symbol pH* with an asterisk will be used to distinguish the acidity of solutions in 80% methanol-water solvent from the corresponding pH of aqueous solutions. pH* has the same meaning as pH for aqueous solutions and is defined by the following relationship

$$pH^* = -\log a_H^* = pH_{obs} - \delta \qquad \text{(II.5)}$$

$$\delta = E_j - \log {}_m\gamma_H \qquad \text{(II.6)}$$

where a_H^* is the activity of hydrogen ion in the mixed solvent, pH_{obs} is the experimental pH-meter reading, δ is an electrode solvent correction factor. The latter accounts for the difference between the liquid-junction potential, E_j, and the medium effect ($\log {}_m\gamma_H$) for 80% methanol-water.

Historically, activity was measured with the molal concentration scale, or

$$a_H^* = m\,\gamma_H^* \qquad \text{(II.7)}$$

where m is molality (moles/kg) and γ_H^* is molal activity coefficient. Operationally, conversion from molal (m) to molar (M) concentration scale can be achieved by

$$M = m\,\rho \qquad \text{(II.8)}$$

where ρ is density (g/L) of the solution in question. For convenience, the molar scale of concentration was used in this work, unless indicated otherwise. Therefore, if $[H^+]$ is the molar concentration of hydrogen ion in 80% methanol, then p[H] could be defined as

$$p[H] = -\log [H^+] \qquad \text{(II.9)}$$

The electrode solvent correction factor δ was calculated from the following

expression

$$\delta = \log K_{H\ exp}^{m*} - \log K_{H\ ref}^{m*} \qquad \text{(II.10)}$$

where $K_{H\ exp}^{m*}$ is the experimental value for the mixed-mode protonation constant of acetic acid in 80% methanol-water and $K_{H\ ref}^{m*}$ is the reference value for the same constant in 80% methanol-water. The mixed-mode protonation constant is defined for the following reaction as

$$L^- + H^+ \rightleftharpoons HL \qquad K_H^{m*} = \frac{[HL]}{a_H^* [L^-]} \qquad \text{(II.11)}$$

where [HL] and [L^-] are the concentrations of the protonated and deprotonated forms of the acid, respectively. The relationships among K_H^{m*}, the thermodynamic protonation constant K_H^{t*}, and the concentration protonation constant K_H^{c*} are represented by

$$\log K_H^{t*} = \frac{a_{HL}^*}{a_H^* a_L^*} = \log K_H^{m*} \frac{\gamma_{HL}^*}{\gamma_L^*} = \log K_H^{c*} \frac{\gamma_{HL}^*}{\gamma_H^* \gamma_L^*} \qquad \text{(II.12)}$$

where a_X^* is hydrogen ion activity and γ_X^* is the activity coefficient in 80% methanol-water of the species *X*, respectively. The value of $K_{H\,ref}^{t*}$ for acetic acid was determined in methanol-water mixtures by several investigators. The published values for 80% methanol-water are presented in Table II.I.

In order to obtain $K_{H\ ref}^{m*}$ and $K_{H\,ref}^{c*}$, the mixed-mode and the concentration mode protonation constants, at 0.05 M ionic strength, the reported thermodynamic values were corrected to the mixed-mode protonation constants using the respective activity coefficients. The values of the mean activity coefficient $\gamma_\pm^*$ for various molal concentrations of hydrochloric acid in methanol-water mixtures have been reported by

Table II.I. Literature values of acetic acid protonation constant in 80% methanol-water

Reference	$\log K_H^{m*}$	$\log K_H^{t*}$
Bacarella et al.[a]		6.50 (below 0.01 M)[d]
Shedlovsky and Kay [b]		6.64
Rorabacher et al. [c]	6.34 (0.1M)[a]	6.57

[a] Reference 15. [b] Reference 16. [c] Reference 17. [d] The value in brackets indicates the ionic strength that was used to obtain the protonation constant.

Oiwa[14]. However, that data did not include the activity coefficient for the experimental conditions of the present work (0.05 M ionic strength). The latter was obtained following procedures described by Craig[18]. In this method available activity coefficint data was fit to a quadratic function derived from the Pitzer equation[19] and the calculated parameters were used to determine the value of $\gamma_{\pm}$* at the desired ionic strength.

The Pitzer equation was developed as an extension of the Debye-Huckel model to calculate activity coefficients in electrolytes over the broad concentration ranges. The general form of Pitzer equation for monovalent cation and anion electrolytes, such as H^+ and Cl^-, is presented below[20]

$$\ln \gamma_{\pm} = f_{\gamma} + IB^{\gamma}_{MX} + I^2C^{\gamma}_{MX} \qquad \text{(II.13)}$$

The coefficients in this quadratic equation are called Pitzer parameters are defined more completely as

$$B^{\gamma}_{MX} = 2\beta^{(0)}_{MX} + \frac{2\beta^{(1)}_{MX}}{\alpha^2 I}\left[1-e^{-\alpha\sqrt{I}}\left(1+\alpha\sqrt{I}-\frac{1}{2}\alpha^2 I\right)\right] \qquad \text{(II.14)}$$

$$C^{\gamma}_{MX} = \frac{3}{2} C^{\phi}_{MX} \tag{II.15}$$

$$f_{\gamma} = -A_0 \left[\frac{\sqrt{I}}{(1+b\sqrt{I})} + \frac{2}{b} \ln(1+b\sqrt{I}) \right] \tag{II.16}$$

where A_0 is Debye limiting slope given as

$$A_0 = \frac{1}{3} \sqrt{\frac{2\pi Nd}{1000} \left(\frac{e^2}{DkT} \right)^3} \tag{II.17}$$

$\beta^{(0)}_{MX}$, $\beta^{(1)}_{MX}$ and C^{ϕ}_{MX} are adjustable parameters that account for short-range ionic interactions

I = ionic strength in molal units

N = Avogadro's number

d = density of solvent

e = unit charge (4.80324×10^{-10} ESU)

D = dielectric constant

k = Boltzmann constant (1.38066×10^{-16} J/K)

T = absolute temperature in Kelvin (298 K)

b = constant with a value of 1.2 for all solvents

α = constant with a value of 2 for all solvents

It was necessary to obtain a reasonable value for A_0 in order to calculate parameter f_{γ}. The required system parameters were available in literature for the 80% methanol-water solvent at 25.0 °C: dielectric constant D = 42.6[21]; density d = 0.8425 g/mL[15]; Debye limiting slope parameter A_0 = 0.904[15]. The available activity coefficient data at various ionic strengths[14], along with the calculated value of f_{γ}, were then plotted

in the form the of function ($\ln \gamma_{\pm} - f_{\gamma}$), obtained by rearranging Pitzer equation (eq II.18), versus the ionic strength expressed in molal concentration units

$$\ln \gamma_{\pm} - f_{\gamma} = IB^{\gamma}_{MX} + I^2C^{\gamma}_{MX} \qquad \text{(II.18)}$$

The Pitzer parameters, B^{γ}_{MX} and C^{γ}_{MX}, were obtained using non-linear least-squares program to fit the data to eq II.18. The resulting curve fit is shown in Figure II.4. The calculated Pitzer parameters were subsequently employed to determine the activity coefficient at the desired ionic strength. The activity coefficient for monovalent ions at ionic strength 0.05 M (0.059 molal) was calculated to be 0.650 and $\log \gamma_{\pm} = -0.187$.

For the conversion between molality (moles of solute/kg solvent) and the molarity (moles of solute/liter solution) concentration scales, the following relationships were used

$$M = \frac{md}{1 - (0.001 \times m \times MW)} \qquad \text{(II.19)}$$

$$m = \frac{M}{d + (0.001 \times M \times MW)} \qquad \text{(II.20)}$$

where M and m are the molar and molal concentrations, respectively, and MW is the molecular weight of the added electrolyte (tetraethylammonium perchlorate in the present study). The value of density of 80% methanol, d = 0.8425 g/mL[15], was used in the conversions.

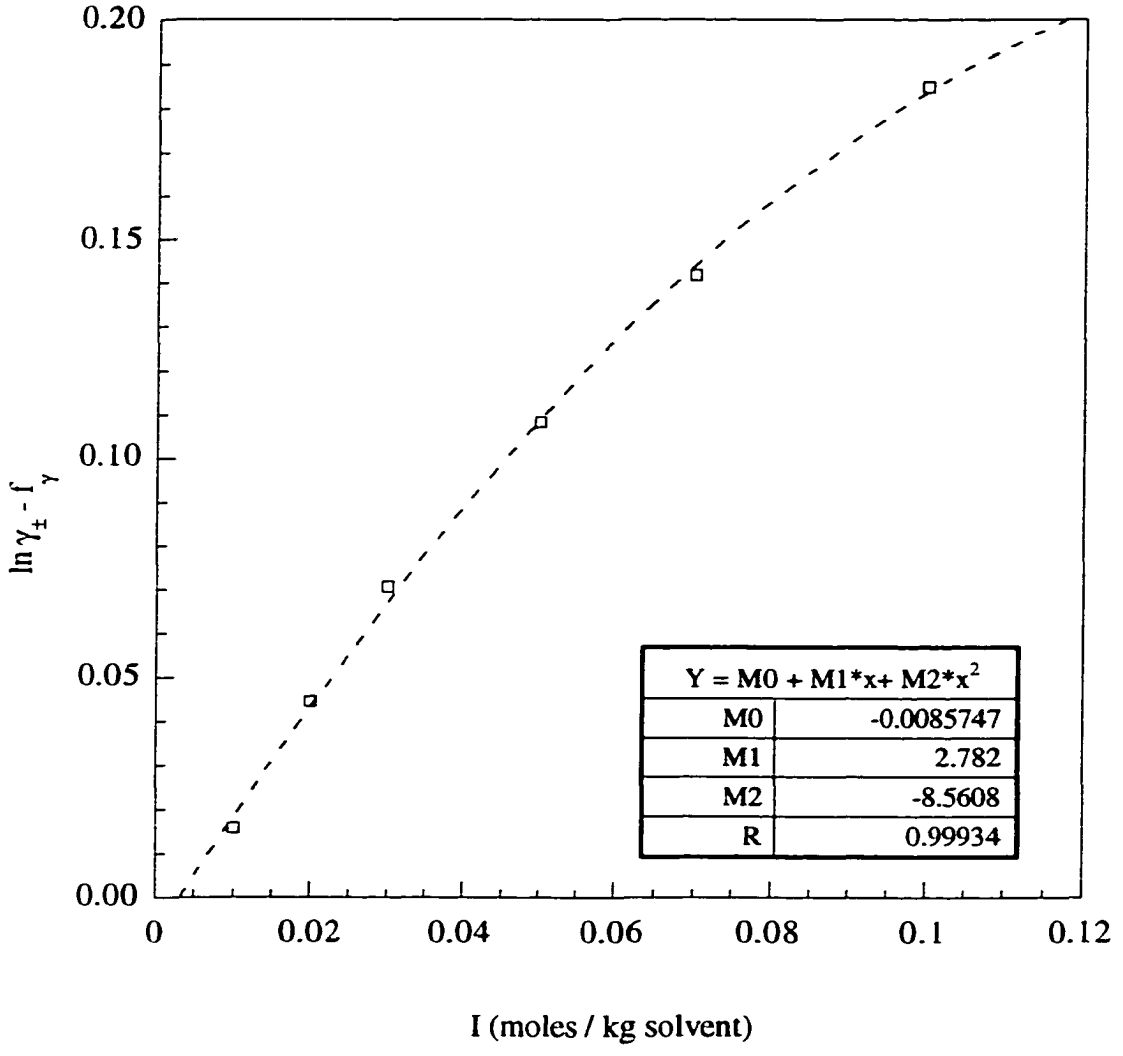

Figure II.4. Plot of experimental activity coefficients (Oiwa, ref. 14) versus molal ionic strength (I) for HCl in 80% methanol-water. The dotted line is the theoretical fit to the modified Pitzer equation (eq II.18).

Rorabacher et al.[17] suggested that the protonation constant of acetic acid obtained by conductance measurements by Shedlovsky and Kay[16] (Table II.1) should be free of errors included into the values obtained by pH* measurements. The average of this thermodynamic value of 6.64 and Rorabacher's value of 6.57 was used to calculate $K_H^{m*}{}_{ref}$, which was found to be 6.44 at 0.05 M ionic strength. The value for $K_H^{m*}{}_{obs}$ was obtained by potentiometric titration of 10-20 mM acetic acid (0.05 M ionic strength in 80% methanol-water) with tetramethylammonium hydroxide base and subsequent analysis of the resulting data using the program PKAS[22]. This procedure was carried out for each electrode one or two times daily before and after the collection of potentiometric titration data.

The PKAS program requires the value for solvent autoprotolysis constant as one of the inputs. The general equation for solvent autoprotolysis may be presented as

$$ROH \rightleftharpoons RO^- + H^+ \qquad \text{(II.21)}$$

The values for the mixed-mode autoprotolysis constant

$$K_S^{m*} = a_H^* [RO^-] \qquad \text{(II.22)}$$

and concentration autoprotolysis constant

$$K_S^{c*} = [H^+] [RO^-] \qquad \text{(II.23)}$$

for 0.05 M ionic strength were calculated using the literature value of thermodynamic autoprotolysis constant (defined in equation II.24) and the calculated value of activity coefficient $\gamma_{\pm}$.

$$K_S^{t*} = a_{H^+}^* a_{OH^-}^* = K_S^{m*} \gamma_{\pm}^* = K_S^{c*} (\gamma_{\pm}^*)^2 \qquad \text{(II.24)}$$

The results are presented in Table II.2. The value of log K_S^{m*} of -14.23 was used as a parameter in the program PKAS to obtain log $K_H^{m*}{}_{obs}$ of acetic acid and the electrode solvent correction factor in 80% methanol-water mixtures.

Table II.2. Calculated and literature values of solvent autoprotolysis constants in 80% methanol-water

	log K_S^{x*} at 0.05 M ionic strength
log K_S^{t*}	- 14.42 [a]
log K_S^{m*}	- 14.23
log K_S^{c*}	- 14.05

[a] Reference 23.

Measurements of pH* in 80% methanol-water medium were made using a Fisher pH meter, model 825MP, or a Corning pH-meter, model 125, and one of the following combination electrodes: Orion Ross Sure Flow semi-micro pH electrode, model 8175BN; Sensorex pHase electrode, model S1021CD; Thomas semimicro electrode, model 4080-B49. The internal filling solution of the electrode was replaced with 0.1M tetraethylammonium perchlorate in 20% methanol or 0.1M tetramethylammonium chloride in 20% methanol-water. The electrode was refilled with fresh filling solution on the day of the measurements.

The method, designed by de Ligny[11-13], for measuring pH* in methanolic solutions was employed, by first calibrating the electrode in aqueous buffers and then equilibrating it in the methanol solution of the desired composition. A three-point calibration of the pH meter-electrode system was performed daily, prior to measurements, using aqueous standard solutions of buffers of pH 4.01, 6.86 and 9.0 or 9.18 (Gram-Pac, Fisher). Buffer solutions for pH 9.18 and 9.00 were stored under argon gas to minimize CO_2 contamination. After calibration, the electrode was equilibrated in 80% methanol-water for at least 2 hours.

To measure pH* values below 4, a different electrode calibration procedure was used. The electrode was equilibrated in 80% methanol-water for 2 hours, then calibrated using a series of standard 0.106 mM to 0.0106 M solutions of $HClO_4$ in 80% methanol-water. The ionic strength of the standard $HClO_4$ solutions was adjusted to 0.05 M with tetraethylammonium perchlorate.

E. Determination of percent CO_2 in the tetramethylammonium hydroxide titrant solutions.

During preparation of 20 mM tetramethylammonium hydroxide titrant solutions care was taken to minimize carbonate contamination. 80% methanol was always prepared from freshly distilled methanol and freshly boiled water. When possible, an atmosphere of argon gas was maintained over the bottled solution to prevent CO_2 penetration. All titrant solutions were analyzed for the presence of carbonate contaminant before they were used for titrations. Gran's method[24] for determination of percent CO_2 was used as recommended by Motekaitis[22]. A solution containing 10 - 20 mM $HClO_4$ in 80% methanol was titrated and the plot of the Gran function, f, versus titrant volume was obtained. The values of f were calculated using the expression

$$f=(V_0+V_b)10^{\pm pH^*} \qquad \text{(II.25)}$$

where V_0 is the initial volume, V_b is the volume of standard base added, pH* is $-\log a_H^*$ in 80% methanol-water, and "+" or "–" are used accordingly for acidic or basic regions of the curve, respectively. The lines for acidic and basic regions were fit separately to a linear equation using the least-squares program in the KaleidaGraph[25] software package and the intersections of these lines with x-axis were found. An example of such a plot is shown in Figure II.5. The percentage CO_2 in the base was calculated according to the following equation

$$\%CO_2 = \frac{(V_- - V_+)}{2V_-}100\% \qquad \text{(II.26)}$$

where V_- is the volume at the intersection of the *x*-axis with the linear segment in the basic region, and V_+ is the volume at the intersection of the *x* -axis with the linear segment in the acidic region. Freshly prepared titrant solutions contained from 0.4 to 1.2% CO_2. Because of the dilute concentrations used in this study, CO_2 content in excess of 2% in the titrant interfered with the titration and the base was not used if the carbonate exceeded this limit[22].

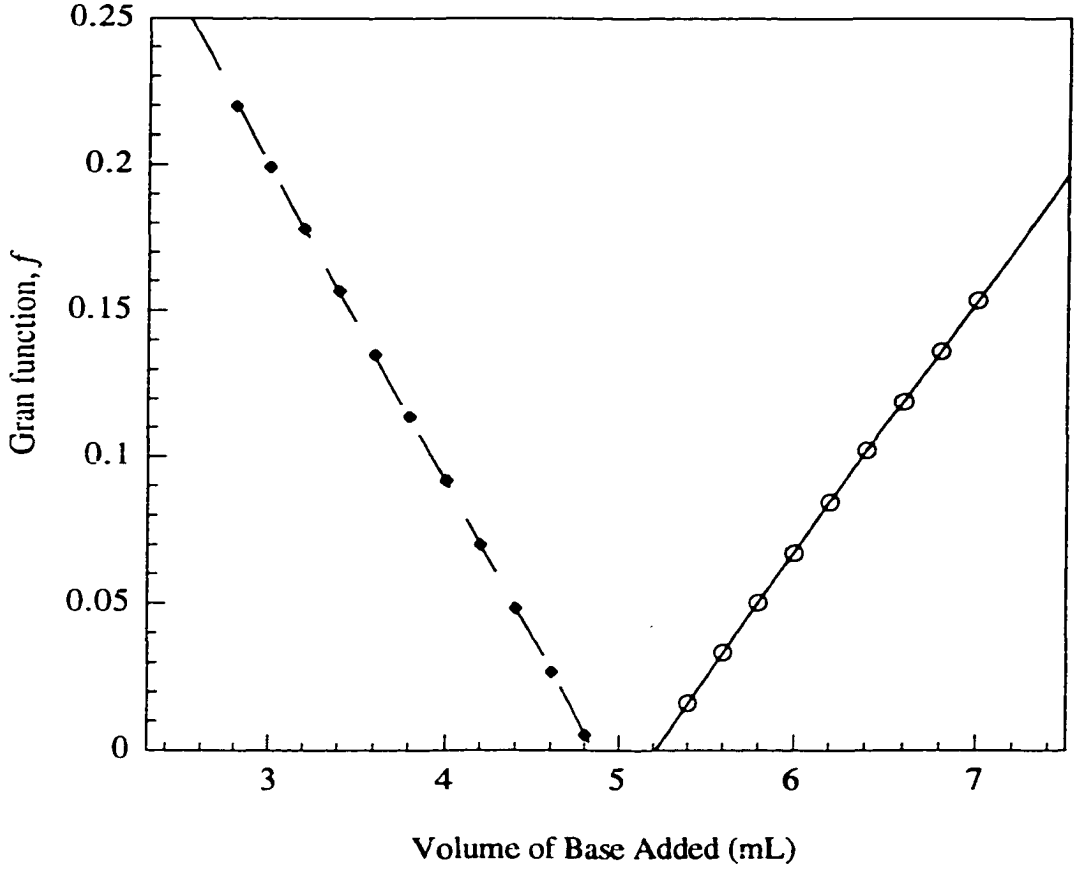

Figure II.5. Gran plot for a titration of perchloric acid with tetramethylammonium hydroxide.

F. Measurement of protonation constants and metal complexation constants of monensin and lasalocid.

Potentiometric titrations.

Potentiometric titrations of the free acid forms of monensin and lasalocid were performed in 80% methanol-water. 80% methanol-water solvent was chosen as a medium for the equilibrium studies because effective solvent polarity of this mixture is thought to resemble the polarity at aqueous-lipid interfaces of cellular membranes or phospholipid vesicles[26]. It has been shown that the equilibrium properties of ionophores in the mixture of this composition mimic those seen at the membrane-interface. For ionophore A23187 the protonation constants and complexation constants of mono- and divalent cations measured in phospholipid vesicle suspensions were in good agreement to those obtained in 80% (w/w) methanol-water[27-30]. Therefore, 80% methanol-water solvent may provide a model for the behavior of the membrane-bound ionophore and the resulting equilibrium constants could be further applied to explain the results of metal-ion transport studies.

pH* titration curves were obtained using 20 mM tetramethylammonium hydroxide as a titrant. Various antibiotic concentrations were employed to evaluate the possibility of dimerization. The upper level of the concentration range was determined by antibiotic solubility. 0.2 mM to 1 mM solutions of monensin A acid and 1 mM – 5 mM solutions of lasalocid A acids were titrated at 25.0 °C and under continuous flow of N_2 to minimize CO_2 contamination. No excess of strong acid was added because it has been reported that monensin can be unstable in a highly acidic medium[31]. Titration data was acquired with the autotitrator system which consisted of a Metrohm model 655 digital buret and a Fisher 825MP pH meter with the electrodes described in section II.D and controlled by a Zenith 158-42 computer[18]. All titrant bases were standardized with KHP and checked for CO_2 contamination as described above. Programs PKAS[22] and BEST[22] were used to calculate the mixed-mode protonation constants from the experimental titration data. The concentration protonation constant was further obtained as follows

$$K_H^{c*} = \frac{[HA]}{[H^+][A^-]} = \frac{\gamma_H^*[HA]}{a_H^*[A^-]} = \gamma_\pm^* K_H^{m*} \qquad \text{(II.27)}$$

$$\log K_H^{c*} = \log K_H^{m*} + \log \gamma_\pm^* \qquad \text{(II.28)}$$

As previously calculated, $\gamma_\pm^*$ has a value of 0.650 in 80% methanol-water at 0.05 M ionic strength. Therefore, the concentration mode and mixed-mode protonation constants are related as follows,

$$\log K_H^{c*} = \log K_H^{m*} - 0.187 \qquad \text{(II.29)}$$

Complexation of lead(II), sodium, calcium(II) and zinc(II) ions with both monensin A and lasalocid A ligands was studied by potentiometric method. A mixture of ligand and the metal of interest in 80% methanol-water was titrated with 20 mM tetramethylammonium hydroxide base. The ionic strength of both the titrant and the titrated solution was kept at 0.05 M using tetramethylammonium perchlorate. Various ligand to metal concentration ratios were employed. No excess of strong acid was added because monensin can be unstable in highly acidic medium[31,32]. Standardized stock solutions of lead perchlorate, sodium chloride, calcium chloride and zinc perchlorate were added to a 10.0 – 20.0 mL aliquot of the ligand at 25.0 °C and under continuos flow of N_2 to minimize CO_2 contamination. Titration data was collected using the autotitrator system described in section II.D.

Potentiometric titration data consisting of $-\log[H^+]$ vs added titrant volume was fit using the program BEST[22] to obtain stability constants of metal-ligand complexes. The pH* data was converted to a molar concentration scale from molar activities by applying a correction of $\log \gamma_\pm$ to the original data set of pH* values.

$$[H^+] = \frac{a_H^*}{\gamma_H^*} \qquad \text{(II.30)}$$

$$p[H] = -\log [H^+] = pH^* + \log \gamma_H^* = pH^* - 0.187 \qquad \text{(II.31)}$$

The program BEST also required the concentration mode protonation constant for the ligand, accurate values of initial sample volume, millimoles of ligand and metal, and molarity of titrant base.

Spectrophotometric studies.

The protonation constant of lasalocid was determined by the spectrophotometric pH titration of the free acid form of lasalocid. A solution of 1 x 10^{-4} M lasalocid in 80% methanol was prepared. Ionic strength was maintained at 0.05 M with TEAP. The solution pH was buffered with 0.001 M DESPEN buffer. Spectra were acquired at constant temperature of 25.0 ^{o}C, which was maintained using an external temperature bath attached to the cuvette holder. The pH* of the solution was adjusted to the required value with a 1.5 M solution of tetraethylammonium hydroxide. After each pH* adjustment, an aliquot of solution was transferred to the cuvette with 1.00 cm pathlength. The cuvette was placed in the thermostated holder and the temperature was allowed to equilibrate for 2-3 minutes. The spectra were recorded with a Hewlett-Packard 8452A diode array spectrophotometer.

The reaction between monensin and lead was studied in 80% methanol. Although monensin is spectroscopically silent, it was observed that formation of the lead-monensin complex resulted in the appearance of an absorbance peak at 240 nm. The titration was accomplished by adding small aliquots (50 μL) of a 1.0 mM solution of tetraethylammonium monensin to 2.50 mL of a solution containing the 5.0 x 10^{-5} M lead perchlorate in 80% methanol. After each addition, the cuvette was inverted several times

to ensure proper mixing. The solution pH* was controlled at 3.11 with 1 mM $HClO_4$ and ionic strength was kept at 0.05 M with TEAP.

The reaction between lasalocid and lead was also studied in 80% methanol. The formation of a lasalocid-lead complex resulted in a small increase of the absorbance at 298 nm and a small decrease at 330 nm. The titration was accomplished by adding small aliquots (5 μL) of a 0.023 M solution of lead perchlorate to 2.50 mL of a solution containing the 0.010 mM lasalocidic acid in 80% methanol. After each addition, the cuvette was inverted several times to ensure proper mixing. The solution pH* was controlled at 3.10 with 1 mM $HClO_4$.

G. Nuclear Magnetic Resonance studies of monensin-lead and lasalocid-lead complexes.

Nuclear Magnetic Resonance (NMR) spectra of various complexes of monensin and lasalocid were recorded using a Varian VXR-500X 500-MHz spectrometer equipped with a 5 mm indirect detection probe, model Nalorac ID500-5, or using a Varian 400-MHz Unity Plus spectrometer equipped with a Varian 5 mm 4-nuclei auto-NMR probe. The goal for doing NMR-experiments was to determine the binding sites for lead and to qualitatively compare the solution structure of the lead-antibiotic complex to that of the sodium or calcium complexes or the free ligand in solution. ^{1}H and ^{13}C NMR spectra of lead complexes having 2:1 ligand-lead stoichiometry were obtained in CD_3OD and 80% CD_3OD/D_2O (w/w) for both lasalocid and monensin at 25.0 °C. The spectra of monensin-lead complexes were acquired in $CDCl_3$ at two temperatures: + 25 °C and – 40 °C. NMR spectra of the monensin sodium and tetramethylammonium salts and monensin free acid were also recorded at the same conditions. In order to make peak assignments, the spectra were compared to the known NMR spectra of the sodium complexes and tetramethylammoium salts. Two-dimensional techniques were employed in order to help

assign chemical shifts in the spectra of lead complexes. Those experiments included COSY[34,33] (^{1}H-^{1}H Correlated Spectroscopy) and homonuclear J-resolved 2-dimensional spectroscopy[35] (J-homo) to find proton-proton connectivity through bonds and the multiplicity of proton signals; APT[36,37] (Attached Proton Test) and DEPT[38] (Distortionless Enhancement by Polarization Transfer) to assign multiplicity to ^{13}C signals; and HETCOR[39,40] (Heteronuclear Correlation spectroscopy) and HMQC[41,42] (Heteronuclear Correlation through Multiple quantum Coherence) to find single-bond carbon-proton connectivities. Standard pulse sequences for all experiments were employed.

Generally, solutions were prepared two, or fewer, days prior to the NMR-measurements. About 10 to 15 mg of sample was dissolved in the solvent of choice to obtain a ^{1}H NMR spectrum, about 20-30 mg of sample was used to provide an adequate signal/noise ratio for a ^{13}C NMR spectrum. When chloroform-d was used as a solvent, it was filtered through dry alumina to eliminate any acid contamination.

References.

1) Gorman, M.; Chamberlin, J. W.; Hamill, R. L. *Antimicrobial Agents and Chemotherapy* **1967**, 363-368.

2) Haney, M. E.; Hoehn, M. M. *Antimicrobial Agents and Chemotherapy* **1967**, 25-29.

3) Walba, D. M.; Hermsmeier, M. *J. Chem. Soc., Chem. Commun.* **1985**, 383-384.

4) Cox, B. D.; van Truong, Ng.; Rzeszotarska, J.; Schneider, H. *J. Am. Chem. Soc.* **1984**, 106, 5965-5969

5) Vaufrey-Mary, F. Doctorate Thesis, Universite Blaise Pascal, Clermont, France, 1990.

6) Tabet, J. C.; Fraisse, D.; David, L. *Int. J. Mass. Spectrom. Ion Processes* **1985**, 63, 29-36.

7) Kiehl, D. E.; Julian, R. K.; Kennington, A. S. *Rapid. Comm. Mass. Spectrom.* **1998**, 12, 903-910.

8) Westley, J. W.; Benz, W.; Donahue, J.; Evans Jr., R. H.; Scott, C. G.; Stempel, A.; Berger, J. *J. Antibiotics* **1974**, 27, 744-753.

9) Westley, J. W.; Blout, J. F.; Evans Jr., R. H.; Stempel, A; Berger, J. *J. Antibiotics* **1974**, 27, 597-604.

10) Vogel, A. I. *Texbook of Quantitative Chemical Analysis*, 5th ed., Longman Group UK Limited: Essex, England, 1989.

11) De Ligny, C. L.; Luykx, P. F. M.; Rehbach, M.; Wieneke A. A. *Recl. Trav. Chim. Pays-Bas* **1960**, 79, 699-712.

12) Gelsema, W. J.; De Ligny, C. L.; Remijne, A. G.; Blijleven, H. A. *Recl. Trav. Chim. Pays-Bas* **1966**, 85, 647-660.

13) Gelsema, W. J.; De Ligny, C. L.; Blijleven, H. A. *Recl. Trav. Chim. Pays-Bas* **1967**, 86, 852-864.

14) Oiwa, I. T. *J. Phys. Chem.* **1956**, 60, 754-759.

15) Bacarella, A. L.; Grunwald, E.; Marshall, H. P.; Purlee, E. L. *J. Org. Chem.* **1955**, 20, 747-762.

16) Shedlovsky, T.; Kay, R. L. *J. Phys. Chem.*, **1956**, 60, 151-155.

17) Rorabacher, D. B.; MacKellar, W. J.; Shu, F. R.; Bonavita, M. *Anal. Chem.* **1971**, 43, 561-573.

18) Craig, M. E. Ph.D. Thesis, The University of Oklahoma, Norman, Oklahoma, 1990.

19) Pitzer, K. S. *J. Phys. Chem.* **1973**, 77, 268-277.

20) Pitzer, K. S.; Mayorga, G. *J. Phys. Chem.* **1973**, 77, 2300-2308.

21) Albright, P. S.; Gosting L. J. *J. Am. Chem. Soc.* **1946**, 68, 1061-1063.

22) Martell, A. E.; Motekaitis, R. J. *Determination and Use of Stability Constants*, 2nd ed., VCH Publishers, Inc.: New York, 1992.

23) Taylor, R. W. Ph.D. Thesis, Wayne State University, Detroit, MI, 1973.

24) Gran, G. *Analyst,* **1952**, 77, 661-671.

25) *KaleidaGraph*, versions 3.0 and 3.5; Synergy Software: Reading, PA, 1986-1997.

26) Fernandes, M. S.; Fromherz, P. *J. Phys. Chem.* **1977**, 81, 1755-1761.

27) Kauffman, R. F.; Taylor, R. W.; Pfeiffer, D. R. *Biochemistry* **1982**, 21, 2426-2435.

28) Taylor, R. W.; Chapman, C. J.; Pfeiffer, D. R. *Biochemistry* **1985**, 24, 4852-4859.

29) Chapman, C. J.; Puri, A. K.; Taylor, R. W.; Pfeiffer, D. R. *Biochemistry* **1987**, 26, 5009-5018.

30) Taylor, R W.; Pfeiffer, D. R.; Chapman, C. J.; Craig, M. E.; Thomas, T. P. *Pure and Appl. Chem.* **1993**, 65, 579-584.

31) Anteunis, M. J. O. In *Polyether antibiotics: Naturally Occurring Ionophores, Vol. 2. Chemistry* , Westley, J. W., Ed.; Marcel Dekker, Inc.: New York, 1983; pp 245-344.

32) Rodios, N. A.; Anteunis, M. J. O. *Bull. Soc. Chim. Belg.* **1980**, 89, 537-550.

33) Bachman, P.; Aue, W. P.; Muller, L.; Ernst, R. R. *J. Magn. Reson.* **1977**, 28, 29-39.

34) Bodenhausen, G.; Freeman, R.; Neidermayer, R.; Turner, D. *J. Magn. Reson.* **1977**, 26, 133-164.

35) Nagayama, K.; Bachmann, P.; Wuthrich, K.; Ernst, R. R. *J. Magn. Reson.* **1978**, 31, 133-148.

36) Rabenstein, D. L.; Nakashima, T. T. *Anal. Chem.* **1979**, 51, 1465A-1474A.

37) Pei, F.-K.; Freeman, R. *J. Magn. Reson.* **1982**, 48, 318-322; Patt, S. L. *J. Magn. Reson.* **1982**, 46, 535-539.

38) Doddrell, D. M.; Pegg, D. T.; Bendall, M. R. *J. Magn. Reson.* **1982**, 48, 323-327.

39) Bax, A.; Morris, G. A. *J. Magn. Reson.* **1981**, 42, 501-505.

40) Bax, A. *J. Magn. Reson.* **1983**, 53, 517-520.

41) Rutar, V. *J. Magn. Reson.* **1984**, 58, 306-310.

42) Bax, A. D.; Griffey, R. H.; Hawkins, B. L. *J. Am. Chem. Soc.* **1983**, 105, 7188-7190; Bax, A.; Subramanian, S. *J. Magn. Reson.* **1986**, 67, 565-569.

CHAPTER III

RESULTS

STUDIES OF MONENSIN–METAL COMPLEXES.

III.A Preparation and characterization of monensin-lead(II) complexes

Complexes having 2:1 monensin-lead stoichiometry were obtained by three different methods. The first method employed the reaction between stoichiometric quantities of the free acid form of monensin and solid lead oxide in methanol. The second method involved back extraction of tetramethylammonium monensin in chloroform with excess of lead nitrate in aqueous solution. In the third method, the reaction of silver monensin with lead chloride in the molar ratio of 2:1 monensin-lead was carried out in methanol. Ternary complexes having 1:1:1 monensin-lead-chloride stoichiometry were prepared by reacting the silver antibiotic salt with lead chloride in a 1:1 stoichiometric ratio. Preparation and isolation of lead-monensin compounds were described in detail in sections II.B and II.C.

Elemental analysis of monensin-lead complexes.

Samples of the isolated monensin-lead complexes were analyzed commercially to determined the percentages of carbon and hydrogen, and for the mixed complexes, chloride. The results of these analyses are presented in Table III.1.

The lead content of monensin-lead complexes was analyzed by flame atomic absorption spectroscopy using a Varian spectrophotometer, model SpectrAA-20. An air-acetylene flame was used with the absorption wavelength set at 283.3 nm. Calibration was carried out with 4 solutions of lead perchlorate in 80% methanol, covering the lead concentration range from 1.5×10^{-5} M to 6.1×10^{-4} M. Samples for atomic absorption were prepared by dissolving 0.015-0.020 g of product in 50.00 mL of 80% MeOH.

After the lead concentration (C) was obtained, %Pb (w/w) was calculated as illustrated in Equation III.1

$$\%Pb = \frac{C \text{ moles/L} \times 0.05 \text{ L} \times 207.19 \text{g/mole}}{\text{g sample}} \times 100\% \qquad \text{(III.1)}$$

As shown in Table III.1, the experimental values of %Pb for binary monensin-lead complexes were in the range between 11.2 and 13.5%, whereas the corresponding value for the mixed monensin-lead-chloride complex was close to 20%. The theoretical values for weight percentages of carbon, hydrogen, lead, and chloride were calculated on the basis of the predicted compound stoichiometries, with and without additional water of crystallization. Comparison between experimental and calculated values for %Pb clearly indicated that the composition and stoichiometry of the samples obtained are close to the ones predicted.

The best correspondence between the calculated and experimental percentages of lead, carbon and hydrogen was observed for those lead-monensin samples that were obtained using the back-extraction method. The composition of the compounds was close to that expected for the complex of 2:1 monensin-lead stoichiometry with 2 additional waters of hydration. The carbon, hydrogen and oxygen contents in the binary lead-monensin complex made by the reaction between lead chloride and silver monensin (in 1:2 ratio) were close to the calculated values if one water of hydration was included. However, the lead content was low in comparison with the calculated one. Unlike that, the good correspondence between the experimental and the calculated values of %Pb was observed in the lead-monensin sample obtained by reacting lead oxide with the free acid form of monensin. However, in the latter case, even allowing for the presence of water, the discrepancies existed between the experimental and calculated carbon, hydrogen and

Table III.1. Experimental and calculated elemental composition of lead-monensin complexes[a].

Compound/ method	%Pb[b]	%Cl[c]	%C[c]	%H	%O[d]
Experimentally obtained					
$PbMon_2$ by reaction of PbO with Hmonensin	13.2		50.12	7.02	29.66
$PbMon_2$ by back extraction	13.0		54.56	7.84	24.60
$PbMon_2$ by reaction of AgMon with $PbCl_2$	11.2		55.65	7.83	25.32
PbMonCl by reaction of AgMon with $PbCl_2$	20.7	5.97	46.13	6.57	20.63
Calculated from the predicted molecular stoichiometries					
1 Pb: 2 Mon ($C_{72}H_{122}O_{22}Pb$)	13.39		55.90	7.95	22.76
1 Pb : 2 Mon : 1 H_2O ($C_{72}H_{122}O_{22}Pb \cdot H_2O$)	13.24		55.26	7.99	23.52
1 Pb : 2 Mon : 2 H_2O ($C_{72}H_{122}O_{22}Pb \cdot 2H_2O$)	13.09		54.63	8.02	24.26
1 Pb : 1 Mon : 1 Cl ($C_{36}H_{61}O_{11}PbCl$)	22.71	3.88	47.38	6.74	19.29
1 Pb : 1 Mon : 1 Cl : 1 H_2O ($C_{36}H_{61}O_{11}PbCl \cdot H_2O$)	22.27	3.81	46.47	6.82	20.63
1 Pb : 1 Mon : 1 OH ($C_{36}H_{62}O_{12}Pb$)	23.17		48.36	6.99	21.48
1 Pb : 1 Mon : 1 OH : 1 H_2O ($C_{36}H_{62}O_{12}Pb \cdot H_2O$)	22.72		47.41	7.07	22.80

[a] All values are presented as %element (w/w). [b] The lead content was determined using flame atomic absorption spectroscopy. %Pb was calculated from eq III.1. [c] The values were obtained using analysis performed commercially. [d] %O was calculated by subtracting the sum of percentages of other elements from 100%.

oxygen contents. Because the compounds were isolated in powder form and attempts at crystallization failed, a non-stoichiometric amount of uncomplexed monensin could be present in the final product. The product could also consist of a mixture of compounds having 1:1 and 2:1 monensin-lead stoichiometries such as PbMonOH or PbMonOMe and $PbMon_2$, and monensin free acid, HMon. The exact composition of the mixture was not determined in this work.

The elemental composition for mixed lead-monensin-chloride complexes exhibited even stronger deviation from the calculated values. The high value for chloride observed may result from the presence of extra chloride from the starting material. The low value for lead may be due to the presence of the free acid form of monensin or complexes having 2:1 monensin-lead stoichiometry in the mixture with the ternary compound. These conclusions were made on the basis of two additional experimental results obtained. First, no peaks corresponding to the silver-monensin complex were observed in the positive ion FAB mass-spectra of the resulting compound. Therefore, monensin ligand was not bound to silver in the resulting product. Second, the experimental yields of both products, the ternary complex and the silver chloride precipitate, were calculated. The silver chloride yields in the two recorded cases exceeded 100% (130 and 110%), whereas the yields for the ternary complex of monensin were less than 80%. This indicated that the silver chloride precipitate contained other reaction material, possibly lead, which could explain its insufficient amount in the main product containing the ionophore complex.

Characterization of monensin–lead complexes by mass-spectrometry.

Mass-spectrometry was one of the tools used to help determine the structure of monensin compounds after their discovery. Chamberlin and Agtarap[1] reported the electron ionization (EI) mass-spectra of monensin A free acid and alkali-metal salts and proposed the fragmentation scheme. With the advent of "softer" ionization techniques and because of the importance of monensin applications to science and agriculture, a number of studies on monensin sodium salt were done using chemical ionization, fast atom bombardment (FAB-MS)[2,3,4] and electrospray ionization mass spectrometry (ESI-MS)[5,6]. In most cases, the molecular ion peak corresponding to the sodium-monensin complex $(Mon+H+Na)^+$ at 693 m/z dominated the spectra, suggesting the high affinity of monensin A for sodium. Here and below in this section, "Mon" refers to the mono-anionic form of monensin, $C_{36}H_{61}O_{11}^-$.

In the present work both FAB and ESI mass-spectra were obtained for isolated 2:1 monensin-lead and 1:1:1 monensin-lead-chloride complexes. Peaks from the molecular ions, corresponding to complexes having both 1:1 and 2:1 monensin-lead stoichiometries, were present in the positive ion ESI mass-spectra of all compounds including ternary complexes. Protons on monensin ligand exhibited a high degree of lability, as they were easily lost or accepted during ionization, which allowed the complex molecular ions with positive unity charge and the specific stoichiometry to be formed. The origin of those the labile protons is unclear. However, it it possible that they can come from the hydroxy groups in the molecule.

Figure III.1 illustrates peaks of interest in the ESI mass spectrum of the compound having 2:1 monensin-lead stoichiometry, obtained by the reaction between lead oxide and monensic acid. Similar spectra were obtained for all other monensin complexes. In positive ion FAB-MS and ESI-MS the presence of a peak at 877 m/z indicated the formation of a strong lead-monensin complex $(Mon+Pb)^+$. Comparison of

the experimental peak intensities in this cluster to the calculated isotopic pattern, shown as the inset in Figure III.2, confirmed the assignment. No peaks for the species of 2:1 monensin-lead stoichiometry were present in the positive ion FAB-MS spectra, whereas in the positive ion ESI-MS the peak cluster centered at 1548 m/z indicated the presence of the 2:1 species $(2Mon+H+Pb)^+$ (Figure III.3). Another peak corresponding to a molecular ion having 2:2 monensin-lead stoichiometry, was present in the positive ion ESI mass spectra as a cluster centered at 1754 m/z $(2Mon+2Pb-H)^+$, as shown in Figure III.4.

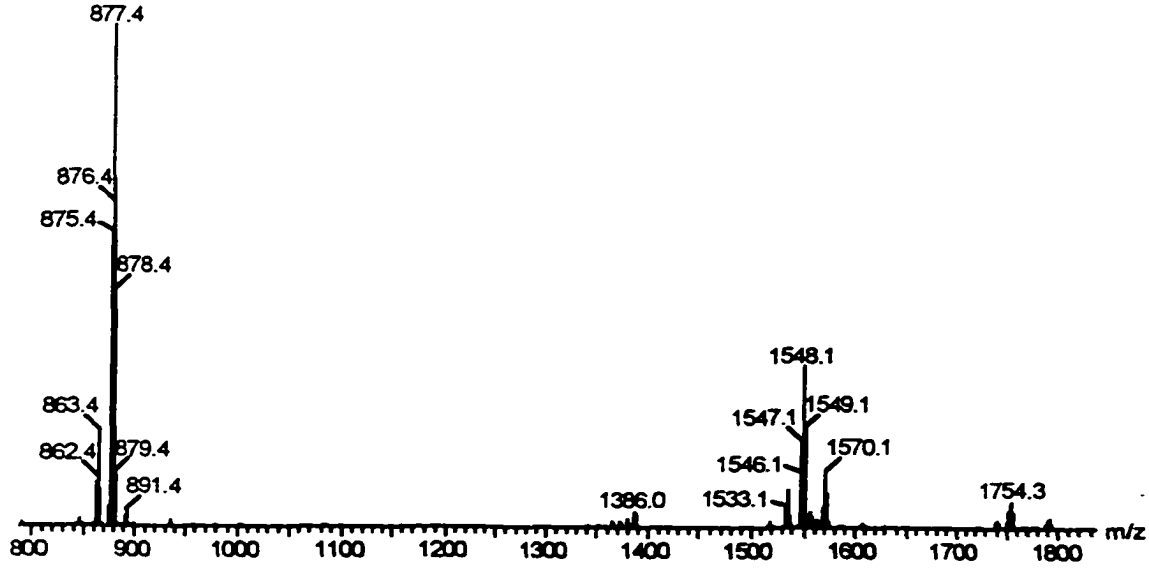

Figure III.1. Part of the positive ion ESI-MS for monensin-lead complex. Peak clusters for molecular ions having 1:1 (877 m/z) and 2:1 (1547 m/z) monensin-lead stoichiometries are observed. The sample was prepared by dissolving the solid 2:1 monensin-lead complex in methanol.

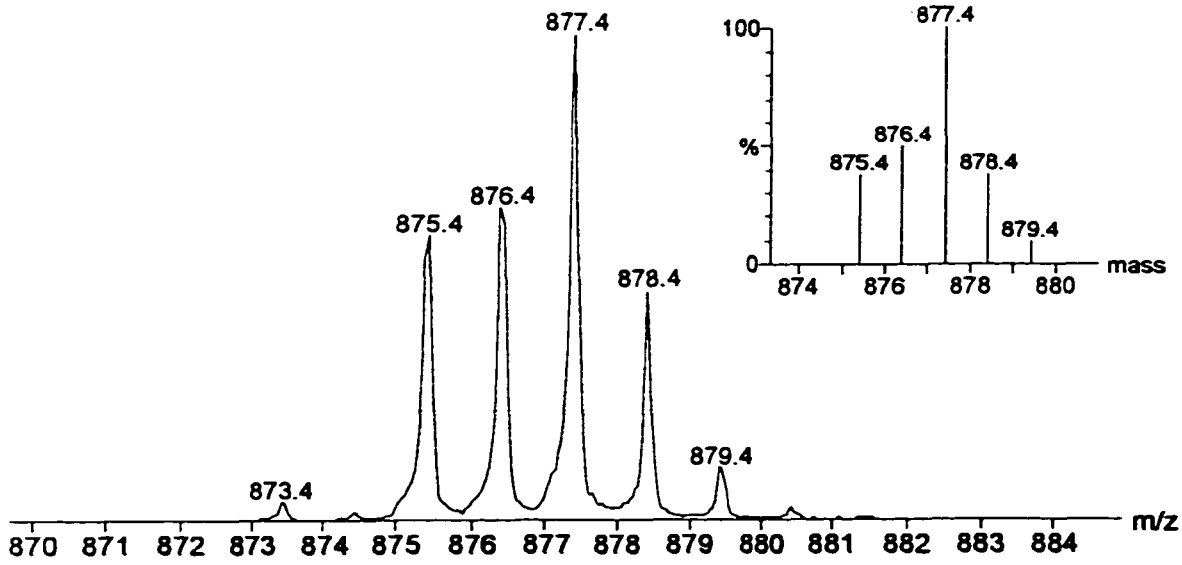

Figure III.2. Peaks for the 1:1 monensin-lead molecular ion in positive ion ESI-MS. The sample was prepared by dissolving the solid 2:1 monensin-lead complex in methanol. The inset shows the calculated isotopic pattern for $C_{36}H_{61}O_{11}Pb$.

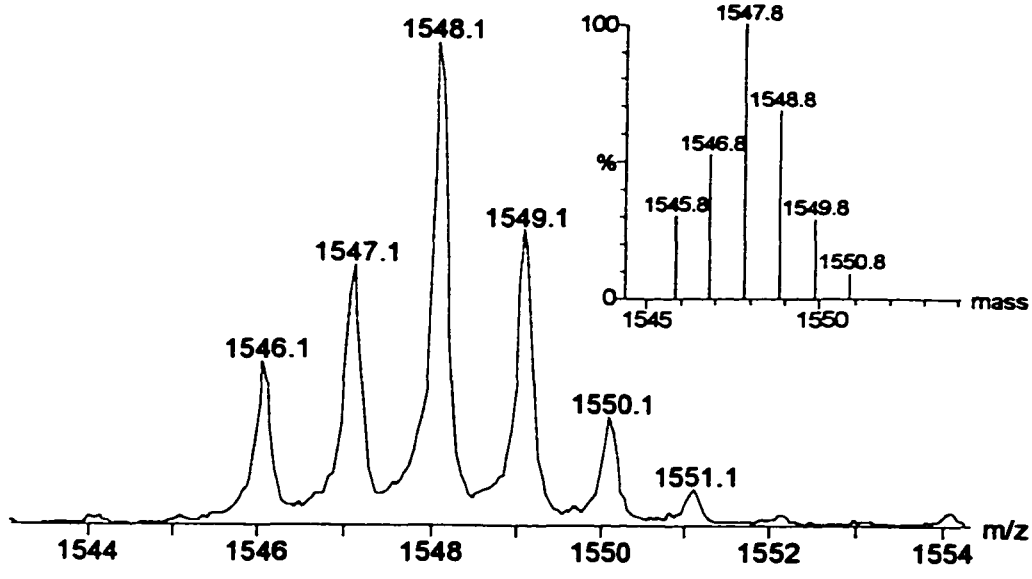

Figure III.3. Peaks for the 2:1 monensin-lead molecular ion in positive ion ESI-MS. The sample was prepared by dissolving the solid 2:1 monensin-lead complex in methanol. The inset shows the calculated isotopic pattern for $C_{72}H_{123}O_{22}Pb$.

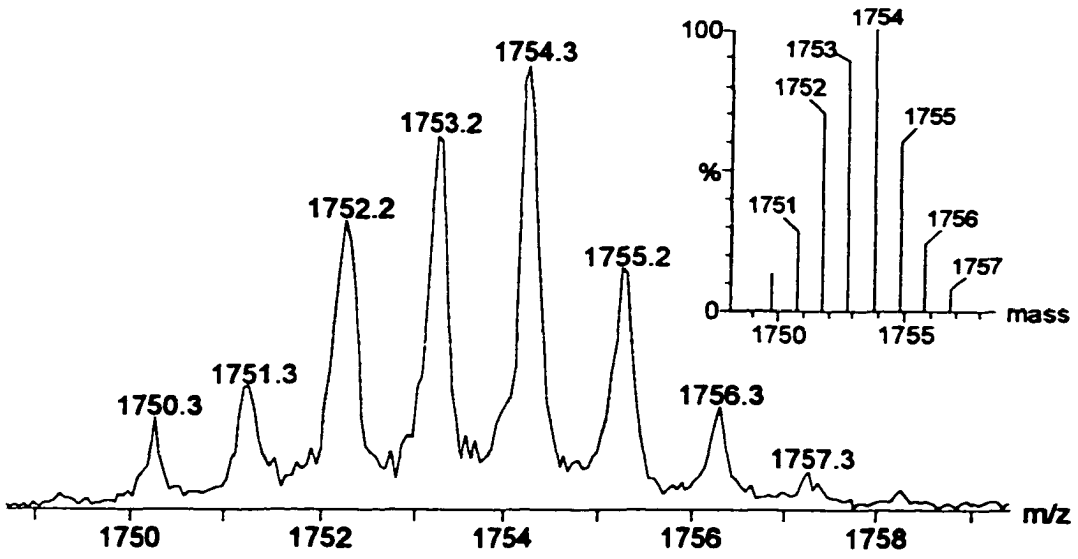

Figure III.4. Peaks for the 2:2 monensin-lead molecular ion in positive ion ESI-MS. The sample was prepared by dissolving the solid 2:1 monensin-lead complex in methanol. The inset shows the calculated isotopic pattern for $C_{72}H_{121}O_{22}Pb_2$.

In the negative ion FAB-MS and ESI-MS peaks corresponding to the mixed lead-monensin–chloride complex were observed at m/z 911 when the samples were prepared by dissolving the isolated complex in either methanol or chloroform. The peak cluster observed is presented in Figure III.5. In chloroform, a set of low intensity peaks, centered at 913 m/z, was present in the positive ion ESI-MS and corresponded to the mixed complex. To simulate biological conditions in the samples (about 0.3 mM total complex concentration), extra chloride, added as $(CH_3)_4NCl$ to the methanol solution, was used to give a total chloride concentration of 0.3 mM. The resulting spectra showed that the intensity of 1:1 lead-monensin peak in the negative ion ESI-MS at 877 m/z significantly decreased and that the peaks for the mixed complex, centered at 911 m/z, became more prominent.

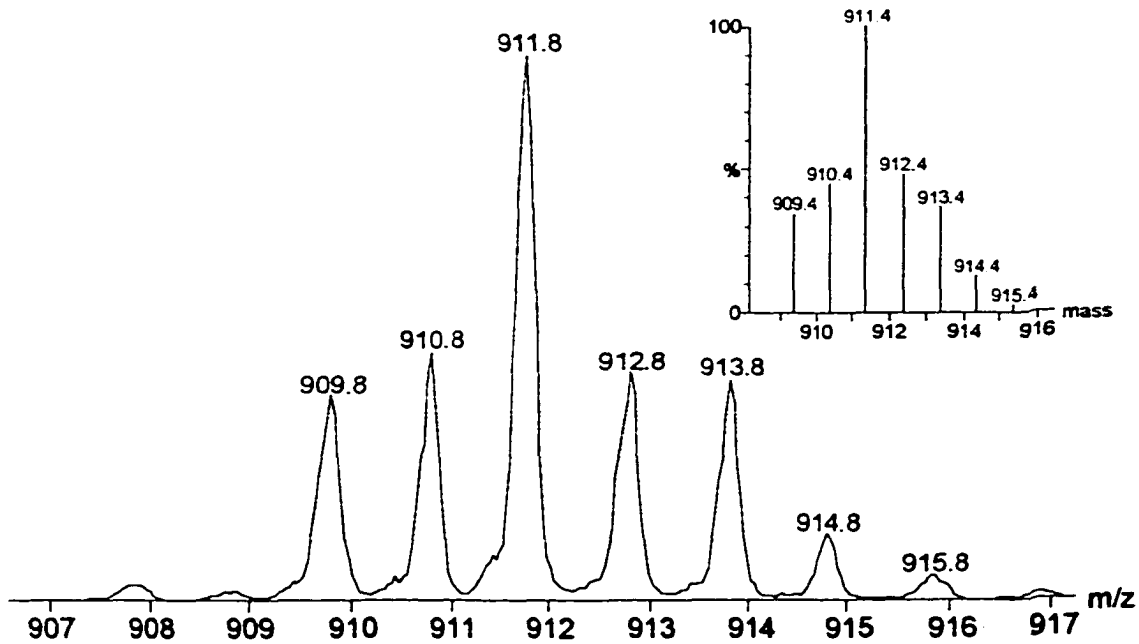

Figure III.5. Peaks for the 1:1:1 monensin-lead-chloride molecular ion in negative ion ESI-MS. The sample was prepared by dissolving the complex in chloroform. The inset shows the calculated isotopic pattern for the $C_{36}H_{60}O_{11}PbCl$.

When samples of the ternary complex were prepared in chloroform without addition of extra chloride, the peak at 911 m/z also was larger in comparison with that in the spectra of the samples dissolved in methanol. The increased intensity of the peak for the mixed complex both in chloroform and in the presence of extra chloride suggests that the formation of this species is more favorable under those conditions.

Ternary mixed complexes having 1:1:1 lead-monensin-nitrate and lead-monensin-acetate stoichiometries were prepared in solution by dissolving the lead-monensin complex in methanol (to yield about 0.3 mM solution) and adding the desired counter ion as the tetraethylammonium salt (0.4–0.9 mM). With negative ion ESI-MS, peaks resulting from the mixed complexes were observed and their assignment was confirmed

by comparison to the calculated isotopic patterns. The value of m/z for the peak with the largest intensity in the molecular ion cluster observed, experimental conditions, and assigned molecular ion compositions are listed in Table III.2 for all experiments.

Table III.2. Peaks for lead-monensin complexes as obtained from the mass-spectra.

m/z[a]	ion composition and charge	stoichiometry	MS method
877.4	$C_{36}H_{61}O_{11}Pb^+$	1Mon:1Pb	+ ESI, +FAB
875.4	$C_{36}H_{59}O_{11}Pb^-$	1Mon:1Pb	- ESI
1548.1	$C_{72}H_{123}O_{22}Pb^+$	2Mon:1Pb	+ESI
1754.2	$C_{72}H_{121}O_{22}Pb_2^+$	2Mon:2Pb	+ESI
911.7	$C_{36}H_{60}O_{11}PbCl^-$	1Mon:1Pb:1Cl	-ESI, -FAB
913.4	$C_{36}H_{62}O_{11}PbCl^+$	1Mon:1Pb:1Cl	+ ESI
938.8	$C_{36}H_{60}O_{11}PbNO_3^-$	1Mon:1Pb:1NO_3	-ESI
935.8	$C_{36}H_{60}O_{11}PbCH_3CO_2^-$	Mon:1Pb:1CH_3CO_2	-ESI

[a] Position of the largest intensity peak in the molecular ion cluster.

III.B. Potentiometric determination of monensin protonation constant in 80% methanol-water.

Monensin A does not possess chromophore groups in its structure and does not have a significant absorbance band in the UV-Vis region of the spectrum. Therefore, the value for the protonation constant of monensin was obtained by potentiometric titration. Figure III.6 shows the titration curve for monensin A in the 80% methanol-water in the pH* range 4–11. In hydroxylic solvents the only possible protonation site on monensin A is the carboxyl group and the data is consistent with the ionization of a single proton.

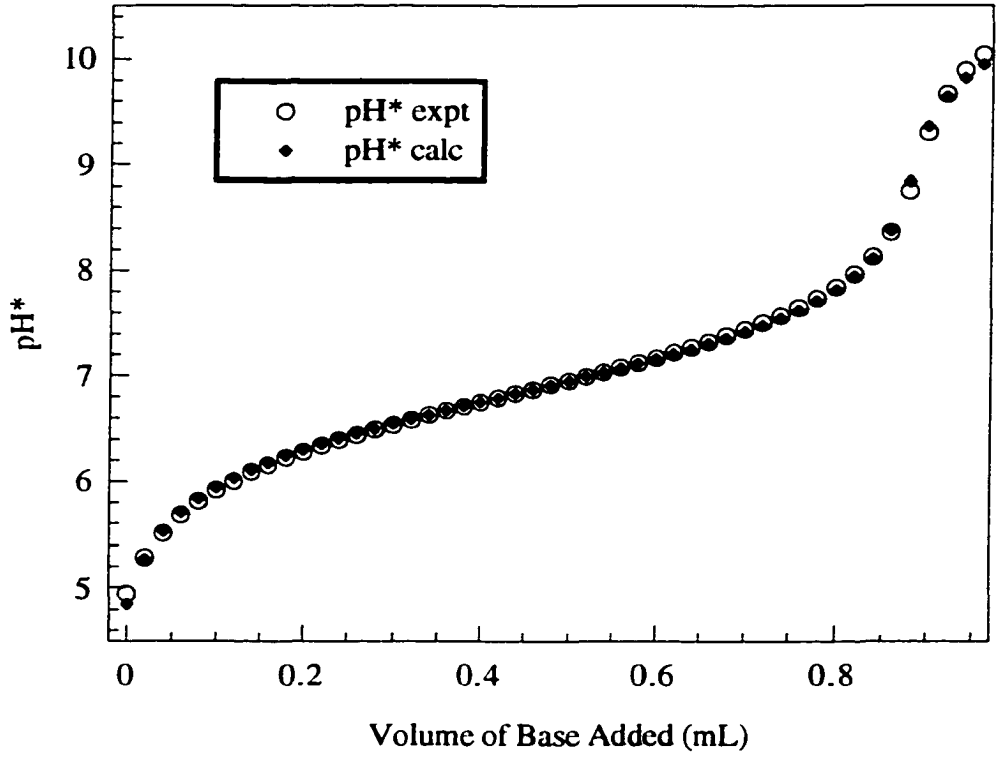

Figure III.6. Experimental titration curve obtained from the titration of 20.0 mL of 0.96 mM monensic acid solution with 0.0194 M Me_4NOH in 80% methanol-water at 25.0 °C and 0.05 M ionic strength (TEAP). The experimental curve is overlaid with the theoretical curve calculated with the program BEST using the known values of ligand and base concentrations and the calculated value of protonation constant.

The potentiometric titration data was first analyzed using the program PKAS[7]. PKAS computes the unknown values of protonation constants using the following algorithm. The p[H] (as defined in eq III.2) at each titration point is calculated using mass balance equations for total ligand and total hydrogen ion concentrations.

$$p[H] = -\log[H^+] \qquad \text{(III.2)}$$

where $[H^+]$ is the molar concentration of hydrogen ion in 80% methanol-water.
These total concentrations are determined using known values of the initial millimoles of the weak acid, millimoles of the strong acid (if added), the initial volume of the sample, and the formality of the titrant base. The value of the solvent autoprotolysis constant and the number of dissociable protons in the neutral ligand are also required input parameters for the program.

An initial estimate of the protonation constant is selected by the program PKAS from the region of the p[H] profile in which the protonation equilibrium in question is predominant. This value is then refined by minimizing the weighted sum of squares of the difference (U) between the computed and the experimental p[H] values, defined in eqs III.3 and III.4

$$U = \Sigma\, w_i\, (p[H]_{exp,i} - p[H]_{calc,i})^2 \qquad \text{(III.3)}$$

The parameter w_i is a weighing factor used to decrease the influence of p[H] values in the steepest regions of the curve and is defined as

$$w_i = \frac{1}{(p[H]_{i+1} - p[H]_{i-1})^2} \qquad \text{(III.4)}$$

The values for stability constants are adjusted until the resulting values of U between two consecutive cycles are different by less than 5×10^{-7} and no further minimization of U can be obtained. The standard deviation in terms of p[H] units is calculated from

$$\sigma_{fit} = \left(\frac{U}{N}\right)^{1/2} \qquad \text{(III.5)}$$

where

$$N = \Sigma\, w_i \qquad \text{(III.6)}$$

The program BEST[7] was subsequently used to recalculate and refine the value of the protonation constant obtained with PKAS. The disadvantage of using PKAS for fitting the acid titration data is that the points around the equivalence point are not included in the fit in order to decrease the influence of the less accurate values in that region. The use of BEST allowed the goodness of fit for the whole curve to be evaluated as well as a more accurate determination of the ligand concentration from the fitted titration end-point.

The program BEST employs a procedure similar to that used in PKAS, but utilizes a more general algorithm that can be used to calculate both protonation and metal complex formation constants. Along with the pH titration input data described for PKAS, the program BEST requires a user-defined model that contains the equilibria that contribute to the pH behaviour. In the case of a single protonation step, the model consists only of equilibrium defined in eq III.7

$$H^+ + L^- \rightleftharpoons HL \qquad \beta^c_{HL} = K^c_H = \frac{[HL]}{[H^+][L^-]} \qquad \text{(III.7)}$$

Equilibrium constants for all reactions included in the model used by BEST were expressed in terms of overall complexation constants (log β values). The reaction was written as the combination of a proton with a basic donor ligand. The input for the program also included an initial estimate for the value of the protonation constant and the concentrations of free monensic acid and titrant base.

Because the experimental pH titration data was obtained in the form of pH* observed vs volume of titrant added, the activity scale of the titration curve was not changed for the purpose of calculating the protonation constant. In this case, $[H^+]$ in eqs III.3, III.4 and III.7 can be substituted by a^*_H which does not affect the general meaning

of these expressions. The mixed-mode value of the protonation constant was thus obtained using programs PKAS and BEST and converted to a concentration constant using the procedure described in section II.F.

The titrations were performed for three different monensin concentrations, 0.2 mM, 0.5 mM and 1.0 mM, to investigate the possibility of monensin dimerization. Titration at each concentration was performed in triplicate. Only those protonation constants where the parameter sigma (eq III.5) is less than 0.1 are included in Table III.3. pH-titrations of monensin at these concentrations in 80% methanol-water gave similar values for the protonation constant, as can be see from the table. This indicates that dimerization of monensin is negligible in the concentration range studied. This conclusion is supported by the results of the studies of the IR-stretch of the monensin carboxyl group in chloroform that also showed no evidence of dimerization in the concentration range from 0.65 mM to 0.065 M[8].

For all concentrations, the average value of log K_H^{m*} is 7.01 ± 0.05 and log K_H^{c*} was calculated as described in section II.F to be 6.83. The latter value was used subsequently in calculations of metal complexation constants.

Table III.3 Calculated values of the mixed-mode protonation constant for monensin in 80% methanol[a]

Monensic acid concentration	log K_H^{m*} [b]	σ_{fit} [c]
0.2 mM	7.01	0.053 (53)
0.5 mM	7.05	0.039 (49)
	7.02	0.037 (29)
	7.02	0.010 (50)
	6.90	0.028 (46)
1.0 mM	7.04	0.044 (47)
	7.01	0.047 (55)
	7.09	0.062 (54)
	6.95	0.023 (55)
	7.00	0.066 (55)
	7.05	0.037 (53)

[a] 25.0 °C, ionic strength = 0.05 M (TEAP). [b] The values of the protonation constants were calculated using the program BEST. [c] $\sigma_{fit} = (U/N)^{1/2}$, as defined in eqs III.5 and III.6. The value in parenthesis indicates the number of points in each titration curve that were used in the curve-fitting procedure.

III.C. Spectrophotometric studies of monensin-lead(II) binding.

To study lead complexation, a solution containing lead perchlorate in 80% methanol was titrated with a solution of tetramethylammonium monensin. To define the stoichiometry of the complex formed from the UV-Vis absorbance change, the pH* of the solution should be significantly higher than the log value of the protonation constant (log K_H^{m*}) to avoid the protonation side-reaction of ligand and to obtain a linear dependence of absorbance on ligand concentration. This condition will be satisfied if at least 99% of the ligand present is deprotonated. In case of monensin, the following relationship holds

$$K_H^{m*} = 10^{-7.01} = \frac{[HMon]}{a_H^*[Mon^-]} = \frac{1}{a_H^* 99} \qquad \text{(III.8)}$$

The calculated value of pH* needed to fulfill this condition was found to be 9.02. Unfortunately, it was not experimentally feasible to carry out titrations at this pH*. Lead precipitation from the solution in the form of lead hydroxide was noticed at pH* 6.5 and interfered with the complexation reaction. Nevertheless, the UV-Vis spectra associated with lead-monensin complexation were obtained at pH* 6.2 by titrating a solution containing 0.065 mM lead with a 1.00 mM solution of monensin tetramethylammonium salt. The pH* of the solution was controlled with 3 mM MES and 5 mM MOPS buffers. The spectra obtained are shown in Figure III.7. Upon addition of monensin, an increase in absorbance occurred with maximum change centered at 240 nm. In Figure III.8 the absorbance values at this wavelength are plotted against the ratio of total lead to total monensin concentrations. Due to the occurrence of the ligand protonation side reaction, the plot exhibits significant curvature in the equivalence point region of lead-monensin complex formation. However, the overall behavior is consistent with 1:1 stoichiometry for the lead-ligand complex. Upon addition of excess monensin the absorbance levels off indicating either that the formation of 1:1 complex was complete or

that formation of higher complexes (e.g., 2:1 monensin-lead) caused no detectable change in the UV-Vis spectra.

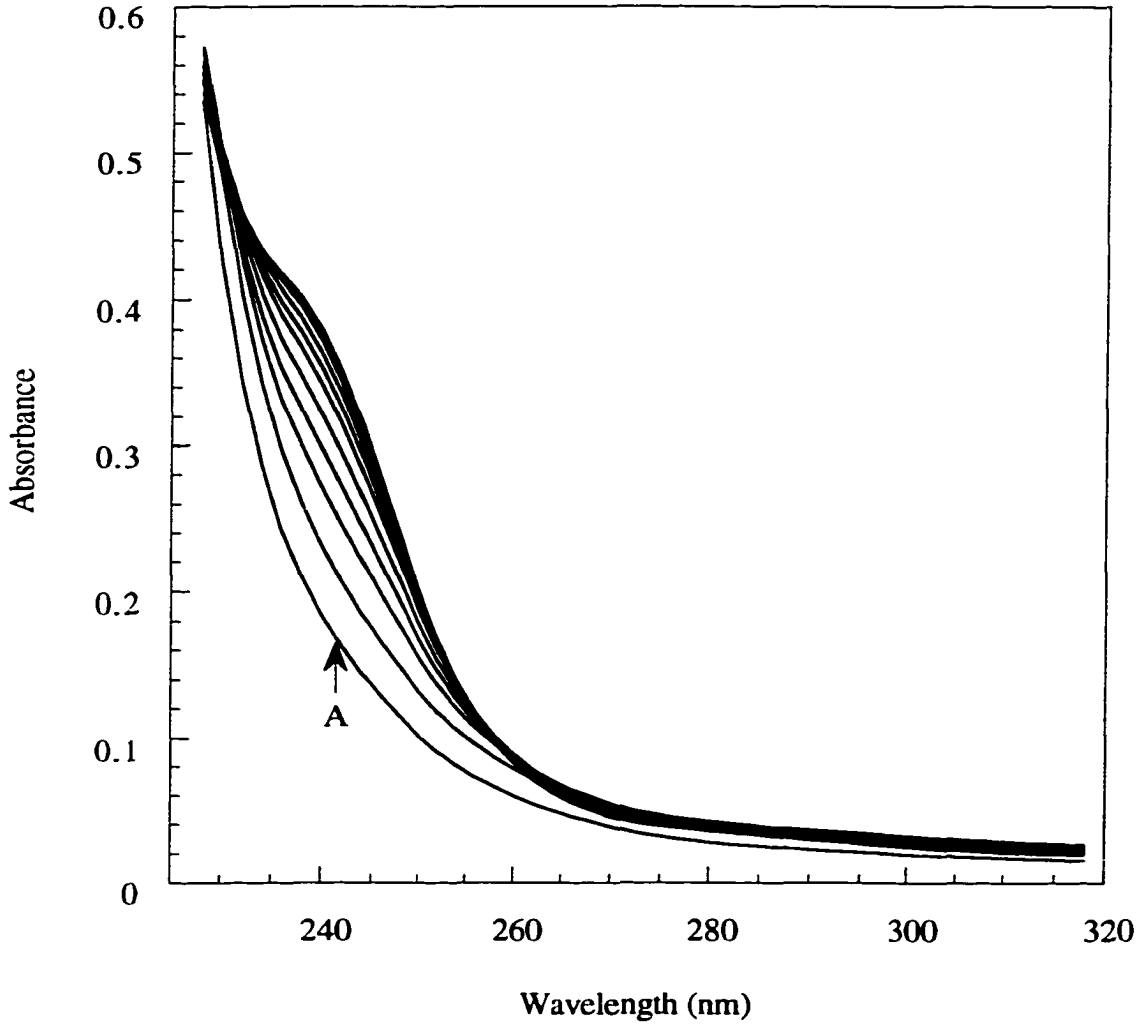

Figure III.7. UV-Vis spectra from the titration of lead perchlorate with monensin A in 80% methanol-water at 25.0 °C. 20.0 μL aliquots of 1.05 mM tetraethylammonium monensin were used to titrate 2.50 mL of a solution containing 0.065 mM lead perchlorate, buffered at pH* 6.2 with 5 mM MES and 5 mM MOPS buffers, at an ionic strength of 0.05 M (TEAP). Curve A – $Pb(ClO_4)_2$ alone, no monensin added.

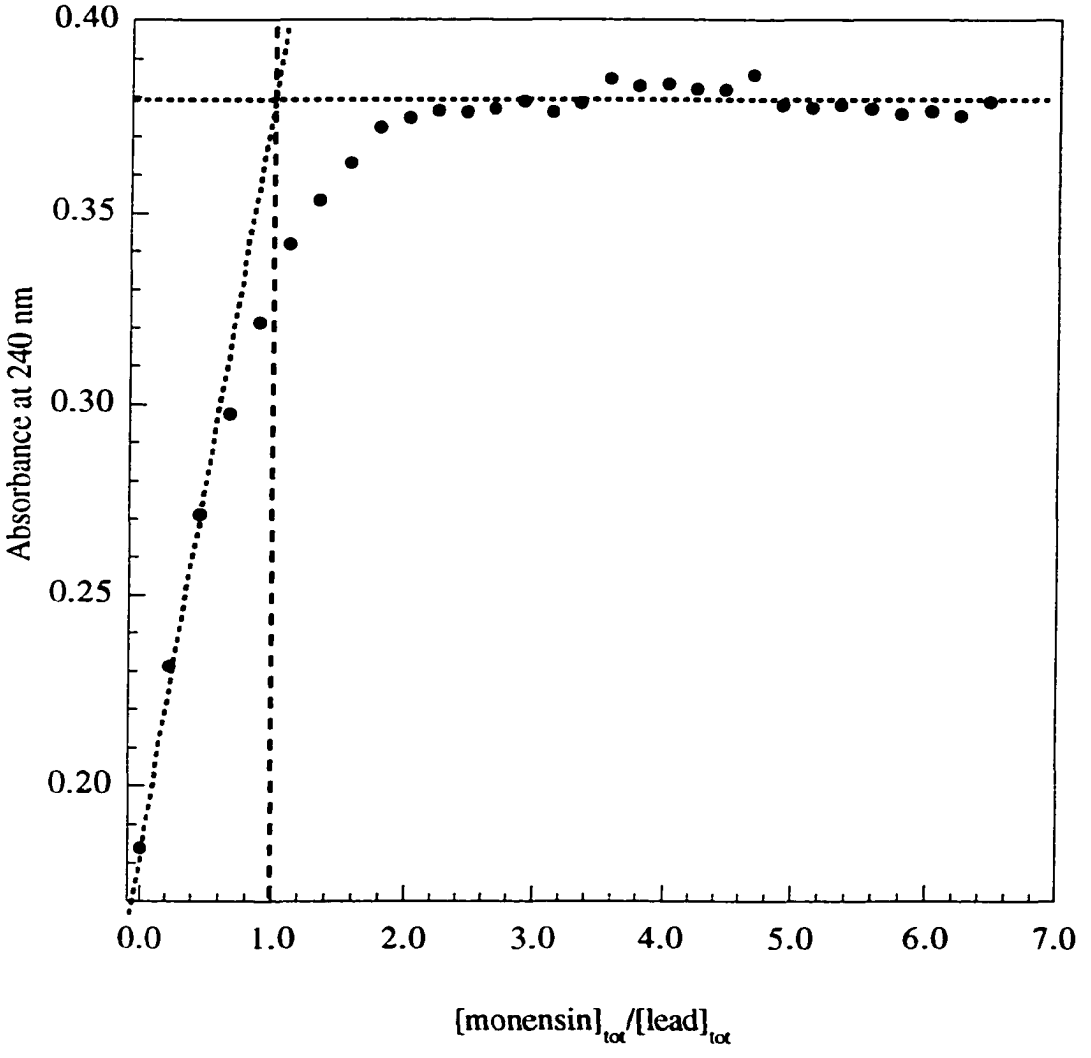

Figure III.8. Plot of the absorbance resulting from each aliquot of tetramethylammonium monensin added versus the concentration ratio of total monensin to total lead.

An estimate for the lead complexation constant was found by titrating lead perchlorate with monensin at a lower pH*, where lead hydroxide does not form. Expressions for the equilibrium reaction between monensin and lead and the corresponding formation constant are presented in equation III.9.

$$Pb^{2+} + L^- \rightleftharpoons PbL^+ \qquad K_{PbL} = \frac{[PbL^+]}{[Pb^{2+}][L^-]} \qquad \text{(III.9)}$$

The intrinsic value of K_{PbL} is related to the apparent, or pH*-dependent, formation constant K'_{PbL} as follows

$$\log K_{PbL} = \log K'_{PbL} - \log \alpha_L \qquad \text{(III.10)}$$

The pH* dependence of the α_L term is given by

$$\alpha_L = \frac{[L^-]}{([L^-]+[HL])} = \left(1 + K_H^{m*}\, a_H^*\right)^{-1} \qquad \text{(III.11)}$$

where K_H^{m*} is the mixed-mode protonation constant. At the pH* where at least 99% of ligand exists in the protonated form, or where $pH^* \leq \log K_H^{m*} - 2$,

$\alpha_L \approx (K_H^{m*}\, a_H^*)^{-1}$, and expression III.10 can be rewritten as

$$\log K_{PbL} = \log K'_{PbL} + \log K_H^{m*} - pH^* \qquad \text{(III.12)}$$

The monensin-lead titration was carried out at pH* 3.25, which is more than 3 pH units lower than $\log K_H^{m*}$. Lead perchlorate solution was prepared using 1.0 mM perchloric acid in 80% methanol-water, and the pH* was adjusted to the required value with 1.4 M tetraethylammonium hydroxide. Small aliquots of monensin were added directly to the spectrophotometric cell and the change in absorbance at 240 nm was recorded. Spectra were recorded after waiting for only one minute following each addition of titrant in order to decrease the possibility of monensin degradation in acidic solution[9]. From the graph of absorbance change vs the concentration of free monensin ($[HL]_i$), the value of

the apparent complexation constant was obtained using non-linear least-squares fit to the expression

$$\Delta Abs_i = \frac{\Delta Abs_\infty K'_{PbL}[HL]_i}{1 + [HL]_i K'_{PbL}} \qquad \text{(III.13)}$$

where ΔAbs_∞ is the difference between the limiting and initial absorbance ($Abs_\infty - Abs_0$), ΔAbs_i is the difference between the limiting absorbance and the absorbance at each titration point ($Abs_\infty - Abs_i$), $[HL]_i$ is the concentration of the total uncomplexed monensin at each point. The derivation for equation III.13 is presented in Appendix 1. Initial estimates for calculated parameters ΔAbs_∞ and K'_{PbL} were required by the curve fitting program. An estimate of ΔAbs_∞ was obtained from the spectra. An initial estimate of K'_{PbL} was obtained from the fraction of change in absorbance when the metal-ligand ratio was unity. At the point where total metal $[Pb^{2+}]_{tot}$ and total ligand $[HL]_{tot}$ concentrations are equal, the fraction of total absorbance change is linearly related to the fraction of the total metal complexed

$$\frac{\Delta Abs_i}{\Delta Abs_\infty} \approx \frac{[PbL^+]'}{[Pb^{2+}]_{tot}} = \chi \qquad \text{(III.14)}$$

where $[PbL^+]'$ represents the sum of the concentrations of all complexes with 1:1 Pb-L stoichiometry, including both protonated and unprotonated species. The concentrations of the uncomplexed reactants can be determined from mass balance equations, assuming only the formation of lead-monensin complexes having 1:1 stoichiometry and that the concentration of the unprotonated form of lasalocid, Mon^-, is negligible at this pH.

$$[Pb^{2+}]_{tot} = [Pb^{2+}]_i + [PbL^+]' \qquad \text{(III.15)}$$

$$[HL]_{tot} = [HL]_i + [PbL^+]' \qquad \text{(III.16)}$$

Those concentrations of $[Pb^{2+}]$ and [HL] calculated at the point where $[Pb^{2+}]_{tot} = [HL]_{tot}$, can be used to provide an initial estimate for K'_{PbL} as follows

$$K'_{PbL} = \frac{[PbL^+]'}{[Pb^{2+}]_i\,[HL]_i} = \frac{\chi\,[Pb^{2+}]_{tot}}{((1-\chi)\,[HL]_{tot})^2} = \frac{\chi}{[Pb^{2+}]_{tot}\,(1-\chi)^2} \qquad \text{(III.17)}$$

This trial value is then utilized to find the concentration of protonated monensin at each titration point, using the following equation

$$[HL]_i = \frac{-(K'_{PbL}([Pb^{2+}]_{tot} - [HL]_{tot}) + 1) + \sqrt{(K'_{PbL}([Pb^{2+}]_{tot} - [HL]_{tot}) + 1)^2 - 4K'_{PbL}[HL]_{tot}}}{2K'_{PbL}} \qquad \text{(III.18)}$$

These values of $[HL]_i$ were used in fitting equation III.13 and a new value for K'_{PbL} was obtained from the non-linear least-squares fit of the data. The iteration cycle was repeated till the resulting parameters were different by less than 1 percent between two consecutive calculations. An example of the results after final curve-fitting step is shown in Figure III.9. The values of the apparent complexation constants obtained and the pH*-independent constants calculated using equation III.12 are listed in Table III.4.

Table III.4 Apparent and pH*-independent complexation constants for lead–monensin derived from UV-Vis titrations in 80% methanol-water[a]

Exp. #	K'_{PbL}	error[b] in K'_{PbL}	ΔAbs_{∞}	error[b] in ΔAbs_{∞}	log K'_{PbL}[c]
1	1647	138	0.348	0.022	6.99
2	2890	193	0.287	0.014	7.20
3	1451	183	0.387	0.037	6.93

[a] 25.0 °C, ionic strength 0.05 M (TEAP). [b] Uncertainty in terms of standard error.
[c] Calculated using eq III.12.

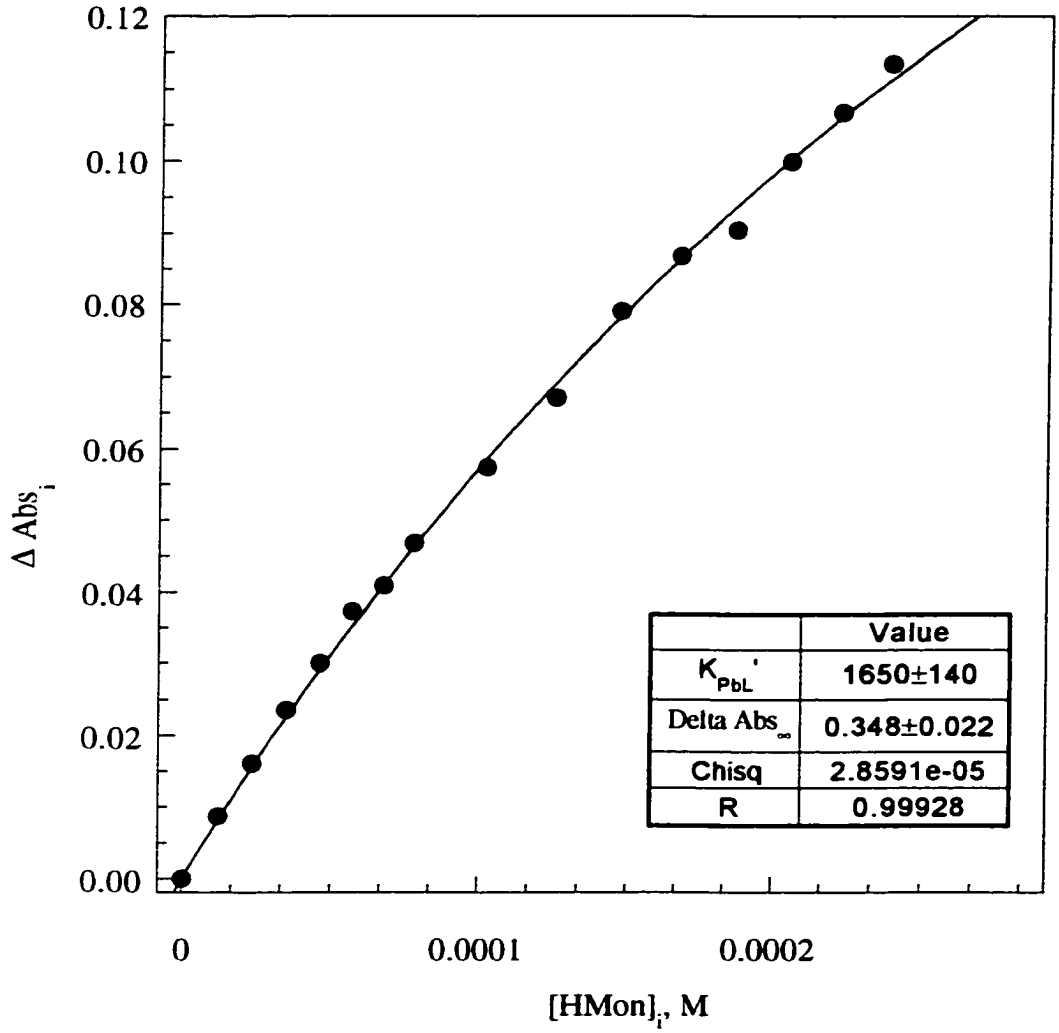

Figure III.9. Change in absorbance at 240 nm as a function of $[HMon]_i$ at pH* 3.25. In order to control the pH* lead solution was prepared using 1 mM solution of $HClO_4$ in 80% methanol-water for a solvent. 20.0 μL aliquots of 1.05 mM monensic acid were used to titrate 2.50 mL of a solution containing 0.065 mM lead perchlorate. The titration was done at 25.0 °C at an ionic strength of 0.05 M (TEAP). The solid line was calculated from eq III.12 using the derived parameters listed in the inset table.

III.D. Potentiometric studies of metal binding.

Titration data sets consisting of observed pH* vs added volume of the base were obtained for solutions of monensic acid in 80% methanol in the presence of metal perchlorates as described in Chapter II.F. Different metal-ligand ratios were used to test for the presence of complexes with varied stoichiometry. Three different metal-ligand ratios (1:1, 1:2, and 1:3) were employed for monensin-lead and monensin-calcium titrations. Metal-ligand ratios of 2:1, 1:1, and 1:2 were used for monensin-sodium and monensin-zinc titrations. Stability constants for monensin complexes of lead, sodium, zinc and calcium were obtained by analyzing each data set (p[H] vs volume titrant) with the program BEST. An electrode solvent correction factor was applied to the pH* values obtained as described in section II.D. The pH* values in each data set were converted to p[H] using the logarithm of the hydrogen activity coefficient. The values of free monensin, metal cation, and titrant base concentrations were also required for the program input file.

Equilibrium constants for all reactions included in the model used to fit the data were considered in terms of overall complexation constants (log β values). Reactions were written as the combination of protons or metals with donor ligands. In addition to the ligand protonation reaction (eq III.7), the expressions for relevant equilibria and corresponding constants that were considered are shown in equations III.19 – III.25, where M stands for the metal ion and L stands for the monensin.

$$M^{n+} + L^- \rightleftharpoons ML^{n-1} \qquad \beta_{ML} = \frac{[ML^{n-1}]}{[M^{n+}][L^-]} \qquad \text{(III.19)}$$

$$M^{n+} + L^- + H^+ \rightleftharpoons MLH^{n+} \qquad \beta_{MLH} = \frac{[MLH^{n+}]}{[M^{n+}][L^-][H^+]} \qquad \text{(III.20)}$$

$$M^{n+} + 2L^- \rightleftharpoons ML_2^{n-2} \qquad \beta_{ML_2} = \frac{[ML_2^{n-2}]}{[M^{n+}][L^-]^2} \qquad \text{(III.21)}$$

$$M^{n+} + L^- + H_2O \rightleftharpoons MLOH^{n-2} + H^+ \qquad \beta_{MLOH} = \frac{[MLOH^{n-2}][H^+]}{[M^{n+}][L^-]} \qquad \text{(III.22)}$$

$$M^{n+} + H_2O \rightleftharpoons MOH^{n-1} + H^+ \qquad \beta_{MOH} = \frac{[MOH^{n-1}]\,[H^+]}{[M^{n+}]} \qquad \text{(III.23)}$$

$$M^{n+} + 2H_2O \rightleftharpoons M(OH)_2^{n-1} + 2H^+ \qquad \beta_{M(OH)_2} = \frac{[M(OH)^{n-2}]\,[H^+]^2}{[M^{n+}]} \qquad \text{(III.24)}$$

$$2M^{n+} + L^- \rightleftharpoons M_2L^{2n-1} \qquad \beta_{M_2L} = \frac{[M_2L^{2n-1}]}{[M^{n+}]^2[L^-]} \qquad \text{(III.25)}$$

In this study log β_{HL} was determined previously, as described in Section III.B and was held constant during calculations. Data fitting started with a simple model including equilibria III.7, III.19, and formation of hydroxy-metal complexes (eqs III.23 and III.24), where applicable. If the value of the parameter sigma fit was above about 0.070 and the calculated values of p[H] were larger in comparison to the experimental points, protonated metal-ligand complexes were added. The 2:1 ligand-metal complex was included in the original model for the titrations with 2:1 and 3:1 monensin-metal ratios. Other species were added to the model to test whether their addition resulted in an improvement of the fit. They were retained in the model if the value of the sigma fit was improved upon their addition.

The values of stability constants obtained for a given model were then used to calculate a species distribution diagram using the program Comics[10]. If a particular complex species constituted less than 5% of the total amount of ligand or metal, it was considered to be insignificant and was eliminated from the model. The values of complexation constants with the updated model were recalculated and the process repeated until the curve fit was satisfactory and the set of equilibrium constants was obtained. The experimental details for each individual metal titration and the associated curve fitting procedures are discussed below.

Sodium-monensin

A 0.0200 M solution of sodium chloride was prepared by dissolving a known weight of oven dried NaCl in 80% methanol and subsequently diluting it to the required concentration. This solution was added to 20.0 mL of monensic acid solution in the titration vessel in the amount required to obtain the stoichiometric metal-ligand ratio desired. The mixture was allowed to equilibrate to 25.0°C for 5 minutes. Titration data was acquired with the addition of small aliquots of 0.02118 M tetramethylammonium hydroxide base and the titration curves obtained are presented in Figure III.10. In addition to HMon and NaMon, the models used to fit the p[H]-curves required the presence of the species $NaMon_2$ for the 1:2 Na-Mon mixture, and $NaMon_2H$ species for all other solution concentration ratios. Results of the fits for 1:1 and 2:1 monensin-sodium solution ratios are shown in Figures III.11 and III.12 and the refined values of the equilibrium constants are listed in Table III.5. Species distribution curves as a function of p[H] were calculated using the average values of the equilibrium constants (Table III.10) and are shown in Figure III.13. Rather unexpectedly, they showed that the species with 1:2 Na-Mon stoichiometry were present in solution in significant

amounts (i.e., they constituted more than 5% of the total concentration of monensin) and were required to fit the data.

Table III.5 Log β_X values obtained from potentiometric titrations of monensic acid (HL) and sodium ion (Na^+) in 80% methanol-water[a]

Exp.	HL-Na	Identity of complex species X				σ_{fit}[d]
No.	ratio	HL[b]	NaL[c]	NaL_2[c]	NaL_2H[c]	
1	1	6.83	4.93		14.89	0.022
2	1	6.83	5.06		15.37	0.025
3	0.5	6.83	4.80		15.25	0.053
4	2	6.83	5.07	8.22		0.015

[a] 25.0 °C, ionic strength 0.05 M (TEAP). [b] The value of log β_{HL} (section III.B) was fixed during refinement. [c] Values were refined by program BEST. [d] $\sigma_{fit} = (U/N)^{1/2}$, as defined in eqs III.5 and III.6.

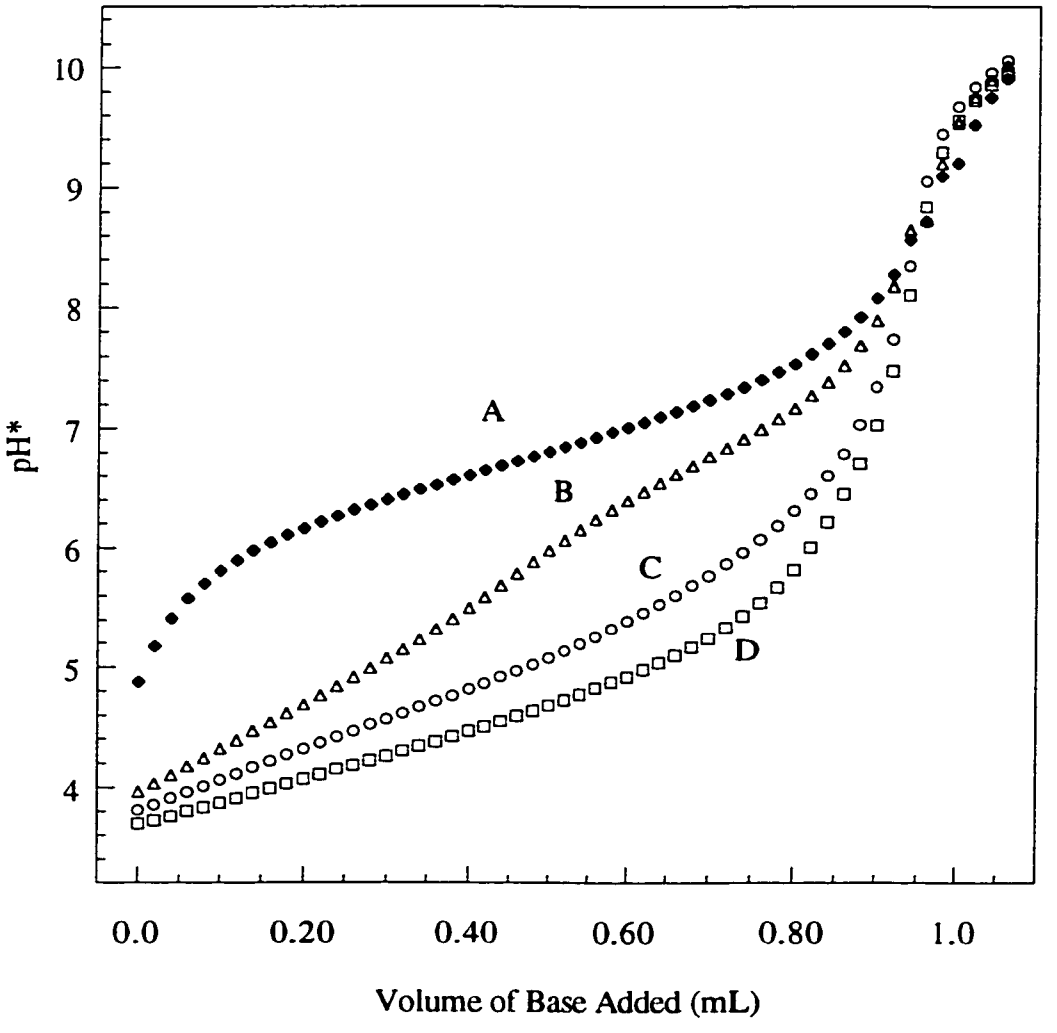

Figure III.10. Potentiometric titration curves for various stoichiometric ratios of monensin-sodium in 80% methanol-water at 25.0 °C. Each solution contained 20.0 mL of 0.60 mM free monensin in the acid form. 0.020 M NaCl was added in the amount to obtain the following stoichiometric ratios: A. no NaCl; B. 2:1 HMon-NaCl; C. 1:1 HMon-NaCl; D. 1:2 HMon-NaCl. All titrations were done at 0.05 M ionic strength (TEAP).

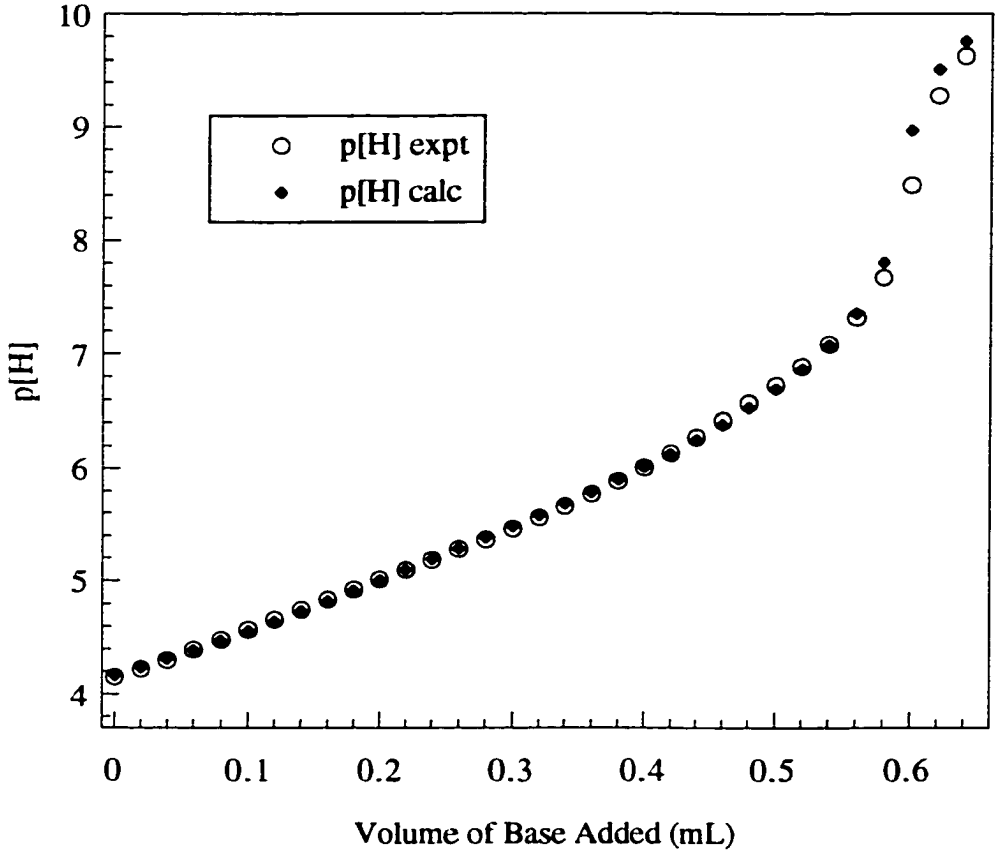

Figure III.11. Potentiometric titration curve for 20.63 mL of a solution containing 0.60 mM monensinc acid and 0.61 mM NaCl at an ionic strength of 0.05 M (TEAP) in 80% methanol-water at 25.0 °C. The titrant is 0.02118 M tetramethylammonium hydroxide with ionic strength maintained at 0.05 M with TEAP. The calculated p[H] values were obtained from the program BEST using refined values of equilibrium constants for the model containing the species listed in Table III.5, Exp.1.

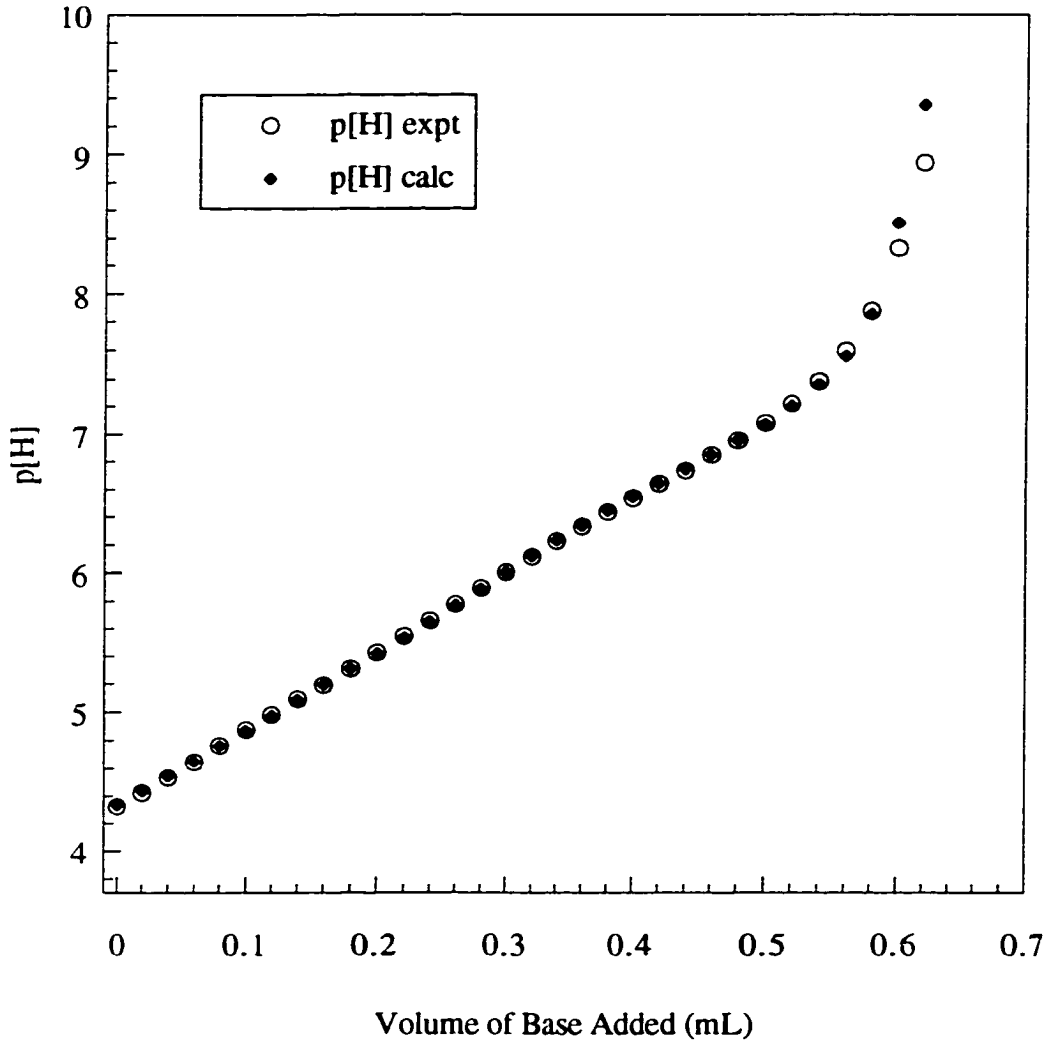

Figure III.12. Potentiometric titration curve for 20.25 mL of a solution containing 0.60 mM monensin acid and 0.31 mM NaCl at an ionic strength of 0.05 M (TEAP) in 80% methanol-water at 25.0 °C. The titrant is 0.02118 M tetramethylammonium hydroxide with ionic strength maintained at 0.05 M with TEAP. The calculated p[H] values were obtained from the program BEST using refined values of equilibrium constants for the model containing the species listed in Table III.5, Exp.4.

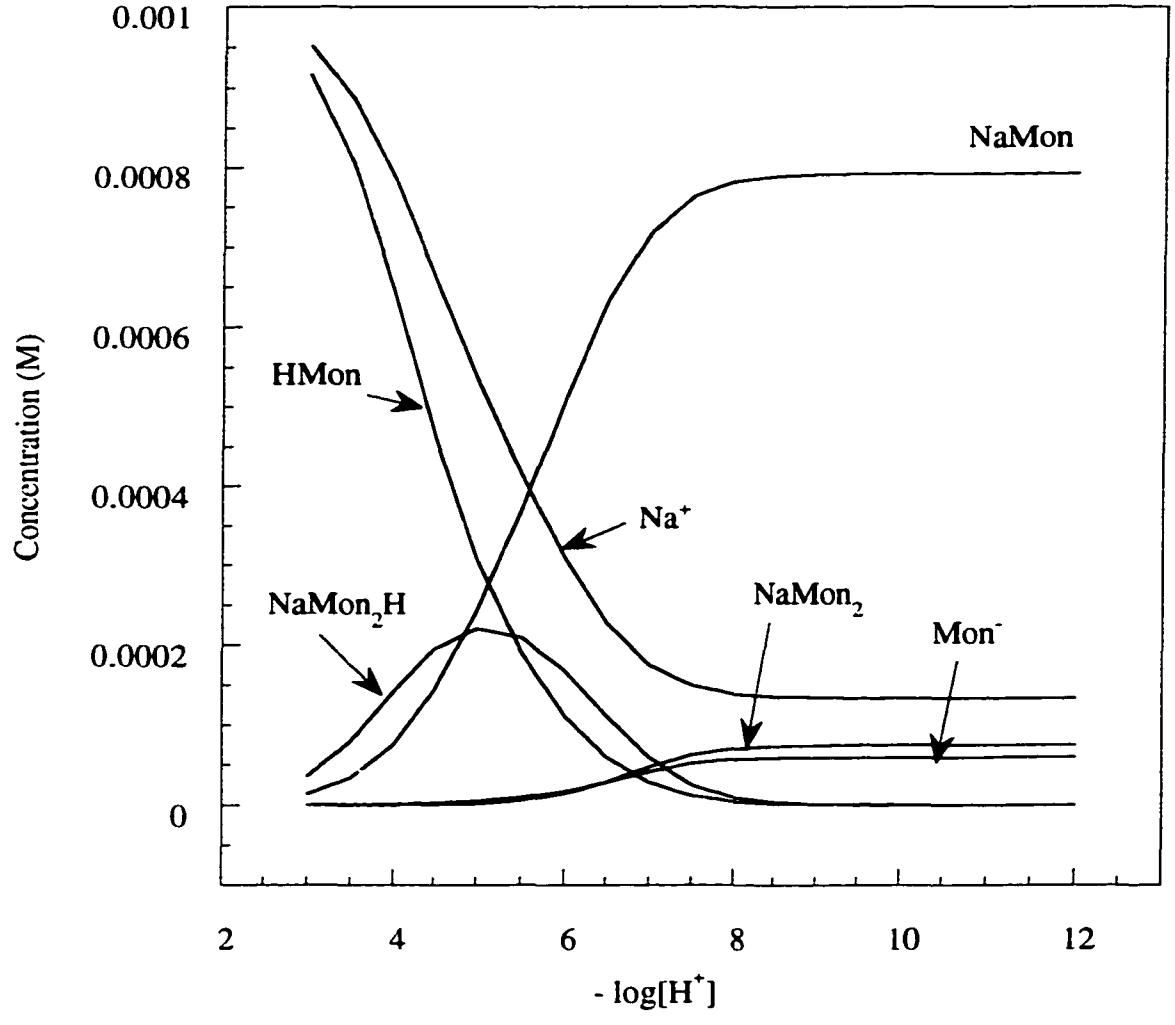

Figure III.13. Species distribution curves for monensin-sodium complexes in solution as a function of p[H] in 80% methanol-water. Species concentrations were calculated using the program Comics for 1.0 mM monensin and 1.0 mM sodium using the average values of the equilibrium constants listed in Table III.10.

Calcium-monensin

An aliquot of a standardized solution of 0.0544 M calcium chloride in 80% methanol was added to the titration vessel containing 20.0 mL of free monensin in the amount required to obtain the metal-ligand stoichiometric ratio desired. The mixture was allowed to equilibrate for 5 minutes at 25.0 °C and was titrated with 0.01935 M tetramethylammonium hydroxide. The resulting pH* curves were analyzed with the program BEST[7]. The model used to fit the calcium-monensin titration data included only the calcium-monensin complex with 1:1 stoichiometry, which was sufficient to obtain reasonably good sigma values. The formation of calcium mono-hydroxide was also included into the model used to fit the data. The value of the formation constant for the calcium mono-hydroxide complex in aqueous solutions was small[11] indicating that the hydroxide complex was rather weak. The aqueous value was converted to the acid dissociation form (eq III.23) using the autoprotolysis constant for 80% methanol-water[12]. This estimate was included in the model and was not refined during calculations. Subsequent analysis showed that the presence of calcium hydroxide in the model used for curve-fitting did not have an effect on the refined value of log β_{CaL}.

Experimental titration curves for solutions with various calcium-monensin concentration ratios are presented in Figure III.14. Figures III.15 and III.16 illustrate the curve fits obtained using the program BEST. The values of equilibrium constants obtained for monensin-calcium complexes are listed in Table III.6. Species distribution curves as a function of p[H] were calculated using the average values of the equilibrium constants (Table III.10) and are shown in Figure III.17.

Table III.6 Log β_X values obtained from potentiometric titrations of monensic acid (HL) and calcium in 80% methanol-water[a]

exp #	HL-Ca ratio	Identity of complex species X			σ fit[e]
		HL[b]	CaL[c]	CaOH[d]	
1	1	6.83	3.04	-13.11	0.026
2	2	6.83	3.15	-13.11	0.025
3	3	6.83	3.11	-13.11	0.026

[a] 25.0 °C, ionic strength 0.05 M (TEAP). [b] The value of log β_{HL} (section III.B) was fixed during refinement. [c] The value was refined by program BEST. [d] Value was fixed during refinement; it was estimated for 80% methanol-water, as described in the text. [e] $\sigma_{fit} = (U/N)^{1/2}$, as defined in eqs III.5 and III.6.

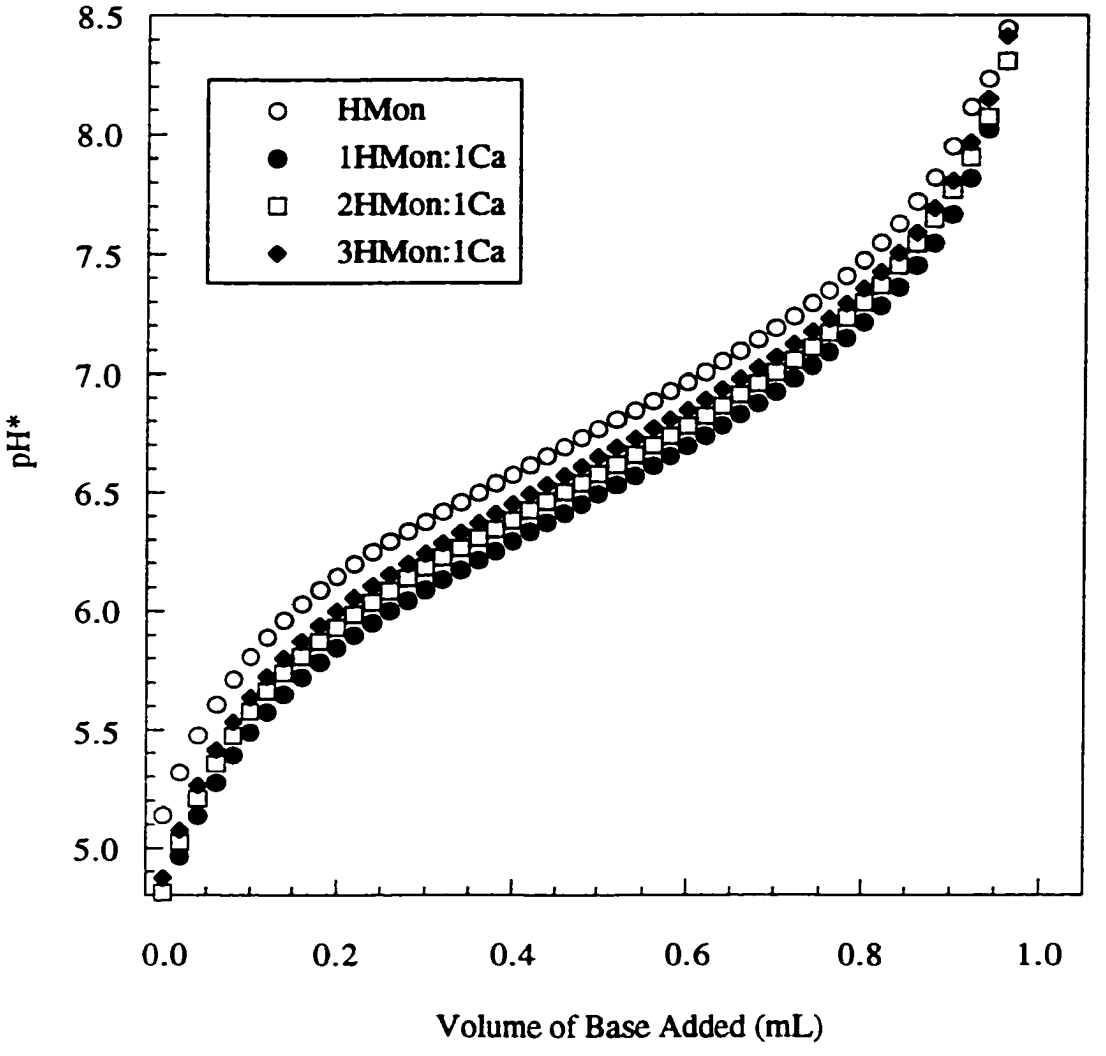

Figure III.14. Potentiometric titration curves for various stoichiometric ratios of monensin-calcium in 80% methanol-water solution at 25.0 °C. Each solution contained 20.0 mL of 0.94 mM monensin in the acid form alone or with indicated amounts of added calcium at 0.05M ionic strength (TEAP).

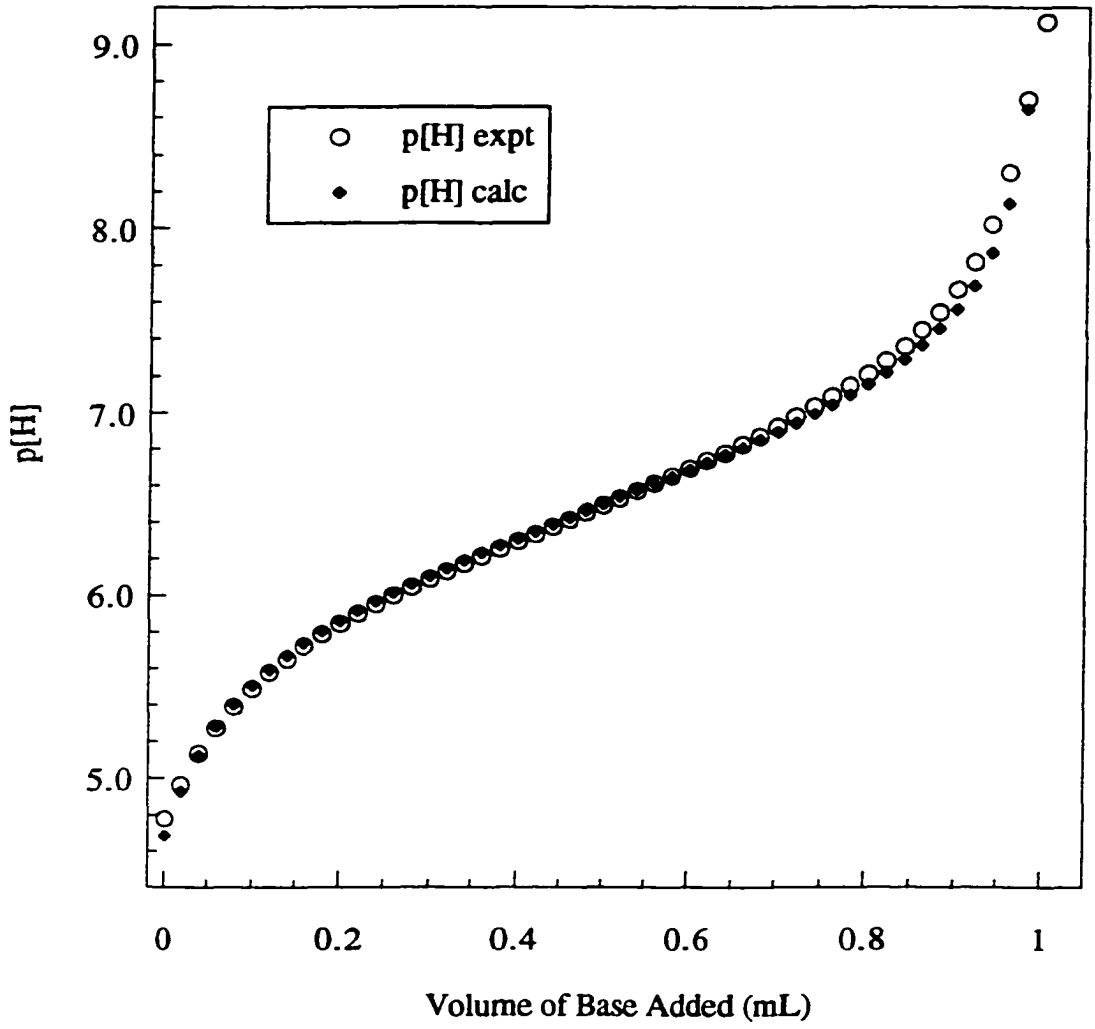

Figure III.15. Potentiometric titration curve for 20.35 mL of a solution containing 0.94 mM monensic acid and 0.95 mM calcium at an ionic strength of 0.05 M (TEAP) in 80% methanol-water at 25.0 °C. The titrant is 0.01935 M tetramethylammonium hydroxide with ionic strength maintained at 0.05 M with TEAP. The calculated p[H] values were obtained from the program BEST using refined values of equilibrium constants for the model containing the species listed in Table III.6, Exp.1.

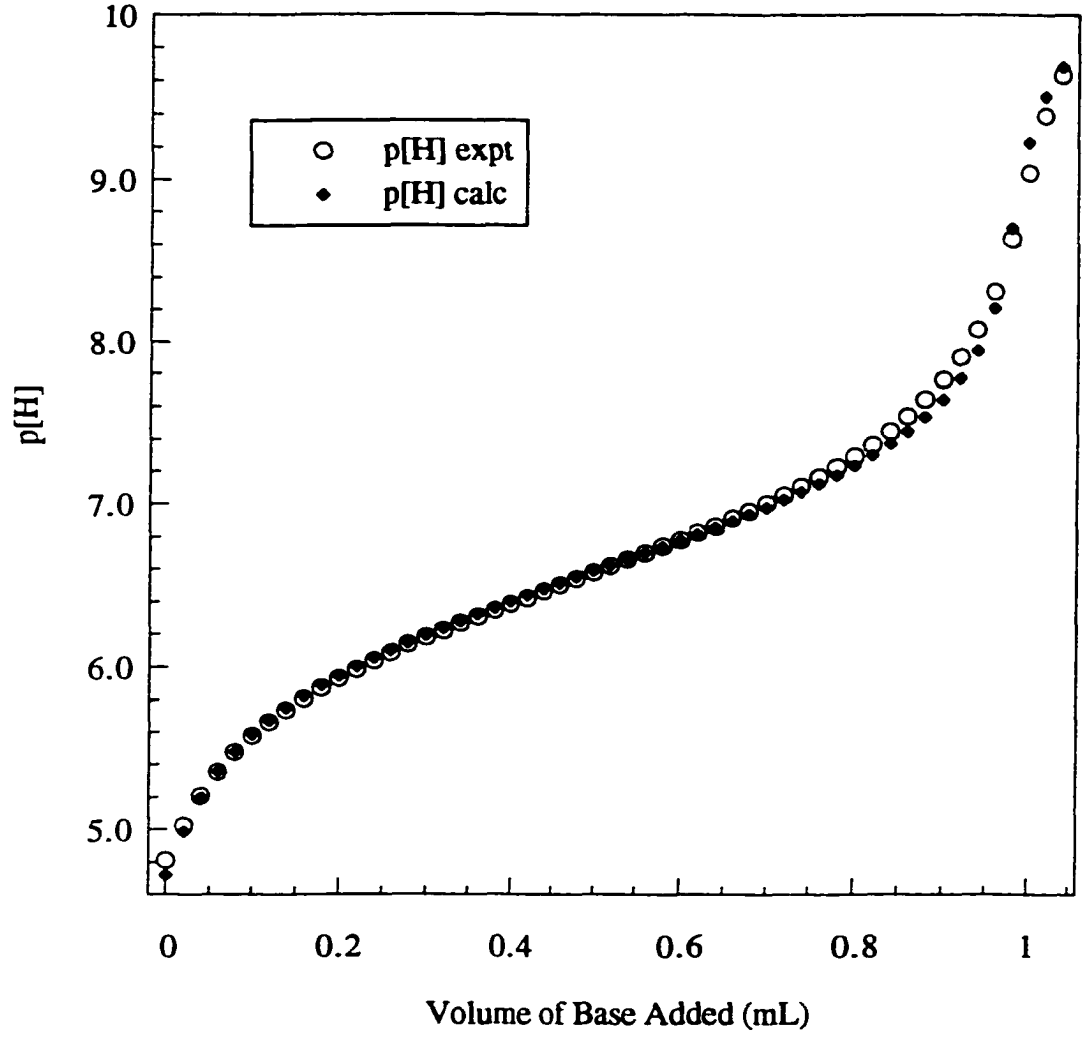

Figure III.16. Potentiometric titration curve for 20.18 mL of a solution containing 0.94 mM monensic acid and 0.48 mM calcium at an ionic strength of 0.05 M (TEAP) in 80% methanol-water at 25.0 °C. The titrant is 0.01935 M tetramethylammonium hydroxide with ionic strength maintained at 0.05 M with TEAP. The calculated p[H] values were obtained from the program BEST using refined values of equilibrium constants for the model containing the species listed in Table III.6, Exp.2.

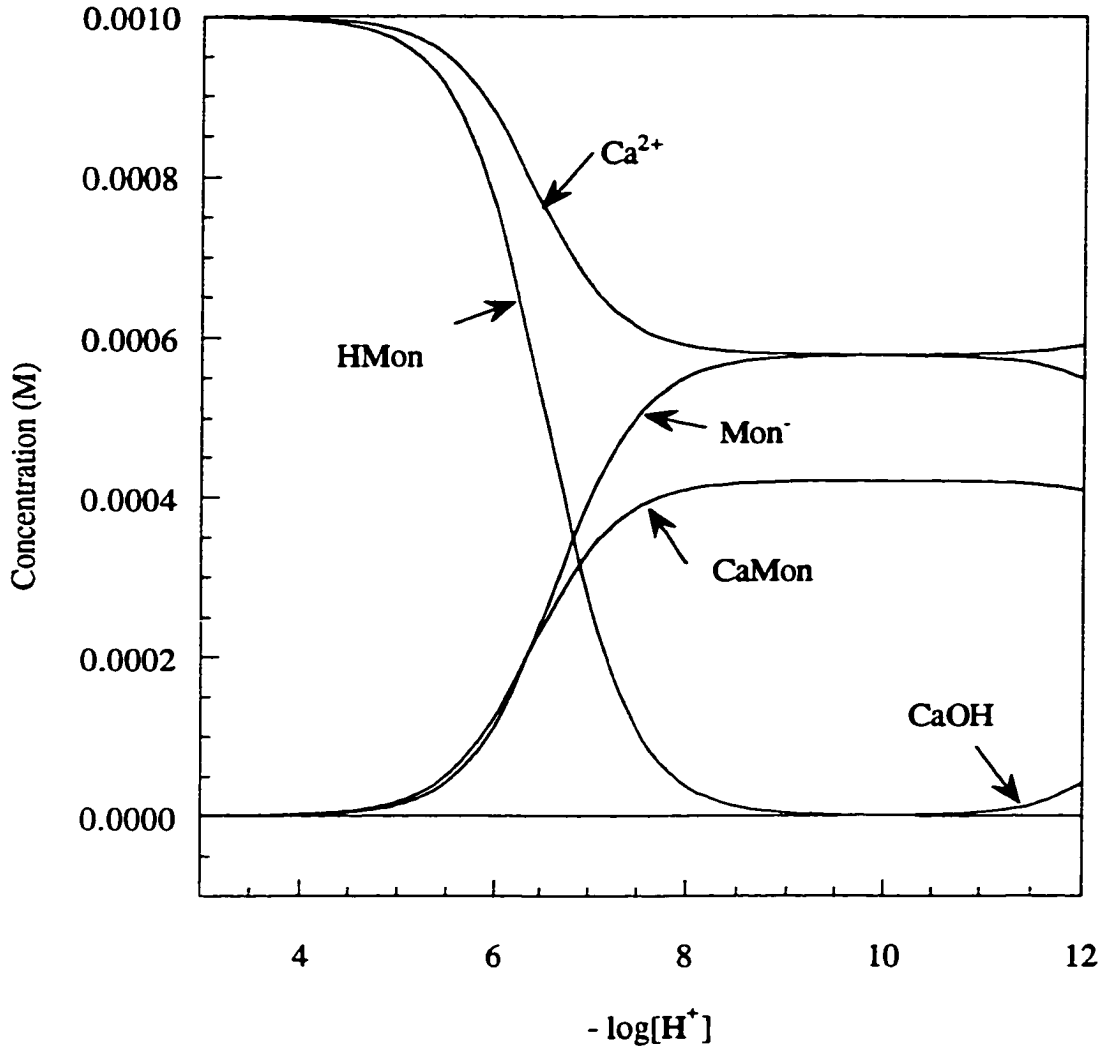

Figure III.17. Species distribution curves for monensin-calcium complexes in solution as a function of p[H] in 80% methanol-water. Species concentrations were calculated using the program Comics for 1.0 mM monensin and 1.0 mM calcium using the average values of the equilibrium constants listed in Table III.10.

Zinc-monensin

An aliquot of a standardized solution of 0.0586 M zinc perchlorate in 80% methanol was added to the titration vessel containing 20.0 mL of free monensin in the amount required to achieve the desired stoichiometric ratio. The mixture was allowed to equilibrate for 5 minutes at 25.0 °C and was titrated with 0.02199 M tetramethylammonium hydroxide. The resulting pH* curves were analyzed using the program BEST[7]. Formation of zinc-hydroxide complexes was included in the model used to fit the titration data. Literature values of the formation constants for zinc-hydroxide complexes measured in aqueous solutions were available[11], but no studies in methanol or methanol-water media were found. To provide estimates of these constants the aqueous stability constants were corrected to 0.05 M ionic strength and converted to the acid dissociation form (e.g., eq III.23) using the water autoprotolysis constant for 80% methanol-water[12]. The estimated values obtained were held constant during calculations.

The model used to fit the zinc-monensin data using BEST also required the presence of a 1:1 zinc-monensin complex and a ternary zinc-monensin-hydroxide species. Experimental titration curves for solutions with various zinc-monensin concentration ratios are presented in Figure III.18. Due to the onset of precipitation, data points above pH* 7.5 for solutions with 2:1 Mon-Zn concentration ratios and above pH* 7.0 for the other ligand-metal ratios were not used in fitting the data. Figures III.19 and III.20 illustrate the curve fits obtained with the program BEST and the values of equilibrium constants are listed in Table III.7. Species distribution curves as a function of p[H] were calculated using the average values of the equilibrium constants (Table III.10) and are shown in Figure III.21.

Table III.7 Log β_X values obtained from potentiometric titrations of monensic acid (HL) and zinc(II) in 80% methanol-water[a]

Exp.	HL-Zn	Identity of complex species X					σ_{fit}[f]
No.	ratio	HL[b]	ZnL[c]	ZnLOH[c,d]	ZnOH[e]	$Zn(OH)_2$[e]	
1	1	6.83	3.81	-3.36	-9.42	-18.2	0.016
2	2	6.83	3.71	-3.81	-9.42	-18.2	0.032
3	0.5	6.83	3.71	-3.76	-9.42	-18.2	0.021

[a] 25.0 °C, ionic strength 0.05 M (TEAP). [b] The value of log β_{HL} (section III.B) was fixed during refinement. [c] Values were refined by program BEST. [d] β_{ZnLOH} is expressed as an acid dissociation constant (eq III.23). [e] Values were fixed during refinement; they were estimated for 80% methanol-water and corrected to 0.05 M ionic strength, as described in the text. [f] $\sigma_{fit} = (U/N)^{1/2}$, as defined in eq III.5 and III.6.

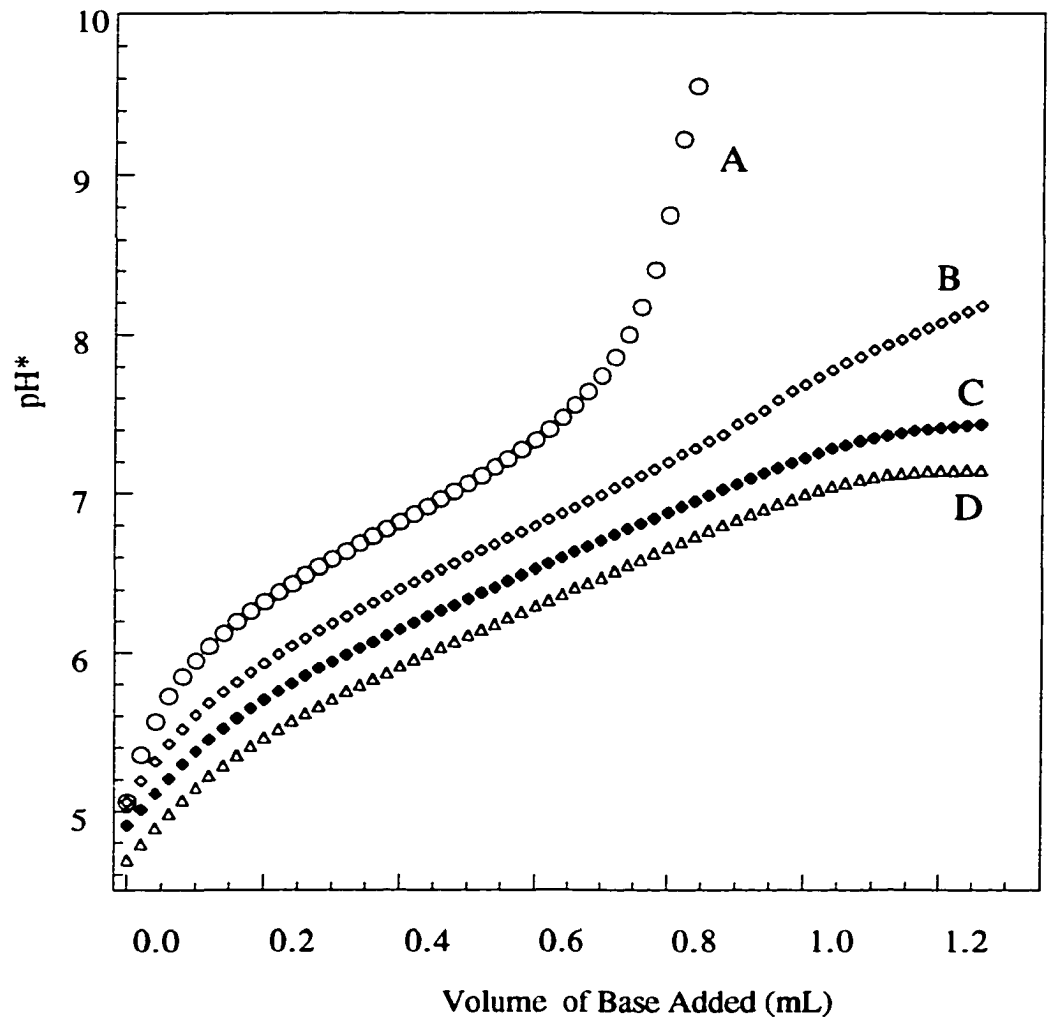

Figure III.18. Potentiometric titration curves for various stoichiometric ratios of monensin-zinc in 80% methanol-water at 25.0 °C. Each solution contained 20.0 mL of 0.88 mM free monensin in the acid form. 0.0586 M zinc perchlorate was added in the amount to obtain the following stoichiometric ratios: A. no Zn; B. 2:1 HMon-Zn; C. 1:1 HMon-Zn; D. 1:2 HMon-Zn. All titrations were done at 0.05 M ionic strength (TEAP).

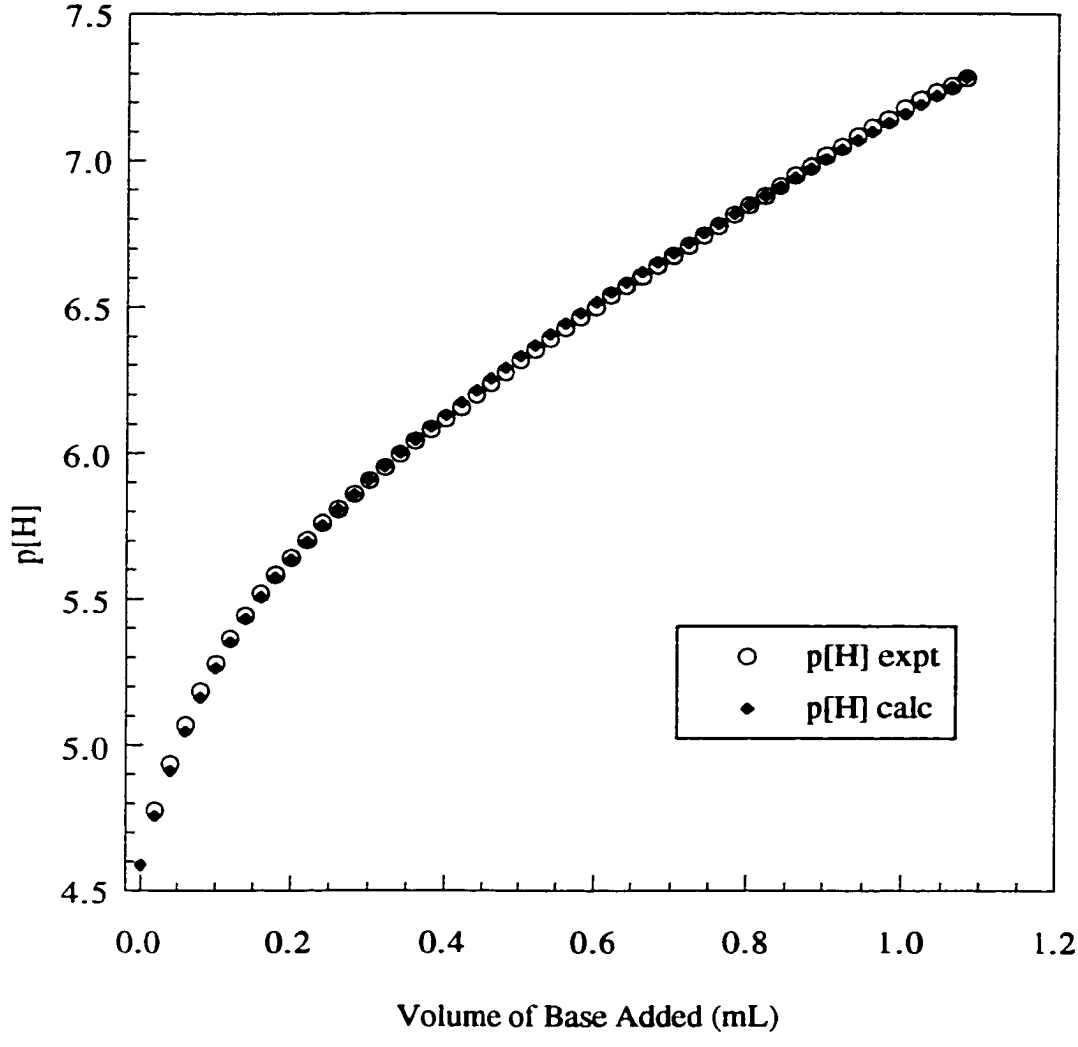

Figure III.19. Potentiometric titration curve for 20.30 mL of a solution containing 0.88 mM monensic acid and 0.88 mM zinc at an ionic strength of 0.05 M (TEAP) at in 80% methanol-water 25.0 °C. The titrant is 0.02199 M tetramethylammonium hydroxide with ionic strength maintained at 0.05 M with TEAP. The calculated p[H] values were obtained from the program BEST using refined values of equilibrium constants for the model containing the species listed in Table III.7, Exp.1.

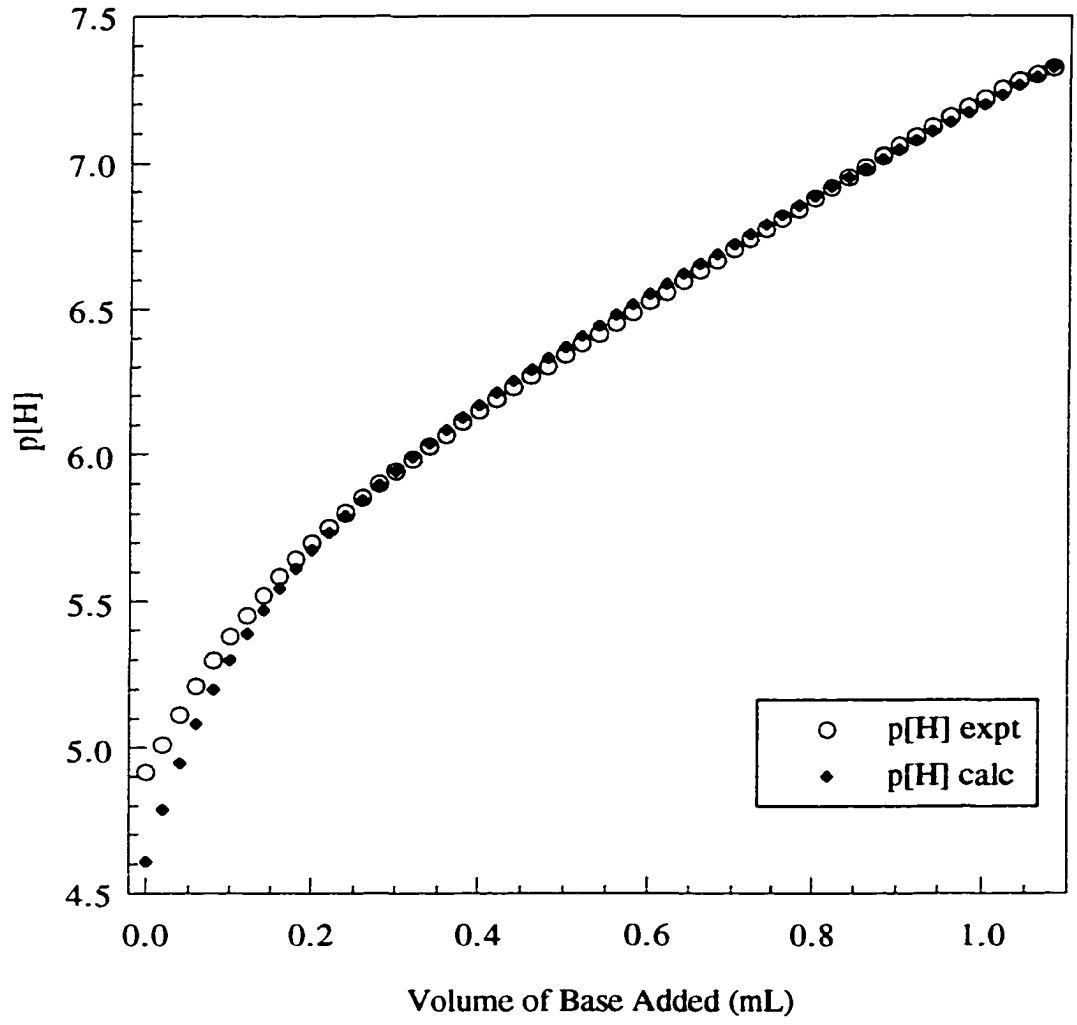

Figure III.20. Potentiometric titration curve for 20.15 mL of a solution containing 0.88 mM monensic acid and 0.44 mM zinc at an ionic strength of 0.05 M (TEAP) at in 80% methanol-water 25.0 °C. The titrant is 0.02199 M tetramethylammonium hydroxide with ionic strength maintained at 0.05 M with TEAP. The calculated p[H] values were obtained from the program BEST using refined values of equilibrium constants for the model containing the species listed in Table III.7, Exp.2.

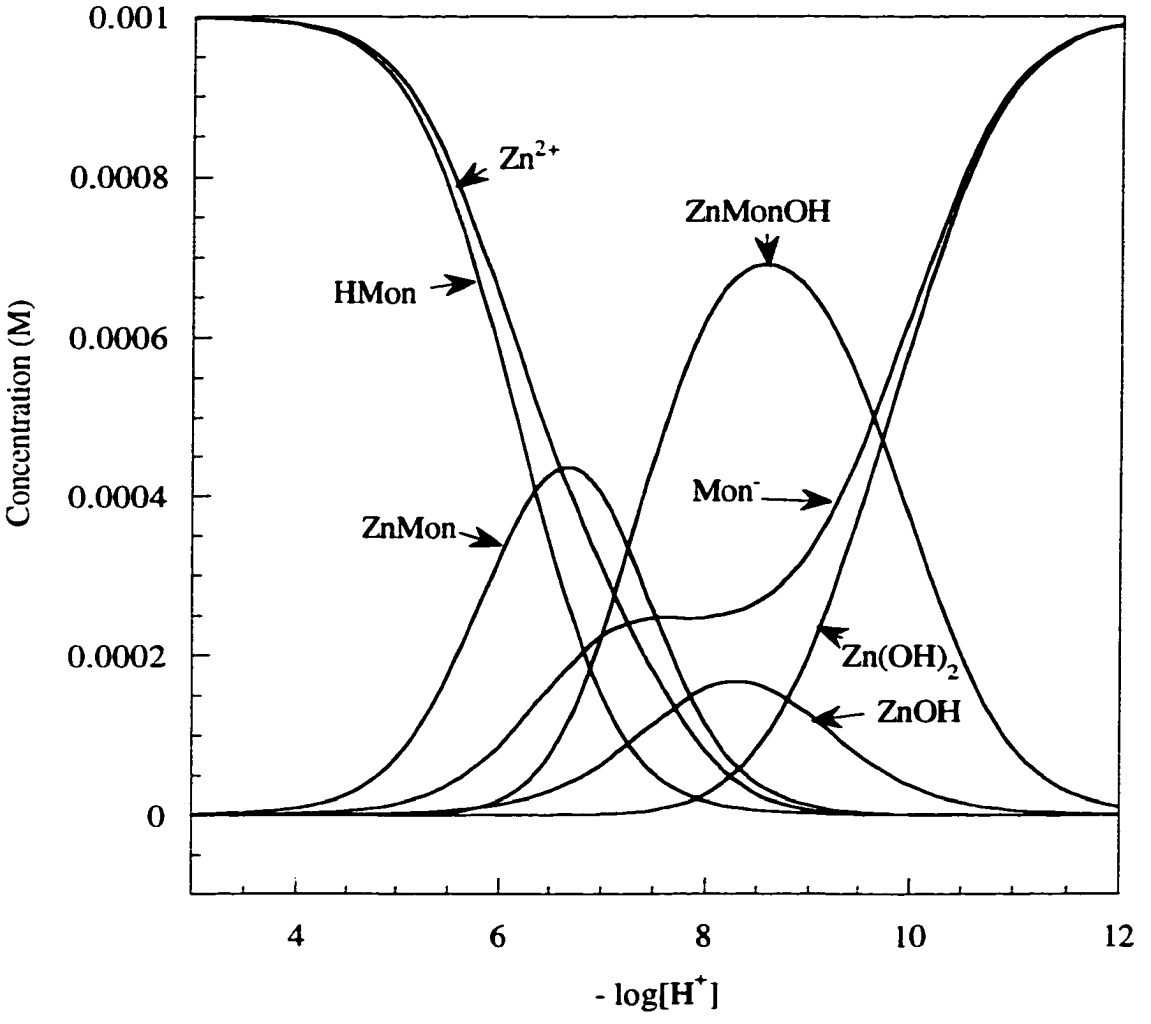

Figure III.21. Species distribution curves for monensin-zinc complexes in solution as a function of p[H] in 80% methanol-water. Species concentrations were calculated using the program Comics for 1.0 mM monensin and 1.0 mM calcium using the average values of the equilibrium constants listed in Table III.10.

Lead(II)-monensin

An aliquot of a standardized solution of 0.0230 M lead perchlorate in 80% methanol was added to the titration vessel containing 20.0 mL of free monensin in the amount required to achieve the desired stoichiometric ratio. The mixture was allowed to equilibrate for 5 minutes at 25.0 °C and was titrated with 0.01950 M to 0.02253 M tetramethylammonium hydroxide. The resulting pH* curves were analyzed using the program BEST[7]. The formation of a lead mono-hydroxide complex was included in the model used to fit the data. Literature values were available for the formation constants for lead-hydroxide and lead-methoxide complexes in water[11,13] and in methanol[14], respectively. Those studies indicated that species with various lead-hydroxide (or lead-methoxide) stoichiometries were present in solution. The relevant formation constants, expressed as overall equilibrium constants (Equation III.25), are listed in Table III.8.

$$x\,Pb^{2+} + y\,OR^- \rightleftharpoons Pb_x(OR)_y^{2x-y} \qquad \beta_{xy} = \frac{[Pb_x(OR)_y^{2x-y}]}{[Pb^{2+}]^x\,[OR^-]^y} \qquad \text{(III.26)}$$

where R = H in water and R = OCH_3 in methanol.

It is obvious that the strength of lead(II) complexation by the methoxide ion is greater than by the hydroxide. No data for 80% methanol was available and the values of the equilibrium constants for lead-hydroxy complexes had to be estimated to be included in the model.

To obtain the approximate dependence of equilibrium constants on the methanol content in the medium, a graph of autoprotolysis constants with changing solution composition[12] was constructed and is presented in Figure III.22. The $K_s'^*$ value at the point corresponding to 80% methanol composition is closer to the value in water than in methanol. The values of autoprotolysis constant start to decrease significantly, compared with those in water, for solvent compositions that contain more than 80% methanol. Therefore, the assumption was made that the values for lead-hydroxide formation

constants in 80% methanol are not much different from those in water, and the latter can be used in the model as estimates for the corresponding reactions in the mixed solvent. Stability constants from reference 13 were chosen since they were obtained at lead concentrations that are close to those employed in this study. The formation constants were corrected to match the ionic strength employed (0.05 M) and the latter values were converted to acid hydrolysis constants (e.g., eq III.23). The values obtained were held constant during the curve-fitting process. As mentioned previously, only the $Pb(OH)^+$ species was included in the model used for the curve-fitting. Attempts to include multinuclear or other mononuclear lead-hydroxy species resulted in their elimination from the model during refinement. The species distribution curves for the lead-hydroxy

Table III.8 Literature values of the overall stability constants for lead-hydroxide and lead-methoxide complexes

	$\log \beta_{Pbx(OR)y}$		
$Pb_x(OR)_y$,x-y	in water, R = H[a]	in water, R = H[a]	in methanol, R = CH_3[b]
1-1	6.0	5.92	8.8
1-2	10.3	-	15.2
1-3	13.3	-	-
3-4	31.7	31.21	41.5
3-5	-	37.15	47.5
4-4	35.2	34.72	-
6-8	67.5	66.8	-
Ionic strength, M	0.5	0.1	0.0
$[Pb^{2+}]_{tot}$, M	unknown	$10^{-4} - 2 \times 10^{-3}$	2.5×10^{-3}
Reference	11	13	14

[a] Concentration constants, as defined by equation III.26. [b] Defined as "overall standard constants of formation".

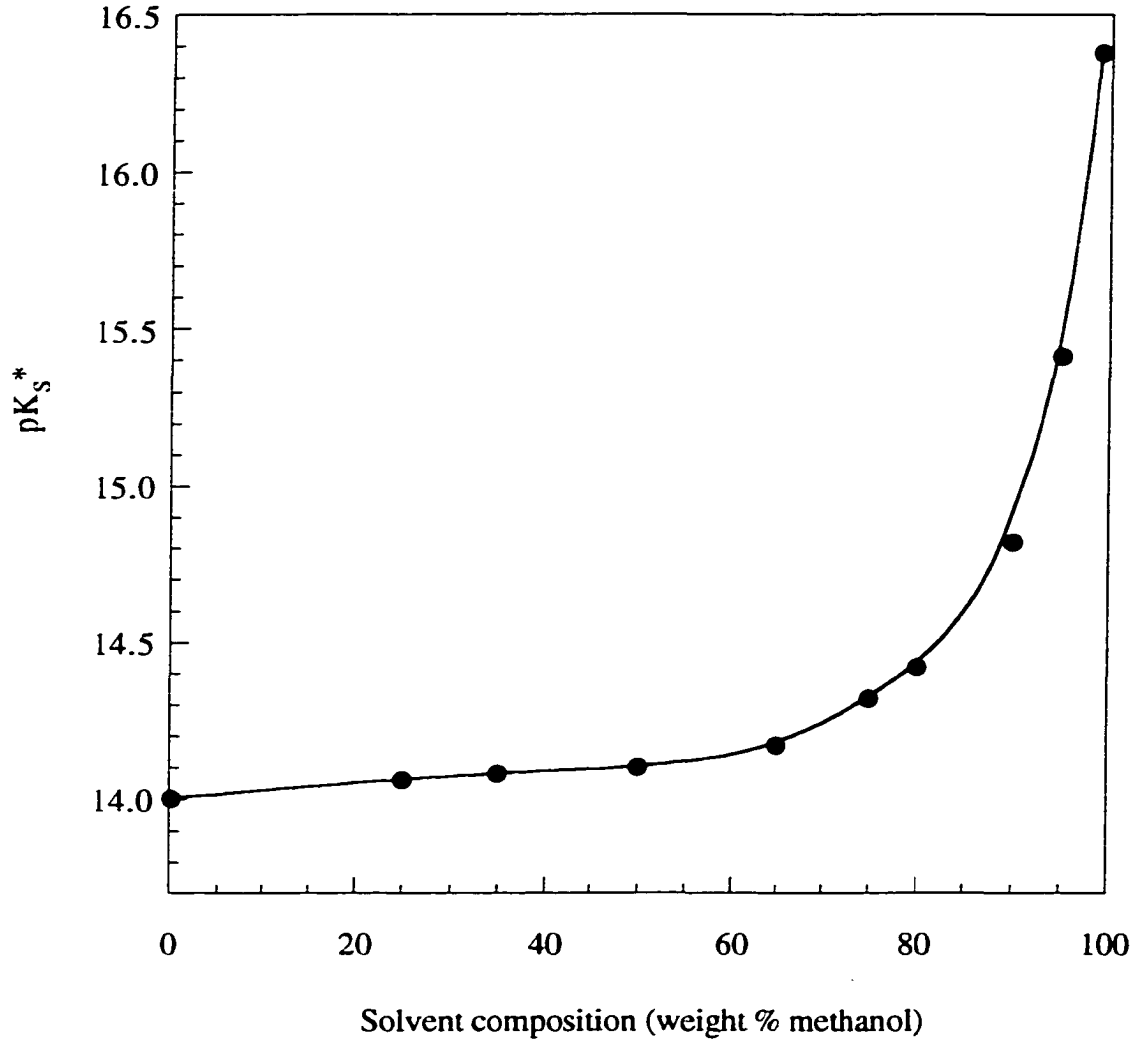

Figure III.22. Plot of thermodynamic solvent autoprotolysis constants as a function of methanol-water solvent composition. The data for the plot was obtained from reference 12.

complexes in water[13] indicated that at 0.1 mM total Pb(II) concentration the only appreciable (≥ 2%) hydrolysis species below pH 7.5 is the $PbOH^+$ cation. Even at the higher concentration of 2.0 mM total lead(II), multinuclear lead complexes do not become important until pH 6.5. In the presence of monensin at pH values above or close to its log K_H^{c*} (6.8) some lead will be complexed, and the concentration of free lead will be decreased, so that the exclusion of multinuclear lead complexes from the model is justified. The same is true for other monomeric species ($Pb(OH)_2$ and $Pb(OH)_3^-$) because in a previous study at low lead(II) concentrations they were not found to be present in solution below pH 8.5[13].

A number of pH* titration data sets were acquired for lead-monensin systems. Experimental titration curves for solutions with various lead-monensin concentration ratios are presented in Figure III.23. For solutions having 1:1 HMon-Pb composition, precipitation was observed at pH* 6.5, therefore data points above this value were not used in the curve fitting process. Equilibria included in the models to fit the experimental data for solutions having 1:1, 2:1 and 3:1 monensin-lead concentration ratios contained the formation reactions of the 1:1 monensin-lead and the ternary 1:1:1 monensin-lead-hydroxide complexes along with that of $PbOH^+$ species. If the ternary complex was excluded from the model while the value for the $PbOH^+$ was allowed to be refined, the resulting formation constant (eq 25) of lead monohydroxy complex was unusually large (about 11.5 in log units). This indicated that the presence of the ternary complex was required in the model for fitting the data, and the value of the equilibrium constant estimated for $PbOH^+$ formation in 80% methanol was kept fixed during further calculations. In addition to the complexes included in the model described above, species of 2:1 Mon-Pb stoichiometry were required to fit the titration data for those solutions that contain an excess of monensin. The curve fits for the titrations of solutions with the 1:1 monensin-lead concentration ratio gave larger values of sigma. It

was necessary to include Pb_2Mon species into the model to improve the match between the experimental and calculated titration curves. The first end-point on the curve occurred at the point when the base concentration was 1/2 to 3/4 of that of total lead, indicating the presence of multinuclear lead species. Because the titration was not complete due to the occurrence of precipitation, large errors might be introduced to the calculated values of equilibrium constants at that solution composition. The species $PbMon_2$ was not important in the model used to fit 1:1 monensin-lead titration data and it was excluded. Introduction of the species PbMonH to all models did not improve the fits. Therefore, it was also omitted from the models used to obtain final results.

Figures III.24, III.25 and III.26 illustrate fits of the pH*-curves obtained using the program BEST. The values of equilibrium constants obtained are listed in Table III.9. Species distribution curves were calculated as a function of p[H] using average values of the equilibrium constants (Table III.10) and are shown in Figures III.27 and III.28. They showed that most complex species, except for the lead-hydroxide complex, were present in the solution in significant amounts ($\geq$ 5%) for both 1:1 and 2:1 monensin-lead concentration ratios.

Table III.9 Log β_X values obtained from potentiometric titrations of monensic acid (HL) and lead (II) in 80% methanol-water[a]

Exp.	HL-Pb	Identity of complex species X						σ_{fit}[f]
No.	ratio	HL[b]	PbL[c]	PbL_2[c]	Pb_2L[c]	PbLOH[c,d]	PbOH[e]	
1	3.3	6.83	7.74	10.83		0.52	-7.96	0.056
2	2.1	6.83	6.88	9.87		-0.22	-7.96	0.017
3	1.6	6.83	7.88	11.14		0.84	-7.96	0.031
4	2.2	6.83	7.23	11.19		1.12	-7.96	0.016
5	2.3	6.83	8.11	11.23		1.22	-7.96	0.026
6	2.0	6.83	7.29	10.75		0.29	-7.96	0.014
7	2.2	6.83	6.80	10.02		-0.40	-7.96	0.014
8	2.0	6.83	6.76	9.81		-0.53	-7.96	0.013
9	2.2	6.83	7.20	10.63		0.02	-7.96	0.024
10	1.0	6.83	6.57		11.29	-0.22	-7.96	0.014
11	0.9	6.83	7.07		12.49	0.87	-7.96	0.038
12	0.81	6.83	7.10		12.39	0.91	-7.96	0.060
13	1.0	6.83	6.97		12.02	0.10	-7.96	0.040

[a] 25.0 °C, ionic strength 0.05 M (TEAP). [b] The value of log β_{HL} was fixed during refinement (section III.B). [c] Values were refined by program BEST. [d] β_{PbOHL} is expressed as an acid dissociation constant (eq III.23). [e] Value was fixed during refinement; it was corrected to 0.05 M ionic strength and estimated for 80% methanol-water, as described in the text. [f] $\sigma_{fit} = (U/N)^{1/2}$, as defined in eq III.5 and III.6.

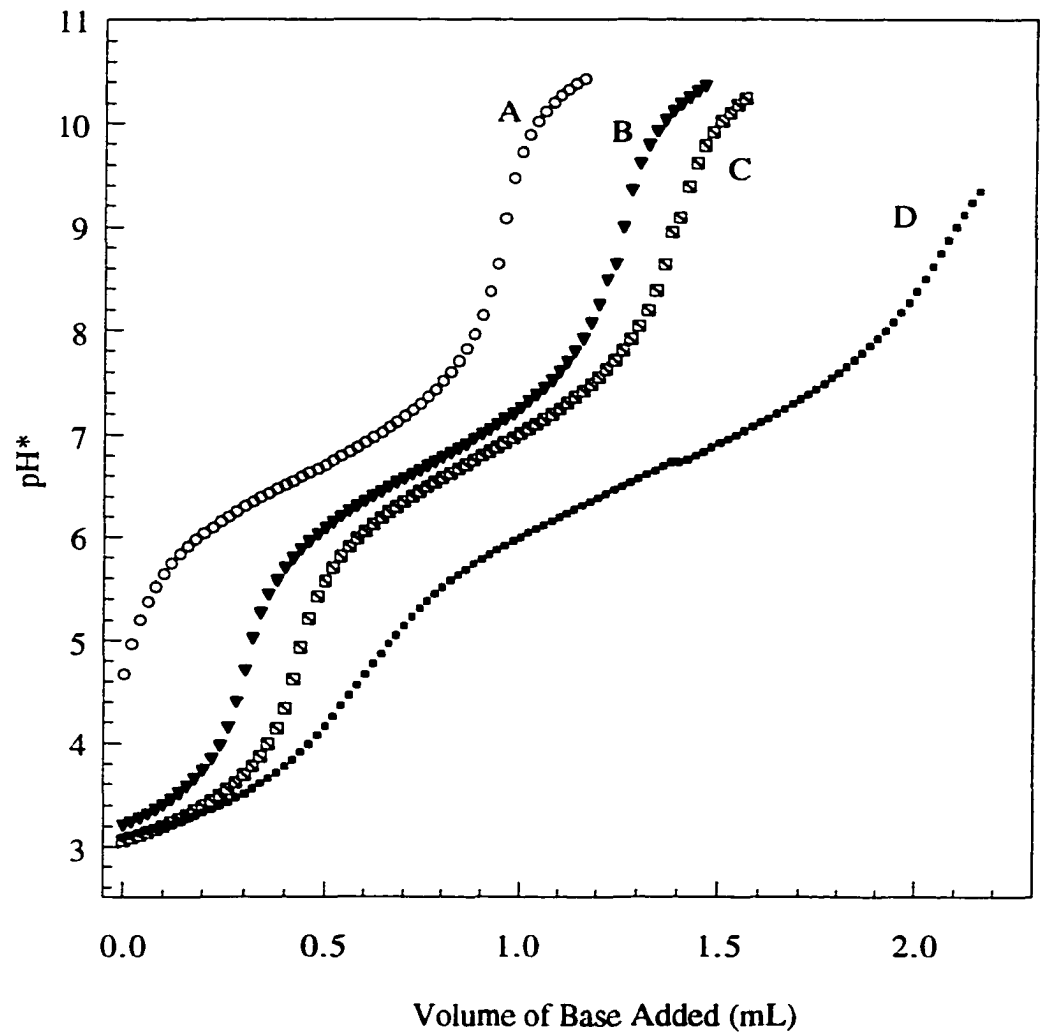

Figure III.23. Potentiometric titration curves for various stoichiometric ratios of monensin-lead in 80% methanol-water at 25.0 °C. Each solution contained 20.0 mL of 0.98 mM free monensin in the acid form. 0.023 M lead(II) perchlorate was added in the amount to obtain the following stoichiometric ratios: A. no Pb; B. 3:1 HMon-Pb; C. 2:1 HMon:Pb; D. 1:1 HMon-Pb. All titrations were done at 0.05 M ionic strength (TEAP).

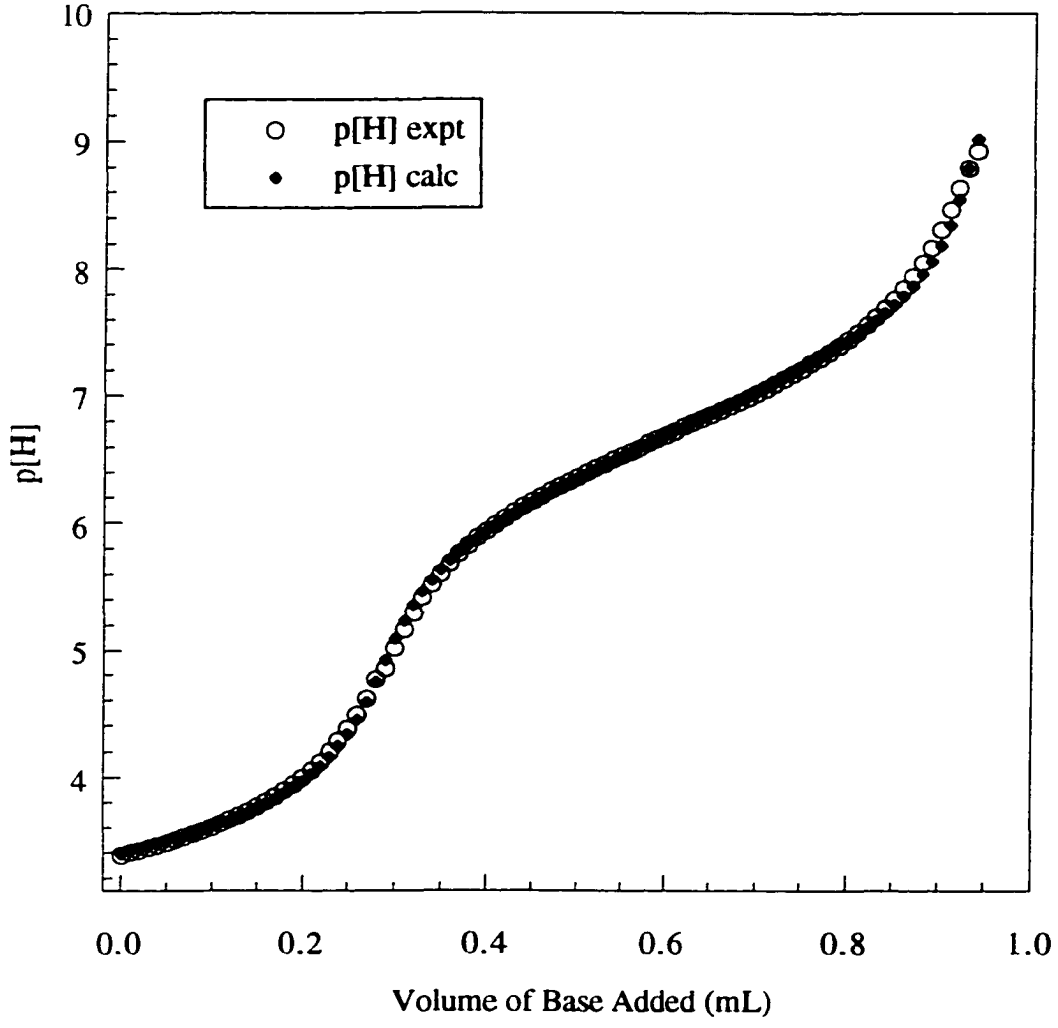

Figure III.24. Potentiometric titration curve for 20.28 mL of a solution containing 0.72 mM monensic acid and 0.32 mM lead(II) at an ionic strength of 0.05 M (TEAP) in 80% methanol-water at 25.0 °C. The titrant is 0.0225 M tetramethylammonium hydroxide with ionic strength maintained at 0.05 M with TEAP. The calculated p[H] values were obtained from the program BEST using refined values of equilibrium constants for the model containing the species listed in Table III.9, Exp.7.

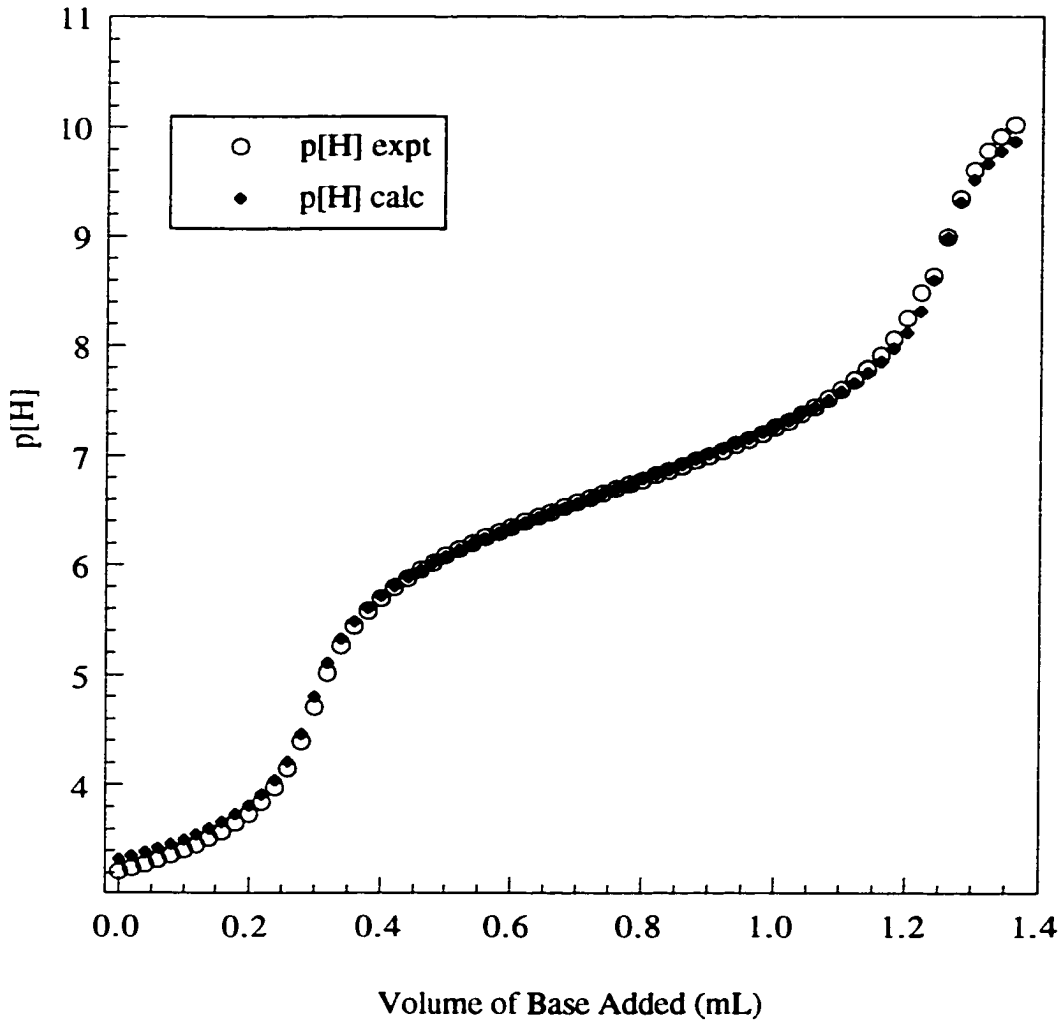

Figure III.25. Potentiometric titration curve for 20.27 mL of a solution containing 1.03 mM monensic acid and 0.32 mM lead(II) at an ionic strength of 0.05 M (TEAP) in 80% methanol-water at 25.0 °C. The titrant is 0.02140 M tetramethylammonium hydroxide with ionic strength maintained at 0.05 M with TEAP. The calculated p[H] values were obtained from the program BEST using refined values of equilibrium constants for the model containing the species listed in Table III.9, Exp.1.

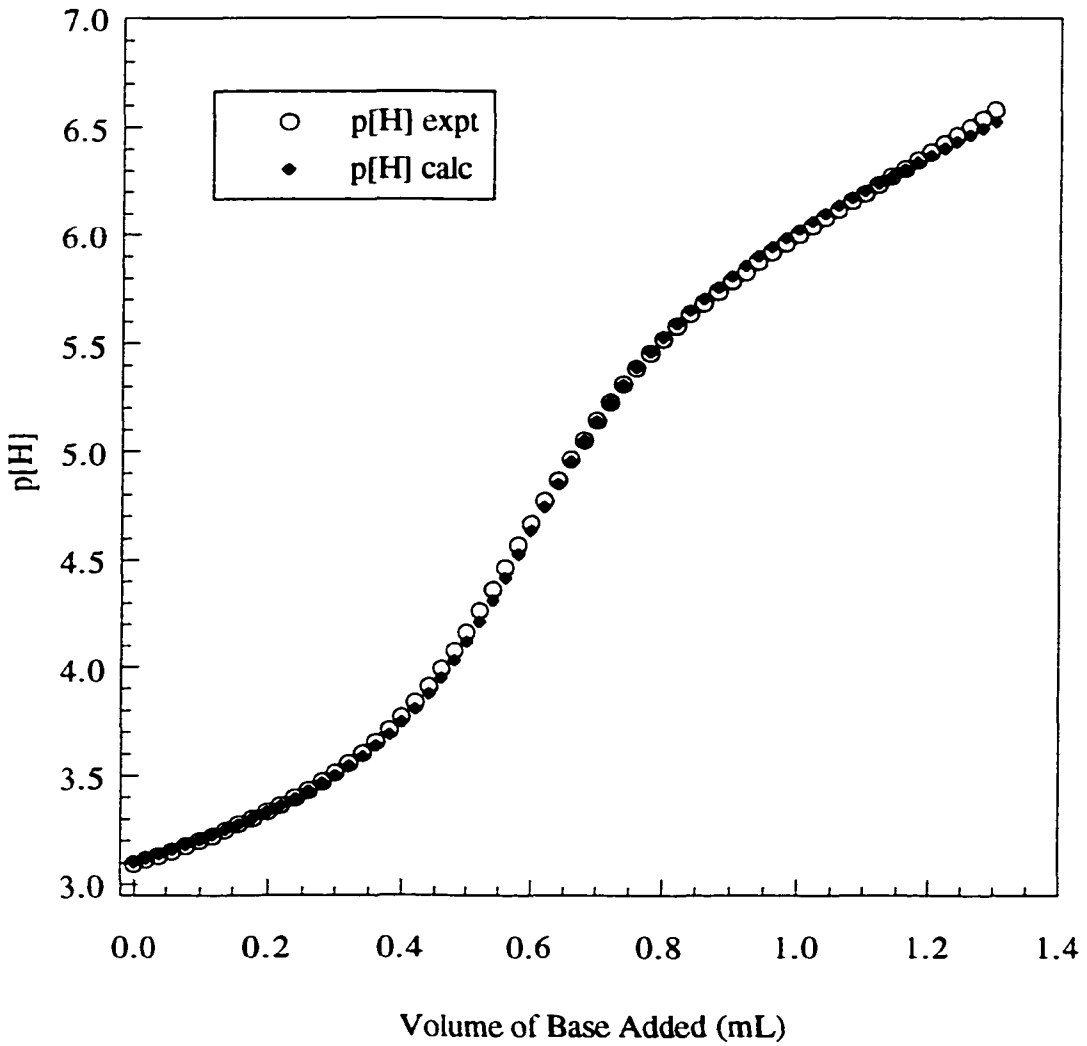

Figure III.26. Potentiometric titration curve for 20.97 mL of a solution containing 0.93 mM monensic acid and 1.11 mM lead(II) at an ionic strength of 0.05 M (TEAP) in 80% methanol-water at 25.0 °C. The titrant is 0.0225 M tetramethylammonium hydroxide with ionic strength maintained at 0.05 M with TEAP. The calculated p[H] values were obtained from the program BEST using refined values of equilibrium constants for the model containing the species listed in Table III.9, Exp.12.

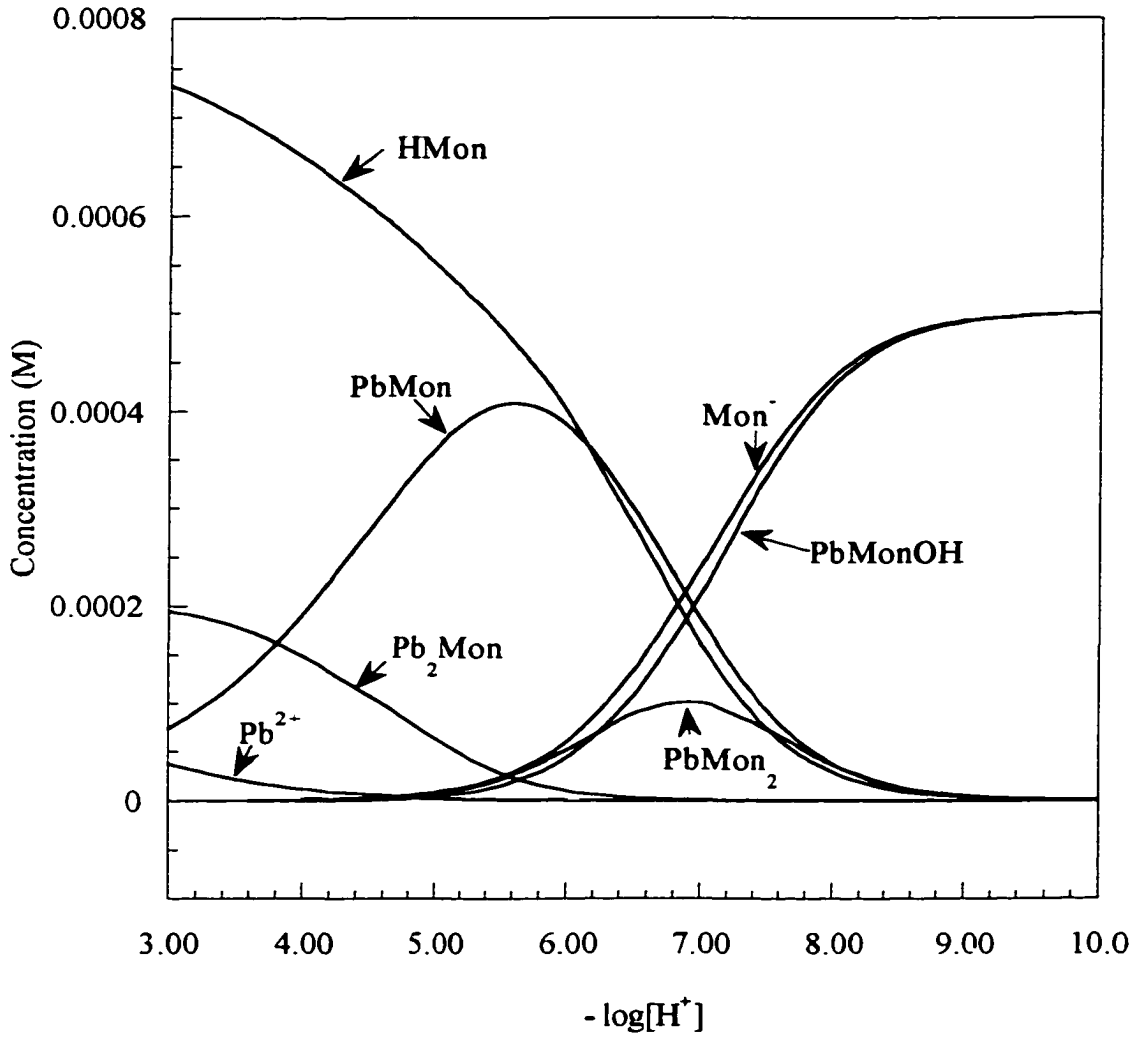

Figure III.27. Species distribution curves for monensin-lead(II) complexes in solution as a function of p[H] in 80% methanol-water. Species concentrations were calculated using the program Comics for 1.0 mM monensin and 0.5 mM lead using the average values of the equilibrium constants listed in Table III.10.

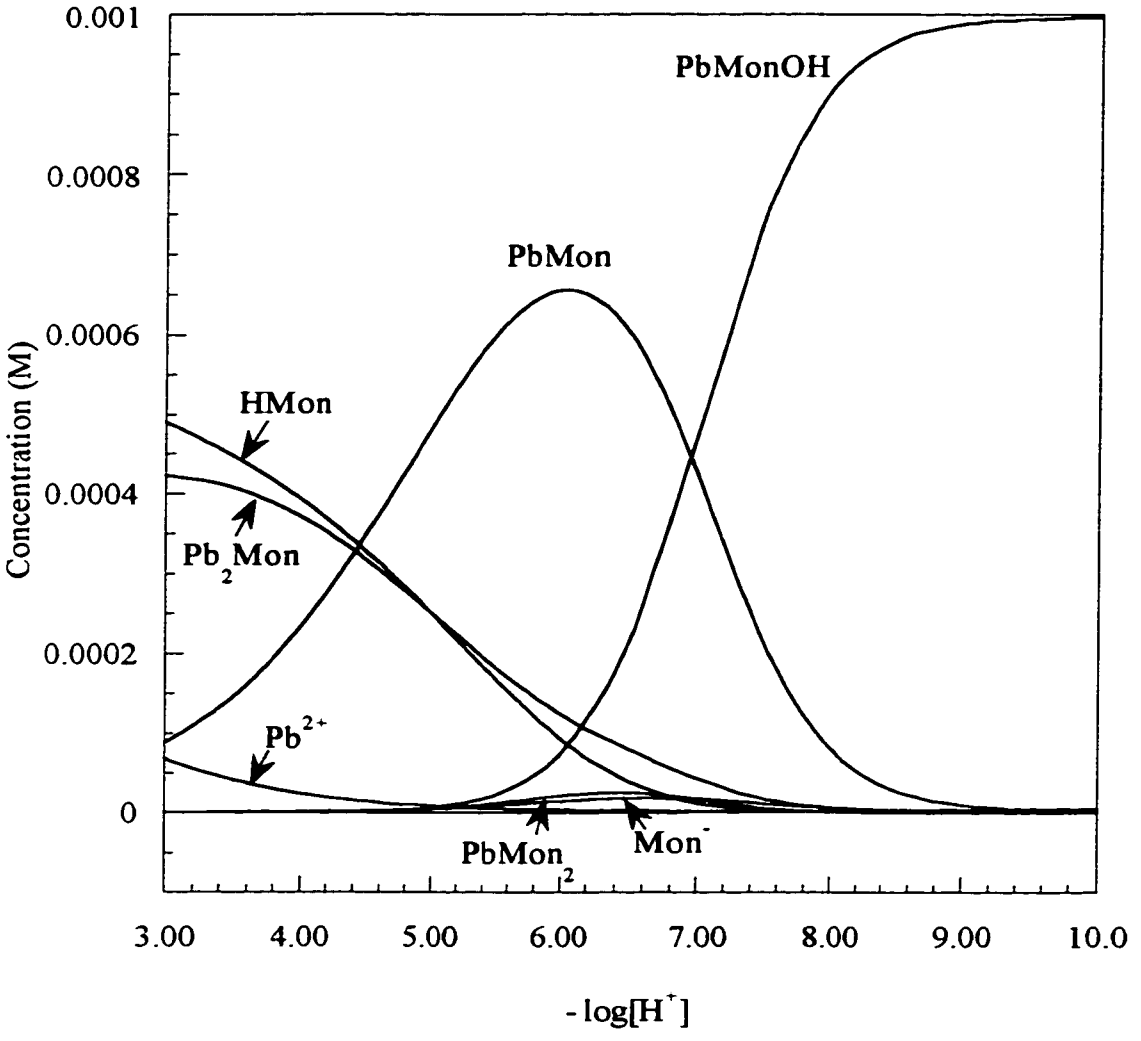

Figure III.28. Species distribution curves for monensin-lead(II) complexes in solution as a function of p[H] in 80% methanol-water. Species concentrations were calculated using the program Comics for 1.0 mM monensin and 1.0 mM lead using the average values of the equilibrium constants listed in Table III.10.

Table III.10. Average values of cumulative equilibrium constants ($\log\beta_X$) for monensin with various ions in 80% methanol-water[a,b]

Ion	Identity of species X[c]				
(M)	ML	ML_2	MLOH[d]	ML_2H	M_2L
H^+	6.83±0.05 (11)	-	-	-	-
Na^+	5.0±0.1 (4)	8.22±0.02[e] (1)	-	15.2±0.2 (3)	-
Ca^{2+}	3.10±0.06 (3)	-	-	-	-
Zn^{2+}	3.74±0.05 (3)	-	-3.6±0.2 (3)	-	-
Pb^{2+}	7.25±0.46(13)	10.6±0.6 (9)	0.3±0.6 (13)	-	12.0±0.5(4)

[a] 25.0 °C; ionic strength 0.05 M (TEAP). [b] Uncertainty expressed in terms of one standard deviation; the number of replicate measurements is indicated in parenthesis. [c] L represents monensin ligand. [d] β_{MLOH} is expressed as an acid dissociation constant (eq III.23). [e] Uncertainty as sigma fit, $\sigma_{fit} = (U/N)^{1/2}$, as defined in eq III.5 and III.6.

III.E. NMR studies of free monensin and monensin complexes. Peak assignments in monensin-sodium, monensin-tetramethylammonium complexes and monensin free acid.

The purpose of the NMR experiments was to determine the ligand binding sites and to qualitatively compare the solution structure of the lead-antibiotic complex to that of the sodium or calcium complexes or that of the free ligand. One approach to this consists of comparing differences in the chemical shifts ($\Delta\delta^{13}C$) of the ionophore in the lead complexes with the uncomplexed anion of the ionophore and with the ionophore complexed to other metals. Therefore, NMR spectra of monensin complexes with lead and other cations and of the free monensin ligand were required. Of special interest are the properties of carbon atoms located next to oxygen donor atoms involved in metal binding in the complexes. Although assignments of ^{1}H and ^{13}C peaks in the NMR spectra of various monensin compounds were available in literature[15,16], their new NMR spectra were recorded in this work. The experimental peak positions were compared to the known values of the chemical shifts to assure that different equipment and conditions did not have an effect on the NMR data.

The numbering scheme for monensin A that was used in this work, was adopted from the most recent publications[15,17] and is shown in Figure III.29. ^{1}H and ^{13}C spectra were recorded for monensin sodium and tetraethylammonium salts and monensin free acid in both deuterated chloroform and methanol solvents. NMR spectra for the sodium monensin complex were also obtained in 80% CD_3OH-D_2O solvent mixture. Because 80% methanol-water was used as a solvent for the solution equilibria studies in this work and in other similar reports from this research group, it was important to compare the data in pure methanol and in the solvent mixture to identify any structural differences, as well as similarities, that might result from this difference in the solvent polarity.

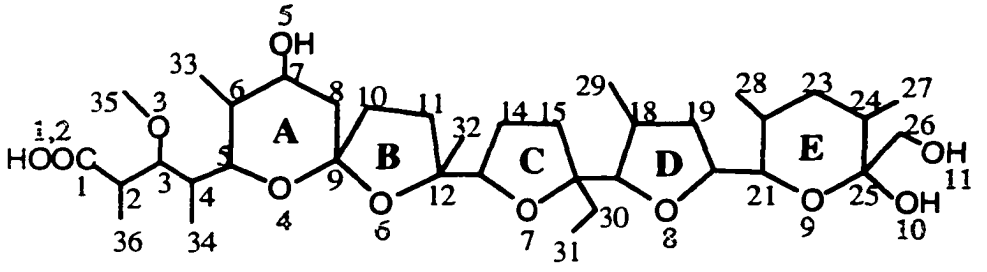

Figure III.29. Monensin A molecule with carbon (plain style) and oxygen (in bold) numbering schemes.

Several two-dimensional techniques were employed in order to help assign resonances in the NMR-spectra. These experiments included COSY[18,19] (^{1}H-^{1}H Correlated Spectroscopy) and homonuclear J-resolved 2-dimensional spectroscopy[20] (J-homo) to help find ^{1}H-^{1}H connectivities through bonds and the multiplicities of ^{1}H signals; J-resolved carbon experiments APT[21,22] (Attached Proton Test) and DEPT[23] (Distortionless Enhancement by Polarization Transfer) to assign multiplicities to carbon signals; and HETCOR[24,25] (Heteronuclear Correlation spectroscopy) and HMQC[26,27] (Heteronuclear Multiple Quantum Coherence) to find single-bond carbon-proton connectivities. The peaks in the ^{1}H and ^{13}C NMR spectra were assigned mostly by, first, comparison to the known values, and, second, the use of the two-dimensional techniques described above. The experimental and literature values of ^{1}H and ^{13}C chemical shifts for the sodium salt in $CDCl_3$ and CD_3OD, and experimental values in 80% CD_3OH-D_2O are listed in Tables III.11 and III.12. Some of the ^{1}H signal multiplicities in the sodium monensin complex are listed along with the similar information taken from the literature[28,29]. The assignments and corresponding literature

values of the chemical shifts for tetramethylammonium monensin and monensin free acid NMR spectra in CD_3OH and $CDCl_3$ are listed in the Tables III.13-III.16. Because most values of the experimentally obtained chemical shifts were close to those found in literature, it was not critical to obtain all of them. The tables contain values for most of the protons and carbons with the gaps corresponding to the heavily overlapping regions, where assignments were not attempted. Only literature values for ^1H and ^{13}C chemical shifts are listed in the tables for monensic acid in CD_3OH. The ^1H and ^{13}C NMR spectra obtained for the sodium-monensin complex in 80% CD_3OH-D_2O are shown in Figures 30 and 31, respectively. The ^{13}C and ^1H chemical shifts in this solvent mixture were not different from those in pure methanol.

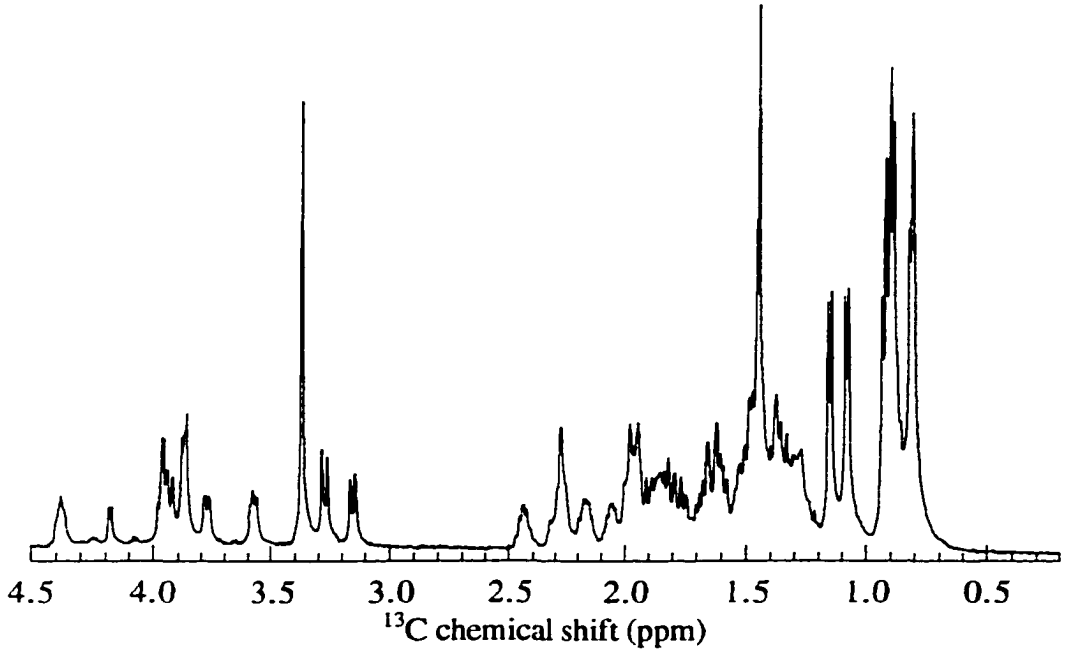

Figure III.30. ^1H NMR spectrum of the sodium-monensin complex in 80% CD_3OH-D_2O.

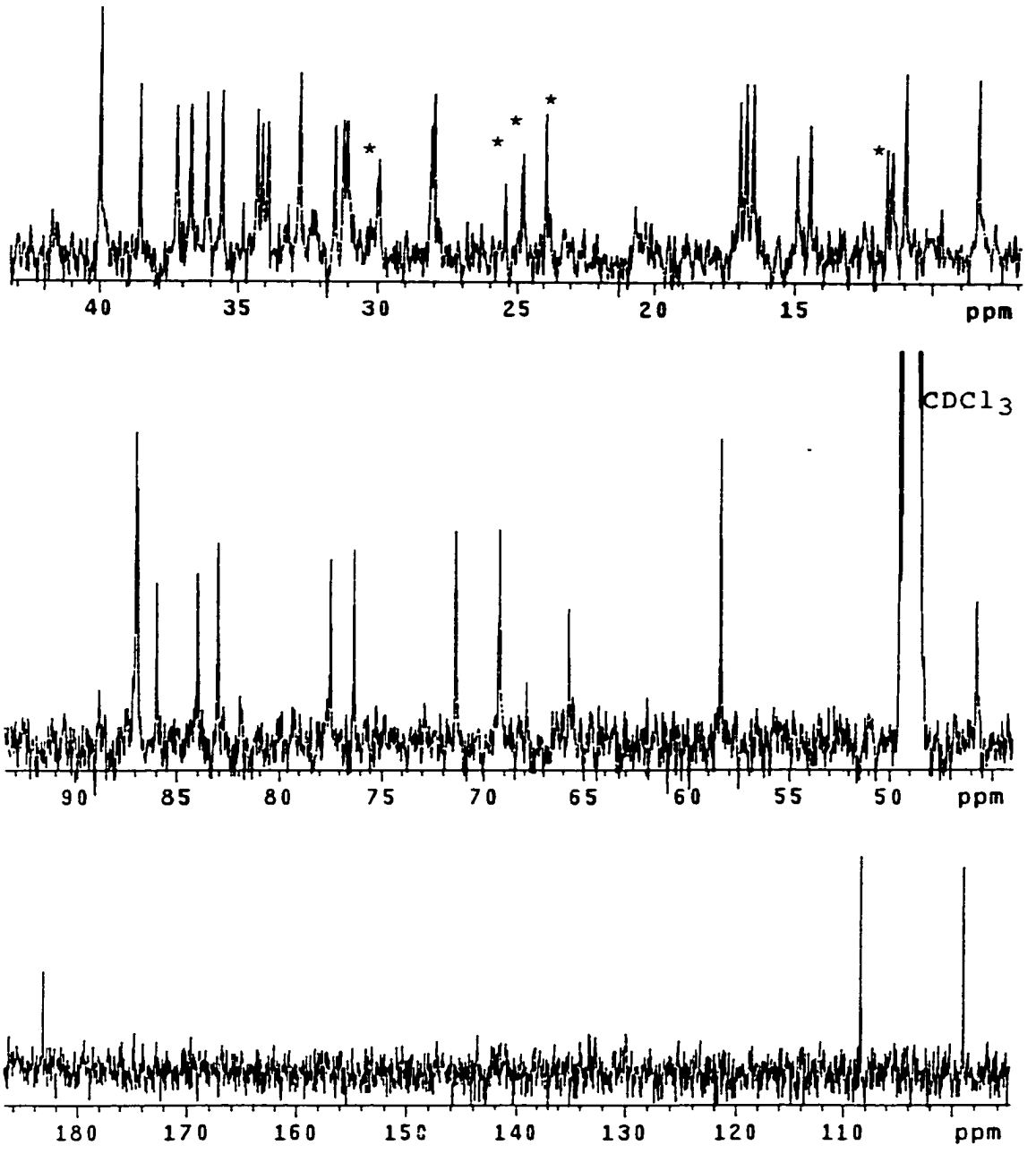

Figure III.31. ^{13}C NMR spectrum of sodium-monensin complex in 80% CD_3OH-D_2O. Peaks with an asterisk mark may result from the unknown impurity. Large peak at 49 ppm is from $CDCl_3$ solvent.

Table III.11. ^{1}H and ^{13}C NMR chemical shifts of sodium monensin in CD_3OD and 80% CD_3OH-D_2O at 25 °C (experimental values) or at room temperature (literature values) and in ppm

carbon #	^{1}H CD_3OD experim[a].	^{1}H 80% CD_3OH-D_2O experimental	^{1}H CD_3OH literature[a,b]	^{13}C CD_3OH experim.	^{13}C 80% CD_3OH-D_2O, experim.	^{13}C, CD_3OD literature[b]
1	-	-	-	183.37	183.30	183.4
2	2.59(dq)	2.44	2.54(dq)	45.98	45.76	46.0
3	3.12(dd)	3.15	3.12(dd)	83.17	83.05	83.2
4	2.07(ddd)	2.06	2.05(dqd)	38.56	38.55	38.6
5	3.96(dd)	3.96	4.16(dd)	69.1	61.23	69.1
6	2.02(dd)	2.00	2.02(dd)	36.151	36.16	36.1
7	3.89(q)	3.87	4.10 (	71.57	71.41	71.6
8	1.99,1.67	1.96,1.63	2.05,1.73(dd)	34.24	34.32	34.3
9	-	-	-	108.4	108.40	108.4
10	1.85	1.85	1.85	40.15	40.00	40.2
11	1.92	1.91	2.00	32.89	34.8	34.4
12	-	-	-	86.81	86.86	86.8
13	3.60	3.58	3.89(dd)	83.9	84.01	84.0
14			1.97,1.57(qd)	28.06	28.01	28.1
15	2.34,1.48	2.31	2.43,2.43(td)	31.28	31.50	31.3
16	-	-	-	87.02	86.96	87.1
17	4.00(d)	4.18	4.09(d)	85.89	85.97	85.9
18	2.30(q)	2.27	2.37(q)	35.7	35.61	35.7
19	2.21,1.61	2.16,1.59	2.30,1.69	34.03	34.13	34.1
20	4.42(dq)	4.38	4.52(dq)	77.52	77.44	77.6
21	3.84(dd)	3.78	3.95(q)	76.22	76.29	76.2
22	1.45	1.39	1.51(qd)	32.9	32.78	33.9
23	1.54		1.63(td)	36.44	36.74	36.9
24	1.57		1.63	36.9	37.22	37.5
25	-	-	-	99.16	99.08	99.2
26	3.89,3.28	3.93, 3.27	4.00,3.38(d)	65.78	65.72	65.8
27	0.85(d)	0.81	0.94(d)	16.49	16.51	16.5
28	0.83(d)	0.80	0.93(d)	16.97	16.99	17.0
29	0.93(d)	0.89	1.04(d)	14.93	14.93	14.9
30	1.72,1.46	1.77, 1.47	1.80,1.57	31.11	31.18	31.1
31	0.94(t)	0.90	1.03(t)	8.32	8.41	8.3
32	1.48(d)	1.45	1.57(d)	28.13	28.10	28.1
33	0.95(d)	0.92	1.04(d)	10.99	10.99	11.0
34	1.10(d)	1.08	1.19(d)	11.5	11.63	11.5
35	3.37(s)	3.37	3.47(s)	58.26	58.43	58.3
36	1.17(d)	1.14	1.26(d)	16.76	16.78	16.8

[a] Letters in parenthesis show the multiplicity of proton signals: 's' stands for singlet, 'd' stands for doublet, 't' stands for triplet, and 'q' stands for quartet. [b] From reference 15. Signal multiplicities were obtained from Refs. 28 and 29.

Table III.12. ^{1}H and ^{13}C NMR peak chemical shifts for the sodium monensin in $CDCl_3$ in ppm

	^{1}H 25.0 °C experimental	^{1}H room temp. literature[a]	^{13}C 25.0 °C experimetal	^{13}C –40 °C experimental	^{13}C room temp. literature[a]
1	-	-	181.10	180.90	181.20
2	2.51	2.530	44.98	44.64	45.07
3	3.17	3.190	82.93	82.49	83.11
4	2.04	2.066	37.41	38.13	37.50
5	4.01	4.029	68.28	67.99	68.33
6	2.22	2.216	34.80	34.57	34.87
7	3.86	3.895	70.38	69.82	70.51
8	1.89,1.65	1.91,1.69	33.39	33.12	33.56
9	-	-	106.90	106.58	107.03
10	1.99,1.67	2.011,1.704	39.19	38.83	39.28
11	1.98,1.72	1.981,1.718	33.15	32.78	33.25
12	-	-	85.14	85.16	85.26
13	3.52	3.540	82.46	82.32	82.52
14	1.72,1.55	1.779,1.536	27.24	27.25	27.26
15	2.27,1.47	2.304,1.468	29.79	29.20	29.91
16	-	-	85.78	85.44	85.90
17	3.92	3.938	84.91	84.84	84.94
18	2.26	2.261	34.29	33.90	34.39
19	2.19,1.51	2.185,1.551	33.21	32.90	33.33
20	4.37	4.403	76.40	76.10	76.45
21	3.80	3.828	74.40	74.20	74.51
22	1.36	1.36	31.81	31.59	31.87
23	1.39,1.26	1.41,1.32	35.60	35.02	35.75
24	1.46	1.46	36.48	36.90	36.56
25	-	-	98.21	97.79	98.31
26	3.96,3.27	3.977,3.298	64.82	64.53	64.92
27	0.83	0.849	16.03	16.07	16.03
28	0.81	0.810	16.68	16.79	16.72
29	0.90	0.903	14.54	14.50	14.56
30	1.58,1.45	1.598,1.507	30.62	30.73	30.60
31	0.94	0.944	8.20	8.40	8.14
32	1.49	1.507	28.89	28.64	27.47
33	0.91	0.939	10.55	10.44	10.48
34	1.16	1.178	11.03	11.34	10.97
35	3.36	3.381	57.87	57.86	57.84
36	1.23	1.238	16.79	16.70	16.72

[a] From reference 28.

Table III.13. ^{13}C NMR chemical shifts of tetramethylammonium monensin in ppm

carbon #	CD_3OH 25 °C experiment.	CD_3OH room temp. literature[a]	$CDCl_3$ 25.0 °C experimental	$CDCl_3$ -40 °C experimental	$CDCl_3$ room temp. literature[a]
1	184.0	183.7	180.29	180.97	180.29
2	45.38	45.6	43.85	43.40	43.42
3	86.36	86.3	83.32	83.95	82.52
4	39.09	39.1	37.28	36.90	37.13
5	69.13	69.2	68.36	68.34	68.13
6	38.54	38.4	35.15	35.07	35.50
7	73.01	73.0	70.85	70.08	70.99
8	35.52	35.6	34.46	34.39	34.46
9	108.82	108.8	107.26	106.88	107.31
10	40.54	40.5	39.26	38.81	39.12
11	32.81	32.8	32.56	32.33	32.33
12	87.88	87.9	85.05	85.27	86.33
13	85.42	85.3	82.55	82.62	83.44
14	28.99	29.0	27.95	27.54	27.593
15	32.47	32.5	31.12	30.59	31.25
16	89.01	89.0	86.40	86.16	86.68
17	86.89	86.9	85.05	84.85	85.31
18	36.55	36.5	34.91	34.90	34.85
19	36.09	36.2	33.20	33.67	33.86
20	79.75	79.7	77.19	77.00	77.22
21	78.20	78.2	75.56	74.47	75.74
22	35.37	35.3	32.83	32.81	33.18
23	38.24	38.3	36.95	36.61	36.98
24	34.65	34.9	34.91	34.68	35.21
25	98.72	98.7	97.00	97.14	96.60
26	67.20	67.5	67.17	66.55	67.10
27	16.50	16.5	16.37	16.59	16.21
28	18.26	18.3	17.47	17.47	17.44
29	16.51	16.5	15.91	15.75	15.74
30	30.10	30.7	29.66	29.00	29.68
31	8.29	8.3	8.14	8.28	8.01
32	26.09	26.0	25.93	26.46	25.65
33	11.85	11.8	10.86	10.70	10.86
34	12.90	14.1	12.15	12.27	12.27
35	59.58	59.5	57.86	57.56	57.86
36	14.11	13.1	14.72	14.63	13.81
Me	55.83	-	55.93	54.53	

[a] From reference 16.

Table III.14. ^1H NMR chemical shifts of tetramethylammonium monensin in ppm

carbon #	CD_3OD 25 °C experimental	CD_3OD room temp. literature[a]	$CDCl_3$ at 25 °C experimental	$CDCl_3$ room temp. literature[a]
2	2.41	2.60	2.42	2.38
3	3.65	3.85	3.60	3.49
4	1.85	2.42	2.05	1.98
5	4.22	4.11	4.06	3.96
6	1.82	1.90	1.83	1.97
7	3.71	4.11	3.75	3.68
8	2.11, 1.69	2.21,1.90	1.95, 1.72	1.90, 1.60
10	1.91 -	2.14,1.93	1.85 -	1.88,1.70
11	- -	2.32,1.89	1.77 -	1.78, 1.69
13	3.73	3.92	3.56	3.44
14	1.99, 1.65	2.02,1.84	1.67, 1.48	1.61,1.39
15	2.08, 1.94	2.22,1.95	2.15, 1.42	2.08, 1.43
17	3.94	4.13	3.96	3.87
18	2.32	2.49	2.27	2.17
19	2.22, 1.57	2.42,1.77	2.18, 1.44	2.09,1.43
20	4.19	4.39	4.28	4.19
21	3.54	3.74	3.81	3.73
22	1.41	1.59	1.31	1.26
23	1.46, 1.32	1.65,1.52	1.87, 1.38	1.85, 1.34
24	1.83	2.05	1.55	1.74
26	3.46, 3.36	3.67,3.56	3.52, 3.47	3.37, 3.37
27	0.87	1.07	0.89	0.81
28	0.93	1.13	0.86	0.80
29	1.00	1.19	0.92	0.87
30	1.60	1.80,1.80	1.49	1.46, 1.34
31	0.92	1.11	0.91	0.85
32	1.35	1.54	1.40	1.32
33	0.93	1.12	0.95	0.75
34	0.99	1.19	1.05	0.95
35	3.39	3.59	3.38	3.26
36	1.09	1.29	1.18	1.11

[a] From reference 16.

Table III.15. ^1H NMR chemical shifts of monensin free acid in ppm

carbon #	$CDCl_3$ room temperature literature[a]	$CDCl_3$ 25 °C experimental	CD_3OD room temperature literature[a]
2	2.63	2.61	2.68
3	3.22	3.21	3.69
4	2.17	2.17	2.20
5	4.07	4.04	3.93
6	2.10	2.10	1.83
7	3.86	3.84	4.10
8	1.99, 1.70	1.87, 1.69	1.80, 1.80
10	1.95, 1.65	-	2.22, 1.72
11	1.91, 1.68	-	2.05, 2.05
13	3.46	3.47	4.04
14	2.25.0, 1.64	-	1.90, 1.70
15	2.21, 1.37	-	2.21, 1.90
17	4.07	4.07	4.04
18	2.24	2.23	2.38
19	2.23, 1.42	2.21, 1.61	2.29, 1.62
20	4.33	4.23	4.30
21	3.94	3.86	3.68
22	1.30	-	1.48
23	1.50, 1.35	-	1.45, 1.45
24	1.49	-	1.90
26	3.68,3.50	3.67, 3.49	3.57, 3.47
27	0.87	0.88	0.96
28	0.86	0.85	1.00
29	0.94	0.92	1.08
30	1.57, 1.57	-	1.68, 1.68
31	0.97	0.95	1.03
32	1.50	1.47	1.43
33	0.89	0.88	1.01
34	1.10	1.09	1.07
35	3.38	3.36	3.45
36	1.28	1.27	1.25.0

[a] From reference 16.

Table III.16. ^{13}C NMR chemical shifts of monensin free acid in ppm

carbon #	CD_3OD room temp. literature[a]	$CDCl_3$ 25.0 °C experimental	$CDCl_3$ -40 °C experimental	$CDCl_3$ room temp. literature[a]
1	179.1	177.13	177.43	177.20
2	42.0	41.98	42.17	42.00
3	83.4	81.56	81.00	81.70
4	38.5	36.68	36.20	36.80
5	69.1	66.99	66.76	67.10
6	37.7	34.50	34.38	34.9
7	72.8	70.70	70.14	71.0
8	35.4	34.09	33.80	34.5
9	108.9	107.78	107.56	107.9
10	40.3	38.37	38.13	38.5
11	32.6	33.75	33.39	33.9
12	87.9	85.11	84.85	85.3
13	85.2	83.44	83.05	83.6
14	26.1	27.86	27.75	27.9
15	36.2	32.56	32.14	32.7
16	89.0	86.33	86.35	86.4
17	86.8	84.95	84.45	85.10
18	36.5	34.43	34.12	34.6
19	35.9	31.52	31.17	31.6
20	79.5	77.09	76.63	77.4
21	78.0	73.77	73.34	74.0
22	35.2	32.84	32.62	32.9
23	38.2	35.61	34.99	36.8
24	34.9	36.68	36.10	35.8
25	98.6	97.06	96.91	97.20
26	67.3	67.91	67.66	68.0
27	16.5	16.39	16.57	16.40
28	18.2	17.58	17.68	17.8
29	16.4	15.79	15.75	15.8
30	30.4	31.18	31.38	31.2
31	8.4	8.62	8.83	8.60
32	29.0	27.73	27.65	27.8
33	11.5	10.35	10.20	10.4
34	12.9	10.75	10.96	10.8
35	58.9	58.02	58.05	56.1
36	12.2	15.65	15.75	15.7

[a] From reference 16.

NMR peak assignments in monensin-lead complexes.

In order to obtain NMR spectra for lead-monensin complexes, the samples were prepared by dissolving the isolated 2:1 monensin-lead compound in the appropriate solvent. The complex prepared by the reaction between solid lead oxide and the free acid form of monensin was used for all experiments. The spectra of the lead-monensin complex in methanol were acquired at 25.0° C. The system behavior was checked by recording ^{1}H spectra in temperature range from +50° C to –70° C. Changing temperature in this range did not result in better spectral resolution and room temperature was chosen for all experiments in methanol. Only one broad signal was present for each proton and carbon of monensin in the NMR spectra in methanol, the signal was assumed to occupy an average position between those from two different monensin ligands. This assumption was based on the behavior of the previously studied 2:1 monensin-calcium[17] and lasalocid-calcium[30] systems where the two ionophore ligands were found to be different with respect to their conformations and metal binding sites, but only one signal for each carbon and proton was found in their NMR spectra at room temperature. When NMR spectra were obtained for the monensin-lead complex using 80% methanol-water solvent, the peaks from proton signals of the lead-monensin complex became broader. It was assumed that the system behavior would be similar to that in pure methanol, and the ^{1}H and ^{13}C NMR spectra in 80% methanol-water were also recorded at 25 °C.

^{1}H NMR spectra of the lead-monensin complex in chloroform were first obtained at 25.0 °C and contained very broad peaks. However, decreasing the temperature to –40 or –50 °C resulted in a significant improvement of the spectral resolution; therefore, all NMR studies of lead-monensin complexes in chloroform were carried out at –40 °C. Two signals were identified for each carbon in the ^{13}C broadband decoupled NMR spectra, shown in Figures III.32 and III.33. It was assumed that the two sets of signals arose from two monensin ligands and indicated that the corresponding atoms were in

were in different chemical environments. Figure III.33 illustrates signals in the ^{13}C NMR spectra at 25 °C and –40 °C in a selected chemical shift region.

Most signals in the NMR spectra acquired were assigned using the following general procedure. The process started by comparing the signals in the ^{13}C and ^{1}H NMR spectra of the lead-monensin complex to the known positions of the corresponding peaks in the spectrum of the sodium complex. Because most peaks in ^{13}C spectra are well separated, their assignment did not present any difficulties. However, there are regions in both ^{1}H and ^{13}C NMR spectra, where the peak overlap is possible. A slight displacement of a given peak in the spectrum of the lead-monensin compound from its known position in the spectrum of the sodium complex could result in errors for assignment of several signals. Other techniques aided in separation and assignment of the resonance signals from carbons and protons in those regions.

The APT experiment identified the number of protons connected to each carbon in question and, thus, helped in distinguishing carbon signals. In this spectrum peaks from tertiary and primary carbons are negative and those from secondary and quaternary carbons are positive. Apart from the carboxylate carbon (C1), signals from four 'quaternary' carbons situated next to oxygens (C9, C25, C12 and C16) in the monensin molecule are located most downfield in the NMR spectrum, and their peaks are positive in the APT spectrum. Seven carbons are tertiary so that their signals are negative, and are located next to oxygen atoms which gives chemical shifts in the general area of 40-85 ppm. There is only one signal in that region from a secondary carbon (C26) which was easily distinguishable by APT. A number of signals from tertiary (six) and secondary (eight) carbons that are not bound to oxygens were also recognized. A portion of the APT spectrum obtained for the lead-monensin complex in chloroform at –40 °C is shown in Figure III.34.

To further separate the ^{13}C signals in those groups, HMQC ^{1}H-^{13}C correlation plots were obtained. Correlations of carbon shifts with the chemical shifts from attached protons provided the necessary information to complete the assignments. An example of a ^{1}H NMR spectrum obtained for the lead-monensin complex in chloroform at –40 °C is shown in Figure III.35. Although ^{1}H signals were heavily overlapped in the region between 1.5 and 2.3 ppm, resonances from protons located at a distance of two bonds from oxygen, were better separated (3 – 4.5 ppm).

The COSY NMR experiment aided in ^{1}H peak assignments in that it identified protons located at a distance of two to three bonds of each other through the vicinal and geminal coupling of their signals and, consequently, allowed the assignments of the attached carbon atoms also to be made. Thus, a cross-peak located at coordinates (3.91; 4.46) showed a coupling between protons 21 and 20 of the same monensin ligand, and allowed their identification. An example of a COSY spectrum is shown in Figure III.36.

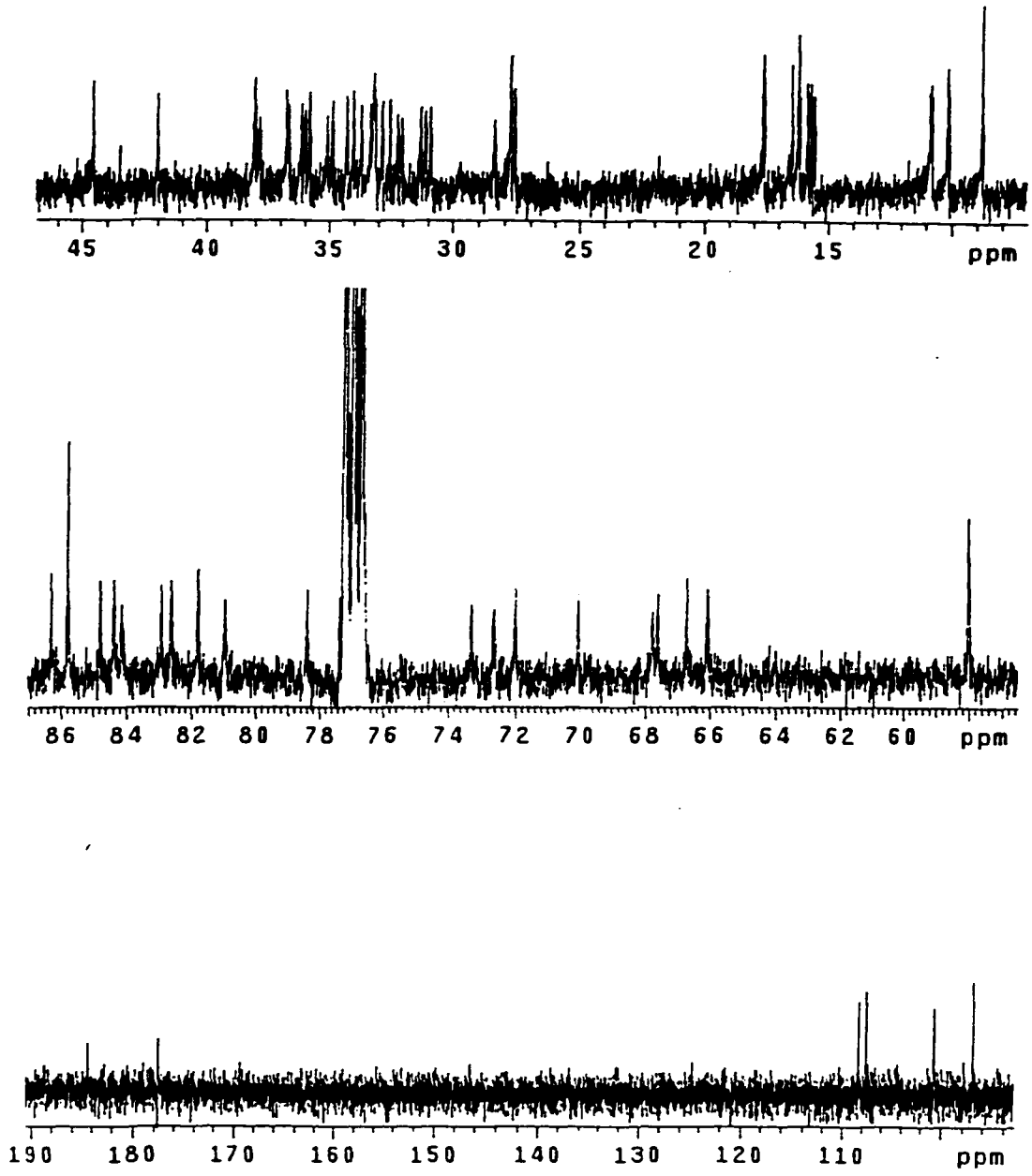

Figure III.32. ^{13}C NMR spectrum of lead-monensin complex in chloroform, acquired at –40 °C with broadband ^{1}H decoupling. Two peaks are observed for each carbon atom. The large triplet at 77.0 ppm is due to the $CDCl_3$ solvent.

A.

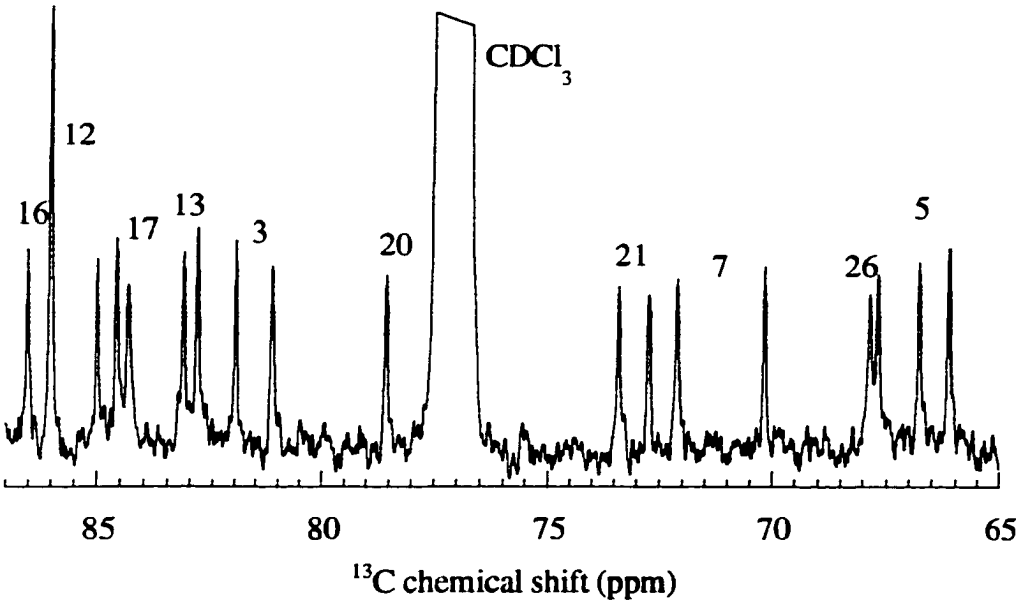

B.

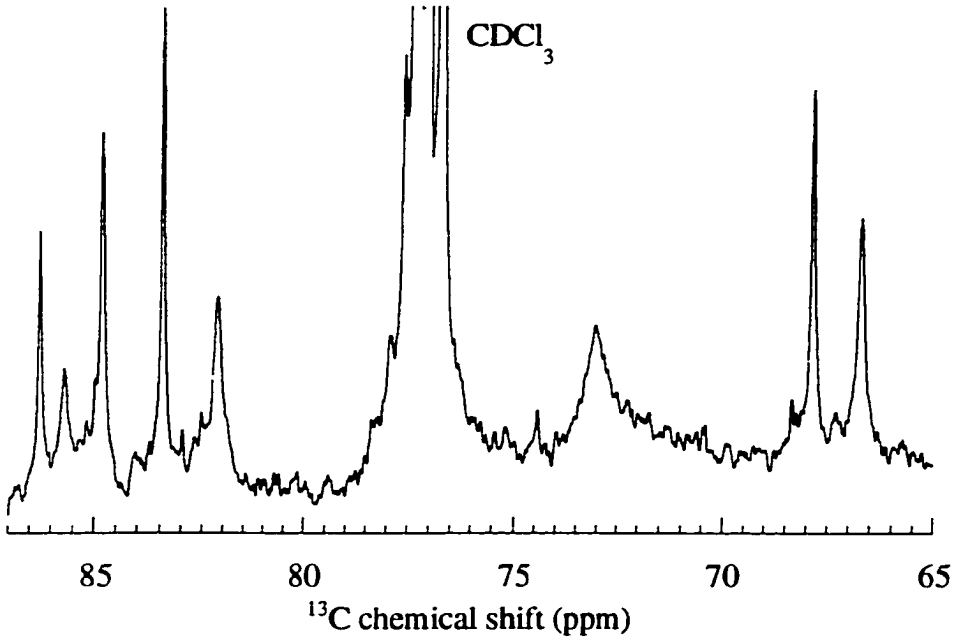

Figure III.33. Selected region in the ^{13}C NMR spectrum of the lead-monensin complex in chloroform: A. at –40 °C; B. at 25 °C. The large triplet at 77.0 ppm is due to chloroform.

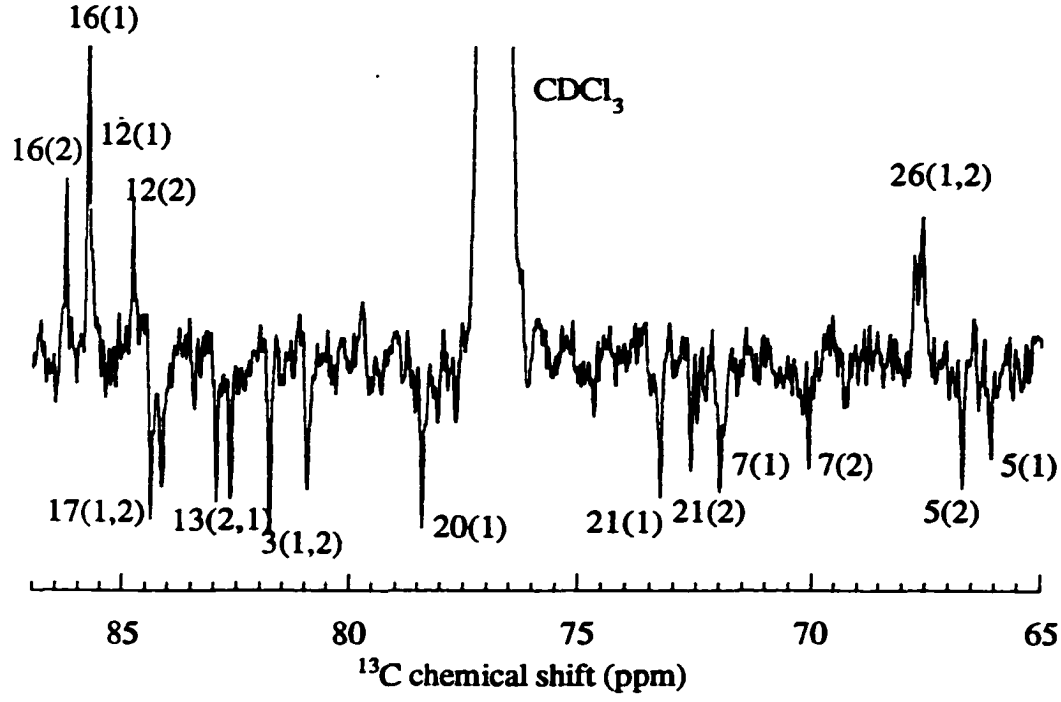

Figure III.34. The region in the J-resolved carbon spectrum (APT) of lead-monensin complex in chloroform obtained at –40 °C. The peaks from tertiary carbons are negative whereas those from secondary and quaternary carbons are positive.

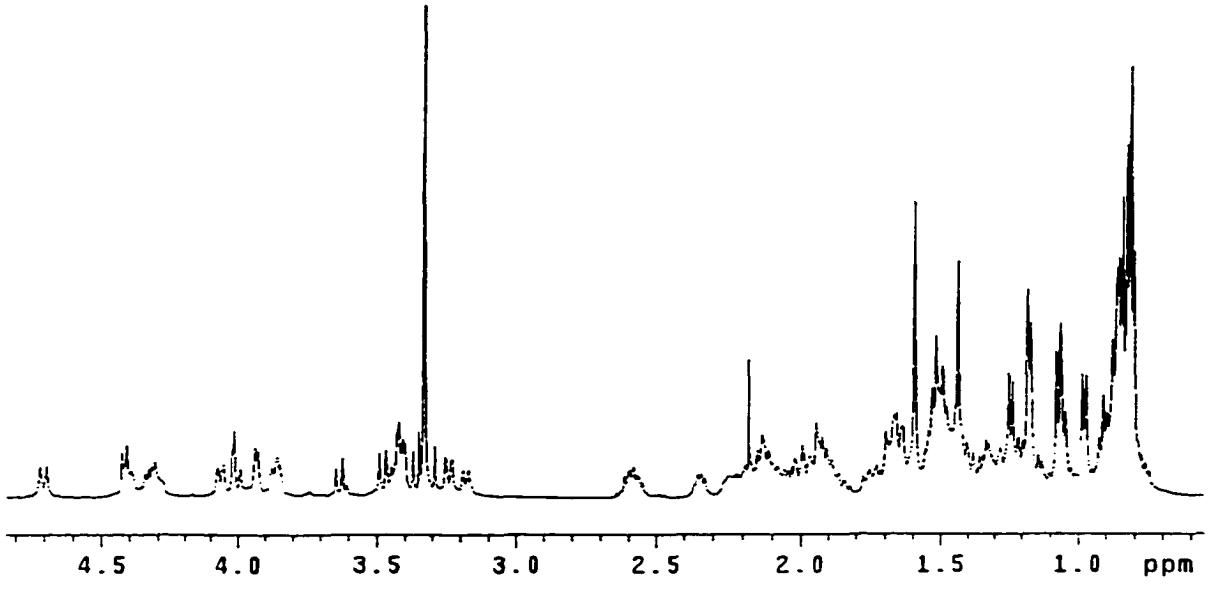

Figure III.35. ^{1}H NMR spectrum of the lead-monensin complex in chloroform acquired at –40 °C.

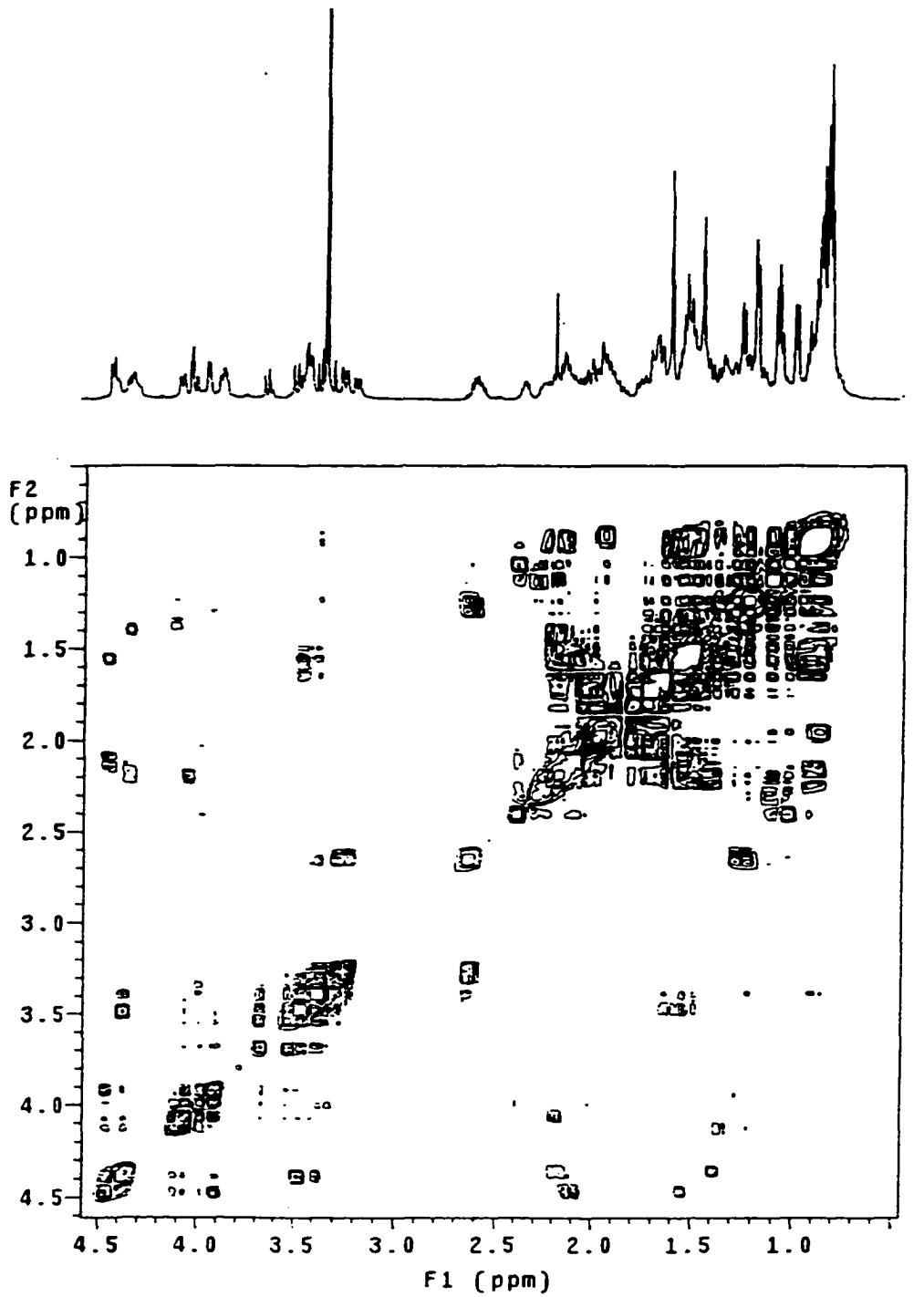

Figure III.36. COSY NMR spectrum for the lead-monensin complex in chloroform, acquired at –40 °C. The off-diagonal cross-peaks indicate coupling between two corresponding proton signals. F1 = ^{1}H chemical shift.

The peaks in the ^{13}C NMR spectra of the lead-monensin complex in chloroform were assigned as described above with the aid of APT and HMQC experiments. When a carbon was bound to hydrogen(s), HMQC pattern obtained at –40 °C showed two separate carbon-hydrogen cross-peaks (Figures III.37 and III.38). The complete assignment of peaks in the ^{13}C NMR spectrum to the particular set (or the assignment of a specific carbon to one out of the two ligands) was not possible without additional experiments (such as finding carbon-carbon through-bond correlations (INADEQUATE)), which were not attempted in this work. Nevertheless, COSY correlations between protons aided in assigning some of the carbon signals to the same ligand. Such groups of interconnected signals included carbons 2-5 and 18-21. The example of such assignment is described below. Two well-defined contours in HMQC map with H1 and C13 chemical shift coordinates of (3.91; 73.31) and (4.12; 72.13) were assigned to carbons and protons 21(1) and 21(2), respectively, based on carbon chemical shifts. (1) and (2) identify the two monensin ligands in the lead complex. COSY correlations (Figure III.36) showed coupling between proton 21(1) at 3.91 ppm and the proton at 4.46 ppm, which was assigned to be 20(1). The carbon correlation gave carbon 20(1) position at 78.41 ppm. ^{1}H and ^{13}C chemical shifts for the carbon and the proton 20(2) were identified as (4.34; 76.85) from the cross peak located in the same general area of the HMQC map as that of 20(1). In a similar fashion, signals from carbons and protons 18 and 19 were separated. Unfortunately, the overlapping proton peaks, magnetically equivalent proton signals from two different sets and poorly defined COSY cross peaks did not allow total separation of the two signal sets. All carbon assignments for lead-monensin complexes obtained are shown in Table III.18.

^{1}H NMR spectrum of the lead-monensin complex in chloroform obtained at low temperature also contained two peaks for most hydrogen atoms in the monensin molecule. The peaks were well separated for some protons from different monensin

ligands and overlapped for others, as mentioned above. ^{1}H-^{13}C chemical shift correlations from the HMQC experiment and COSY ^{1}H-^{1}H correlations aided in peak assignments. J-resolved 2-dimensional ^{1}H spectrum was also obtained which allowed to take into account some of the peak multiplicities. Unfortunately, it was not possible to resolve and assign a lot of overlapping ^{1}H signals in the region of 1.5-2.3 ppm. The ones that were assigned are listed in Table III.17.

Broad and poorly resolved peaks were observed in the ^{1}H NMR spectrum of lead-monensin complex in methanol. These peaks were broader in comparison to those in the spectra of sodium complex or of free acid in the same solvent. Most peaks were heavily overlapped and it was not possible to make an unambiguous assignment for all of them. However, chemical shift correlations obtained using COSY and HMQC, and comparisons to the known peak positions in the sodium monensin complex resulted in the assignment of most peaks (Table III.17 and III.18). ^{1}H and ^{13}C NMR peaks in the spectra of the lead-monensin complex in 80% methanol medium were assigned in a similar manner.

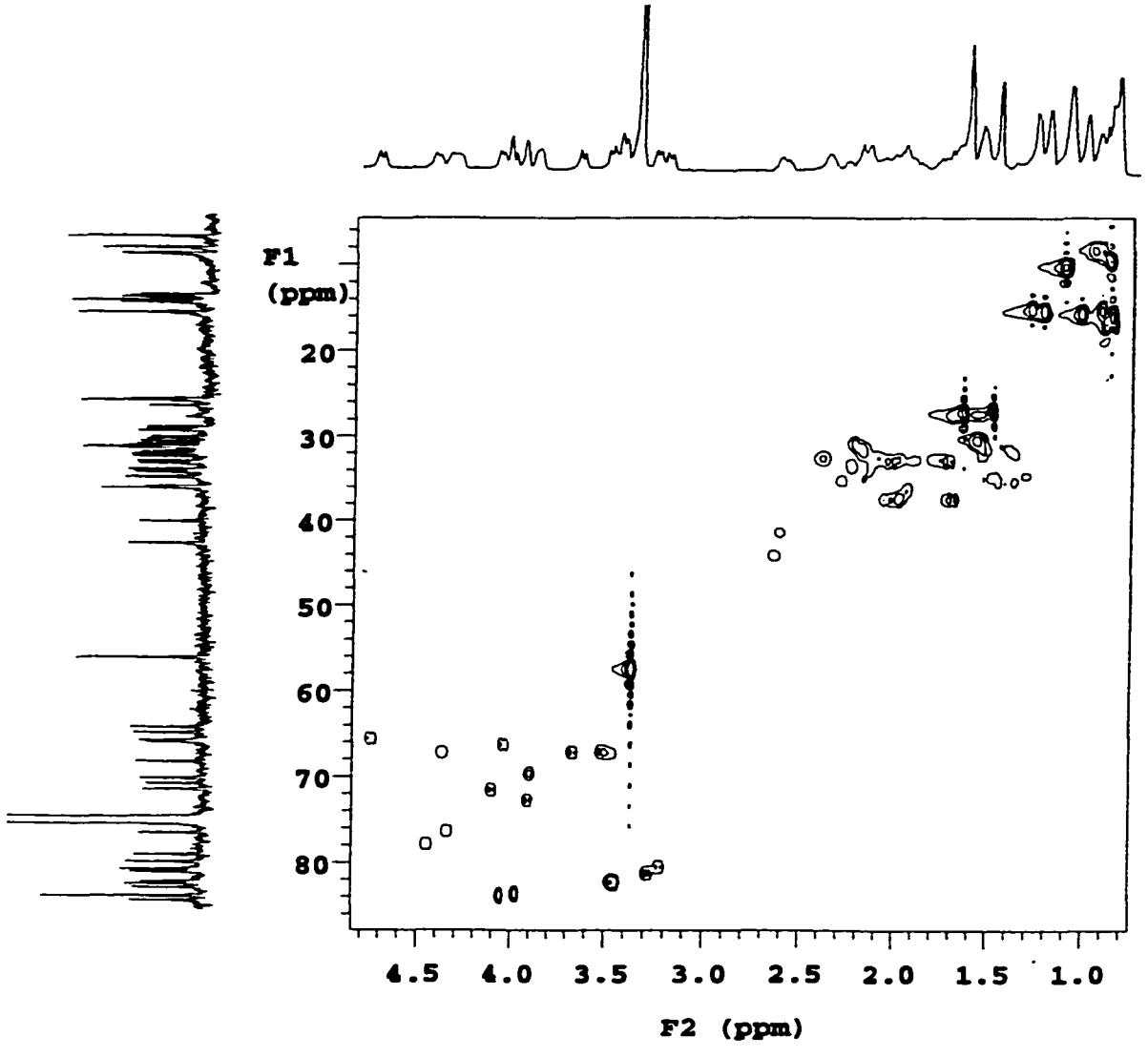

Figure III.37. One-bond heteronuclear $^{1}H - ^{13}C$ correlation spectrum of the lead-monensin complex in $CDCl_3$ acquired using HMQC technique at –40 °C and presented as a contour map. Two cross-peaks are visible for each carbon-hydrogen pair.
F1 = ^{13}C; F2 = ^{1}

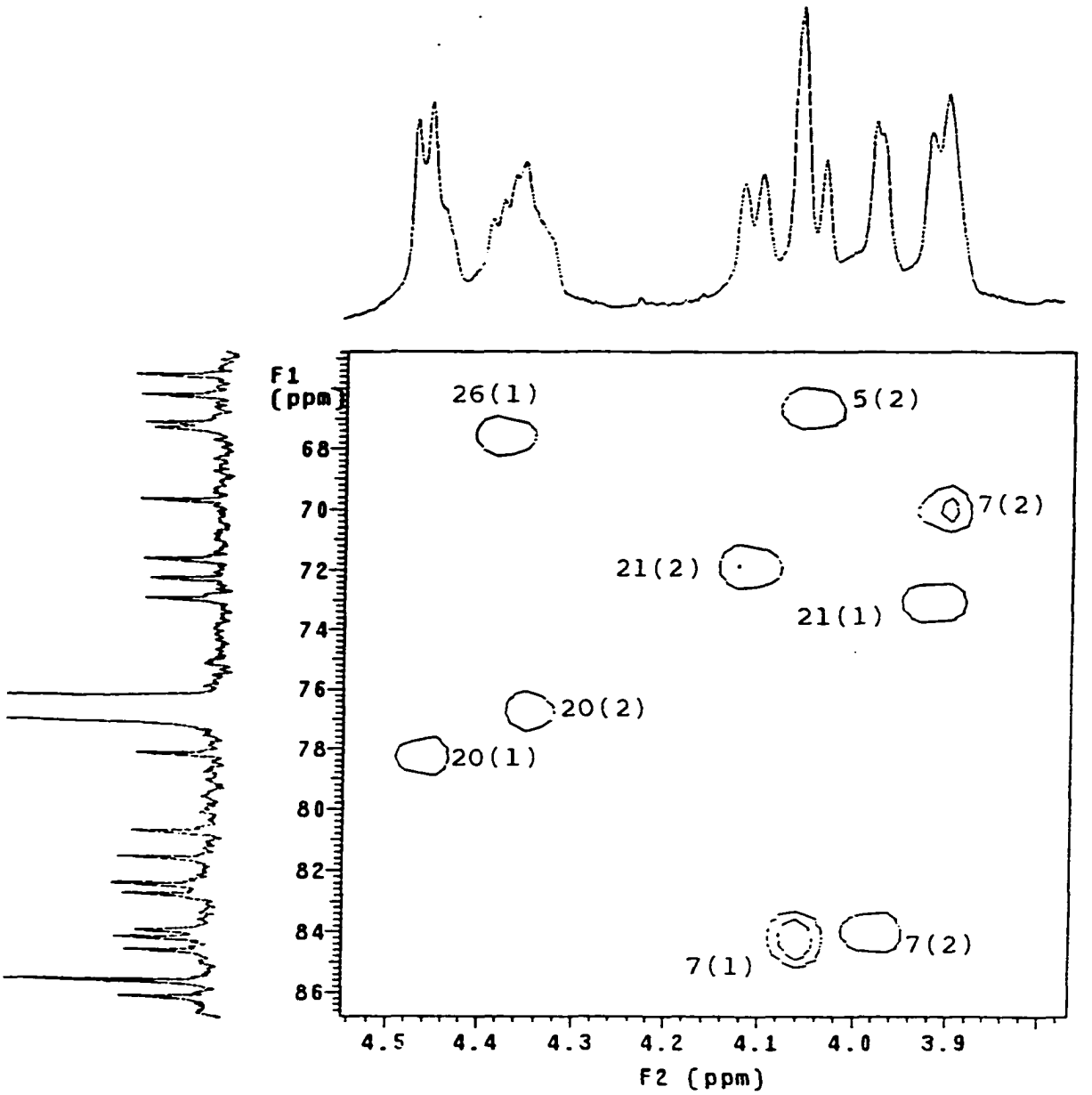

Figure III.38. Enlarged area of HMQC contour map from Figure III.37 showing the areas or ^{13}C-^{1}H correlations from two different monensin ligands. F1 = ^{13}C; F2 = ^{1}H.

Table III.17. Experimental ^1H NMR chemical shifts of the lead-monensin complex in ppm

carbon #	CD_3OD 25 °C	80% CD_3OD–D_2O 25 °C	$CDCl_3$ -40 °C set (1)	$CDCl_3$ -40 °C set (2)
2	2.44	2.40	2.56	2.59
3	3.37	3.36	3.18	3.24
4	2.11	2.09	2.21	2.26
5	4.20	4.13	3.99	4.70
6	-	-	-	-
7	4.12	4.11	3.85	-
8	1.93, 1.69	1.63	2.07	-
10	-	-	2.04, 1.65	-
11	-	-	1.93, 1.66	-
13	3.63	3.63	3.41	3.43
14	1.78, 1.62	-	-	-
15	2.22	2.15	-	-
17	4.05	4.00	4.93	4.02
18	2.33	2.31	2.34	2.34
19	2.28, 1.54	2.22, 1.53	2.18, 1.54	2.13, 1.48
20	4.34	4.34	4.41	4.32
21	3.76	3.75	3.86	4.07
22	1.35	-	-	-
23	1.91	-	-	-
24	1.76	-	-	-
26	3.67, 3.53	3.66, 3.53	4.32, 3.36	3.63, 3.48
27	0.88	0.86	-	-
28	0.90	0.87	-	-
29	0.98	0.94	-	-
30	1.96, 1.59	-	-	-
31	0.94	0.90	-	-
32	1.46	1.44	1.56	1.44
33	0.94	0.91	-	-
34	1.04	1.02	-	-
35	3.37	3.36	3.33	3.33
36	1.16	1.30	1.25.0	1.18

Table III.18. Experimental ^{13}C NMR chemical shifts of the lead-monensin complex in ppm

carbon #	CD_3OD 25 °C	80% CD_3OD-D_2O 25 °C	$CDCl_3$ -40 °C set (1)	$CDCl_3$ -40 °C set (2)
1	184.05	184.11	183.98	177.47
2	45.95	46.01	44.50	42.04
3	84.92	84.34	81.81	80.97
4	38.48	38.08	34.06	36.02
5	68.81	68.75	66.08	66.72
6	38.48	36.82	34.88	34.05
7	73.2	73.06	72.00	70.09
8	35.72	35.29	32.88	32.60
9	108.94	109.14	108.25	107.53
10	40.25	39.80	37.86	38.07
11	33.18	33.87	33.45	33.45
12	87.65	87.67	85.82	84.81
13	84.92	84.34	82.66	82.96
14	28.79	28.38	27.96	27.96
15	32.58	32.31	31.55	31.55
16	88.6	88.23	85.82	86.33
17	86.54	86.19	84.40	84.17
18	36.35	36.19	33.17	33.17
19	36.35	34.3	32.24	32.24
20	79.55	79.10	78.41	76.85
21	77.39	77.03	73.30	72.50
22	35.51	34.10	30.97	32.07
23	38.09	37.59	36.78	36.69
24	35.33	33.87	35.81	35.84
25	99.54	100.07	100.67	96.88
26	67.54	67.35	67.62	67.79
27	16.63	16.63	15.88	15.88
28	18.14	17.85	16.51	17.63
29	16.4	16.63	16.25	16.35
30	30.44	30.99	31.14	31.14
31	8.44	8.57	8.82	8.82
32	26.92	27.64	27.81	27.67
33	11.43	11.16	10.18	10.14
34	14.08	12.29	10.90	10.80
35	59.05	58.93	58.04	58.04
36	12.67	14.76	15.61	15.73

Results of additional NMR experiments with monensin-lead complexes using Pb-207 enriched lead.

A complex having 2:1 monensin-lead stoichiometry was made with ^{207}Pb-enriched lead by the reaction between the lead oxide and the free acid form of monensin in a manner described in section III.B. The complex obtained was dissolved in chloroform, and the ^{13}C and ^{1}H NMR spectra were recorded at –40 °C. Most of the signals were broader compared to those from the monensin complex made with natural abundance lead. Because the ^{207}Pb nucleus has a spin of 1/2, its complexation to an oxygen atom located within 2-3 bonds of a ^{13}C or a ^{1}H and coupling to the latter spins could introduce a multiplet structure to the ^{13}C and ^{1}H signals. Multiplets resulting from three-bond coupling have been observed previously for the signals in the ^{1}H NMR spectrum of ^{207}Pb-EDTA complexes[31]. However, the observed peak broadening can be also caused by a more efficient relaxation mechanism through chemical shielding anisotropy, characteristic of the heavier metal nuclei in complexes with less than tetrahedral symmetry[32]. Such broadened or multiplet signals were observed in the ^{13}C NMR spectrum for both monensin ligands and are illustrated for the peaks of carbon number 2 in Figure III.39. By comparing the widths of carbon peaks from the monensin complex with natural abundance lead versus those containing enriched ^{207}Pb, the signals from some carbons were considered to be doublets. The values of coupling constants J (Hz) were estimated directly from the ^{13}C NMR spectrum and are presented in Table III.19.

The reported values of $^{n}J(^{207}Pb^{13}C)$ coupling constants were mostly for organometallic compounds. Values of two-bond coupling constants (^{2}J) were generally larger than 3-bond coupling constants (^{3}J) when measured across aliphatic carbons and other nuclei (Sn, Si) in plumbylsilanes, plumbylstannanes and tetraorganolead complexes containing the $^{t}Bu_3Pb$ group[33]. However, the magnitude of coupling

constants in various tetraorganolead compounds[34] did not appear to follow any given trend and depended on the structure and number of the organic ligands. For example, in tetrabutyllead, $^{2}J(^{207}Pb^{13}C)$ was found to be larger in comparison with $^{3}J(^{207}Pb^{13}C)$, whereas in tetraphenyllead the following trend[34] was observed: $^{2}J < {}^{3}J > {}^{4}J$.

A)

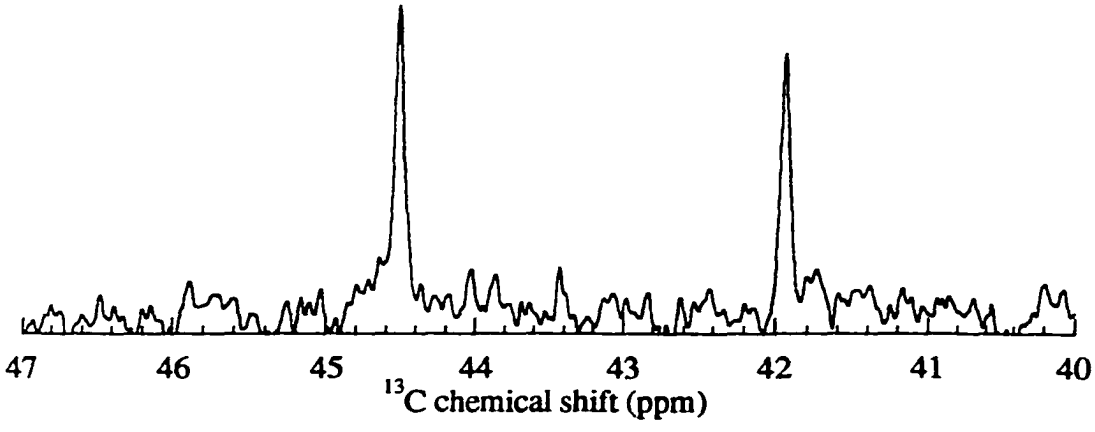

B)

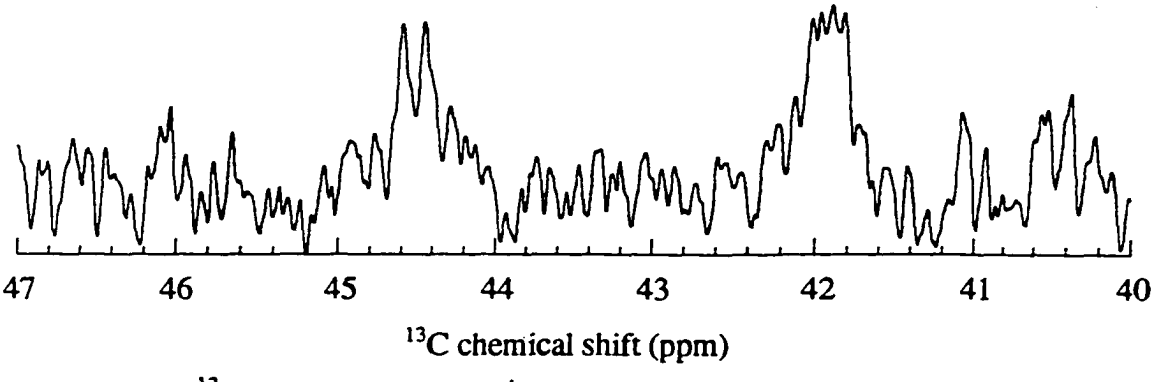

Figure III.39. ^{13}C NMR broadband ^{1}H–decoupled spectra showing resonance peaks for carbon number 2(1) at 44.60 ppm and carbon number 2(2) at 42.10 ppm in $CDCl_3$ at -40 °C. A) for lead-monensin complex with natural abundance lead, B) with ^{207}Pb-enriched lead.

Table III.19. Position of doublet peaks and the values of coupling constants as observed in the ^{13}C NMR spectrum of lead-monensin complex with ^{207}Pb-enriched lead

peak, ppm	carbon number[a]	peak shape or coupling ^{n}J, Hz	Coordinated oxygen atom[c]
108.25	9(1)	broad peak[b]	6
107.53	9(2)	singlet	-
100.67	25(1)	broad peak[b]	9 or 10 or 11
96.88	25(2)	broad peak[b]	9 or 10 or 11
86.33	16(2)	singlet	-
85.82	16(1)	singlet	-
85.81	12(1)	singlet	-
84.81	12(2)	singlet	-
84.43	17(1)	>10	8
84.15	17(2)	>10	8
83.01	13(2)	<10	6
82.64	13(1)	9	6
81.81	3(1)	singlet	-
80.97	3(2)	singlet	-
78.40	20(1)[d]	>10	8
73.30	21(1)	21.5	9
72.50	21(2)	>15	9
72.00	7(1)	>15	5
70.09	7(2)	21.5	5
67.9	26(2)	broad peak[b]	9 or 10 or 11
67.60	26(1)	broad peak[b]	9 or 10 or 11
66.70	5(2)	21.5	4
66.12	5(1)	>20	4
44.60	2(1)	20.9	1 or 2
42.01	2(2)	broad peak[b]	1 or 2
37.90	10(1)	broad peak[b]	4 or 6
38.10	10(2)	broad peak[b]	4 or 6
32.88	8(1)	broad peak[b]	4 or 5 or 6
32.60	8(2)	< 10	4 or 5 or 6

[a] (1) and (2) designate carbons from two different monensin ligands in the complex. [b] Some peaks were broadened, their multiplicity was not obvious and coupling constant value was not obtained. [c] Coordinating oxygens were assigned based on coupling constant values, as discussed in the text. [d] Carbon signal from the second set was not evaluated due to its overlap with the broad solvent peak.

Taking this literature data into account, it was assumed for the purpose of the present study that the values of coupling constants (through a coupling path that involves oxygen and coordination rather than covalent bonding) would decrease as the number of bonds between carbon and lead increases. Based on this assumption, the available coupling constant values, and observations of broader than usual peaks, the coordinating oxygens were assigned as shown in Table III.19.

Analysis of NMR data in methanol.

Although the stoichiometry of isolated lead-monensin complex used to obtain NMR spectra was found to be close to 2:1 monensin-lead, only one signal was present for ^{1}H and ^{13}C resonances at room temperature. It was concluded that the two ligands exchange rapidly and it was not possible to separate their signals in methanol. The values of coupling constants were not obtained due to the above reason. Therefore, chemical shifts assignments for protons and carbons represent the mean values between the two ligands.

In spite of this problem, the pattern of ^{13}C chemical shifts provides important information. In Figure III.40 the difference in ^{13}C chemical shifts ($\Delta\delta^{13}C$) in methanol between monensin anion (Me_4NMon) and various monensin salts, or monensic acid is presented for each carbon. As can be seen in case of the acid, where no complexation takes place, virtually no changes in the ^{13}C chemical shift are observed, except for the carboxylate group end of the molecule (carbons 1-5, 35-36), the middle furan ring (carbons 1415), and the methyl group adjacent to furan ring B (C32). However, upon complex formation several factors can contribute to changes in the ^{13}C chemical shifts. The first is cation coordination or hydrogen bonding that will change the environment of the participating oxygen atoms and of the adjacent carbon nuclei. Shift of the associated

^{13}C peaks downfield will occur in the ^{13}C NMR spectrum resulting in a positive value of $\Delta\delta^{13}C$. This change caused by coordination or hydrogen bonding was found to be less marked for monovalent cation complexes[15] and less pronounced in methanol. In a polar hydroxylic solvent such as methanol, the oxygen atoms are involved in the interactions with solvent molecules and substitution of a metal cation results in only slight differences in chemical shifts. The second factor contributing to the substantial differences in the ^{13}C NMR chemical shifts, is the change in molecular conformation of the ligand that accompanies metal ion coordination. In the case of monovalent cation salts, most of the $\Delta\delta^{13}C$ values were negative and were ascribed to such conformational changes[15].

Values of $\Delta\delta^{13}C$ obtained for the lead complex more closely resembled those in calcium complexes rather than that in sodium, indicating conformational similarities between monensin in the calcium and lead complexes. In the lead complex larger values of $\Delta\delta^{13}C$ were observed for carbons located in the carboxylate arm and ring E of the monensin molecule (see Figure III.29 for labeling diagram), carbons in ring A were not affected, and those in rings B, C and D were affected slightly. This trend is almost identical to that found in the 1:1 calcium-monensin complex[17]. The similarities of the pattern of $\Delta\delta^{13}C$ for the lead complex with the available data on calcium-monensin and manganese-monensin complexes[17] revealed that changes in ^{13}C chemical shifts in rings C and D of the lead-bound monensin might be a result of a conformational change in the ligand upon complexation. Also, the interaction of monensin with lead cation can be suggested to take place through a carboxylate group and oxygens 6 and 9, or 10 or 11.

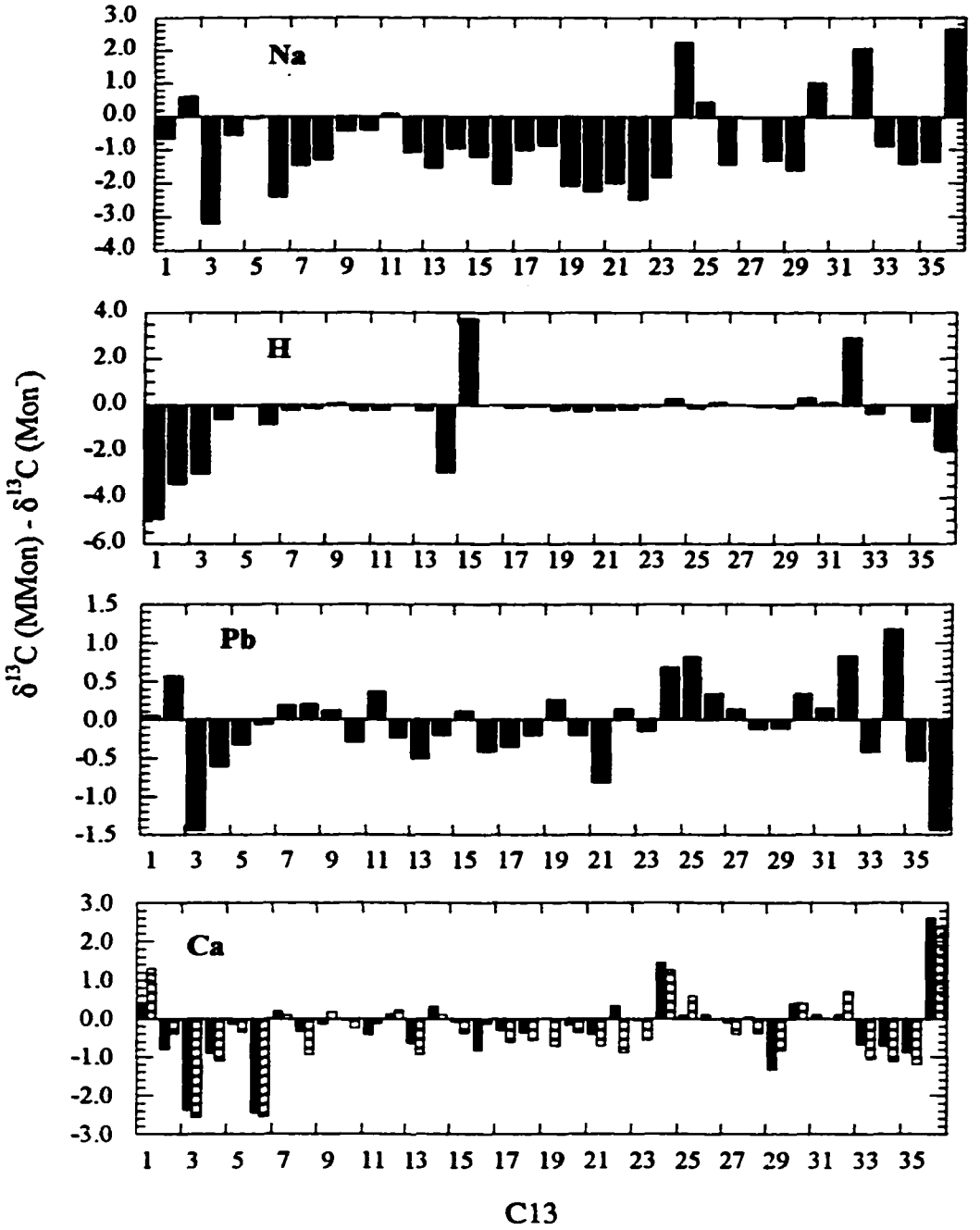

Figure III.40. Variation of ^{13}C chemical shifts differences of all the carbons in the monensin molecule from the free monensin anion Mon^- to the metal complex and free acid in methanol. Both variations to the first (darkened) and second (lighter areas) anion ligands in calcium complex are shown, the values of ^{13}C chemical shifts were adopted from literature[17]. Experimentally obtained ^{13}C resonances from Tables III.11, 12, 14 and 17 were used for monensic acid, free monensin anion, sodium and lead complexes.

The ^{1}H and ^{13}C chemical shifts obtained for protons and carbons in the monensin-lead complex in 80% methanol-water solvent closely resembled those obtained in pure methanol as can be seen from Tables III.17 and III.18. However, variations with magnitudes larger than 0.5 between the values of chemical shift in the two solvents were also observed for some carbons. Upon going from methanol to 80% methanol-water, large changes were observed for all carbons on ring E, which points to the fact that major conformation changes or interactions with more polar solvent might occur in that part of the monensin molecule. The magnitude of changes in the chemical shift of carbons on ring C and the carboxylate arm of monensin in two solvents was not as large, but it was substantial to suggest that the conformational change can also affect those areas.

Analysis of NMR data in chloroform.

Divalent cation coordination by monensin in chloroform was previously studied in calcium, manganese and copper complexes[17]. In order to obtain information about binding sites in monensin ligands positive variations in carbon chemical shift were identified when going from anion species to metal cation salts. This method was applied to the acquired ^{13}C chemical shift data for the lead-monensin complex in chloroform. The plot of differences in the chemical shift for each carbon ($\Delta\delta^{13}C$) in going from monensin anion to monensic acid or monensin-metal complexes are shown in Figure III.41. The values of $\Delta\delta^{13}C$ for both ligands ((1) and (2)) in the lead-monensin complex are shown.

It is obvious from Figure III.41 that the second set of carbon chemical shifts (corresponding to ligand 2 in lead-monensin complex) in chloroform closely resembles that of monensic acid. This conclusion is based on the similarity of their carbon shift variations from monensin anion. Several different explanations of this result may be

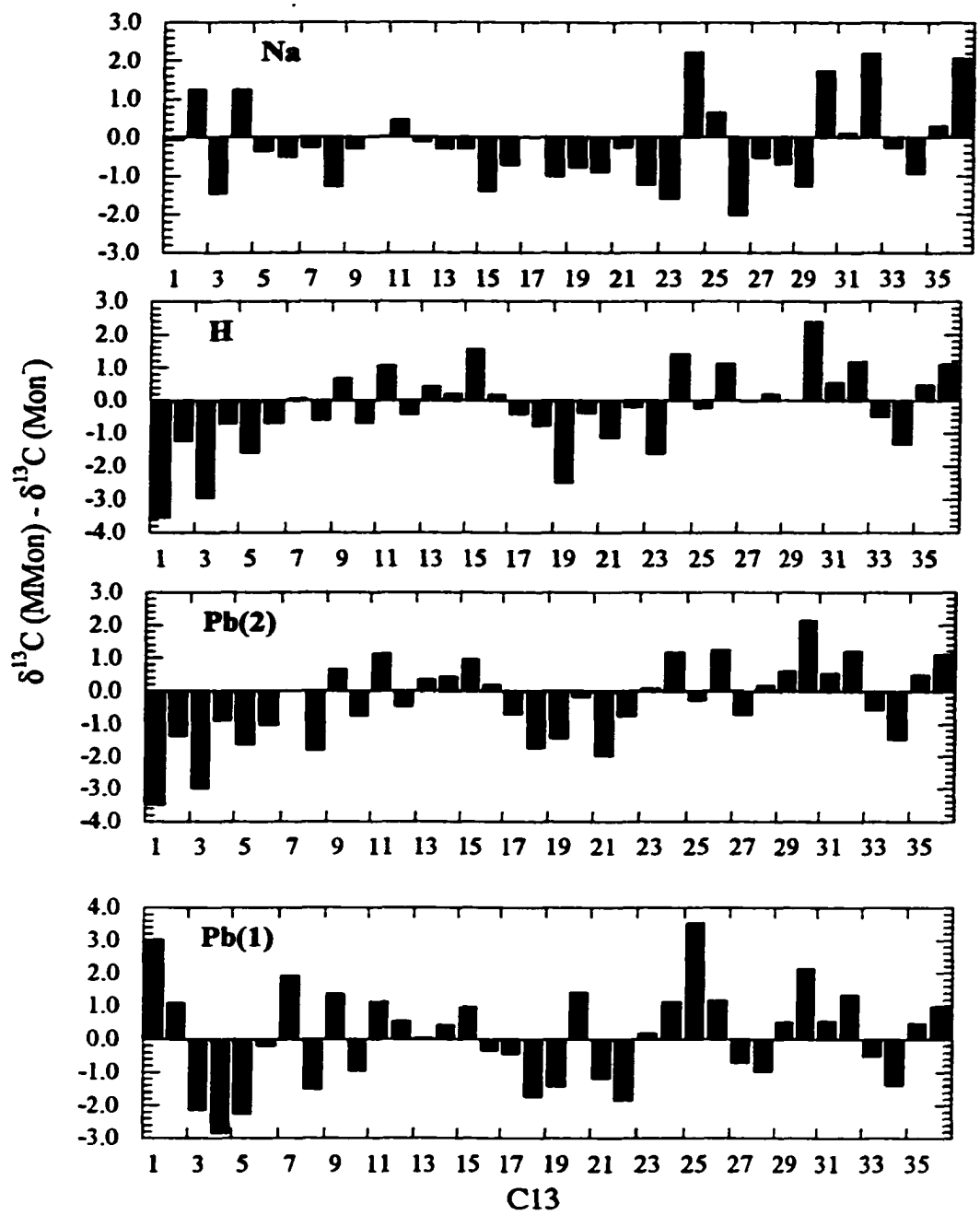

Figure III.41. Variation of ^{13}C chemical shifts of all the carbons in the monensin molecule from the free monensin anion Mon^- to the metal complex and free acid in chloroform. Variations to both anion ligands in lead complex are shown. Experimentally obtained ^{13}C resonances from Tables III.11, 12, 15 and17 were used for monensic acid, free monensin anion, sodium and lead complexes.

proposed which are discussed in more detail in Chapter V. In addition, it is important to note that the two sets of carbon signals in the lead-monensin complex differed significantly from one another possibly indicating different conformation or lead binding of the two monensin ligands.

From the analysis of Figure III.41 positive values of $\Delta\delta^{13}C$ between monensin anion and the first ligand in the lead-monensin complex were observed for carbons 7, 9, 12, 20, 25 and 26. Overall, the changes affected the carboxylate end and all rings, except for ring C, where the variations were not large. This suggests that oxygens 1 or 2, and 5, 6, 8, and 9 or 10 may be involved in lead coordination. Positive value of $\Delta\delta^{13}C$ for carbon 26 has the same magnitude as that in the monensic acid. In the acid structure, this positive difference may be caused by the involvement of oxygen 11 in the hydrogen bond. The same process or the involvement of that oxygen in lead coordination may be responsible for the positive shift difference of this carbon in the lead complex.

Positive values of $\Delta\delta^{13}C$ between monensin anion and the second ligand in the lead-monensin complex were observed for carbons 9, 13, 16 and 26, which are located next to possible binding oxygens 6, 7 and 9, 10 or 11.

References.

1) Chamberlin, J. W.; Agtarap, A. *Org. Mass Spectrom.* **1970**, 3, 271-285.

2) Havlicek, V.; Ryska, M.; Pospisil, S. *J. Mass. Spectrom.* **1995**, 30, 1089-1094.

3) Chang, T. T.; Lay,Jr., J. O.; Francel, R. J. *Anal. Chem.* **1984**, 56, 111-113.

4) Siegel, M. M.; McGahren, W. J.; Tomer, K. B.; Chang T. T. *Biomed. Environ. Mass Spectrom.* **1987**, 14, 29-38.

5) Kiehl, D. E.; Julian, R. K.; Kennington, A. S. *Rapid Commun. Mass Spectrom.* **1998**, 12, 903-910.

6) Volmer, D. A.; Lock, C. M. *Rapid Commun. Mass Spectrom.* **1998**, 12, 157-164.

7) Martell, A. E.; Motekaitis, R. J. *Determination and Use of Stability Constants*, 2nd ed., VCH Publishers, Inc.: N.Y., 1992.

8) Lutz, W. K.; Wipf, H.-K.; Simon, W. *Helv. Chim. Acta* **1970**, 53, 1741-1746.

9) Anteunis, M. J. O. In *Polyether antibiotics: Naturally Occurring Ionophores, Vol. 2. Chemistry* , Westley, J. W., Ed.; Marcel Dekker, Inc.: New York, 1983; pp 245-344.

10) Perrin, D. D.; Sayce, I. G. *Talanta* **1967**, 14, 833-842.

11) Smith R. M.; Martell, A. E. *NIST Critically Selected Stability Constants of Metal Complexes Database*, Version 5.0, U.S.Secretary of Commerce, USA, 1998.

12) Taylor, R. W. Ph.D. Thesis, Wayne State University, Detroit, MI, USA, 1973.

13) Sylva, R. N.; Brown, P. L. **1980**, *J. Chem. Soc., Dalton Trans.*, 1577-1581.

14) Palma, M.; Ouahabi, A.; Malfreyt, P.; Juillard, J. **1995**, *J. Chem. Res., Synop.*, 404-405.

15) Mimouni, M.; Hebrant, M.; Dauphin, G.; Juillard, J. *J. Chem. Res., Miniprint* **1996**, 1416-1433.

16) Vaufrey-Mary, F. Doctorate Thesis, Universite Blaise Pascal, Clermont, France, 1990.

17) Hebrant, M.; Mimouni, M.; Tissier, M.; Pointud, Y.; Juillard, J. *New J. Chem.* **1992**, 16, 999-1008.

18) Bachman, P.; Aue, W. P.; Muller, L.; Ernst, R. R. *J. Magn. Reson.* **1977**, 28, 29-39.

19) Bodenhausen, G.; Freeman, R.; Neidermayer, R.; Turner, D. *J. Magn. Reson.* **1977**, 26, 133-164.

20) Nagayama, K.; Bachmann, P.; Wuthrich, K.; Ernst, R. R. *J. Magn. Reson.* **1978**, 31, 133-148.

21) Rabenstein, D. L.; Nakashima, T. T.; *Anal. Chem.* **1979**, 51, 1465A-1474A.

22) Pei, F.-K.; Freeman, R. *J. Magn. Reson.* **1982**, 48, 318-322.; Patt, S. L. *J. Magn. Reson.* **1982**, 46, 535-539.

23) Doddrell, D. M.; Pegg, D. T.; Bendall, M. R. *J. Magn. Reson.* **1982**, 48, 323-327.

24) Bax, A.; Morris, G. A. *J. Magn. Reson.* **1981**, 42, 501-505.

25) Bax, A. *J. Magn. Reson.* **1983**, 53, 517-520.

26) Rutar, V. *J. Magn. Reson.* **1984**, 58, 306-310.

27) Bax, A. D.; Griffey, R. H.; Hawkins, B. L. *J. Am. Chem. Soc.* **1983**, 105, 7188-7190; Bax, A.; Subramanian, S. *J. Magn. Reson.* **1986**, 67, 565-569.

28) Anteunis, M. J. O. *Bull. Soc. Chim. Belg.* **1977**, 86(5), 367-381.

29) Ajaz, A. A.; Robinson, J. A.; Turner, D. L. *J. Chem. Soc., Perkin Trans. 1* **1987**, 27-36.

30) Lyazghi, R.; Pointud, Y.; Dauphin, G.; Juillard, J. *J. Chem. Soc., Perkin Trans. 2* **1993**, 1681-1686.

31) Claudio, E. S.; ter Horst, M. A., Forde, C. E.; Stern, C. L.; Zart, M. K.; Godwin, H. A. *Inorg. Chem.* **2000**, 39, 1391-1397.

32) Wasylishen, R.E. In *NMR Spectroscopy Techniques*, 2nd edition, Brush, M.D., Ed.; Marcell Dekker, Inc.: New York, 1996; pp. 105-144.

33) Herberhold, M.; Trobs, V.; Wrackmeyer, B. *J. Organomet. Chem.* **1997**, 541, 391-400.

34) Wrackmeyer, B.; Horchler, K. *Annu. Rep. NMR Spectrosc.* **1989**, 22, 249-306.

CHAPTER IV

RESULTS

STUDIES OF LASALOCID–METAL COMPLEXES

IV.A. Preparation and characterization of lasalocid - lead(II) complexes.

Complexes having 2:1 lasalocid-lead stoichiometry were obtained by the reaction between stoichiometric quantities of the free acid form of lasalocid and solid lead oxide in methanol. A ternary complex having 1:1:1 lasalocid-lead-chloride stoichiometry was prepared by reacting the silver lasalocid salt with lead chloride in a 1:1 stoichiometric ratio. Preparation and isolation of lead-lasalocid compounds were described in detail in sections II.B and II.C.

Elemental analysis of lasalocid - lead complexes.

Samples of the isolated lasalocid-lead complexes were analyzed commercially to determine the percentages of carbon and hydrogen, and for the mixed complexes, chloride. The results of these analyses are presented in Table IV.1.

The lead content of lasalocid-lead complexes was analyzed by flame atomic absorption spectroscopy as described in section III.A for lead-lasalocid compounds. After the lead concentration (C) was obtained, %Pb (w/w) was calculated as illustrated in Equation IV.1.

$$\%Pb = \frac{C \text{ moles/L} \times 0.05 \text{ L} \times 207.19 \text{g/mole}}{\text{g sample}} \times 100\% \qquad \text{(IV.1)}$$

The experimental values for %Pb in the binary lasalocid-lead complex were found to be between 13.5 and 14.5%, and one of these results is shown in Table IV.1, whereas the corresponding value for the mixed lasalocid-lead-chloride complex was close to 17%. The theoretical values for weight percentages of carbon, hydrogen, lead

and chloride were calculated on the basis of the predicted compound stoichiometries, with and without additional water of crystallization.

Comparison of the experimental and calculated values for %Pb indicated that the composition of the binary complex was closest to that predicted for a 2:1 Mon-Pb complex with two added molecules of water of hydration. A non-stoichiometric amount of the water molecules (nH_2O, with $1<n<2$) associated with the isolated complex could account for the small differences observed. However, the elemental composition for the mixed 1:1:1 lead-lasalocid-chloride complex exhibits large deviations from the calculated values. Although amounts of lead and chloride were found to be lower than calculated, their ratio indicated that about 1.3 chlorine atoms were present for each lead. This points to the possible presence of the unreacted lead chloride in the final product. Because no peaks corresponding to the silver lasalocid complex were identified in the recorded mass-spectra, this reagent is not present in the isolated complex. The carbon to hydrogen and carbon to oxygen ratios suggested that most of the organic matter in the final product is present in the form of lasalocid. Slightly higher amounts of oxygen and hydrogen may indicate the presence of several waters of hydration. The determination of the exact composition of the final product containing ternary ionophore complex was not attempted.

Table IV.1. Experimental and calculated elemental composition of lead-lasalocid complexes[a]

Compound/ method	%Pb[b]	%C[c]	%H[c]	%O[d]	%Cl[c]
Experimentally obtained					
$PbLas_2$ by the reaction of PbO with HLas	14.2[b]	57.95[c]	7.71[c]	20.14[d]	
PbLasCl by reaction of AgLas with $PbCl_2$	17.12[b]	51.61[c]	6.82[c]	20.66[d]	3.79[c]
Calculated from the predicted molecular stoichiometries					
1 Pb: 2 Las ($C_{68}H_{106}O_{16}Pb$)	14.94	58.89	7.71	18.46	
1 Pb : 2 Las : 1 H_2O ($C_{68}H_{106}O_{16}Pb \cdot H_2O$)	14.75	58.14	7.75	19.36	
1 Pb : 2 Las : 2 H_2O ($C_{68}H_{106}O_{16}Pb \cdot H_2O$)	14.56	57.40	7.80	20.24	
1 Pb : 1Las : 1 Cl ($C_{34}H_{53}O_8PbCl$)	24.89	49.06	6.42	15.37	4.26
1 Pb : 1 Las : 1 Cl :1 H_2O ($C_{34}H_{53}O_8PbCl \cdot H_2O$)	24.36	48.02	6.52	16.93	4.17
1 Pb : 1 Las : 1 OH ($C_{34}H_{54}O_9Pb$)	25.45	50.17	6.69	17.69	

[a] All values are given as weight percentages. [b] The lead content was determined using flame atomic absorption spectroscopy. %Pb was calculated from eq IV.1. [c] The values were obtained using analysis performed commercially. [d] %O was calculated by subtracting the sum of percentages of other elements from 100%.

Characterization of lasalocid–lead complexes by mass-spectrometry.

The first electron ionization mass spectra of lasalocid were recorded after its discovery[1] in 1974. The fragmentation patterns obtained aided in the characterization of various lasalocid homologs, but no molecular ion peak for the sodium salt was observed. The highest peak at m/z 528 resulted from the loss of sodium, CO_2 and water. Later, when the softer ionization methods were used to analyze lasalocid, including chemical ionization[2], FAB-MS and ESI-MS[3,4], the spectra showed the presence of lasalocid-sodium molecular ion peaks at 613 m/z $(Las+H+Na)^+$ and at 635 m/z $(Las+2Na)^+$. Here and below in this section "Las" refers to the monoanionic form of lasalocid, $C_{34}H_{53}O_8^-$.

In the present work, FAB-MS and ESI-MS spectra were obtained for isolated 2:1 lasalocid-lead and 1:1:1 lasalocid-lead-chloride complexes. Peaks from the molecular ions, corresponding to complexes having both 1:1 and 2:1 lasalocid-lead stoichiometries, were present in the positive ion ESI mass-spectra of all compounds including the mixed complexes. Protons on lasalocid ligand exhibited of a high degree of lability, as they were easily lost or accepted during ionization, which allowed the complex molecular ions with positive unity charge and the specific stoichiometry to be formed. Figure IV.1 illustrates peaks of interest in the positive ion ESI mass spectrum of the compound with 2:1 lasalocid-lead stoichiometry. The peaks with the highest intensity in the spectrum were centered at 797 m/z $(Las+Pb)^+$ and indicated the formation of the species with 1:1 lasalocid-lead stoichiometry. Other smaller but significant clusters of peaks were centered at m/z 1204 $(2Las+Na+2H)^+$, 1220 $(2Las+2H+K)^+$, 1226 $(2Las+H+2Na)^+$, 1242 $(2Las+Na+K+H)^+$, 1388 $(Pb+2Las+H)^+$ and 1410 $(Pb+2Las+Na)^+$. The group of peaks at 1199 m/z may correspond to the ammonia adduct of lasalocid $(2Las+3H+NH_3)^+$ because lasalocid is known to complex various amines by forming hydrogen-bonds to the $-NH_3$ group with donor oxygen atoms[5]. However, the source of the ammonia contamination is not known. Comparison of the experimental peak intensities to the calculated isotopic pattern, shown as the inset in Figure IV.2 for the 797 m/z peak

cluster, confirmed the assignment. Peaks centered at 1388 m/z and corresponding to 2:1 Las-Pb complex are shown in Figure IV.3.

Both positive and negative ion ESI-MS spectra were obtained for the mixed lasalocid-lead-chloride complexes, where excess chloride, in the form of tetramethylammonium chloride (0.3 mM total chloride), was added to the methanol solution containing the mixed compound PbLasCl. Only the peaks from the molecular ions of ternary complexes were present in the negative ion mass spectra, whereas no peaks from binary compounds were observed. The negative ion ESI mass-spectrum was dominated by the large peaks corresponding to the lasalocid anion $(Las)^-$ (m/z 589). Sets of low intensity peaks resulting from the mixed lead-lasalocid-chloride complexes were also present. Figure IV.4 shows one set of peaks, centered at m/z 831, that correspond to the species with 1:1:1 lasalocid-lead-chloride stoichiometry $(Las\text{-}H+Pb+Cl)^-$. Figure IV.5 shows another set of peaks, centered at m/z 1422 that are consistent with a species with 2:1:1 lasalocid-lead-chloride stoichiometry $(2Las+Pb+Cl)^-$. Isotopic distribution patterns were calculated for the expected ion compositions and are shown as insets with the corresponding mass spectrum peaks. The identical isotopic distribution between both the experimental and calculated peaks confirmed the assignments. The values of m/z for the most intense peak in the molecular ion cluster observed, the assigned molecular ion compositions and stoichiometries, and the experimental method are listed in Table IV.2 for all experiments.

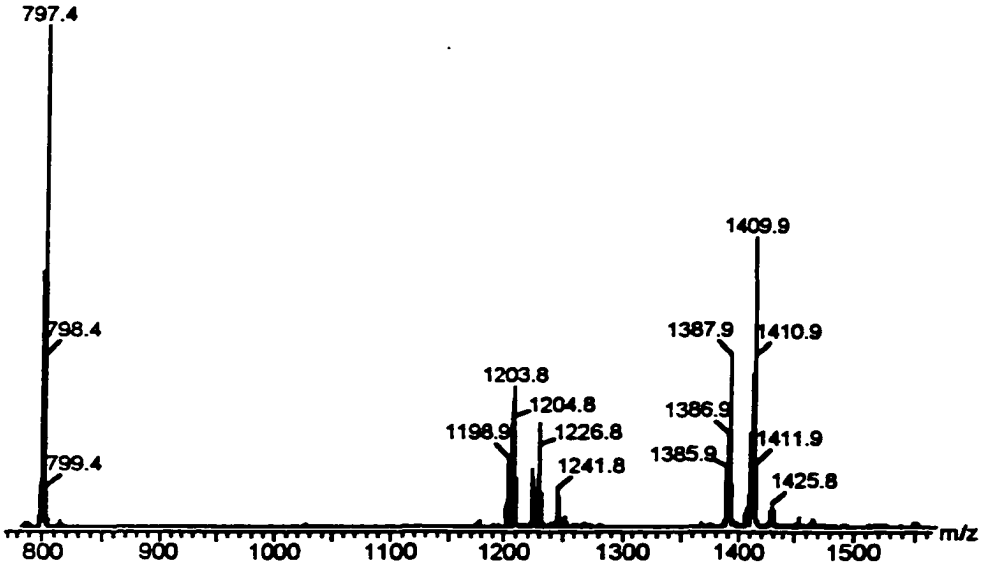

Figure IV.1. Part of the positive ion ESI-MS for 2:1 lasalocid-lead complex. Peak clusters for molecular ions having 1:1 (797 m/z) and 2:1 (1388 m/z) lasalocid-lead stoichiometries are observed. The sample was prepared by dissolving the 2:1 lasalocid-lead complex in methanol yielding about 0.3 mM solution.

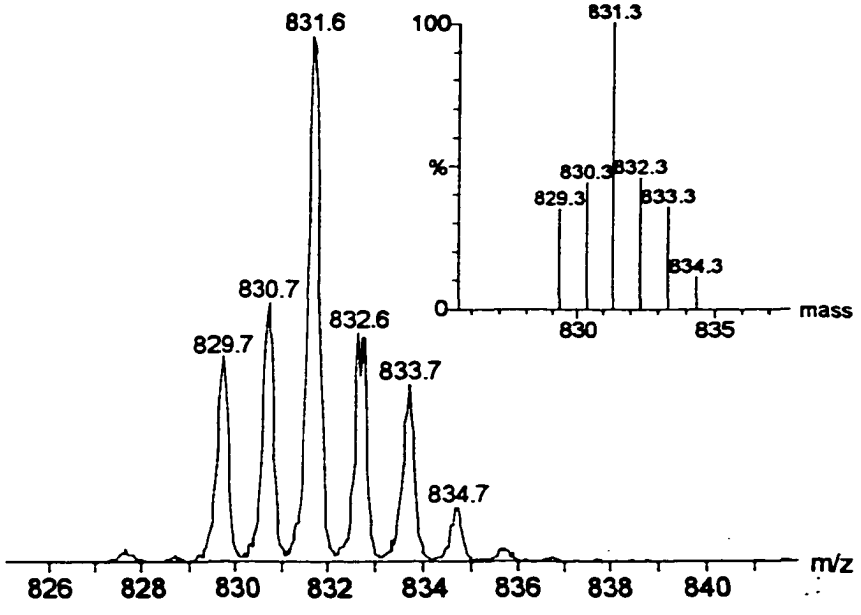

Figure IV.2. Peaks for the 1:1 lasalocid-lead molecular ion in the positive ion ESI-MS. The sample was prepared by dissolving the solid 2:1 lasalocid-lead complex in methanol. The inset shows the calculated isotopic pattern for $C_{34}H_{53}O_8Pb$.

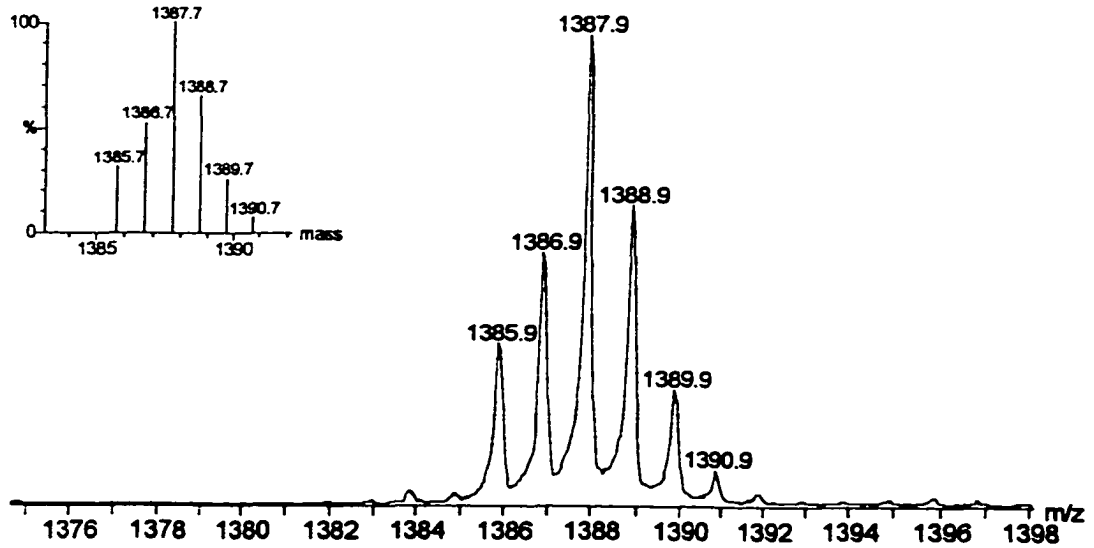

Figure IV.3. Peaks for the 2:1 lasalocid-lead molecular ion in the positive ion ESI-MS. The sample was prepared by dissolving the solid 2:1 lasalocid-lead complex in methanol. The inset shows the calculated isotopic pattern for $C_{68}H_{107}O_{16}Pb$.

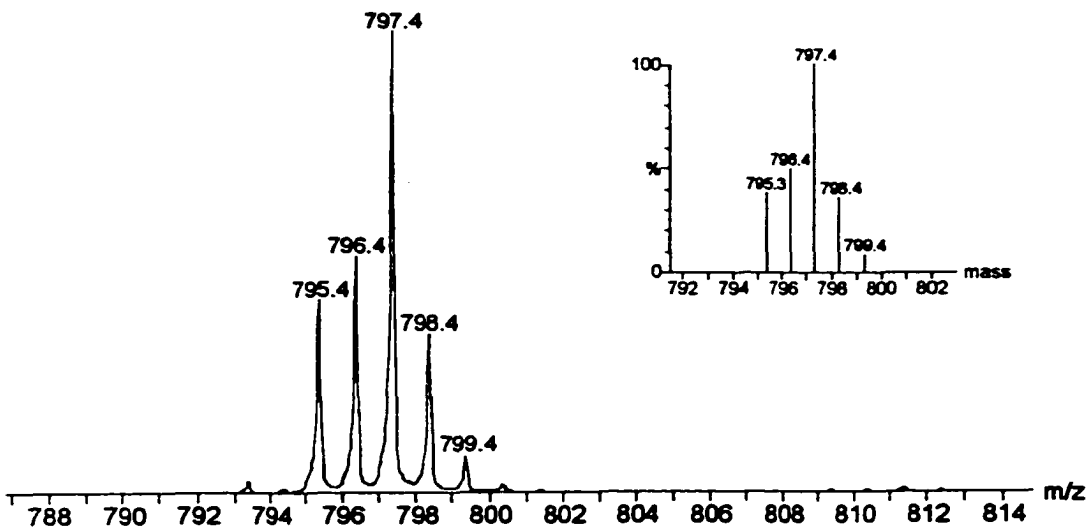

Figure IV.4. Peaks for the 1:1:1 lasalocid-lead-chloride molecular ion in negative ion ESI-MS. The sample was prepared by dissolving the isolated mixed complex in methanol with the addition of about 0.3 mM excess of chloride in the form of tetramethylammonium chloride. The inset shows the calculated isotopic pattern for $C_{34}H_{52}O_8PbCl$.

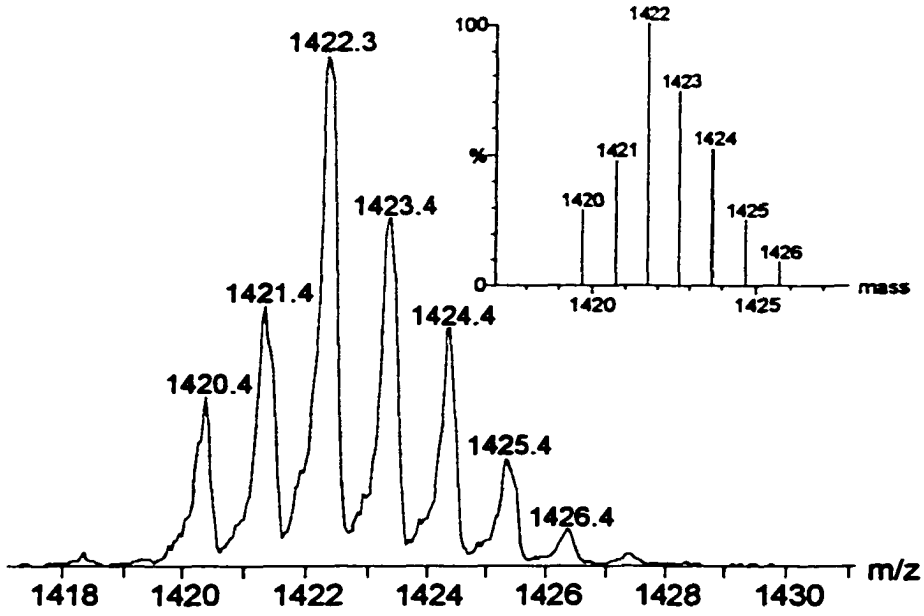

Figure IV.5. Peaks for the 2:1:1 lasalocid-lead-chloride molecular ion in negative ion ESI-MS. The sample was prepared by dissolving the isolated mixed complex in methanol with the addition of 0.3mM excess of chloride in the form of tetramethylammonium chloride. The inset shows the calculated isotopic pattern for $C_{68}H_{106}C_{.5}PbCl$.

Table IV.2 Peaks for lead-lasalocid complexes as obtained from the mass spectra[a]

m/z[a]	ion composition and charge	Stoichiometry	MS method
797.4	$C_{34}H_{53}O_8Pb^+$	1 Las : 1 Pb	positive ion ESI, FAB
1387.7	$C_{68}H_{107}O_{16}Pb^+$	2 Las : 1 Pb	positive ion ESI
831.3	$C_{34}H_{52}O_8PbCl^-$	1 Las :1 Pb : 1 Cl	negative ion ESI
1422.4	$C_{68}H_{106}O_{16}PbCl^-$	2 Las :1 Pb : 1 Cl	negative ion ESI

[a] Position of the highest intensity peak in the molecular ion cluster observed.

IV.B. Determination of lasalocid protonation constant in 80% methanol-water.

Lasalocid exhibits significant absorbance in the UV-Vis region of the spectrum due to the presence of several chromophore groups in its structure. The change in the protonation state of the carboxylic acid group, located on the benzene ring and a part of the conjugated system, results in a change of the UV-Vis spectrum, as reported previously[6]. The value for the mixed-mode protonation constant of lasalocid in 80% methanol was obtained both from UV-Vis and potentiometric titrations.

Potentiometric Method

Figure IV.6 shows the titration curve for lasalocid in the pH* range 3–11. The data is consistent with the ionization of a single proton. The potentiometric titration data in the form of pH* observed vs volume of titrant added was first analyzed using the program PKAS[7] to calculate the value of the protonation constant. The program BEST[7] was used subsequently to recalculate and refine the value obtained. The disadvantage of using PKAS lies in the fact that the data around the equivalence point are not included in the fit in order to decrease the influence of the less accurate values in that region. The use of BEST allows the goodness of fit for the whole curve to be evaluated as well as a more accurate determination of the ligand concentration from the fitted titration end-point.

The titrations were performed for three different lasalocid concentrations, 0.5 mM, 1.0 mM and 5.0 mM, to investigate the possibility of lasalocid dimerization. Titration at each concentration was performed in triplicate. Only those protonation constants where the parameter sigma is less than 0.1 are included in Table IV.3. pH*-titrations of lasalocid at these concentrations in 80% methanol-water gave similar values

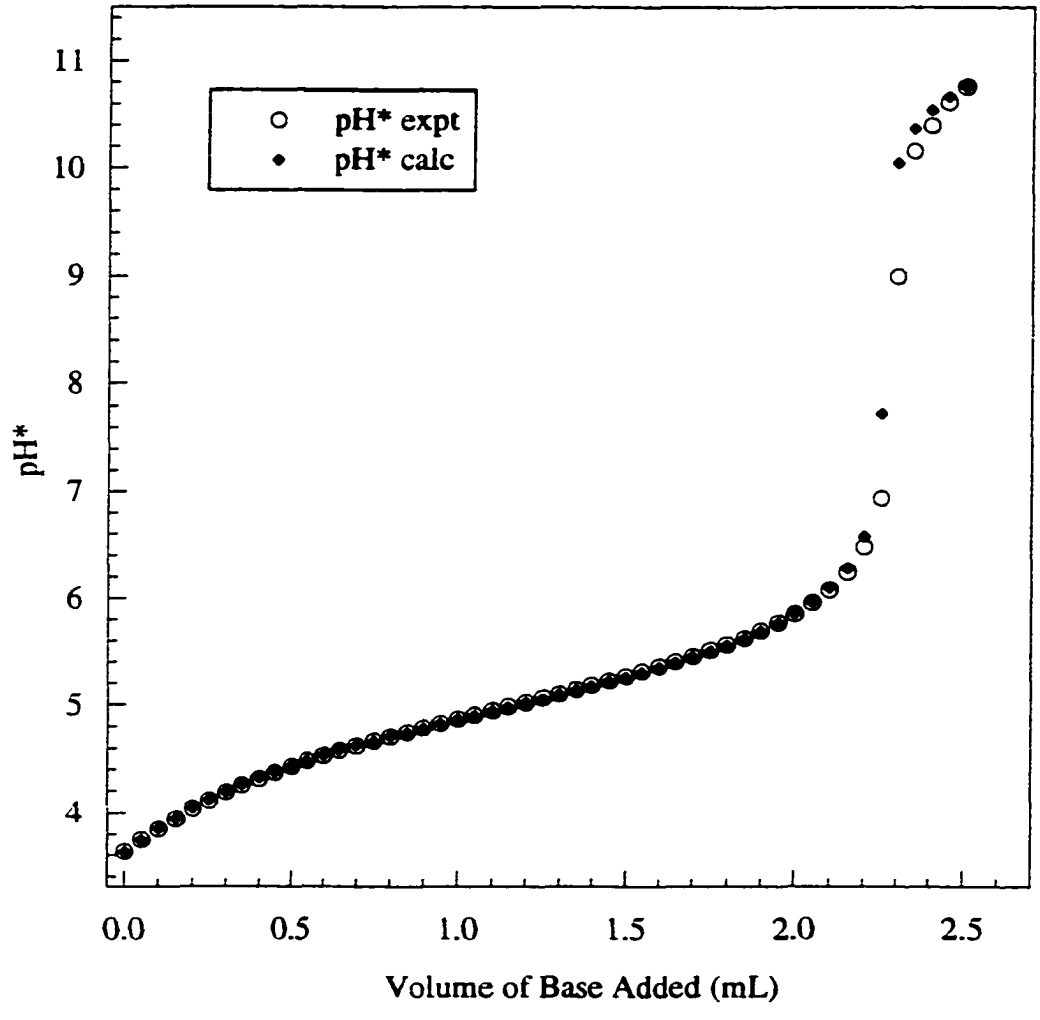

Figure IV.6. Experimental titration curve obtained from the titration of 10.0 mL of 4.50 mM lasalocidic acid solution with 0.02108 M Me_4NOH in 80% methanol-water at 25.0 °C and 0.05 M ionic strength (TEAP). The experimental curve is overlaid with the theoretical curve calculated with the program BEST using the known values of ligand and base concentrations and the calculated value of protonation constant.

Table IV.3 Calculated values of the mixed-mode protonation constant for lasalocid in 80% methanol[a]

Lasalocid concentration	log K_H^{m*} [b]	σ_{fit} [c,d]
0.5 mM	5.06	0.024 (51)
	5.04	0.038 (24)
1.0 mM	4.83	0.060 (52)
	5.05	0.031 (61)
	5.05	0.043 (53)
	5.00	0.035 (41)
	5.00	0.016 (50)
5.0 mM	5.03	0.019 (50)
	5.02	0.009 (51)
	5.04	0.016 (52)

[a] 25.0 °C, ionic strength = 0.05 M (TEAP). [b] The values of the protonation constants were calculated using the program BEST. [c] Standard deviation expressed as σ_{fit}, $\sigma_{fit} = (U/N)^{1/2}$, where $U = \Sigma w_i (p[H]_{exp,i} - p[H]_{calc,i})^2$, $N = \Sigma w_i$ and $w_i = (p[H]_{i+1} - p[H]_{i-1})^{-2}$ [d] The values in parenthesis indicate the number of points in each titration curve that were used in the curve-fitting procedure.

for the protonation constant, as can be seen from the table. This indicates that dimerization of lasalocid is negligible in the concentration range studied. This conclusion is supported by the results of the studies of ^1H and ^{13}C relaxation times by NMR which suggested that lasalocid in the form of free acid was present as a monomer in both chloroform[8] and methanol[9] solutions.

For all concentrations, the average calculated value of log K_H^{m*} is 5.01 ± 0.07 and log K_H^{c*} was calculated as described in section II.F to be 4.83. The latter value was used subsequently in the calculations of metal complexation constants.

UV-Vis spectrophotometric method.

Spectrophotometric titrations were carried out using sample solutions containing 4.50 mM lasalocid free acid, 1.0 mM DESPEN buffer and sufficient TEAP to maintain the ionic strength at 0.05 M. Temperature was controlled at 25.0 °C by an external water bath, attached to the cell-holder. The total pH* range included was from 2.8 to 7.0.

Figure IV.7 shows representative spectra obtained for a spectrophotometric titration covering the full pH* range. Changes were recorded in the UV-Vis spectrum of lasalocid in 80% methanol as the pH* was varied. The fully protonated compound (pH* 2.8) has peaks of maximum absorbance at 318 and 248 nm. As the pH* was increased, the peak at 318 nm shifts to a shorter wavelength and the one at 248 nm disappears into a shoulder. This behavior is similar to that reported in the literature for lasalocid solutions in methanol[6] and ethanol[10]. Isosbestic points were observed at 243, 270 and 314 nm. Although they were not well defined because of experimental errors in solution volume transfers, their presence indicated that there were only two absorbing components in solution. Figure IV.8 shows the plot of measured absorbance at 255 nm versus the hydrogen ion activity. The data was fit to equation IV.2 in order to obtain the value of protonation constant

$$A_i = \frac{A_1 K_H^{m*} a_H^* + A_0}{K_H^{m*} a_H^* + 1} \qquad \text{(IV.2)}$$

where A_0 is the absorbance of unprotonated lasalocid, A_1 is the absorbance of the monoprotonated compound, $K_H^{m}*$ is the mixed-mode protonation constant and a_H* is the hydrogen ion activity, which was calculated from the corrected pH* values as

$$a_H* = 10^{-pH*} \qquad \text{(IV.3)}$$

The protonation constants and their log values, obtained from data at different wavelengths, are shown in Table IV.4.

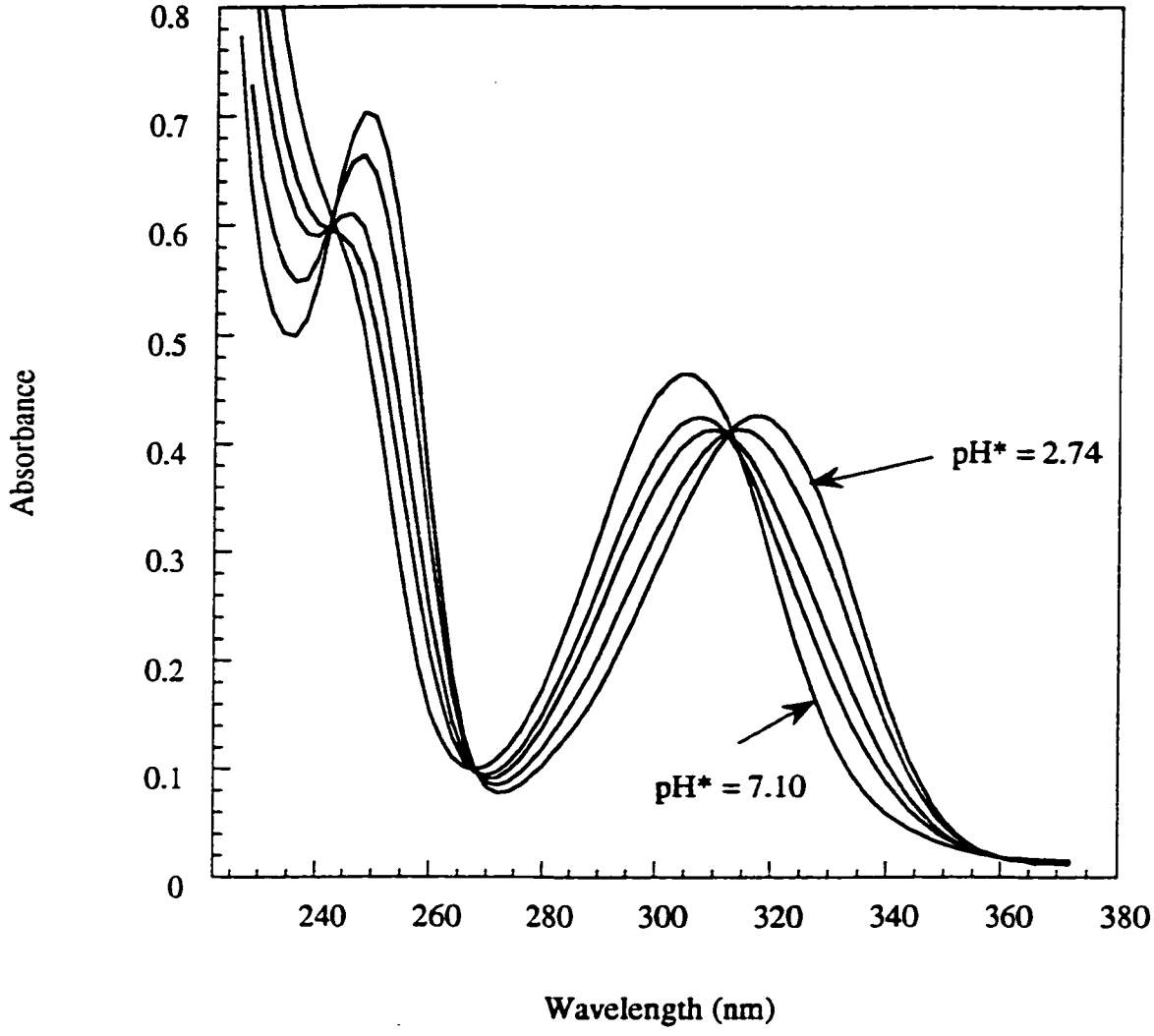

Figure IV.7. Representative spectra from the spectrophotometric pH-titration of lasalocid in 80% methanol-water at 25.0 °C. The solution contained 4.50 mM lasalocid, 1.0 mM DESPEN buffer and TEAP to maintain ionic strength at 0.05 M. HLas was titrated by adding small aliquots (0.5-2 uL) of 1.3 M tetraethylammonium hydroxide.

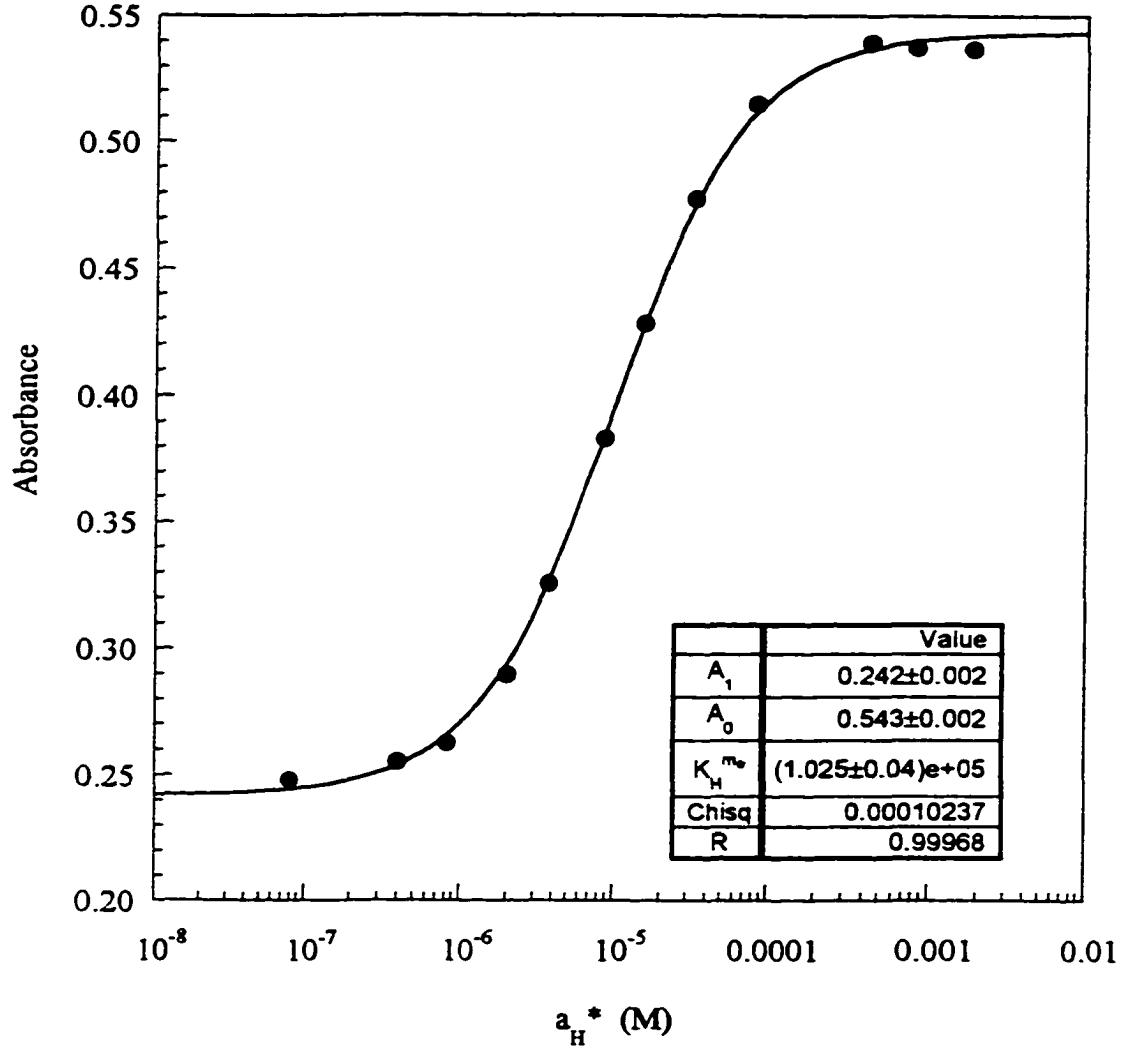

Figure IV.8. Plot of the absorbance at 255 nm as a function of a_H^* for the titration of lasalocid shown in fig. IV.7. The data were fit to eq IV.3. The solid line was calculated using the values of the parameters in the inset table.

Table IV.4. Calculated values for the mixed-mode protonation constants of lasalocid from spectrophotometric titrations in 80% methanol-water[a]

Exper. #	λ, nm	$K_H^{m*} \times 10^{-5}$ [b]	$\log K_H^{m*}$
1	230	1.03±0.03	5.01
1	255	1.03±0.04	5.01
1	300	1.08±0.08	5.03
1	330	1.01±0.02	5.00
2	255	1.08±0.08	5.03
2	300	1.36±0.15	5.13
2	330	1.13±0.10	5.05

[a] At 25.0 °C; ionic strength = 0.05 M (TEAP). [b] Uncertainty expressed as standard error.

IV.C. Spectrophotometric studies of lead(II)-lasalocid binding.

To study lead complexation, a solution containing 0.100 M lasalocid in 80% methanol was titrated with a 0.0230 M solution of lead perchlorate. To define the stoichiometry of the complex formed from the UV-Vis absorbance change, the pH* of the solution should be significantly higher than the log value of the ligand protonation constant (log K_H^{m*}) to avoid the protonation side-reaction of ligand and to obtain a linear dependence of absorbance on metal concentration. This condition would be satisfied if at least 99% of the ligand present is deprotonated. In case of lasalocid, the following relationship holds

$$K_H^{m*} = 10^{5.01} = \frac{[HLas]}{a_H^{\bullet}[Las^-]} = \frac{1}{a_H^{\bullet}99} \qquad (IV.4)$$

The calculated value of pH* needed to fulfill this condition was found to be 7.01. Precipitation from the solution, possibly in the form of lead hydroxyde, was noticed at pH* 6.8 when the lead-lasalocid ratio exceeds unity. The precipitation interfered with any further complexation reaction. Nevertheless, the UV-Vis spectra associated with lead-lasalocid complexation were recorded prior to that occurrence. The pH* of the solution was controlled at 6.77 with 3 mM MES and 5 mM MOPS buffers. The spectra obtained are shown in Figure IV.9. Upon addition of lead, the position of the absorbance peak of lasalocid ligand shifted from 304 to 310 nm, and it was accompanied by the increase in absorbance at 320 nm which was monitored. An increase in absorbance at 244 nm was also observed, but at that wavelength absorbance resulting from increasing lead concentration of the solution (maximum at 218nm) could also have contributed to the change. In Figure IV.10 the absorbance values at 320 nm are plotted against the ratio of total lead to lasalocid concentrations. Due to the occurrence of precipitation reactions, the absorbance curve did not level off but continued to increase with the addition of lead beyond the first equivalence point. The break in the curve occurred where the lead to lasalocid concentration ratio was unity. This behavior is

consistent with the formation of complex with 1:1 lead-lasalocid stoichiometry in solution.

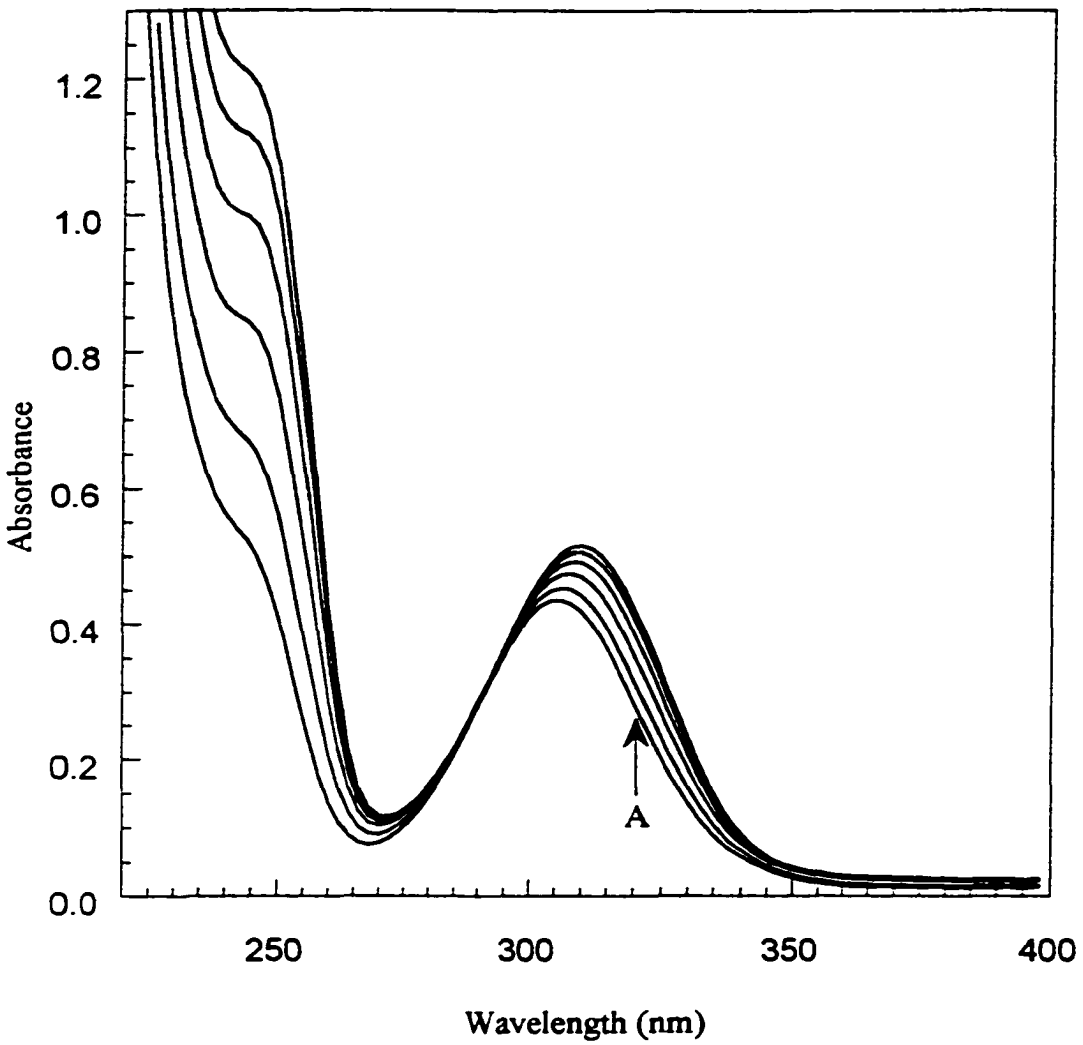

Figure IV.9. Representative UV-Vis spectra from the titration of lasalocid with lead perchlorate in 80% methanol-water at 25.0 °C. 3-5 uL aliquots of 0.0230 M lead perchlorate were used to titrate 2.50 mL of a solution containing 0.100 mM lasalocid. pH* was controlled at 6.5 with 5 mM MES and 5 mM MOPS buffers, at ionic strength 0.05 M (TEAP). The spectra were recorded 2 minutes after the lead addition to allow reaction equilibrium to be established. Curve A – lasalocid alone, no $Pb(ClO_4)_2$ added.

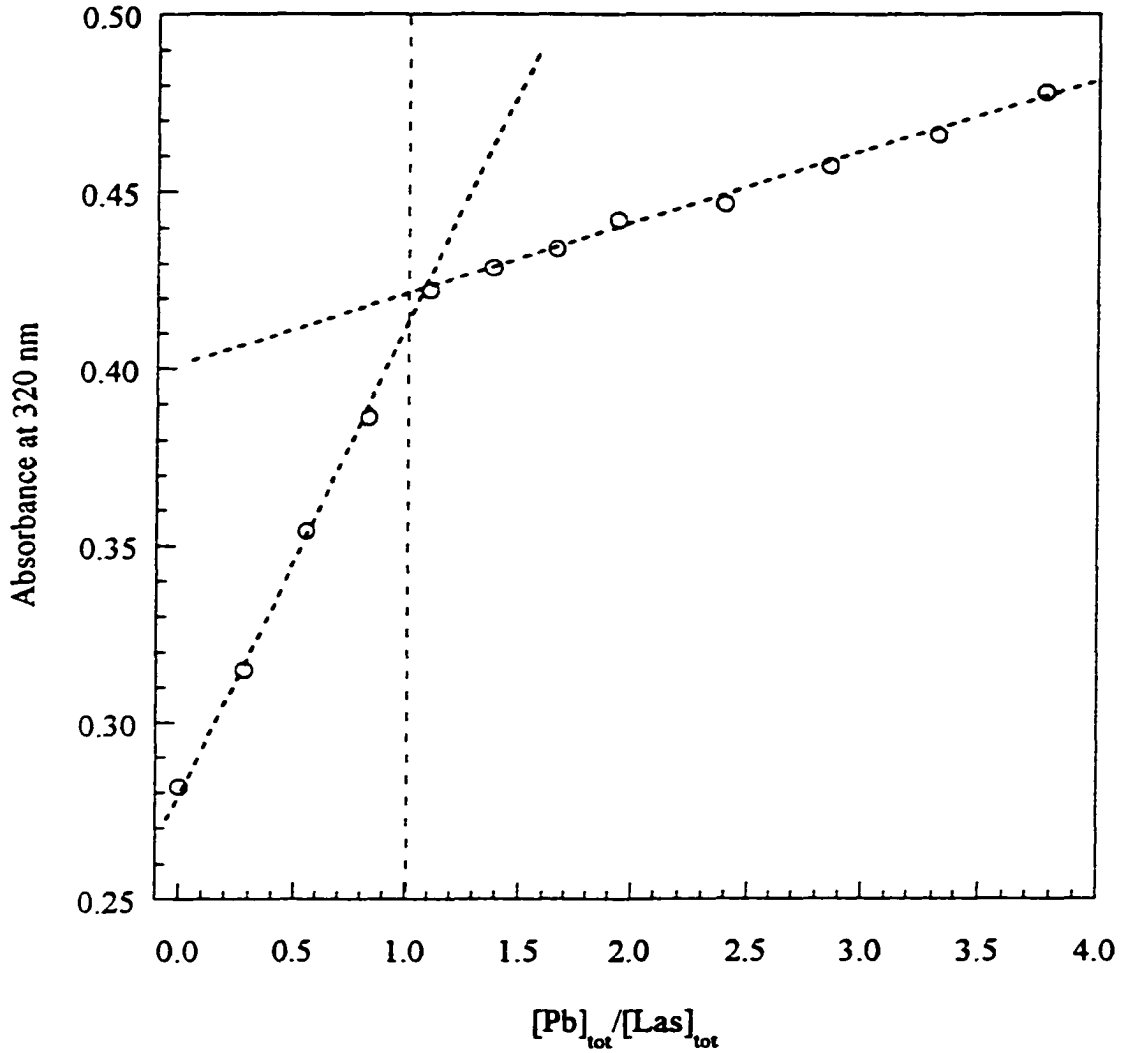

Figure IV.10. Plot of the absorbance change resulting from each aliquot of lead perchlorate added versus the concentration ratio of total lead to total lasalocid.

An estimate for the lead complexation constant was found by titrating lasalocid with lead perchlorate at a lower pH*, where lead hydroxide does not form and, therefore, does not interfere with reaction. Expressions for the lasalocid-lead equilibrium reaction and the corresponding complex formation constant are presented in Equation IV.5, where L^- stands for the anion of lasalocid.

$$Pb^{2+} + L^- \rightleftharpoons PbL^- \qquad K_{PbL} = \frac{[PbL^-]}{[Pb^{2+}][L^-]} \tag{IV.5}$$

The intrinsic value of K_{PbL} is related to the apparent, or pH*-dependent, formation constant K'_{PbL} as follows

$$\log K_{PbL} = \log K'_{PbL} - \log \alpha_L \tag{IV.6}$$

The pH* dependence of the α_L term is given by

$$\alpha_L = \frac{[L^-]}{([L^-]+[HL])} = \frac{1}{(1+K_H^{m*}a_H^*)} \tag{IV.7}$$

where K_H^{m*} is the mixed-mode acid protonation constant. At the pH* where at least 99% of ligand exists in the protonated form, or where $pH^* \leq \log K_H^{m*} - 2$, $\alpha_L = (K_H^{m*} a_H^*)^{-1}$, and expression IV.6 can be rewritten as

$$\log K_{PbL} = \log K'_{PbL} + \log K_H^{m*} - pH^* \tag{IV.8}$$

The lasalocid-lead titration was carried out at pH* 3.1, which is about 2 pH* units lower than $\log K_H^{m*}$. The lasalocid solution was prepared using 1.0 mM perchloric acid in 80% methanol-water as a solvent, and the pH* was adjusted to the required value with 1.4 M tetraethylammonium hydroxide. Prior to that, stability of the free acid form of lasalocid was checked by monitoring its UV-Vis spectra with time. No spectral change was recorded during a 4 hour period and protonated lasalocid was concluded to be stable at this pH. Small aliquots of lead perchlorate solution were added directly to the spectrophotometric cell and the absorbances at 298 nm and 320 nm were

recorded. The absorbance decreased at 330 nm and increased at 298 nm as shown in Figure IV.11. This behavior differs from the UV-Vis behavior observed for the reaction between unprotonated lasalocid with lead. The difference is probably due to the differences in the UV-Vis spectra of protonated and unprotonated free lasalocid. Spectra were recorded after waiting 3-5 minutes following each addition of lead in order to allow the true reaction equilibrium to be established. Figure IV.12 shows a plot of the absorbance change at 330 nm vs the concentration of free lead. The value of the apparent complexation constant was obtained using non-linear least-squares to fit the data to the expression

$$\Delta Abs_i = \frac{\Delta Abs_\infty \, K'_{PbL}[Pb^{2+}]_i}{1+[Pb^{2+}]_i K'_{PbL}} \qquad (IV.9)$$

where ΔAbs_∞ is the difference between the limiting and initial absorbance ($Abs_\infty - Abs_0$), ΔAbs_i is the difference between the limiting absorbance and the absorbance at each titration point ($Abs_\infty - Abs_i$) , $[Pb^{2+}]_i$ is the concentration of the free lead cation at each point. The derivation for equation IV.9 is similar to that of equation III.13 which is presented in Appendix 1. Initial estimates for calculated parameters ΔAbs_∞ and K'_{PbL} were required by the curve-fitting program. An estimate of ΔAbs_∞ was obtained from the spectra. An initial estimate of K'_{PbL} was obtained from the fraction of change in absorbance when the metal-ligand ratio was unity. At the point where total metal $[M]_{tot}$ and total ligand $[HL]_{tot}$ concentrations are equal, the fraction of the total absorbance change is linearly related to the fraction of the total metal complexed

$$\frac{\Delta \, Abs_i}{\Delta \, Abs_\infty} \approx \frac{[PbL^+]'}{[Pb^{2+}]_{tot}} = \chi \qquad (IV.10)$$

where $[PbL^+]'$ represents the sum of the concentrations of all complexes with 1:1 Pb-L stoichiometry, including both protonated and unprotonated species. The concentrations of the uncomplexed reactants can be determined from mass balance equations, assuming the formation of only lead-lasalocid complexes with 1:1 stoichiometry and that the concentration of the unprotonated form of lasalocid, Las^-, is negligible at this pH.

$$[Pb^{2+}]_{tot} = [Pb^{2+}] + [PbL^+]' \qquad \text{(IV.11)}$$

$$[HL]_{tot} = [HL] + [PbL^+]' \qquad \text{(IV.12)}$$

Those concentrations of $[Pb^{2+}]$ and [HL] calculated at the point where $[Pb^{2+}]_{tot} = [HL]_{tot}$, can be used to provide an initial estimate for K'_{ML} as follows

$$K'_{PbL} = \frac{[PbL^+]'}{[Pb^{2+}]_i\,[HL]_i} = \frac{\chi\,[Pb^{2+}]_{tot}}{((1-\chi)\,[HL]_{tot})^2} = \frac{\chi}{[Pb^{2+}]_{tot}\,(1-\chi)^2} \qquad \text{(IV.13)}$$

This trial value is then used to find the concentration of free lead at each titration point, using the following equation

$$[Pb^{2+}]_i = \frac{-(K'_{PbL}([Pb^{2+}]_{tot}-[HL]_{tot})+1)+\sqrt{(K'_{PbL}([Pb^{2+}]_{tot}-[HL]_{tot})+1)^2-4K'_{PbL}[HL]_{tot}}}{2K'_{PbL}} \qquad \text{(IV.14)}$$

These new values of $[Pb^{2+}]_i$ were used in fitting equation IV.9 and a new estimate for K'_{PbL} was obtained from the non-linear least-squares fit of the data. The iteration was repeated until the resulting parameters differed by less than 1 percent between two consecutive cycles. An example of the results after final curve-fitting step is shown in Figure IV.12. The values of the apparent complexation constants obtained and the pH-independent constants calculated using equation IV.6 are listed in Table IV.5

Addition of 0.05 M TEAP to control ionic strength resulted in a dramatic change of the system behavior. At pH* 3.01 the addition of the first few lead aliquots resulted in the increase of absorbance over the entire wavelength range indicating the formation of

precipitate. A change in absorbance indicative of complex formation (increase at 298nm and decrease at 330 nm) occurred at much larger lead/lasalocid concentration ratios than expected (more than unity). Therefore, because the higher ionic strength of solution interfered with the complexation reaction, this data was not used to calculate K'_{PbL}.

Table IV.5 Apparent and pH*-independent complexation constants for lead–lasalocid derived from UV-Vis titrations in 80% methanol-water[a]

Exp. #	λ, nm	K_{ML}	error[b] in K_{ML}	ΔAbs_∞	error[b] in ΔAbs_∞	pH*	calc. α_L[c]	calc.[d] log K_{ML}
1	298	3460	185	0.107	0.006	3.04	0.00806	5.63
	330	2290	188	-0.125	0.003	3.04	0.00806	5.45
2	298	6513	273	0.097	0.001	3.14	0.0130	5.81
	332	1551	76	-0.129	0.003	3.14	0.0130	5.19

[a] at 25 °C and about 1 mM ionic strength. [b] Uncertainty in terms of standard error. [c] Calculated from eq IV.7 using the value of $K^m_H* = 10^{5.13}$, corrected to 0.004 M ionic strength. [d] Calculated from eq IV.6.

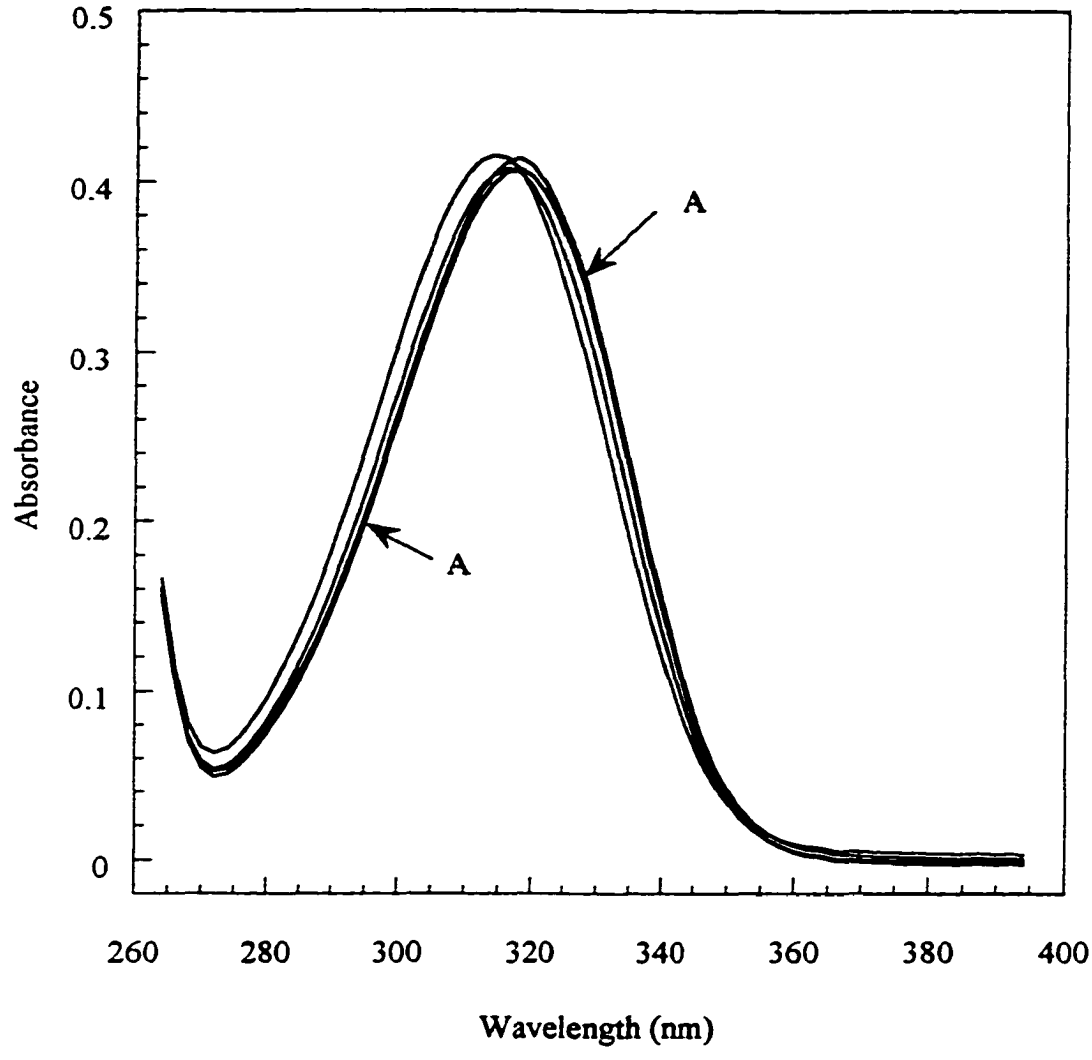

Figure IV.11. Representative UV-Vis spectra from the titration of the lasalocid with lead perchlorate in 80% methanol-water at pH * 3.14 and 25.0 °C. 3-5 uL aliquots of 0.0230 M lead perchlorate were used to titrate 2.50 mL of a solution containing 0.100 mM lasalocid. In order to control the pH* lasalocid solution was prepared using 1 mM solution of $HClO_4$ in 80% methanol-water for a solvent. No ionic strength control was employed. Spectrum A is for HLas alone, no lead added.

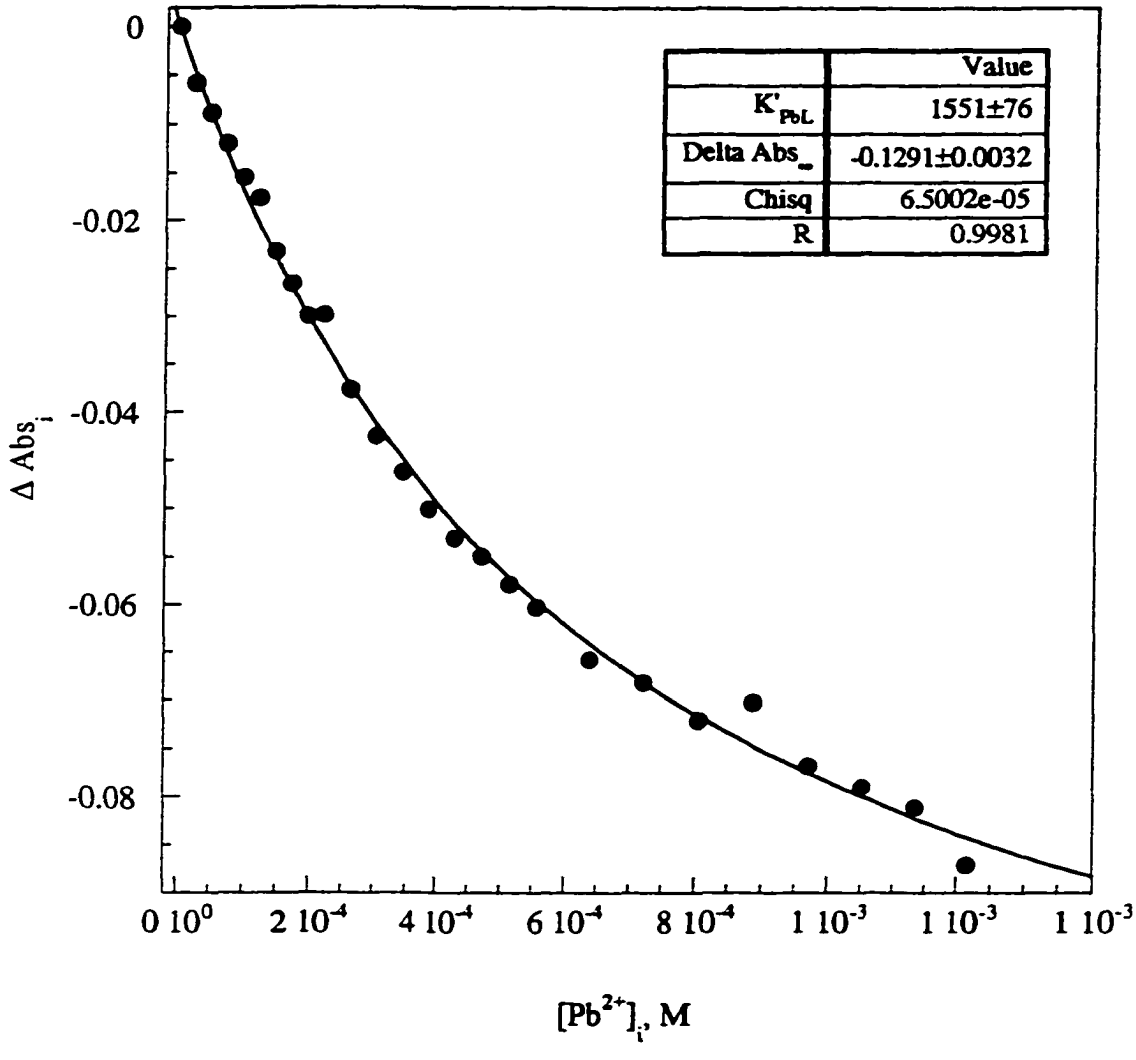

Figure IV.12. Change in absorbance at 330 nm as a function of $[Pb^{2+}]_i$ at pH* 3.14. In order to control the pH* lasalocid solution was prepared using 1 mM solution of $HClO_4$ in 80% methanol-water for a solvent. 3-5 μL aliquots of 0.0230 mM lead perchlorate were used to titrate 2.50 mL of a solution containing 0.100 mM lasalocid. The titration was done at 25.0 °C and ambient (from 1.1 mM to 5 mM) ionic strength. The solid line was calculated from eq IV.8 using the derived parameters listed in the inset table.

IV.D. Potentiometric studies of metal binding.

Titration data sets were obtained for solutions of lasalocid free acid in 80% methanol in the presence of metal perchlorates as described in Chapter II.F. Different metal-ligand ratios were used to test for the presence of complexes with varied stoichiometry. Ratios of 1:1 and 1:2 metal-ligand were employed for lasalocid-calcium and lasalocid-sodium titrations, ratios of 2:1, 1:1 and 1:2 were used for and lasalocid-zinc titrations, and three different ratios (1:1, 1:2, 1:3) were used for lasalocid-lead titrations. Stability constants for lasalocid complexes were obtained by analyzing each data set (p[H] vs volume titrant) with the program BEST[7]. The p[H] is defined in eq IV.15, where $[H^+]$ is the molar concentration of the hydrogen ion in 80% methanol-water.

$$p[H] = -\log[H^+] \qquad \text{(IV.15)}$$

An electrode solvent correction factor was applied to the pH* values obtained as described in Chapter II.B. The pH* values in each data set were converted to p[H] using the logarithm of the hydrogen activity coefficient. The values for the total concentrations of free lasalocid, metal cation, and titrant base were also required for the program input file.

Equilibrium constants for all reactions included in the model used to fit the data were expressed in terms of overall complexation constants (log β values). Reactions were written as the combination of protons or metals with donor ligands. The overall equilibria for the formation of hydroxy complexes were written in the form of acid dissociation reactions. The expressions for equilibria and corresponding constants are shown in equations IV.16 – IV.23, where M stands for the metal ion and L^- stands for the lasalocid anion

$$H^+ + L^- \rightleftharpoons HL \qquad \beta_{HL} = K_H = \frac{[HL]}{[H^+][L^-]} \qquad \text{(IV.16)}$$

$$M^{n+} + L^- \rightleftharpoons ML^{n-1} \qquad \beta_{ML} = \frac{[ML^{n-1}]}{[M^{n+}][L^-]} \qquad \text{(IV.17)}$$

$$M^{n+} + 2\,L^- \rightleftharpoons ML_2^{n-2} \qquad \beta_{ML_2} = \frac{[ML_2^{n-2}]}{[M^{n+}][L^-]^2} \qquad \text{(IV.18)}$$

$$M^{n+} + L^- + H^+ \rightleftharpoons MLH^{n+} \qquad \beta_{MLH} = \frac{[MLH^{n+}]}{[M^{n+}][L^-][H^+]} \qquad \text{(IV.19)}$$

$$M^{n+} + 2\,L^- + H^+ \rightleftharpoons ML_2H^{n-1} \qquad \beta_{ML_2H} = \frac{[ML_2H^{n-1}]}{[M^{n+}][L^-]^2[H^+]} \qquad \text{(IV.20)}$$

$$M^{n+} + L^- + H_2O \rightleftharpoons MLOH^{n-2} + H^+ \qquad \beta_{MLOH} = \frac{[MLOH^{n-2}][H^+]}{[M^{n+}][L^-]} \qquad \text{(IV.21)}$$

$$M^{n+} + H_2O \rightleftharpoons MOH^{n-1} + H^+ \qquad \beta_{MOH} = \frac{[MOH^{n-1}]\,[H^+]}{[M^{n+}]} \qquad \text{(IV.22)}$$

$$M^{n+} + 2H_2O \rightleftharpoons M(OH)_2^{n-1} + 2H^+ \qquad \beta_{M(OH)_2} = \frac{[M(OH)^{n-2}]\,[H^+]^2}{[M^{n+}]} \qquad \text{(IV.23)}$$

In this study log β_{HL} was determined previously, as described in Section IV.B and was held constant during calculations. Data fitting started with a simple model including

equilibria IV.15, IV.16 and formation of hydroxy-metal complexes (eqs IV.22 and IV.23), where applicable. A 2:1 ligand-metal complex (eq IV.18) was included in the original model for the titrations of solution with 2:1 lasalocid-metal concentration ratio. Other species, for example, mixed hydroxide-metal-lasalocid complexes, were added to the model to test whether their addition resulted in an improvement of the fit. They were retained in the model if the value of the σ_{fit} (eqs III.5 and III.6) was improved upon their addition.

The values of stability constants obtained for a given model were then used to calculate a species distribution diagram with the program Comics[11]. If a particular complex species constituted less than 5% of the total amount of ligand or metal, it was considered to be insignificant and was eliminated from the model. The values of complexation constants with the updated model were recalculated and the process repeated until the satisfactory curve fit and the set of binding constants was obtained. The experimental details for each individual metal titration and the associated curve fitting procedures are discussed below.

Sodium-lasalocid and calcium-lasalocid.

Plots for the titrations of lasalocid with sodium or calcium present showed that the addition of calcium or sodium ions to the solution of lasalocid did not result in a significant shift of the acid titration curve toward lower pH* values. This behavior indicated that even if the complex is formed, it is very weak. A general limitation of the potentiometric titration method is that it does not give reliable equilibrium constants for weak complexes (i.e., $\log \beta_{ML} < 2$). In these cases the $\log \beta_{ML}$ value would be less than 2 and could not be obtained from the curve-fitting procedures. The plots of the experimental titration curves are shown in Figures IV.13 and IV.14 for sodium and calcium, respectively.

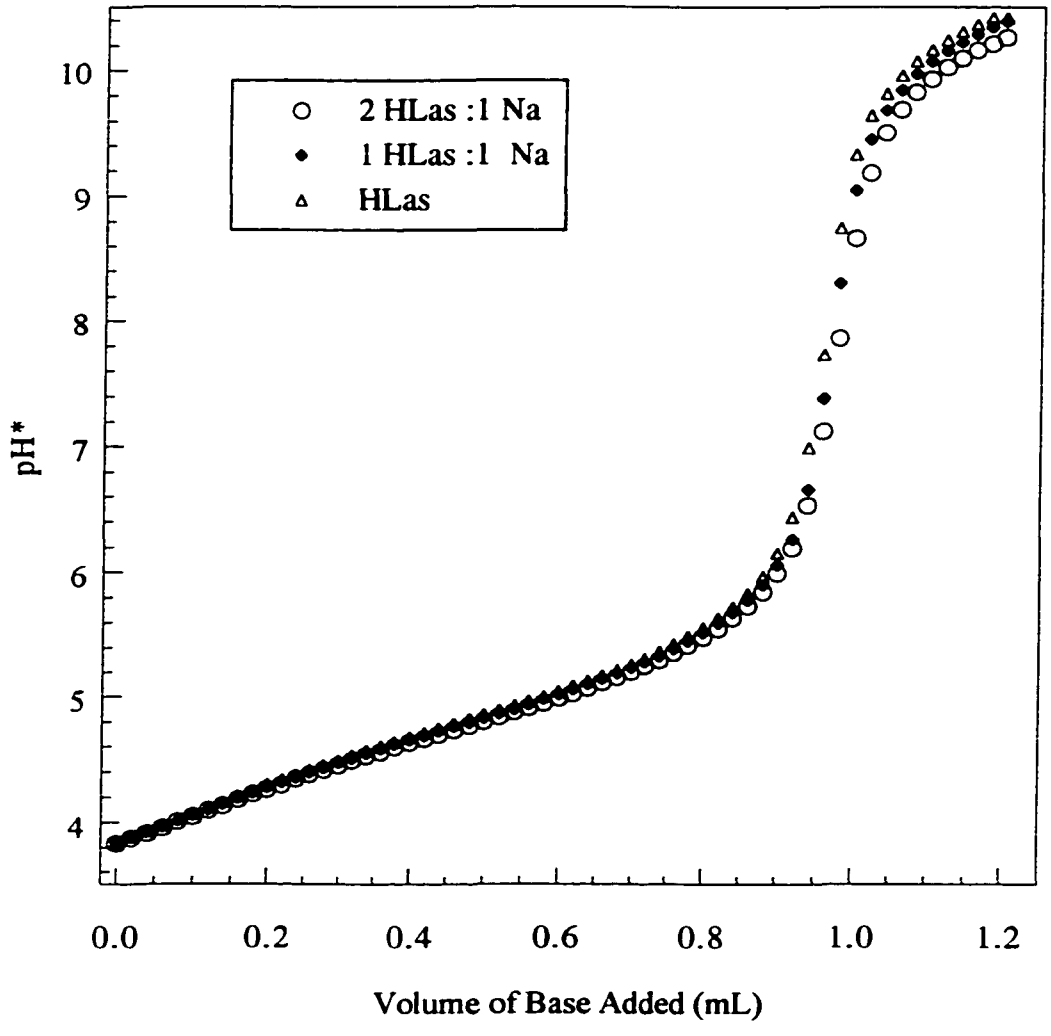

Figure IV.13. Potentiometric titration curves for various stoichiometric ratios of lasalocid-sodium in 80% methanol-water solution at 25.0 °C. Each solution contained 10.0 mL of 4.50 mM lasalocid in the acid form alone or with indicated amounts of added sodium at 0.05M ionic strength (TEAP).

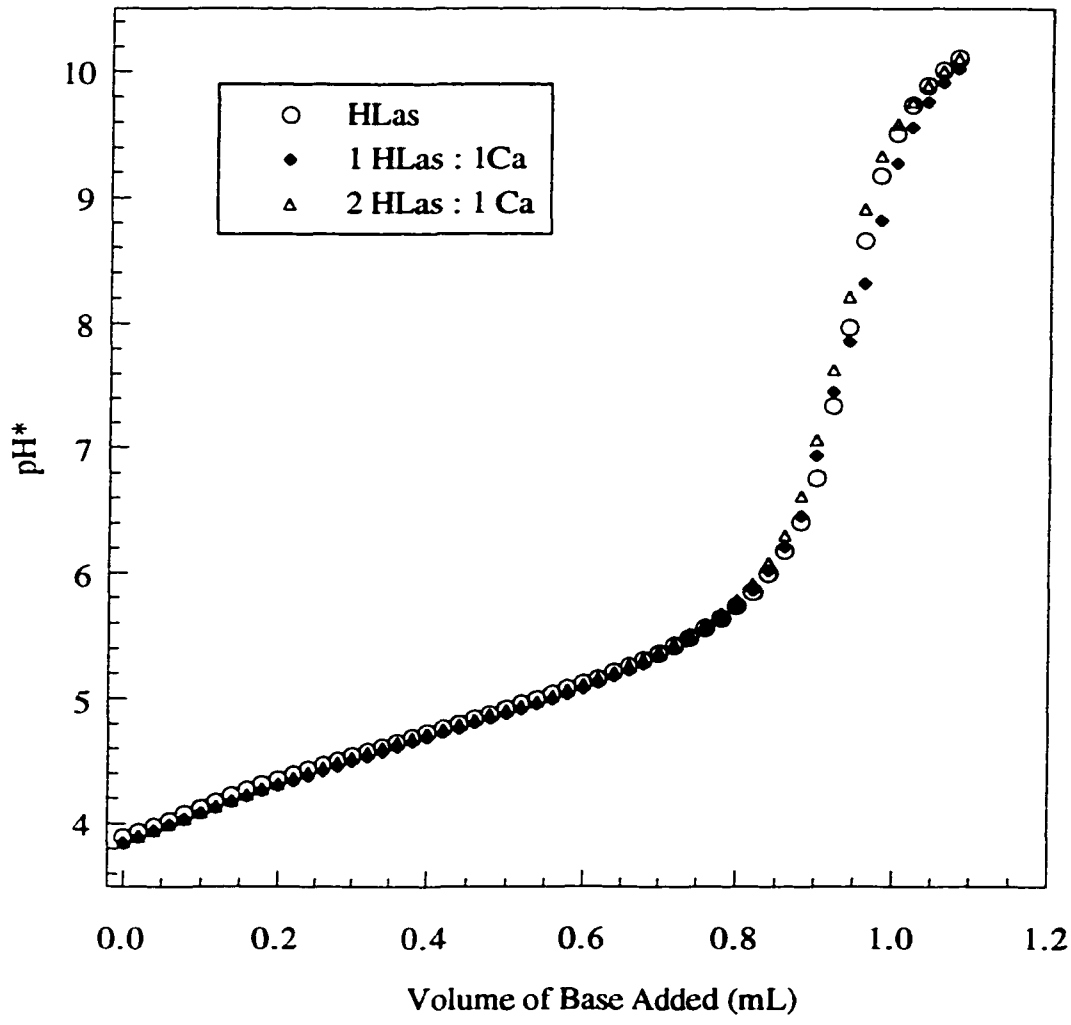

Figure IV.14. Potentiometric titration curves for various stoichiometric ratios of lasalocid-calcium in 80% methanol-water solution at 25.0 °C. Each solution contained 10.0 mL of 4.50 mM lasalocid in the acid form alone or with indicated amounts of added calcium at 0.05M ionic strength (TEAP).

Lasalocid-zinc titrations.

Aliquots of a standardized solution of zinc perchlorate in 80% methanol were added to the titration vessel containing 10.0 mL of lasalocid free acid in the amounts required to achieve the desired stoichiometric ratio. The mixture was allowed to equilibrate for 5 minutes at 25.0 °C and was titrated with 0.02118 M tetramethylammonium hydroxide. The resulting pH* curves were analyzed using the program BEST[7]. Formation of zinc-hydroxide complexes was included in the model used to fit the titration data. Values of formation constants for zinc-hydroxide complexes in 80% methanol-water were estimated as previously described in Section III.D for zinc-monensin titrations. The model used to fit the data with the program BEST also included the presence of a 1:1 zinc-lasalocid complex and a ternary zinc-lasalocid-hydroxide species. The complex species $ZnLas_2H$ was also required in order to obtain a better curve fit. Experimental titration curves for solutions having various zinc-lasalocid stoichiometries are presented in Figure IV.15. Due to the observed precipitation, data points above pH* 6.0 were not used to fit the data. Figures IV.16 and IV.17 illustrate the results of the refined fits for the 1:1 and 2:1 lasalocid-zinc solution concentration ratios . The values of equilibrium constants for the individual experiments are listed in Table IV.6. The average values of the equilibrium constants are listed in Table IV.8. Species distribution curves as a function of p[H] were calculated using the average values of these equilibrium constants and are shown in Figure IV.18.

Table IV.6. Log β_X values obtained from potentiometric titrations of lasalocid and zinc(II) in 80% methanol-water[a].

exp	HL-Zn	Identity of complex species X						σ_{fit} [f]
#	ratio	HL[b]	ZnL[c]	$ZnLas_2H$[c]	ZnLOH[c,d]	ZnOH[e]	$Zn(OH)_2$[e]	
1	1	4.83	2.64	9.58	-5.09	-9.4	-18.2	0.035
2	1	4.83	2.60	9.54	-5.65	-9.4	-18.2	0.018
3	2	4.83	2.51	9.63	-5.85	-9.4	-18.2	0.012
4	0.5	4.83	2.61	9.39	-5.07	-9.4	-18.2	0.018

[a] 25.0 °C, 0.05 M ionic strength (TEAP); [b] The value of log β_{HL} (section IV.B) was fixed during refinement [c] Values were refined by program BEST. [d] β_{ZnLOH} is expressed as the acid dissociation constant (eq IV.21). [e] Values were fixed during refinement. [f] Standard deviation expressed as σ_{fit}, $\sigma_{fit} = (U/N)^{1/2}$, where $U = \Sigma w_i (p[H]_{exp,i} - p[H]_{calc,i})^2$, $N = \Sigma w_i$, and $w_i = (p[H]_{i+1} - p[H]_{i-1})^{-2}$.

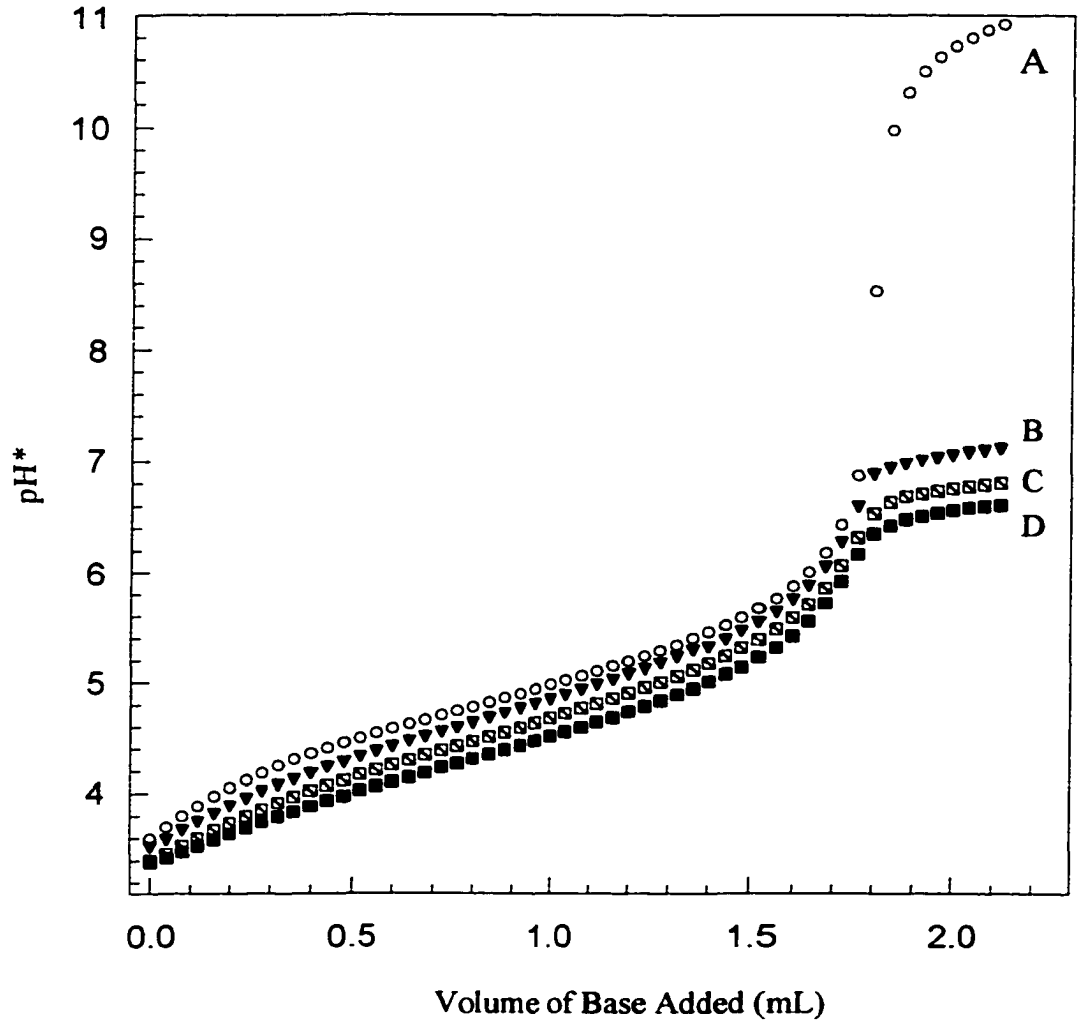

Figure IV.15. Potentiometric titration curves for various stoichiometric ratios of lasalocid-zinc in 80% methanol-water at 25.0 °C. Each solution contained 10.0 mL of 3.81 mM free lasalocid in the acid form. 0.0586 M zinc perchlorate was added in the amount to obtain the following stoichiometric ratios: A. no Zn; B. 2:1 HLas-Zn; C. 1:1 HLas-Zn; D. 1:2 HLas-Zn. All titrations were done at 0.05 M ionic strength (TEAP).

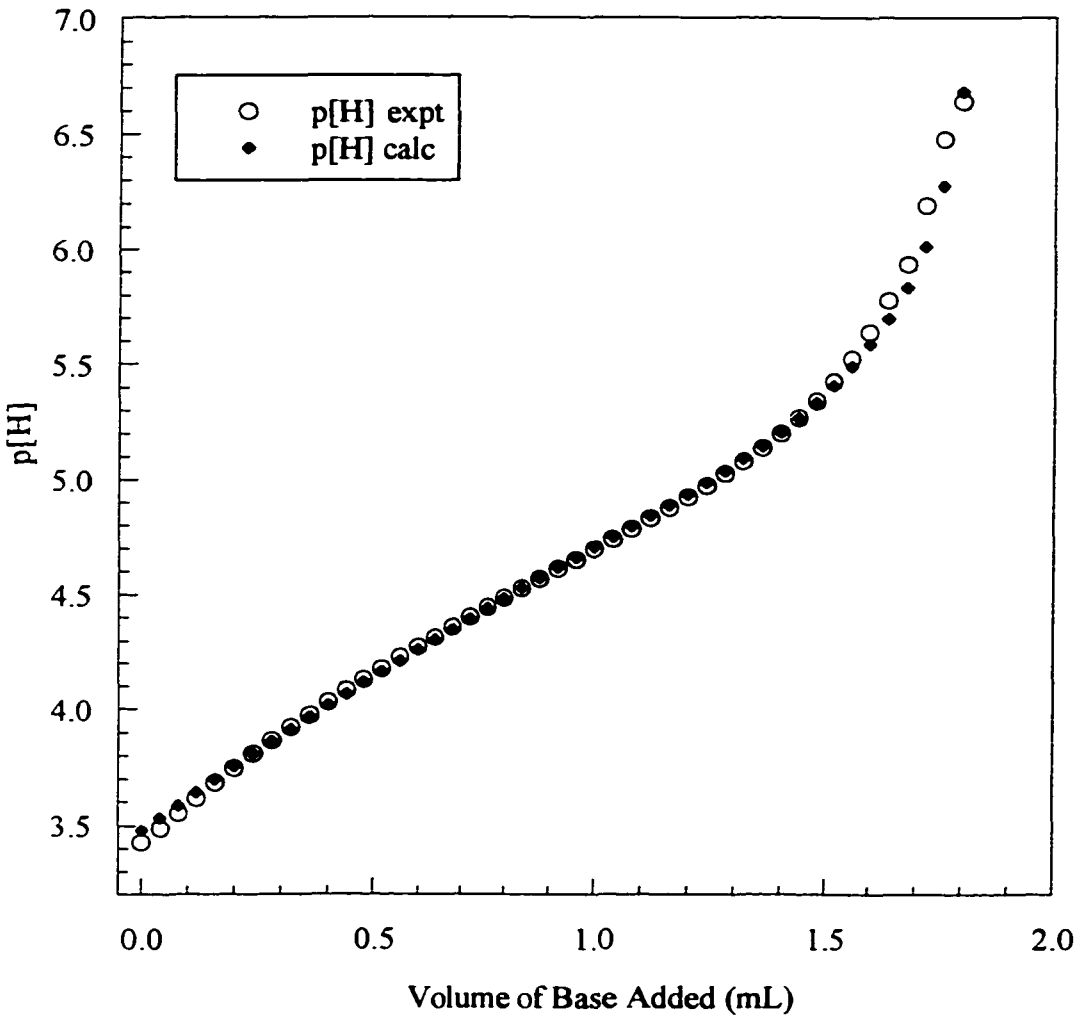

Figure IV.16. Potentiometric titration curve for 10.66 mL of a solution containing 3.81 mM lasalocid free acid and 3.87 mM zinc at an ionic strength of 0.05 M (TEAP) in 80% methanol-water at 25.0 °C. The titrant is 0.02118 M tetramethylammonium hydroxide with ionic strength maintained at 0.05 M with TEAP. The calculated p[H] values were obtained from the program BEST using refined values of equilibrium constants for the model containing the species listed in Table IV.6, Exp.2.

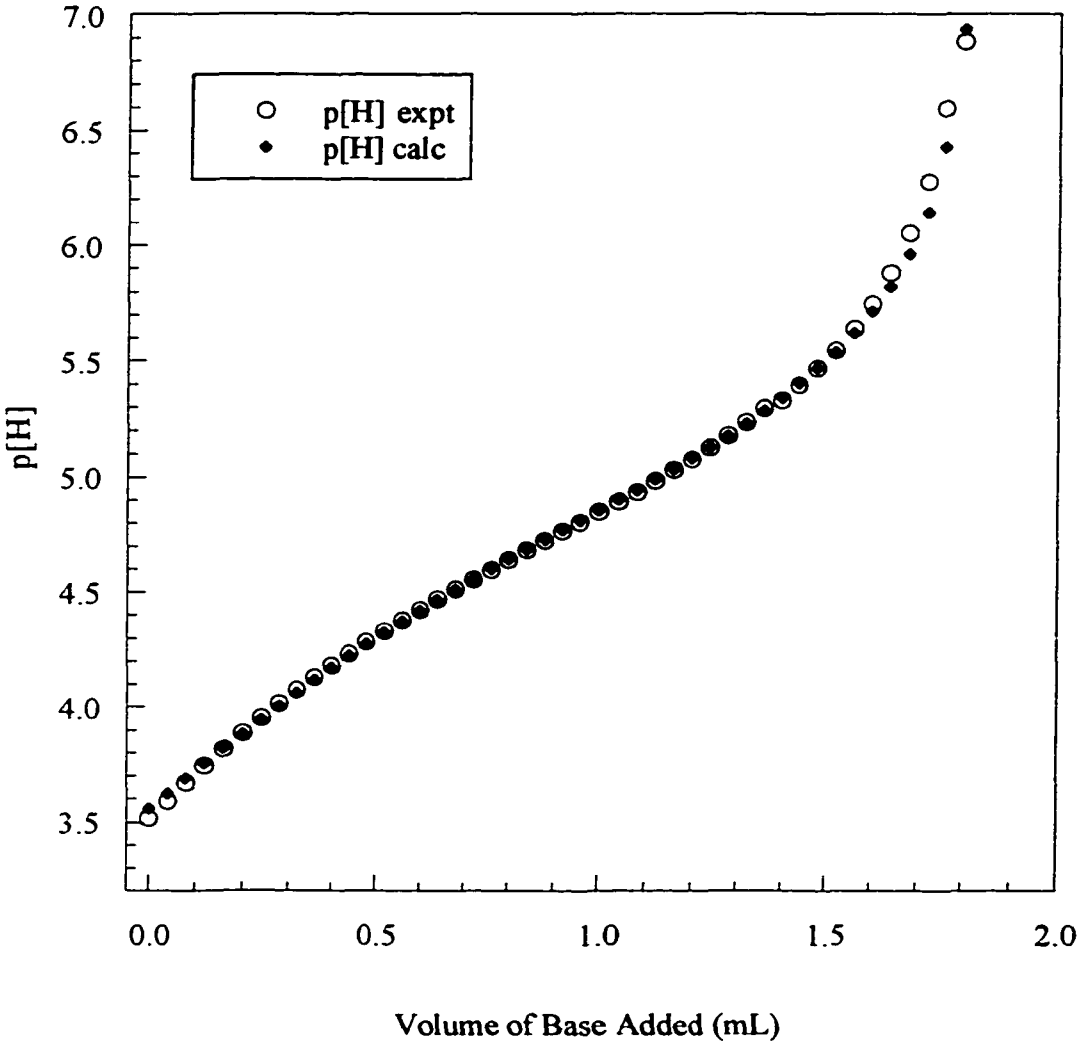

Figure IV.17. Potentiometric titration curve for 10.33 mL of a solution containing 3.81 mM lasalocid and 1.93 mM zinc at an ionic strength of 0.05 M (TEAP) at in 80% methanol-water 25.0 °C. The titrant is 0.02118 M tetramethylammonium hydroxide with ionic strength maintained at 0.05 M with TEAP. The calculated p[H] values were obtained from the program BEST using refined values of equilibrium constants for the model containing the species listed in Table IV.6, Exp.3.

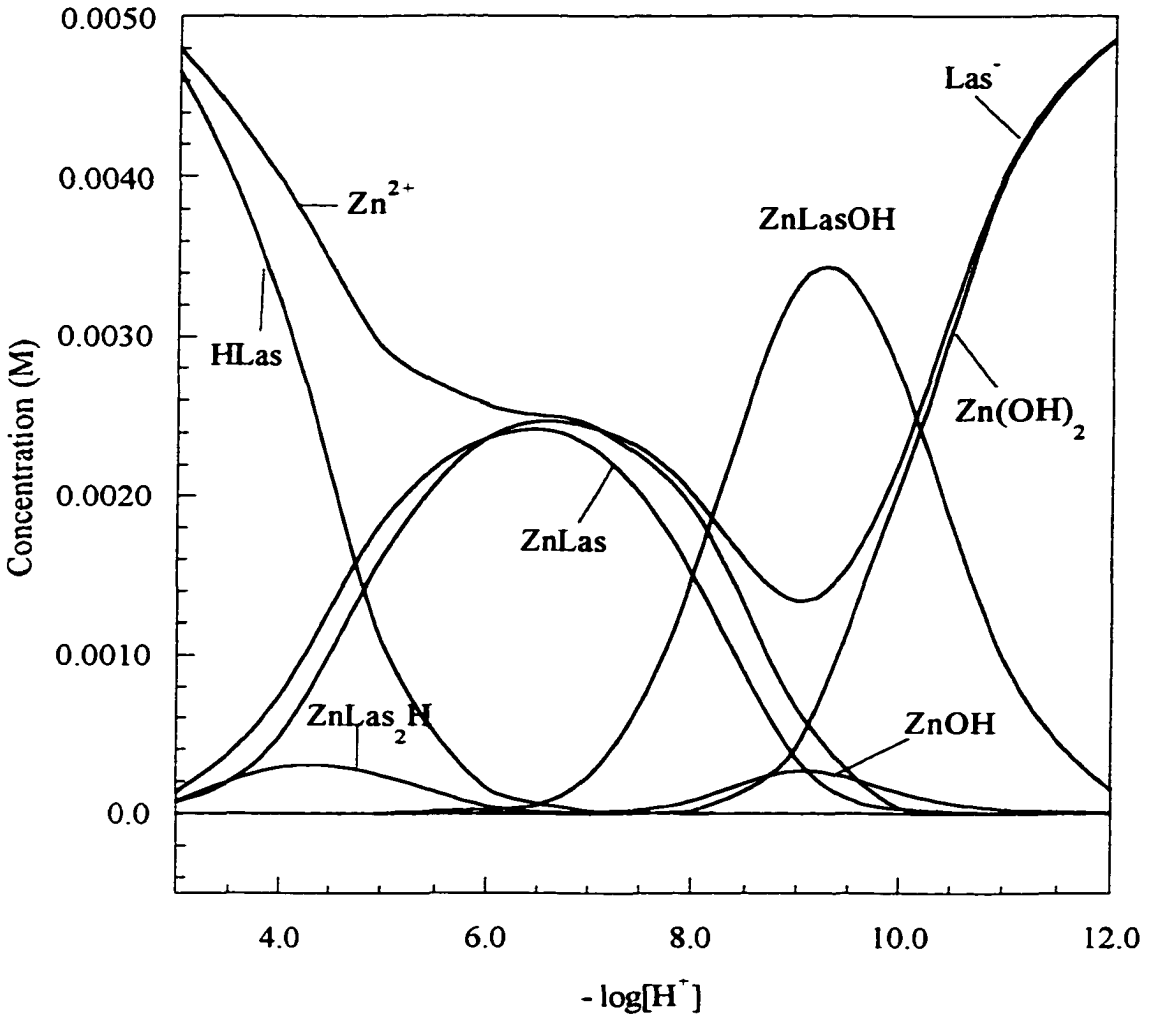

Figure IV.18. Species distribution curves for lasalocid-zinc complexes in solution as a function of p[H] in 80% methanol water. Species concentrations were calculated using the program Comics (Ref.11) for 5.0 mM lasalocid and 5.0 mM zinc using the average values of the equilibrium constants listed in Table IV.8.

Lead(II)-lasalocid.

An aliquot of a standardized solution of 0.0230 M lead perchlorate in 80% methanol was added to the titration vessel containing 10.0 mL of 4.25 mM solution of lasalocid free acid in the amount required to achieve the desired stoichiometric ratio. The mixture was allowed to equilibrate for 5 minutes at 25.0 °C and was titrated with 0.02029 M tetramethylammonium hydroxide. The resulting pH* curves were analyzed using the program BEST[7].

A number of pH* titration data sets were acquired for lead-lasalocid systems. Experimental titration curves for various lead-lasalocid concentration ratios are presented in Figure III.19. The end-point in all pH*-curves occurred when the amount of mmoles of base added was equal to the mmoles of lasalocid present. For titrations where Las-Pb concentration ratio exceeded 1.5, an additional end-point was observed at the point where the millimoles of the base added were equal to the mmoles of lead present. The last end-point in the pH*-curves occurred when the amount of mmoles of base added was equal to the sum of mmoles of lasalocid and mmoles of lead. Precipitation at p[H] > 7.5 occurred before the last end-point on the curve was reached. Therefore, data points beyond the second equivalence point on the curve (p[H] ≈ 7.0) were not used in the curve fitting process.

Equilibria included in the models used to fit the experimental data included 1:1 lead-lasalocid, mixed 1:1:1 lead-lasalocid-hydroxide, and 1:1 lead-hydroxide species. The value of the equilibrium constant for the formation of $PbOH^+$ in 80% methanol-water was estimated as described for monensin-lead titrations, and was kept fixed during calculations. In addition to the complexes included in the model described above, species having 2:1 Mon-Pb stoichiometry were required to fit the data for solutions that contained an excess of lasalocid. Including the species PbMonH in the model did not

result in a significant improvement of the fit. Therefore, it was excluded from the final model used to fit the data.

Curve fits for the solutions where lasalocid-lead concentration ratio was less than 1.5, showed large systematic differences between the calculated and experimental values of p[H] and had large values of the parameter σ_{fit}. The results of these fits were not included in Table IV.7, which lists the values for equilibrium constants obtained. For titrations with lasalocid-lead concentration ratios higher that 1.5, the first few calculated p[H] points (6 or 7) were systematically higher that the corresponding experimental data. Attempts to improve the calculated curve by including polynuclear lasalocid-lead complexes (3:2 and 4:3 Las-Pb) into the model used for data fitting were not successful, as they resulted in significant differences in the location of the first equivalence point in the calculated and the experimental titration curves. As a result, the polynuclear species were not included into the data set used to obtain the final results.

Figures IV.20 and IV.21 illustrate the results of these refined fits for the data obtained with lasalocid-lead concentration ratios of about 2:1 and 3:1, respectively. The values of equilibrium constants obtained are listed in Table IV.7. A species distribution curve was calculated as a function of p[H] using the average values of these equilibrium constants and is shown in Figure IV.22.

Table IV.7 Log β_X values obtained from potentiometric titrations of HLas and lead(II) in 80% methanol-water[a]

exp	HL-Pb	Species identity X					σ_{fit}[f]
#	ratio	HL[b]	PbL^c	PbL_2[c]	PbLOH[c,d]	PbOH[e]	
1	1.83	4.83	6.43	9.15	-1.13	-7.90	0.023
2	1.83	4.83	6.75	9.50	-0.79	-7.90	0.030
3	2.75	4.83	6.47	9.48	-0.89	-7.90	0.061

[a] 25.0 °C, 0.05 M ionic strength (TEAP); [b] The value of log β_{HL} (section IV.B) was fixed during refinement. [c] Values were refined by program BEST. [d] β_{PbLOH} is expressed as an acid dissociation constant (eq IV.21). [e] The value was fixed during refinement. [f] Standard deviation expressed as σ_{fit}; $\sigma_{fit} = (U/N)^{1/2}$, where $U = \Sigma\, w_i\, (p[H]_{exp,i} - p[H]_{calc,i})^2$; $N = \Sigma\, w_I$ and $w_i = (p[H]_{i+1} - p[H]_{i-1})^{-2}$.

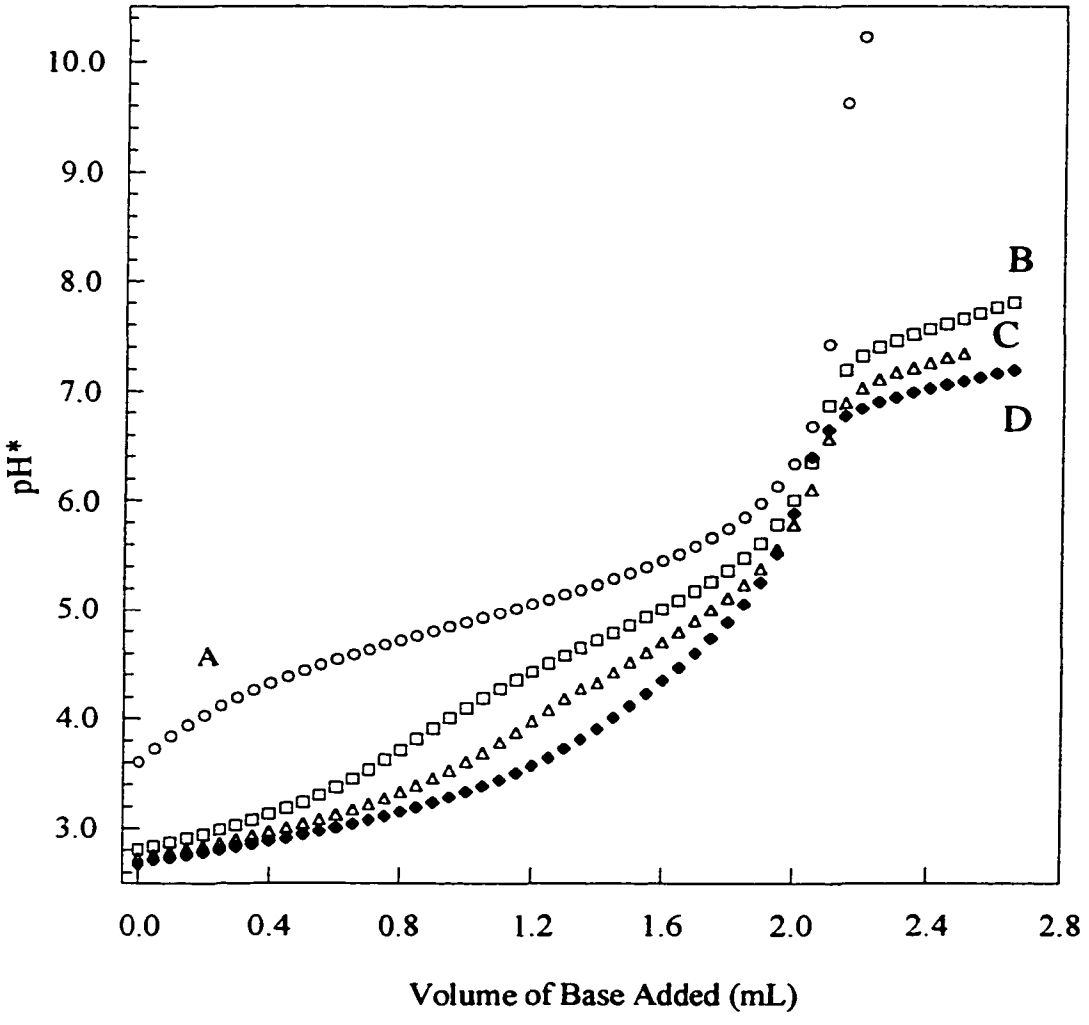

Figure IV.19. Potentiometric titration curves for various stoichiometric ratios of lasalocid-lead in 80% methanol-water at 25.0 °C. Each solution contained 10.0 mL of 4.20 mM free lasalocid in the acid form. 0.023 M lead(II) perchlorate was added in the amount to obtain the following stoichiometric ratios: A. no Pb; B. 2.75:1 HLas-Pb; C. 1.83:1 HLas-Pb; D. 1.37:1 HLas-Pb. All titrations were done at 0.05 M ionic strength (TEAP).

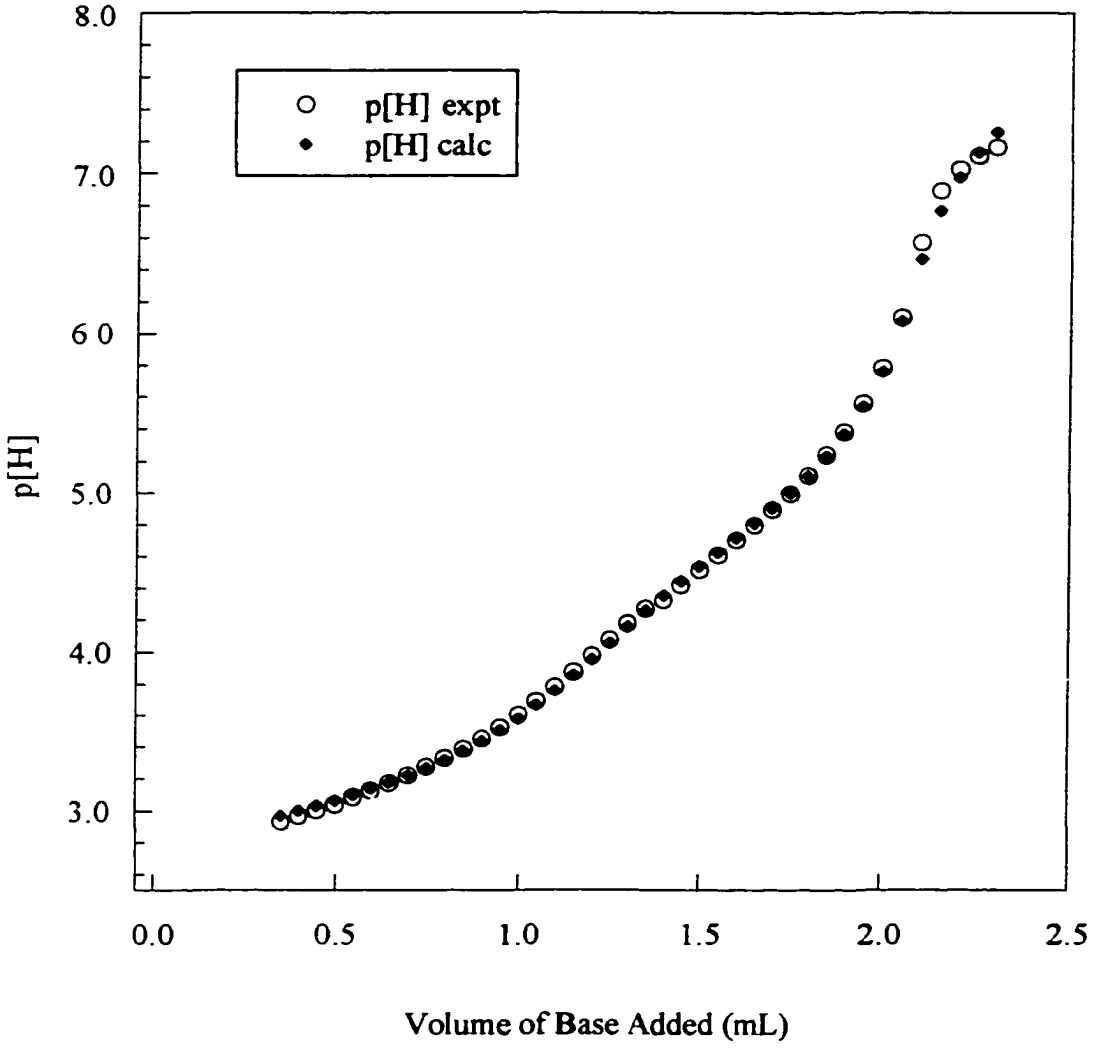

Figure IV.20. Potentiometric titration curve for 10.0 mL of a solution containing 3.73 mM lasalocid free acid and 2.0 mM lead(II) at an ionic strength of 0.05 M (TEAP) in 80% methanol-water at 25.0 °C. The titrant is 0.02029 M tetramethylammonium hydroxide with ionic strength maintained at 0.05 M with TEAP. The calculated p[H] values were obtained from the program BEST using refined values of equilibrium constants for the model containing the species listed in Table IV.7, Exp.1.

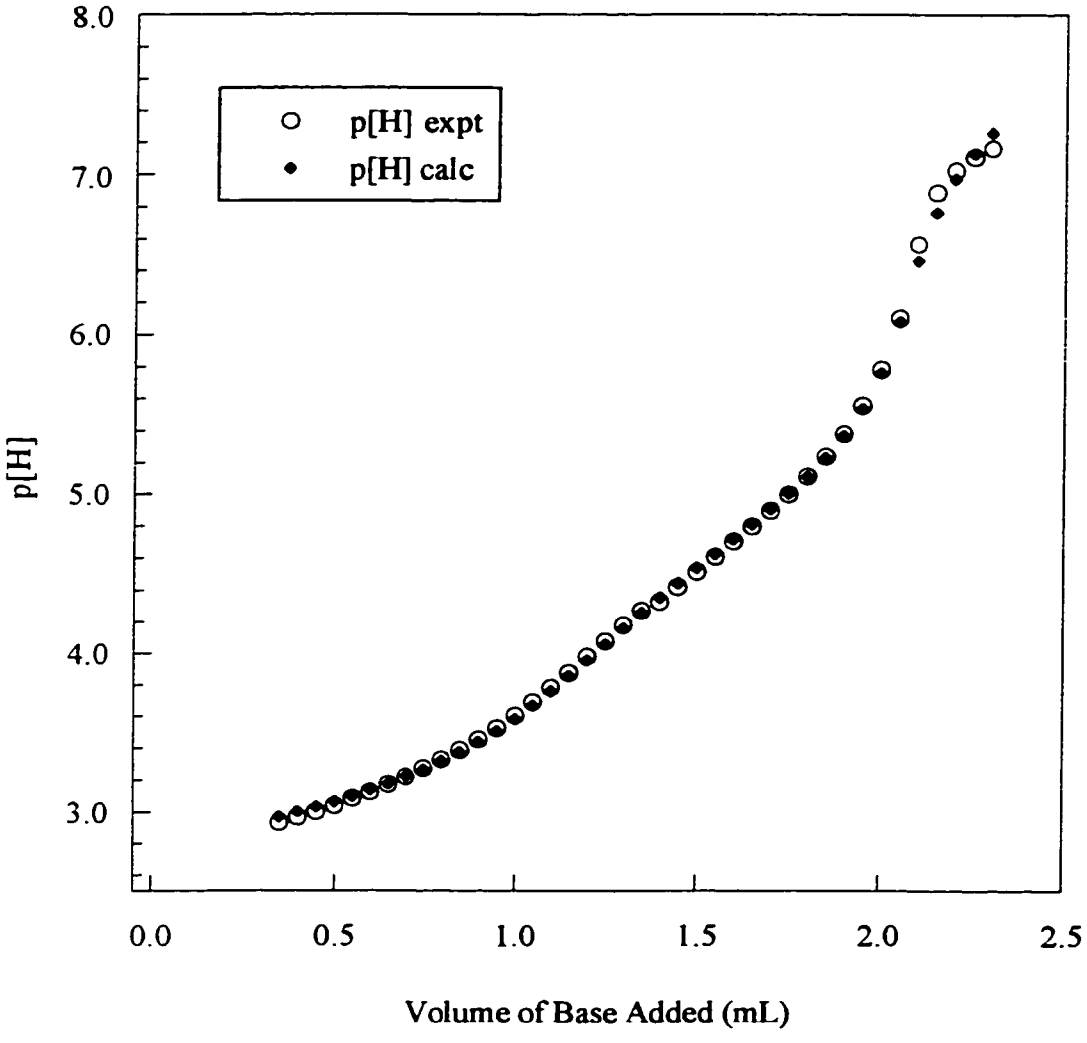

Figure IV.21. Potentiometric titration curve for 10.0 mL of a solution containing 3.73 mM lasalocid free acid and 2.0 mM lead(II) at an ionic strength of 0.05 M (TEAP) in 80% methanol-water at 25.0 °C. The titrant is 0.02029 M tetramethylammonium hydroxide with ionic strength maintained at 0.05 M with TEAP. The calculated p[H] values were obtained from the program BEST using refined values of equilibrium constants for the model containing the species listed in Table IV.7, Exp.1.

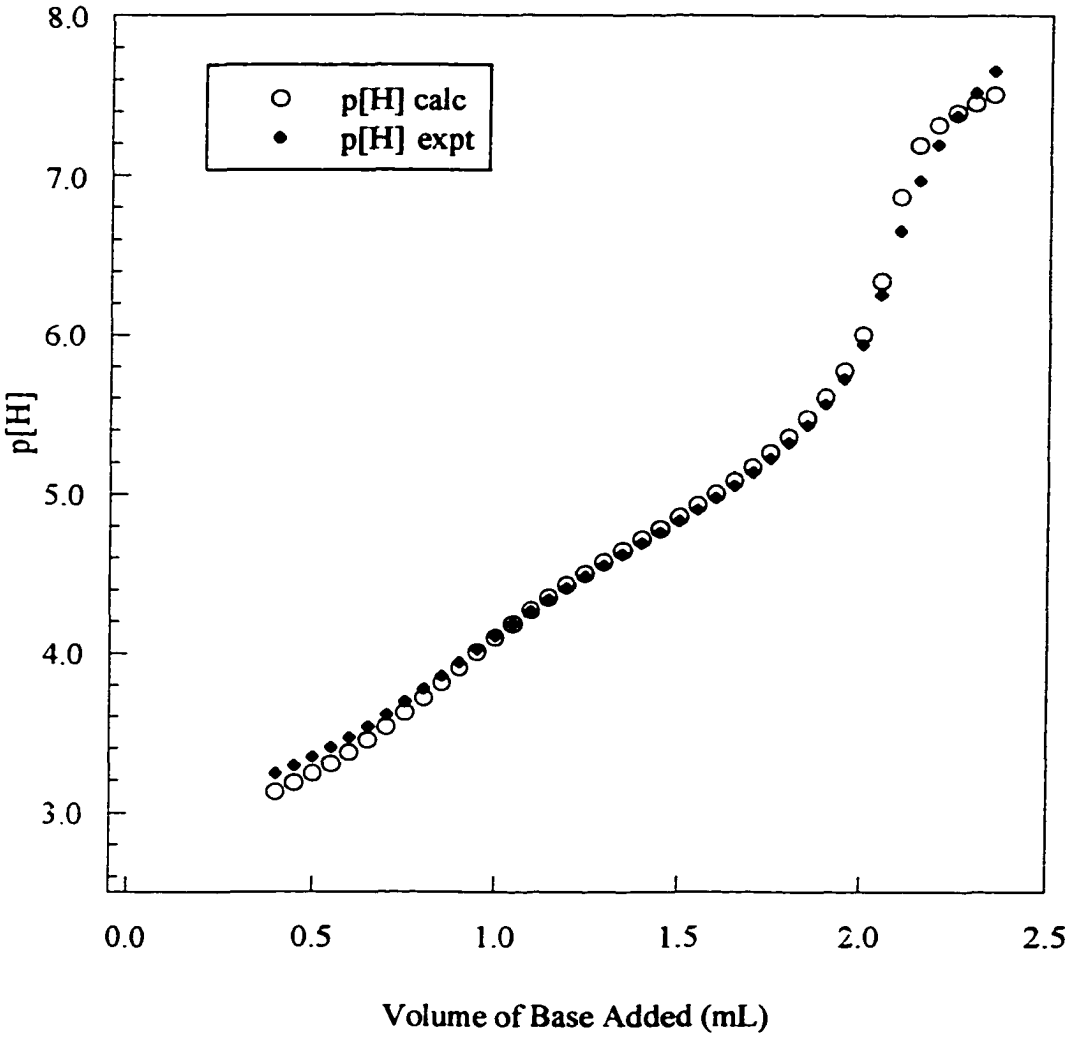

Figure IV.22. Potentiometric titration curve for 10.0 mL of a solution containing 3.88 mM lasalocid free acid and 1.41 mM lead(II) at an ionic strength of 0.05 M (TEAP) in 80% methanol-water at 25.0 °C. The titrant is 0.02029 M tetramethylammonium hydroxide with ionic strength maintained at 0.05 M with TEAP. The calculated p[H] values were obtained from the program BEST using refined values of equilibrium constants for the model containing the species listed in Table IV.7, Exp.3.

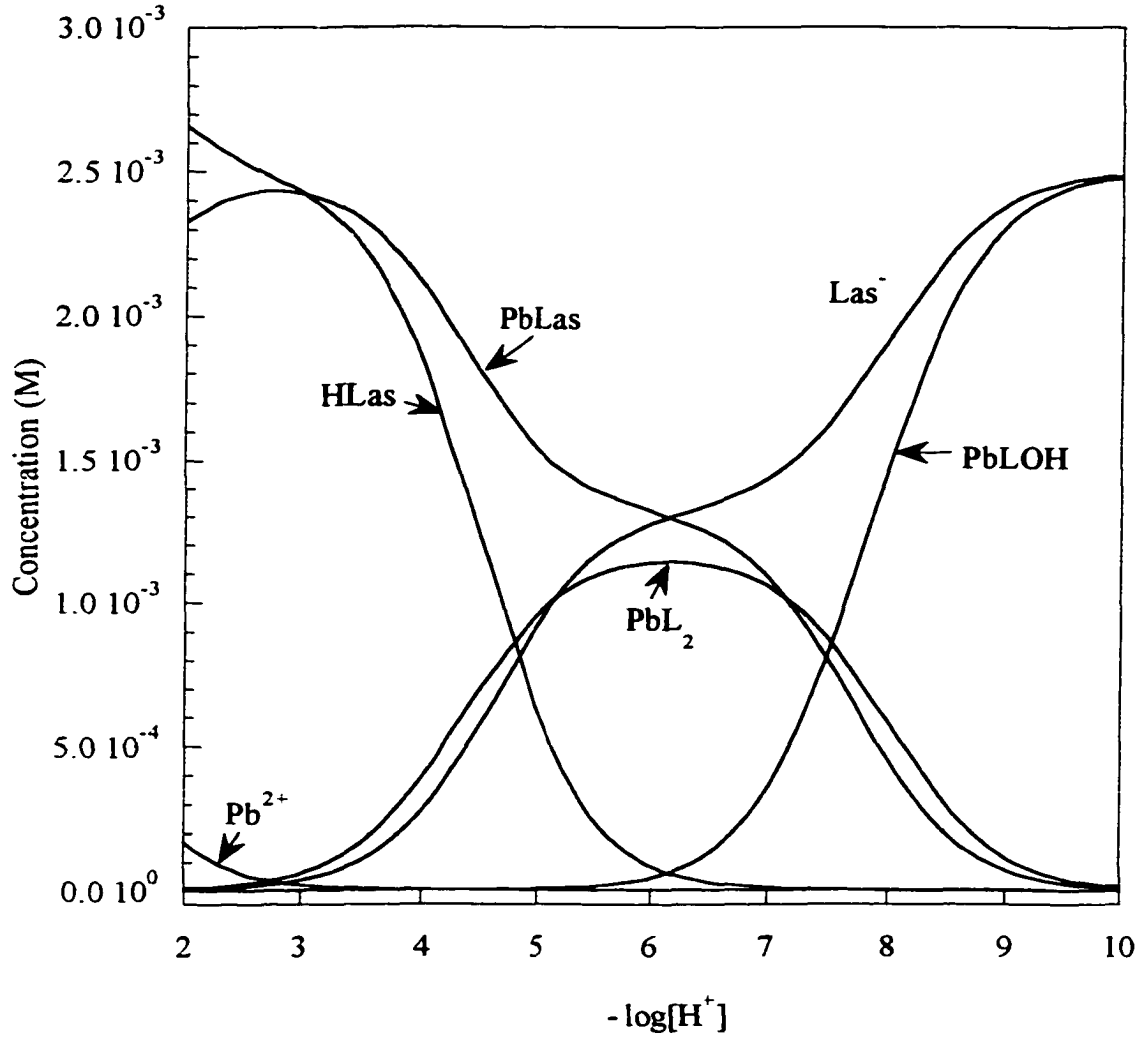

Figure IV.23. Species distribution curves for lasalocid-lead(II) complexes in solution as a function of p[H] in 80% methanol-water. Species concentrations were calculated using the program Comics for 5.0 mM lasalocid and 2.5 mM lead using the average values of the equilibrium constants listed in Table IV.8.

Table IV.8 Average values of cumulative equilibrium constants (log β_X) for lasalocid with various ions in 80% methanol-water[a,b]

Ion	Identity of species X[c]			
(M)	ML	ML_2	MLOH[d]	ML_2H
H^+	5.02 ± 0.01 (17)			
Na^+	<2	-	-	-
Ca^{2+}	< 2	-	-	-
Zn^{2+}	2.59 ± 0.06 (4)	-	-5.42 ± 0.40 (4)	9.5 ± 0.1(3)
Pb^{2+}	6.55 ± 0.17 (3)	9.38 ± 0.20 (3)	-0.94 ± 0.17 (3)	-

[a] 25 °C; ionic strength 0.05 M.(TEAP). [b] The number of replicate measurements is indicated in parentheses. Uncertainty is expressed in terms of one standard deviation. [c] L represents the monoanion of lasalocid. [d] β_{MLOH} is expressed as the acid dissociation constant (eq IV.21).

IV.E. NMR studies of the lasalocid complexes with lead (2:1 Las-Pb stoichiometry) in methanol.

NMR peak assignments for lasalocid complexes with other cations.

The purpose of the NMR experiments was to determine the ligand binding sites and to qualitatively compare the solution structure of the lead-antibiotic complex to that of the sodium or calcium complexes or of the free lasalocid ligand. One approach to this consists of comparing differences in the chemical shifts ($\Delta\delta^{13}C$) of the ionophore in the lead complexes with the uncomplexed anion of the ionophore and with the ionophore complexed to other metals. Therefore, NMR spectra of the lasalocid complexes and the free lasalocid ligand were required. Assignments of ^{1}H and ^{13}C peaks in the NMR spectra of the sodium, tetramethylammonium, and calcium lasalocid salts, and those of free lasalocid were available in literature[12-14] and aided in this process. NMR spectra for the sodium-lasalocid complex were obtained in this work as well. The experimental peak positions were compared to the known assignments to assure that different equipment and conditions did not have an effect on the NMR data. The numbering scheme for lasalocid A that was used in this work is shown in Figure IV.24.

Several two-dimensional and multipulse techniques were employed in order to help assign resonances in the NMR-spectra. These experiments included COSY[15,16] (^{1}H - ^{1}H Correlated Spectroscopy) which helped to find ^{1}H -^{1}H connectivities through bonds; J-resolved carbon experiments APT[17,18] (Attached Proton Test) - to assign multiplicities to carbon signals, and HMQC[19,20] (Heteronuclear Multiple Quantum Coherence) - to find single-bond carbon-proton connectivities. The peaks in the ^{1}H and ^{13}C spectra of the sodium lasalocid salt were assigned mostly by, first, comparison to the known values, and, second, the use the two-dimensional techniques described above. Both experimentally obtained and literature values for the peak chemical shifts in the NMR

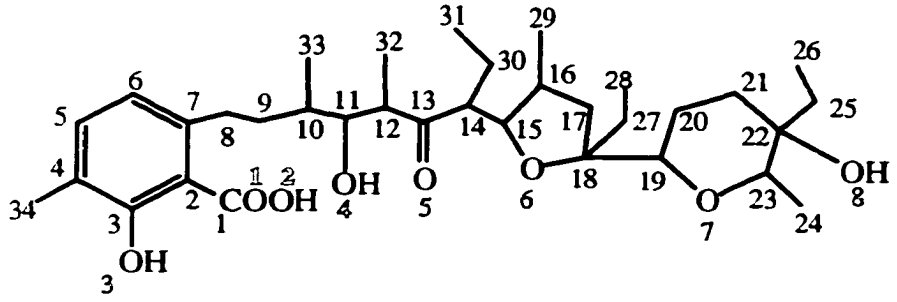

Figure IV.24. Lasalocid A molecule with carbon (plain style) and oxygen (outlined) numbering schemes.

spectrum of the sodium-lasalocid complex are listed in Tables IV.9 and IV.10. Most assigned ^{13}C chemical shifts were similar to those found in literature. However, some discrepancies were noticed between the experimental and the literature ^{1}H chemical shifts. These might be attributed to the possible presence of water in the deuterated methanol solvent employed, which may result in a slightly different overall conformation and solvent interaction involved. Two-dimensional NMR spectra obtained for the sodium-lasalocid complex served as models of those for the lead-lasalocid complex.

NMR peak assignment in the spectra of the lead-lasalocid complex in methanol.

NMR samples were prepared by dissolving the isolated lead-lasalocid complex in deuterated methanol. The complex prepared by the reaction between solid lead oxide and the free acid form of monensin was used for all experiments. Elemental analysis results indicated that the complex had 2:1 lasalocid-lead stoichiometry (section IV.A). However, only one resonance peak was present in the NMR spectra for both protons and carbons of lasalocid at room temperature, and the spectra were well-resolved. The NMR resonances observed could be the time-averaged signals for two different ligands involved when the ligands exchange rapidly. This assumption was based on the

behavior of the previously studied 2:1 lasalocid-calcium systems[13,14] where two ionophore ligands were found to be different with respect to their conformations and metal binding sites, but only one signal for each carbon and proton was found in their NMR spectra at room temperature. Because the peak separation using lower acquisition temperature was not attempted in this work, the possibility of only one ^{13}C signal from the two ligands with same conformations and lead binding sites also could not be ruled out. The ^{13}C resonances obtained were assigned as follows.

The process started from comparing the signals in the ^{13}C and ^{1}H spectra to the known positions of the corresponding peaks in the spectrum of the sodium complex. Because most peaks in ^{13}C spectra are well separated (Figure IV.25), their assignment did not present any difficulties. Assignments of the peaks in the areas of the overlap in the ^{1}H NMR spectrum presented more difficulties and other techniques aided in the assignment process. The ^{1}H NMR spectrum for the lasalocid-lead complex in methanol is shown in Figure IV.26. Along with 1-dimensional ^{1}H and broad-band decoupled ^{13}C spectra for the lead-lasalocid complex, APT, COSY, and HMQC experimental data was acquired. The map of COSY cross peaks is shown in Figure IV.27 and the HMQC contour map is shown in Figure IV.28.

The APT experiment identified the number of protons connected to each carbon in question and, thus, helped in distinguishing carbon signals. Signals from four quaternary carbons on the benzine ring, from the carboxylic acid group and ketone carbons, and from two quatenary carbons located next to oxygens in the furan and pyran rings were easily distinguishable because they are located most downfiled in the NMR spectrum. It was assumed that their general position closely resembled that in the spectrum of the sodium complex. Eight signals from tertiary carbons and seven from secondary carbons were also identified. Four of the tertiary carbons are located next to oxygens in the lasalocid structure and, thus, were easily distinguished.

To further separate the signals in those groups, HMQC ^{1}H-^{13}C correlation plots were obtained. Correlations of carbon chemical shifts with the chemical shifts from the attached protons provided the necessary information to complete the assignments. The COSY NMR experiment aided in ^{1}H peak assignments in that it identified neighboring protons through the vicinal and geminal coupling of their signals and, consequently, allowed to complete the assignments of the attached carbon atoms as well. The assigned ^{13}C and ^{1}H peaks in the spectra of the lead-lasalocid complex are shown in Tables IV.9 and IV.10

Table IV.9 ^{1}H NMR chemical shifts of complexed lasalocid in methanol at room temperature in ppm

carbon #[a]	NaLas, experimental	NaLas, literature[b]	PbLas, experimental
5	7.07	7.07	7.01
6	6.52	6.58	6.55
8A	3.63	3.76	3.50
8B	2.50	2.50	2.70
9A	1.66	1.75	1.65
9B	1.46	1.53	1.55
10	1.69	1.78	1.66
11	4.18	4.29	4.16
12	2.93	3.00	2.92
14	2.79	2.87	2.77
15	3.78	3.85	3.89
16	2.22	2.23	2.21
17A	1.90	1.98	1.90
17B	1.52	1.56	1.58
19	3.67	3.73	3.74
20A	1.86	1.94	1.78
20B	1.48	1.52	1.53
21A	1.69	1.77	1.77
21B	1.69	1.77	1.77
23	3.80	3.89	4.01
24	1.21	1.29	1.14
25A	1.58	1.71	1.98
25B	1.35	1.46	1.42
26	0.92	0.99	0.87
27A	1.83	1.92	1.81
27B	1.39	1.43	1.44
28	0.85	0.93	0.79
29	1.05	1.13	0.97
30A	1.94	2.00	1.97
30B	1.43	1.49	1.45
31	0.87	0.94	0.78
32	0.97	1.04	0.86
33	0.86	0.94	0.85
34	2.14	2.20	2.13

[a] "A" and "B" stand for two geminal protons. [b] From ref. 12.

Table IV.10 ^{13}C chemical shifts of complexed lasalocid in methanol at room temperature in ppm

C13	NaLas, experim.	NaLas, literature[a]	PbLas, experim.
1	176.8	177.1	178.3
2	118.1	118.4	118.3
3	161.4	161.7	161.4
4	123.7	124.0	124.3
5	133.6	133.1	131.1
6	121.8	121.4	121.9
7	144.7	144.8	145.2
8	34.4	34.2	33.9
9	38.2	38.5	38.16
10	35.2	35.2	35.09
11	73.2	73.2	72.8
12	50.6	50.2	50.1
13	219.8	220.2	219.5
14	57.0	56.6	57.0
15	84.4	84.4	85.9
16	36.1	35.9	36.9
17	38.8	39.0	39.7
18	87.9	88.1	88.0
19	70.3	70.6	70.9
20	20.8	20.9	21.5
21	30.7	30.7	30.6
22	71.8	71.9	72.51
23	77.1	77.1	77.78
24	13.9	13.9	14.37
25	32.0	32.3	32.3
26	6.50	6.70	6.86
27	30.6	30.6	30.6
28	9.8	9.6	9.31
29	15.5	15.6	16.1
30	17.8	17.5	18.3
31	12.6	12.8	12.8
32	13.2	13.0	13.26
33	13.4	13.4	13.46
34	16.3	16.2	16.2

[a] From Ref. 12.

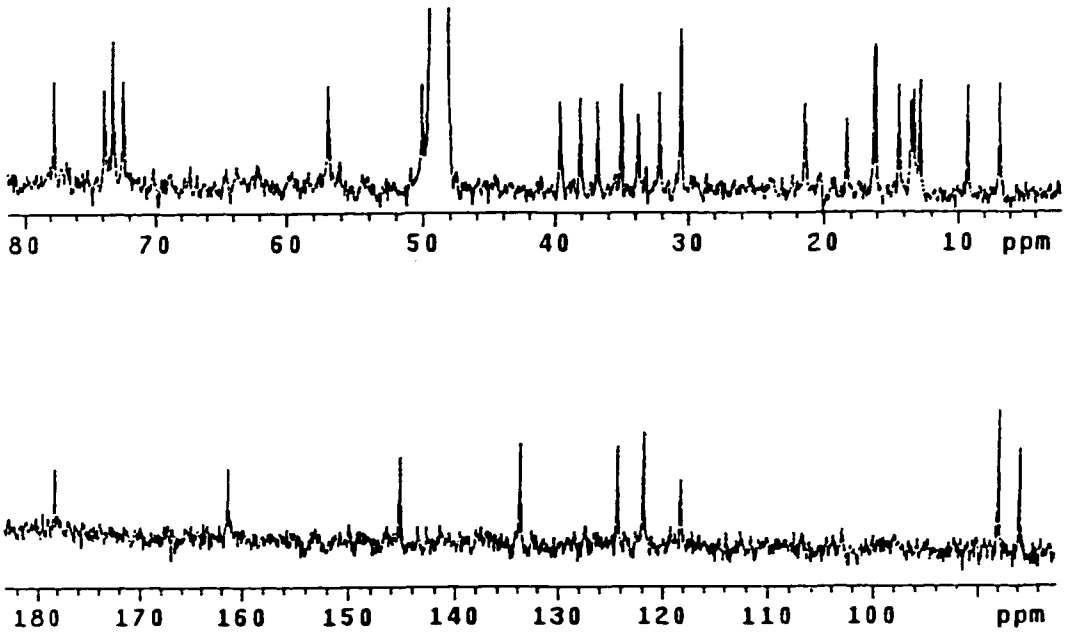

Figure IV.25. ^{13}C broad-band decoupled NMR spectrum of the lasalocid-lead complex in methanol at room temperature.

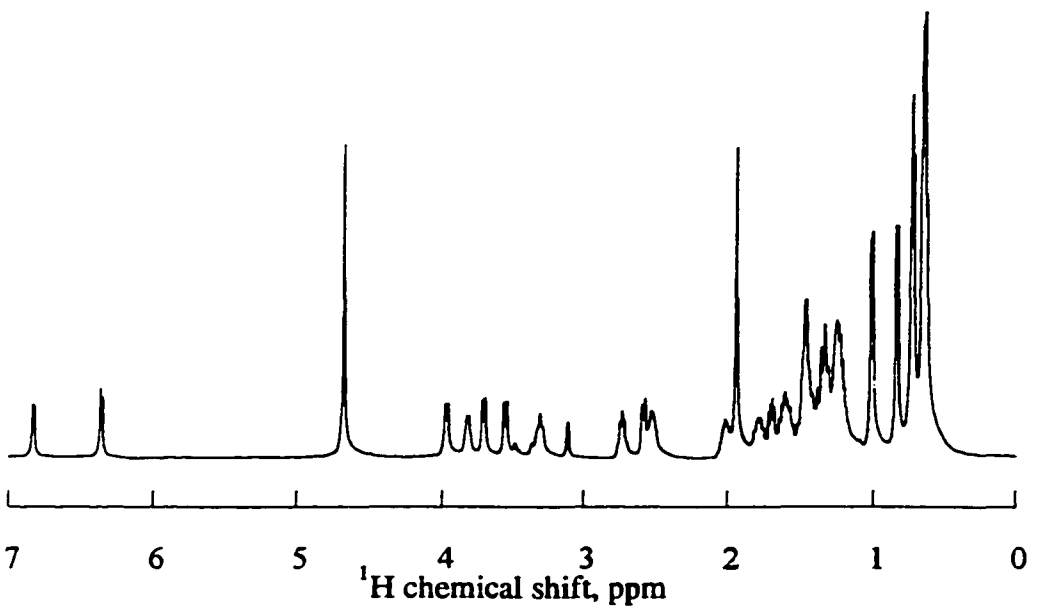

Figure IV.26. ^{1}H NMR spectrum of the lasalocid-lead complex in methanol at room temperature.

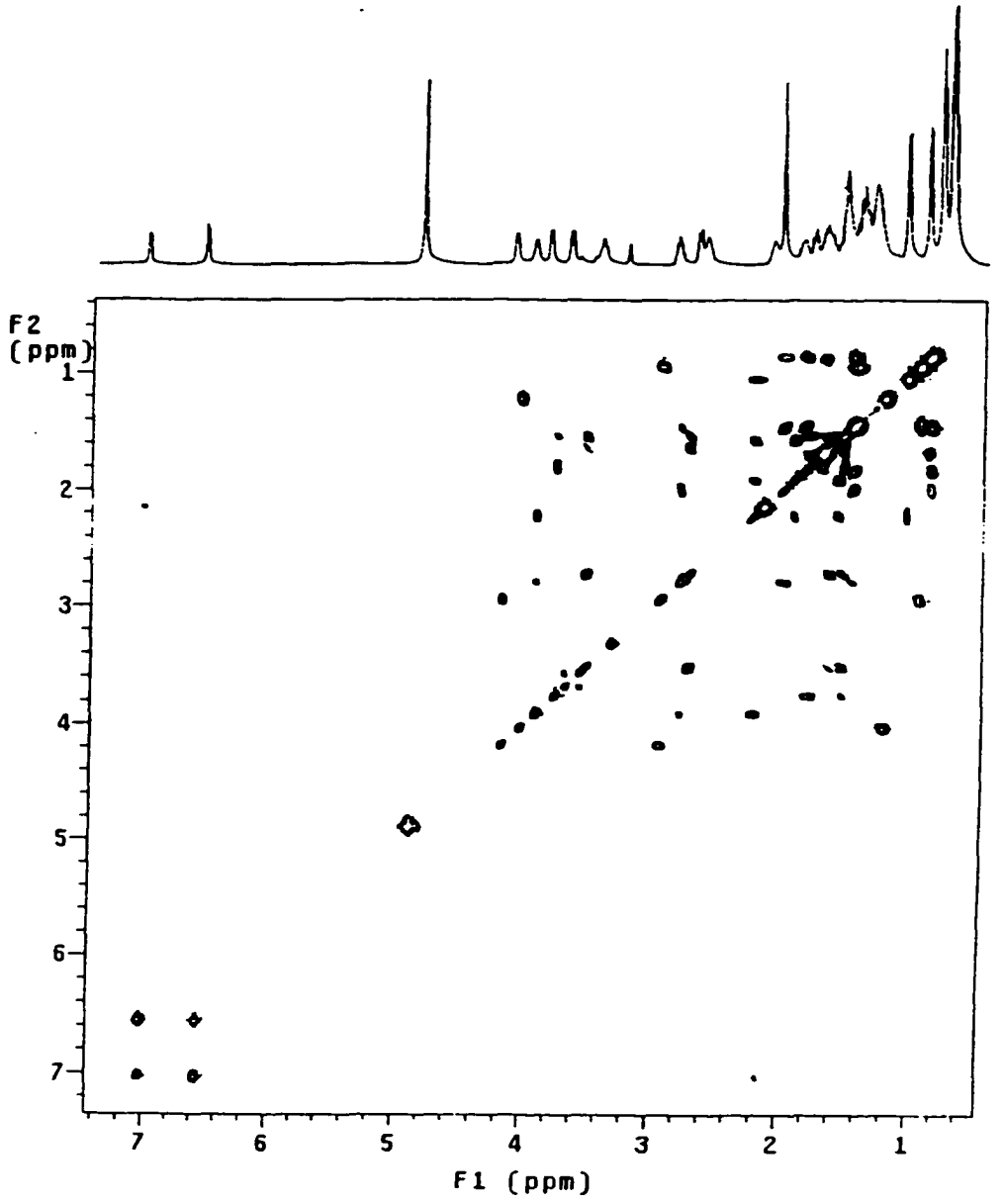

Figure IV.27. COSY spectrum for the lasalocid-lead complex in methanol at room temperature. F1 = F2 = ^{1}H chemical shift (ppm).

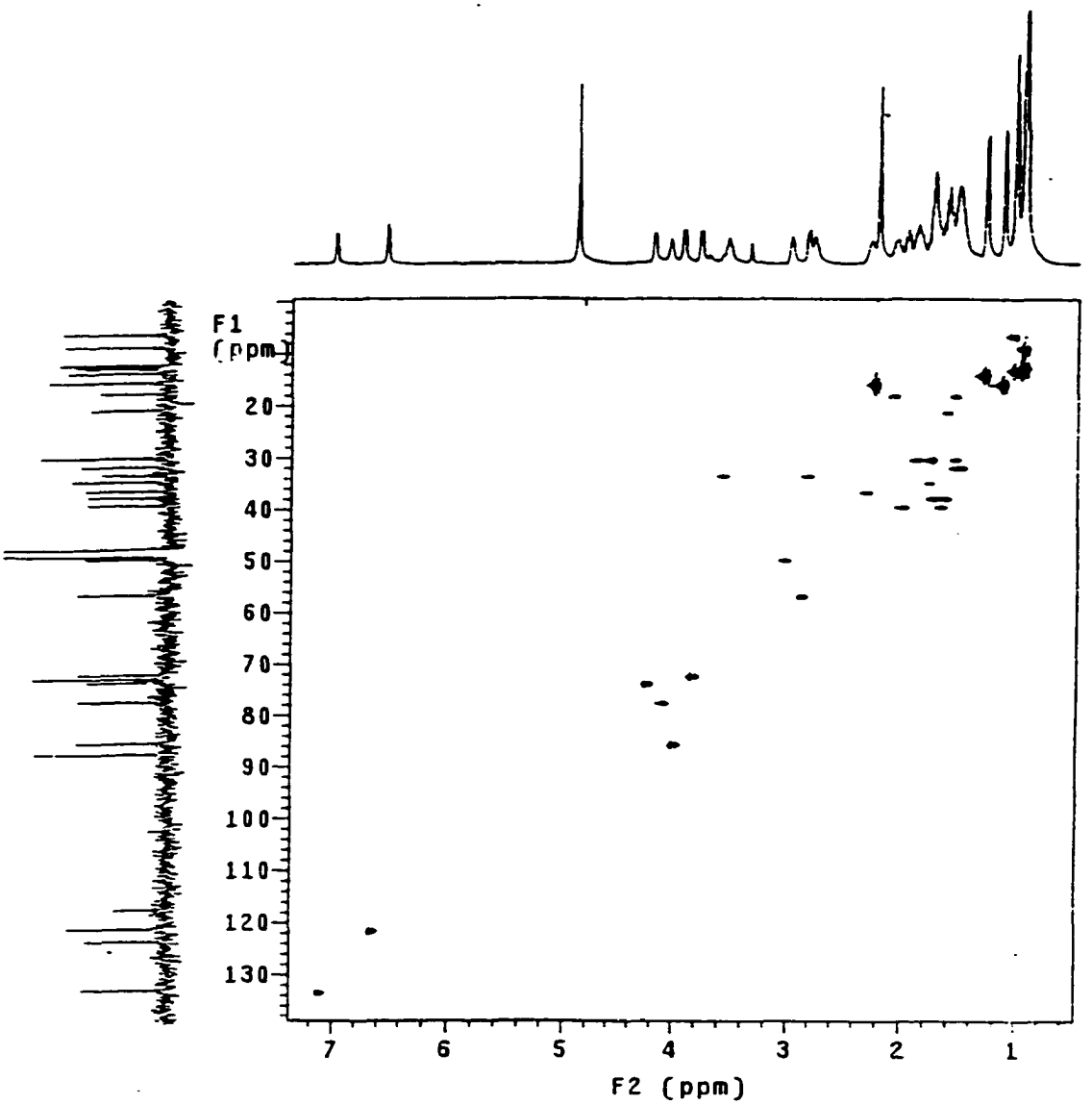

Figure IV.28. HMQC contour map for the lasalocid-lead complex at room tempearature. F1= ^{1}H and F2 = ^{13}C chemical shifts.

Results of the NMR experiments.

Although the stoichiometry of the isolated lasalocid-lead complex used to obtain NMR spectra was found to be close to 2:1, only one signal was present for ^{1}H and ^{13}C resonances at room temperature. It was concluded that the two ligands either exchange rapidly or have similar conformations and lead-coordination patterns. The separation of their signals in methanol was not attempted and it was not possible to rule out any of the possibilities. The values of coupling constants were not obtained since they could reflect the mean situation which would be difficult to interpret.

Figure IV.29 presents the calculated differences in ^{13}C resonance frequencies in methanol ($\Delta\delta^{13}C$) between these of lasalocid salts and lasalocid acid, and lasalocid anion (in the form of Me_4NLas). Literature values of ^{13}C chemical shifts in the calcium-lasalocid complex[14], lasalocid anion[21], and lasalocid acid[21], and the experimental values of ^{13}C chemical shifts for lead lasalocid and sodium lasalocid complexes were used in the calculations. For the acid form of the lasalocid, where no complexation takes place, only very slight ($\leq$ 0.5 ppm) changes in the carbon chemical shifts occur, except for the carboxylic acid end of the molecule (carbons 1-7), where transmission of electronic effects across the benzene ring take place. Upon complex formation, differences in the chemical shift for a given carbon atom may be related to either interactions of a metal cation with a neighboring oxygen (resulting in a downfield shift), or conformational changes in its neighborhood, or local changes due to the interactions with solvent molecules. Previously, it was found that the chemical shift changes, caused by complexation, were smaller for lasalocid complexes with monovalent cations[12] that for those with divalent cation ones[14].

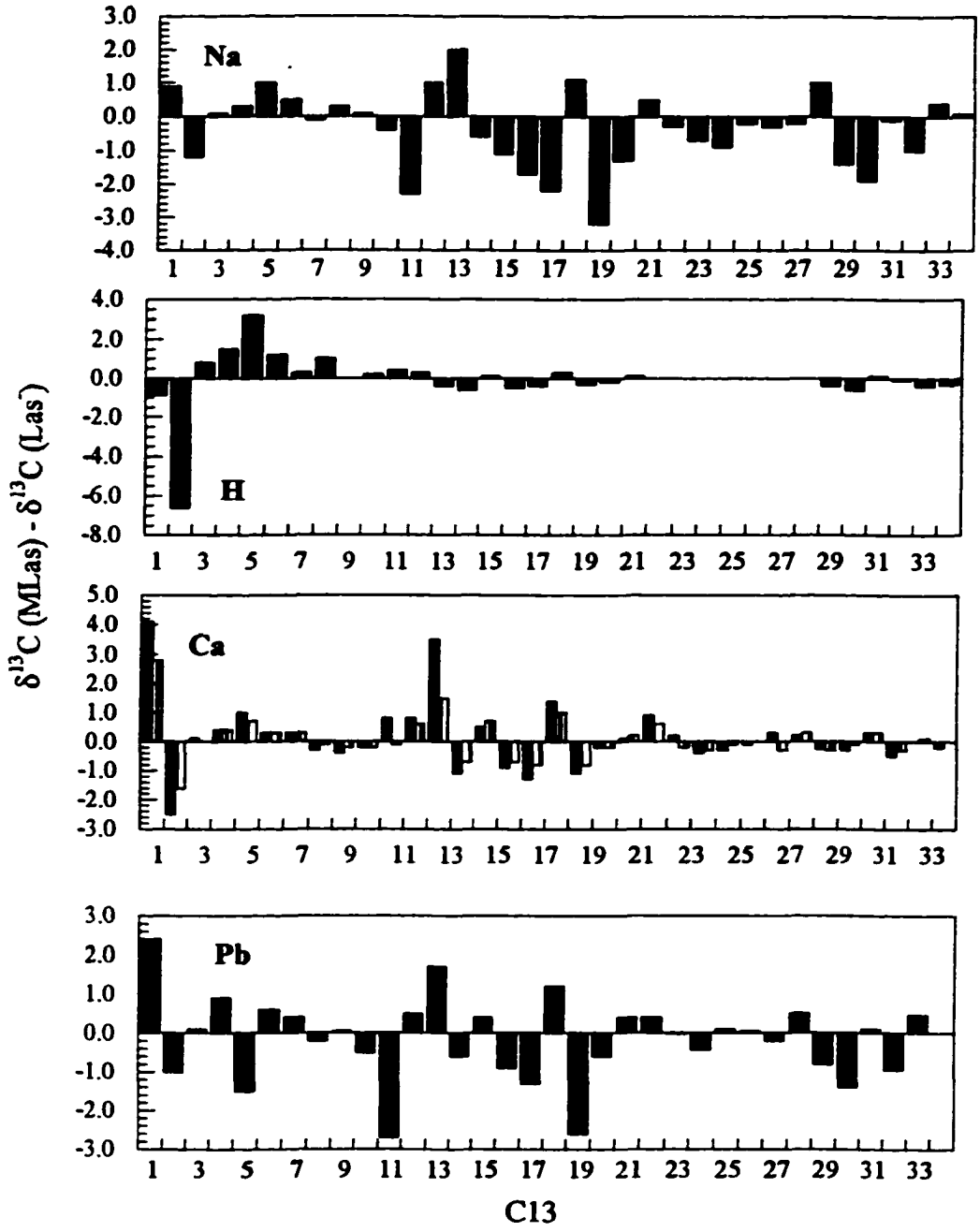

Figure IV.29. Variation of ^{13}C chemical shifts of all the carbons in the lasalocid molecule from the free lasalocid anion Las$^-$ to the metal complex and free acid in methanol. Both variations to the first (darkened) and second (lighter areas) anion ligands in calcium complex are shown.

Nevertheless, as can be seen from Figure IV.29, patterns of $\Delta\delta^{13}C$ for the lead complex of lasalocid are very similar to that of the sodium complex for most carbon atoms. Positive chemical shift differences at carbons 13, 15, 18 and 22 suggest the possibility of lead binding to oxygens 5, 6 and 8 of both ligands. The value for the chemical shift difference at carbon 1 for the lead complex is intermediate to that in the first lasalocid ligand in the calcium complex and in the sodium complex. It was suggested that carboxylates of both ligands participate in calcium binding[13,14]. The results of studies of lasalocid complexes with alkaline earth metal cations indicated that the involvement of the carboxylate in cation coordination decreases with increase in the ionic radius[14]. Also, it is known from the X-ray structures of the sodium complex that lasalocid carboxylate function is only involved in hydrogen bonding with a water or a methanol molecule, but does not participate directly in coordination[22,23]. Therefore, two possibilities exist for the carboxylate group binding in lead-lasalocid complex on the basis of the $\Delta\delta^{13}C$ value obtained. On one hand, the carboxylate of only one of lasalocid ligands may be bound to lead (with $\Delta\delta^{13}C$ of about 4 ppm), with the second carboxylate not participating in coordination (with $\Delta\delta^{13}C$ similar to that in the sodium complex). On the other hand, both carboxylates may be bound to lead and $\Delta\delta^{13}C$ for both carbons number 1 may close to that in the first lasalocid in the calcium complex (2.4 to 2.8 ppm).

References.

1) Westley, J. W.; Benz, W.; Donahue, J.; Evans Jr., R. H.; Scott, C. G; Stempel, A.; Berger, J. *Antibiot.* **1974**, 27, 744-753.

2) Bose, A. K.; Fujiwara, H.; Pramanik, B. N. *Tetrahedron Lett.* **1979**, 42, 4017-4020.

3) Blanchflower, W. J.; Kennedy, D. G. *Analyst* **1995**, 120, 1129-1132.

4) Volmer, D. A.; Lock, C. M. *Rapid Commun. Mass Spectrom.* **1998**, 12, 157-164.

5) Degani, H; Friedman, H. L. *Biochemistry* **1974**, 13, 5022-5032.

6) Lindoy, L. F. *Coord. Chem. Rev.* **1996**, 148, 349-368.

7) Martell, A. E.; Motekaitis, R. J. *Determination and Use of Stability Constants*, 2nd ed., VCH Publishers, Inc.: N.Y., 1992.

8) Patel, D. J.; Shen, C. *Proc. Natl. Acad. Sci. USA*, **1976**, 73, 1786-1790.

9) Shen, V.; Patel, D. J. *Proc. Natl. Acad. Sci.USA*, **1976**, 73, 4277-4281.

10) Painter, G. R.; Pressman, B. C. In *Host Guest Complex Chemistry II*, Vogtle, F., Ed. Topics in Current Chemistry Series 101; Springer-Verlag: New York; 1982, pp.84-110.

11) Perrin, D. D.; Sayce, I. G. *Talanta* **1967**, 14, 833.

12) Malfreyt, P.; Lyazghi, R.; Dauphin, G.; Pascal, Y.; Juillard, J. *J. Chem. Soc., Perkin Trans. 2*, **1996**, 1971-1979.

13) Everett, G. W.; Parker, S. B.; Williams, R. J. P. *Biochemistry*, **1983**, 22, 6149-6155.

14) Mimouni, M.; Malfreyt, P.; Lyazghi, R.; Palma, M.; Dauphin, G.; Pascal, Y.; Juillard, J. *J. Chem. Soc., Perkin Trans. 2*, **1995**, 1941-1947.;

15) Bachman, P.; Aue, W. P.; Muller, L.; Ernst, R. R. *J. Magn. Reson.* **1977**, 28, 29-39.

16) Bodenhausen, G.; Freeman, R.; Neidermayer, R.; Turner, D. *J. Magn. Reson.* **1977**, 26, 133-164.

17) Rabenstein, D. L.; Nakashima, T. T.; *Anal. Chem.* **1979**, 51, 1465A-1474A.

18) Pei, F.-K.; Freeman, R. *J. Magn. Reson.* **1982**, 48, 318-322.; Patt, S. L. *J. Magn. Reson.* **1982**, 46, 535-539.

19) Rutar, V. *J. Magn. Reson.* **1984**, 58, 306-310.

20) Bax, A. D.; Griffey, R. H.; Hawkins, B. L. *J. Am. Chem. Soc.* **1983**, 105, 7188-7190; Bax, A.; Subramanian, S. *J. Magn. Reson.* **1986**, 67, 565-569.

21) Lyazghi, R.; Cuer, A.; Dauphin, G.; Juillard, J. *J. Chem. Soc., Perkin Trans. 2* **1992**, 35-42.

22) Schmidt, P. G.; Wang, A. H.-J.; Paul, I. C. *J. Am. Chem. Soc.* **1974**, 96, 6189-6191.

23) Duesler, E. N. and Paul, I. C. In *Polyether Antibiotics: Naturally Occuring Acid Ionophores, Volume 2: Chemistry*, Westley, J. W., Ed.; Marcel Dekker, Inc.: New York, 1983, pp. 170-178.

CHAPTER V
DISCUSSION

Discovery of the importance of metal ions in biological processes brought a demand for non-destructive methods to control their intracellular concentrations in order to study and further understand their roles in physiological functions. Ionophore compounds have been widely used as mediators of cation transport across lipid membranes. The equilibria and kinetics involved in these transport processes have been extensively studied. Although most studies concentrated on the biologically important metal ions (e.g., alkali metals, calcium, iron, zinc), several recent studies reported very efficient transport of lead(II) compared with that of other divalent metal ions[1,2]. Several compounds from the family of carboxylic acid polyether ionophore antibiotics mediated this transport. Because several of these naturally occurring compounds, including the antibiotics monensin and lasalocid, are widely used in agriculture and can be present in the environment, their lead transporting properties may present a health concern.

To gain a better understanding of the transport mechanism, in-depth knowledge of the structure, stability, stoichiometry and kinetics of the transporting complexes is necessary. The transport selectivity of a particular ionophore towards a given metal cation can be governed by any of the above factors. This study focussed on the identification of the stoichiometry and composition of the complexes that can participate in transport, on the examination of the complex formation equilibria in solution, and the determination of complex solution structure.

V.A. Isolation and characterization of the ionophore antibiotic lasalocid and monensin complexes with lead(II).

Knowledge of possible stoichiometries and compositions of complexes formed between ionophore antibiotics and metal cations, such as lead(II), is important in order to identify the species that can participate in cation transport, to identify the mode(s) of transport, and to provide a chemical basis for the ionophore transport selectivities found.

Isolation of complexes and their elemental analysis

A number of ionophore complexes with lead were isolated and their compositions were characterized. Complexes having 2:1 monensin-lead and lasalocid-lead stoichiometries were made by reacting solid lead oxide with the free acid form of the ionophore in methanol. Complexes having the same 2:1 monensin-lead stoichiometry were also isolated as products of the back-extraction of a chloroform solution of tetraethylammonium monensin with an excess of aqueous lead nitrate, and the reaction between a solution of silver monensin in methanol with a solution of lead chloride (sections III.B and IV.A). Complexes having 1:1:1 ionophore-lead-chloride stoichiometry were obtained from the reaction between silver monensin and lead chloride in 1:1 stoichiometric ratio (sections III.C and IV.A). For all compounds isolated the stoichiometries obtained from the results of elemental analysis were close to those predicted for reactions that are quantitative (100% completed).

For monensin, the back-extraction method used to prepare the 2:1 Mon-Pb complex gave the best correlation between the calculated and the experimental composition of the final product. For complexes having 2:1 ionophore-lead stoichiometry made by reacting solid lead oxide with the free acid form of the ionophore, the composition of the 2:1 lead-lasalocid complex was closer to the predicted values than that of monensin. This can be the result of the differences in the acidity of the carboxylic

acid group in the two ionophores. Because lasalocid ononizes easier (as discussed below in section V.B), it could form a better stoichiometrically defined 2:1 complex with lead through the reaction with lead oxide than monensin. The ratio of equilibrium constants for the complex formation reaction (eq V.1) for lasalocid and monensin can be estimated from the available thermodynamic data.

$$PbO + 2HL \rightleftharpoons PbL_2 + H_2O \qquad K_{Overall} = K_O \qquad (V.1)$$

The following schematic reactions for the separate steps in the process shown in eq V.1 and their corresponding equilibrium constants are as follows

$$PbO \rightleftharpoons Pb^{2+} + O^{2-} \qquad K_1 \qquad (V.2)$$

$$2HL \rightleftharpoons 2H^{+} + 2L^{-} \qquad K_a = 1/K_H \qquad (V.3)$$

$$Pb^{2+} + 2L^{-} \rightleftharpoons PbL_2 \qquad \beta_{ML_2} \qquad (V.4)$$

$$2H^{+} + O^{2-} \rightleftharpoons H_2O \qquad K_1 \qquad (V.5)$$

Therefore,

$$K_O \propto K_1 K_4 \times \beta_{ML_2}/(K_H)^2$$

The steps in the process that are described by eqs V.2 and V.5 have the corresponding values of equilibrium constants K_1 and K_4 that are the same for either ionophore. Consequently, only the term $\beta_{ML_2}/(K_H)^2$ determines the ratio of the overall reaction constants K_O. This term for each ionophore can be calculated using the equilibrium constants obtained in this work which are presented in detail in section V.C. Then for lasalocid

$$\beta_{ML_2}/(K_H)^2 = 10^{9.38}/(10^{4.84})^2 = 0.50 \qquad (V.6)$$

and for monensin

$$\beta_{ML_2}/(K_H)^2 = 10^{10.6}/(10^{6.83})^2 = 8.7 \times 10^{-4} \qquad (V.7)$$

The ratio of equilibrium constants for the overall process can be calculated as

$$\frac{K_{O\,(Las)}}{K_{O\,(Mon)}} \propto \frac{0.50}{8.7 \times 10^{-4}} = 574 \qquad (V.8)$$

The fact that the equilibrium constant for the formation of 2:1 lasalocid-lead complex is more than 500 times larger than that for the formation of 2:1 monensin-lead complex indicates that the reaction with lasalocid is more likely to proceed to completion than that with monensin. As the result, the final product for lasalocid could be closer to the desired 2:1 ligand-lead stoichiometry, as was the case in this work.

Characterization of complexes by mass spectrometry.

ESI and FAB mass spectra were obtained for both 2:1 Mon-Pb and 1:1:1 Mon-Pb-Cl complexes. Molecular ion peaks corresponding to the complexes having both 1:1 and 2:1 ionophore-lead stoichiometries were observed in all mass spectra. In the case of lasalocid, molecular ions corresponding to 2:1 ligand-lead and other higher stoichiometry (2:2) complexes were observed to a greater extent. Formation of the latter may be the result of the lasalocid molecule having fewer donor oxygen atoms in comparison with monensin. Previous studies indicated that ESI-MS results can semi-quantitatively reflect the solution behavior because they were used to reliably predict the binding selectivities[3] among the complexes with 1:1 metal–crown-ether stoichiometry. However, the observation of ionophore-lead complexes with higher stoichiometries in the gas phase does not necessarily indicate their formation in solution, but points to the possible formation of such species and the high affinity of both monensin and lasalocid for lead.

Mixed complexes having 1:1:1 monensin-lead-anion stoichiometry were observed not only with chloride anion but also with nitrate and acetate using ESI-MS. A complete list of ternary complexes observed is given in Table V.1. The identification of such ternary complexes points to the fact that they can be formed when all three components are available, which may be the case in the some model systems and in cells. The concentration of chloride in biological media can be as high as 0.14 M, carboxylates may be present in biological and model systems, and the presence of hydroxide anions becomes significant at pH values above 7.5. Ternary hydroxide complexes were previously proposed to explain the electroneutral transport of La(III) cations mediated by A23187 ($La(L)_2OH$) and ionomycin ($LaLOH$)[4]. Likewise, a study of the complexation

Table V.1 Ternary complexes of Pb^{+2} having 1:1:1 lead-L-X stoichiometry identified in the present study.

Identity of L^- and X^-	methods of detection
monensin, Cl	elemental composition analysis
	negative ion ESI-MS and FAB-MS
lasalocid, Cl	elemental composition analysis
	negative ion ESI-MS and FAB-MS
monensin, NO_3	negative ion ESI-MS of methanol solution
monensin, CH_3COO	negative ion ESI-MS of methanol solution
monensin, OH	potentiometric titrations[a]
lasalocid, OH	potentiometric titrations[a]

[a] The presence of the ternary complex with hydroxide anion was required in the model to fit pH*-curves with the program BEST (reference 5).

equilibria between ionophore A23187 and Zn^{2+}, Ni^{2+}, Co^{+2} cations in 80% methanol-water reported[6] the formation of ternary hydroxy complexes above pH* 6.

Concentration studies of the monensin-mediated Pb^{2+} transport showed a first-order dependence on both lead (II) and ionophore concentrations[1]. For lasalocid, the transport studies showed 0.6-order dependence on the concentration of lead, whereas that on the concentration of lasalocid was found to be between first and second-order[2]. This indicated that species having 1:1 lead-ionophore stoichiometry are involved in the monensin-mediated transport, and species having both 1:1 and 2:1 lead-ionophore stoichiometries take part in lasalocid-mediated Pb^{2+} transport. Two transport models can be suggested to account for the 1:1 lead-ionophore stoichiometry of the participating species. First, electrogenic transport could take place through a positively charged 1:1 Pb-ionophore complex (PbL^+). Secondly, the process could involve electroneutral transport by a mixed 1:1:1 lead-ionophore-anion complex (PbLX). In case of the lasalocid-mediated transport, electroneutral transport by the 2:1 lasalocid-lead complex (PbL_2) can also occur. The formation of all these types of ionophore-lead complexes was confirmed in this study by the results of the elemental analysis and from the mass-spectra.

V.B. Protonation constants of lasalocid A and monensin A.

A key step in the process of cation transport across a lipophilic membrane may involve the deprotonation/protonation equilibria of the participating ionophore at the membrane-water interface. The extent of complex formation with metal ions depends on side reactions of the ionophore with protons. Therefore, the knowledge of the protonation state of ionophore molecule at physiological pH (6.8 – 7.5) is important to any discussion of the ionophore-mediated transport in biological or model systems. Measurements of protonation and complex formation equilibria were made in 80% methanol-water as the solvent. It was previously found that effective polarity of the 80% methanol-water medium resembles the polarity at the aqueous-lipid interface of cellular membranes and liposomes[7]. In addition, the values obtained for protonation and complex formation constants of ionophore A23187 in 80% methanol-water were similar to the corresponding values obtained in phospholipid vesicle systems[6,8-10]

1. Mean values.

The value for the protonation constant of monensin was determined using potentiometric method only, because monensin does not possess a chromophore group and, therefore, does not have a significant absorbance peak in the UV-Vis spectra. The pH*-titrations were performed at 25 °C with ionic strength kept at 0.05 M with TEAP. The values were calculated from the potentiometric data using the programs PKAS[5] and BEST[5]. Table V.1 presents the average values expressed as both the mixed-mode (log K_H^{m}*) and the concentration mode (log K_H^{c}*) constants.

Protonation constants for lasalocid were determined using both spectrophotometric and potentiometric methods at 25 °C with ionic strength maintained at 0.05 M with TEAP. The values from two different methods are in good agreement. The

average values obtained for each method and a composite value for both methods are listed in Table V.2.

The value of log K_H^c for lasalocid was previously calculated from the pH-dependence of lasalocid-mediated manganese transport in a phospholipid vesicle suspension[11]. The protonation constant from Table V.2. is in good agreement with the literature value of 5.0 ± 0.2 which was reported as a concentration constant.

The values of the mixed-mode protonation constants show that lasalocid is present in the unprotonated form (about 99%) at physiological pH whereas about 50% to 60% of monensin molecules are protonated at the same conditions. If the assumption holds that the K_H* values in 80% methanol-water are similar in magnitude to the protonation constants of the membrane-bound ionophore[9,10], then at physiological pH the large fraction of the unprotonated form of lasalocid should be efficient in metal complexation. However, as shown in the diagram of the transport process (Figure I.4), the presence of both protonated and unprotonated forms of the ionophore are required in order to complete the transport cycle; and according to the data obtained only 1% of

Table V.2 Average values for protonation constants of monensin A and lasalocid A obtained from potentiometric and spectrophotometric titrations in 80% methanol-water and composite values for both methods[a,b]

		Composite values	
Method	log K_H^{m}*	log K_H^{m}*	log K_H^{c}*
	Monensin		
Potentiometric	7.01 ± 0.05 (11)		
	Lasalocid		
Potentiometric	5.01 ± 0.07 (10)	5.02 ± 0.01[c]	4.84 ± 0.01
Spectrophotometric	5.03 ± 0.05 (7)		

[a] 25 °C; ionic strength = 0.05 M (TEAP); error expressed in terms of one standard deviation unless stated otherwise [b] (n) = number of replicate titrations averaged. [c] The value is calculated as a weighted average of the log K_H^{m}* mean values from both methods. The error is expressed as $e_{ave}/(\Sigma n_i)^{-1/2}$ for the mean of all measurements from both methods.

lasalocid is present in its protonated form at neutral pH. In case of monensin, both protonated and unprotonated forms that are required for transport cycle are present at appreciable concentrations.

2. General trends.

The values of the protonation constants obtained in this work were compared to values of similar compounds determined in 80% methanol-water. Experimental values were also compared to those reported for ionophores in pure methanol solvent and for simple carboxylic acids in methanol and aqueous media. As can be seen from Table V.3, the values of log K_H for ionophore antibiotics are about 2.9 to 3.5 orders of magnitude lower when measured in 80% methanol-water solvent composition versus pure methanol. The reported values of simple carboxylic acids (acetic and benzoic acids) also differed by about 3 log units for these two solvent systems. The dependence of log K_H* values of simple carboxylic acids upon solvent composition was studied previously[12,13]. The overall changes in the protonation behavior were attributed to both electrostatic and proton solvation effects of the solvent mixtures.

The protonation constant value of monensin is similar to that of the carboxylic acid group in ionomycin in 80% methanol and is similar to the value for propionic acid in 80% methanol among simple carboxylic acids (CA). This indicates that the carboxylic acid group of monensin behaves in a similar manner to that of the propionic acid and no extra intramolecular hydrogen bonds are present in that solvent composition.

The value of the protonation constant of lasalocid in pure methanol lies closest to that of salicylic acid among the compounds considered. The hydroxyl group, located in position ortho to the carboxylic acid on the benzene ring, increases the acidity of lasalocid in comparison with the carboxylic groups of other antibiotics. The same correlation is observed for the acidity of the salicylic acid versus that of a simple aliphatic or benzoic

acid in all three solvents. However, unlike salicylic acid, the benzene ring in lasalocid contains a *m*-methyl group and a bulky *o*-substituent. The inductive effects of those groups are transmitted to the carboxylate, and the resulting increase in the electron density is reflected in the higher values for the lasalocid protonation constants compared with those of salicylic acid.

Table V.3 Protonation constants of ionophore antibiotics and simple carboxylic acids in 80% methanol-water and pure water and methanol solvents at 25 °C

Compound	log K_H*		
	H_2O	80% (w/w) CH_3OH-H_2O	CH_3OH
Monensin A		7.20[a]	10.24[b]
Lasalocid A		5.21[a,c]	8.23[d]
A23187		8.04[e]	10.7[f]
Ionomycin		6.99[g]	
Acetic acid	4.76[h]	6.57[j]	9.52[k]
Propionic acid	4.87[h]	6.81[l]	9.71[m]
Benzoic acid	4.20[h]	6.29[l]	9.38[h]
Salicylic acid	3.04[n]	4.48[n]	7.69[o]

[a] The value was obtained in this work and corrected to 0 M ionic strength. [b] Ionic strength = 0 M; from reference 14. [c] For lasalocid the value is the average between those found by potentiometric and spectrophotometric methods. [d] Ionic strength = 0 M; from reference 15. [e] From reference 8; the value is listed for the protonation of the carboxylate group in A23187, corrected to 0 M ionic strength. [f] Ionic strength 0.10 M; from reference 16. [g] The value is listed for the protonation of the carboxylate group in ionomycin; from reference 17, corrected to 0 M ionic strength. [h] Ionic strength = 0 M; from reference 18. [j] Ionic strength = 0 M; from reference 12. [k] Ionic strength = 0 M; from ref. 19. [l] Ionic strength = 0 M. The value was obtained in 80% methanol-water solvent, prepared by volume; from reference 18. [m] Ionic strength = 0.1-1.0 mM; from ref. 20 [n] Ionic strength = 0.1 – 1.0 mM. The value was obtained in 75.9 % (w/w) methanol-water; from ref. 21. [o] Ionic strength = 0.005 M; from reference 22.

V.C. Complex formation constants of ionophores monensin and lasalocid with metal ions.

The strength of metal ion complexation by an ionophore can have a significant effect on the selectivity and specificity of its transport. The value for the complex formation constant has to be large enough to form appreciable concentrations of transporting species from the membrane bound ionophore and metal cations in the aqueous phase. On the other hand, it should not be so large as to prevent the release of metal ion following transport. The stoichiometry and the resulting charge of the complex formed determine the transport mode for a particular cation-ionophore system.

The formation constants of complexes with biologically important cations (Na^+, Ca^{2+}, and Zn^{2+}) and Pb^{2+} were measured in an 80% methanol-water medium, which is considered to be a model for the polarity of the lipid-aqueous interface. Both spectrophotometric and potentiometric methods were employed to obtain the values of the formation constants for lead complexes.

1. Mean values.

Data from potentiometric titrations were input into the program BEST[5] and the model was refined to determine equilibrium constants for the metal complexes formed. In addition to a 1:1 ligand(L)-metal(M) complex, most cases required a complex having 2:1 L-M stoichiometry in the models used to fit the titration curves. The mixed hydroxy-complex was included into the final models for zinc and lead(II) ionophore systems, but was not required in the models for calcium or sodium systems. Protonated complexes (MLH) were omitted from the model in all cases because they did not have a significant influence on the fit. Complex formation constants of lasalocid with sodium and calcium could not be determined potentiometrically due to the low affinity of those ions for lasalocid in 80% methanol-water solvent.

Determinations of the formation constants of both monensin and lasalocid complexes with lead(II) were also done using spectrophotometric titrations to complement the studies using the potentiometric method. The results of the UV-Vis titrations were analyzed to obtain the conditional stability constant, which was then corrected for the side reaction of the ligand with protons. The average values of stability constants of the lead complexes with ionophores obtained by each method are listed in Table V.4. For monensin the two values differ only by 0.2 log units, and they were both used to calculate the composite stability constant. However, a large discrepancy can be seen between the spectrometric and potentiometric values for lasalocid. Differences in the conditions of ionic strength used to obtain these values can not account for this discrepancy. On the other hand, the UV-Vis absorbance changes resulting from each aliquot of lead added to the lasalocid solution were small (total absorbance change for the reaction only about 0.1). The successive approximation process was used to fit the titration data and obtain the value for the conditional complex formation constant. The value obtained from this curve-fitting procedure could be subject to large errors due to

Table V.4. Average values for formation constants of ionophore complexes having 1:1 stoichiometry with lead obtained from both potentiometric and spectrophotometric titrations in 80% methanol-water[a,b].

Ionophore	log K_{PbL}		
	spectrometric	potentiometric	composite[c]
monensin	7.04 ± 0.14 (3)	7.25 ± 0.46 (13)	7.21 ± 0.10
lasalocid	5.52 ± 0.26 (4)[d]	6.55 ± 0.17 (3)	

[a] 25 °C; ionic strength = 0.05 M with TEAP. [b] (n) = number of titrations averaged. Error is expressed in terms of one standard deviation, unless indicated otherwise. [c] The value is calculated as a weighted average of the log K_{PbL} mean values from both methods. The error is expressed as $e_{ave}/(\Sigma\ n_i)^{-1/2}$ for the mean of all measurements from both methods. [d] 25 °C; ionic strength = 0.1–5.0 mM.

the large relative errors in the absorbance values recorded. Therefore, the value obtained by spectrophotometric titration was not included in the calculation of the composite stability constant for lasalocid.

Average values of the overall formation constants found in this work in 80% methanol and those available in literature in pure methanol for lasalocid and monensin complexes with several metal cations are listed in Table V.5. Most of the experimental values were obtained from the potentiometric data analyzed using the program BEST[5]. These results were presented previously for monensin and lasalocid complexes in Tables III.10 and IV.7, respectively. The equilibrium constants obtained were defined in terms of the overall formation or acid hydrolysis reactions. For the ternary hydroxide complex, the stepwise complex formation constant, K_{MLOH}, defined in eq V.9, can be calculated using the overall hydrolysis constant, β_{MLOH}, and the formation constant for 1:1 ionophore-lead complex, β_{ML}

$$ML^+ + OH^- \rightleftharpoons MLOH \qquad K_{MLOH} = \frac{[MLOH]}{[ML^+][OH^-]} \qquad (V.9)$$

β_{MLOH} and K_{ML} were defined as

$$\beta_{MLOH} = \frac{[MLOH][H^+]}{[M^{2+}][L^-]} \qquad (V.10)$$

$$\beta_{ML} = \frac{[ML^+]}{[M^{2+}][L^-]} \qquad (V.11)$$

Therefore, equation V.9 can rewritten as

$$K_{MLOH} = \frac{\beta_{MLOH}}{\beta_{ML}\, K_W^*} \qquad (V.12)$$

or

$$\log K_{MLOH} = \log \beta_{MLOH} - \log \beta_{ML} + pK_W^{c*} \qquad (V.13)$$

For these calculations a value of 14.05 was used for pK_W^{c*} in 80% methanol-water (from Table II.2).

The equilibrium in V.9 can be also presented as an acid dissociation as

$$ML^+ + H_2O \rightleftharpoons MLOH + H^+ \qquad K_{a\,(MLOH)} = \frac{[MLOH][H^+]}{[ML^+]} \qquad (V.14)$$

where the acid dissociation constant $K_{a\,(MLOH)}$ can be calculated as

$$K_{a\,(MLOH)} = K_{MLOH}\, K_W^{c*} \quad \text{or} \quad pK_{a\,(MLOH)} = p\,K_W^{c*} - \log K_{MLOH} \qquad (V.15)$$

Table V.5. Average experimental and literature values of overall complexation constants of monensin and lasalocid with metal cations.

Identity of X ($M_s L_t H_u$) or (MLOH)	Average values of log β_X or log K_X for the complex species X			
	L = monensin		L = lasalocid	
	80% methanol[a]	100% methanol	80% methanol[a]	100% methanol
NaL	5.0	6.30[e]	< 2	2.8 [h]
NaL_2	8.22			
NaLH		2.30[e]		0.7
ZnL	3.74	6.5[f]	2.59	5.4[j]
ZnL_2		10.6[f]		8.8[j]
ZnL_2H			9.50	
ZnL(OH)	6.71[b]		6.04[b]	
	(-7.34)[c]		(-8.01)[c]	
CaL	3.10	5.6[f]	< 2	5.0[k]
CaL_2		8.9[f]		7.50[k]
PbL	7.21[d]	7.7[g]	6.55	7.7[g]
PbL_2	10.6	12.1[g]	9.38	11.0[g]
PbL(OH)	7.20[b]		6.56[b]	
	(-6.85)[c]		(-7.49)[c]	

[a] Values obtained in the present work at 25 °C and 0.05 M ionic strength (with TEAP); expressed as overall formation constant: $p\ M^{n+} + q\ L^- \rightleftharpoons M_pL_q^{p(n+)-q}$. [b] The equilibrium constant is expressed as shown in eq V.9. [c] The value in parentheses corresponds to log $K_{a\ (MLOH)}$ (eq V.14). [d] Composite value from the results of both spectrophotometric and potentiometric titrations. [e] Ionic strength = 0 M; from ref. 14. [f] Ionic strength = 0 M; from ref. 23. [g] Ionic strength = 0 M; from ref. 24. [h] Ionic strength = 0 M; from ref. 25. [j] Ionic strength = 0 M; from ref. 26 [k] Ionic strength = 0 M; from ref. 27.

It was possible to compare the log value of the formation constant obtained for the monensin-sodium complex in 80% methanol-water (5.0) with those reported previously in a similar solvent[28] and in phopholipid vesicles[29]. These values were calculated to be 5.1 for log of the complexation constant in 70% (v/v) methanol at 0 M ionic strength[28], and 1.52 for log of the apparent stability constant in the liposome suspension[29]. The value in 80% methanol-water is very close to the former; the small difference can be accounted for by the differences in the solvent composition and ionic strength. The value in phospholipid vesicle suspension was calculated from the apparent association and dissociation rate constants for the sodium complex obtained from analysis of dynamic ^{23}Na NMR spectra[29]. The NMR spectra were recorded in the presence of $DyCl_3$ shift reagent at 1 M concentration which gives ionic strength values of about 6 M that can account for some of the difference in the value of the complex formation constant.

General trends.

The complex species and the values of their formation constants shown in Table V.5 were obtained through the refinement of the models used to fit the potentiometric data using the program BEST[5]. The presence or absence of any species in solution was determined on the basis of the impact of its presence in the model on the goodness of fit. Unlike those in pure methanol, studies in 80% methanol-water identified only complexes having 1:1 Zn-monensin and Ca-monensin stoichiometry, whereas 2:1 metal-monensin complexes were not found to be present for those metals at the conditions employed in this study. A 2:1 Lasalocid-Zn complex also was not identified although its monoprotonated form (Las(Hlas)Zn) was included into the model to improve the data fit. Both ionophores formed complexes with 1:1 and 2:1 ligand-lead stoichiometries for titrations employing concentrations of 1 mM monensin and 4.2 mM lasalocid. However, when the species distribution curves were calculated at lower ionophore concentrations

(Figures V.1 and V.2) that are typical of those used in biological systems, the concentrations of 2:1 ionophore-lead complexes were negligible.

The values of complex formation constants in 80% methanol-water were compared to those in pure methanol. The values for zinc and calcium complex formation were different by about 3 orders of magnitude, which is the same difference found for the protonation constants in those two solvents. However, the difference in the values for the 1:1 sodium-monensin complex was only 1.3 log units, and in the 1:1 lead-ionophore complexes, only 0.55 log units for monensin and 1.2 for lasalocid. These findings indicate that the latter values are less dependent on solvent polarity. The behavior mimics the relative insensitivity of complex formation constants to the solvent composition for alkali-metal complexes of A23187[31].

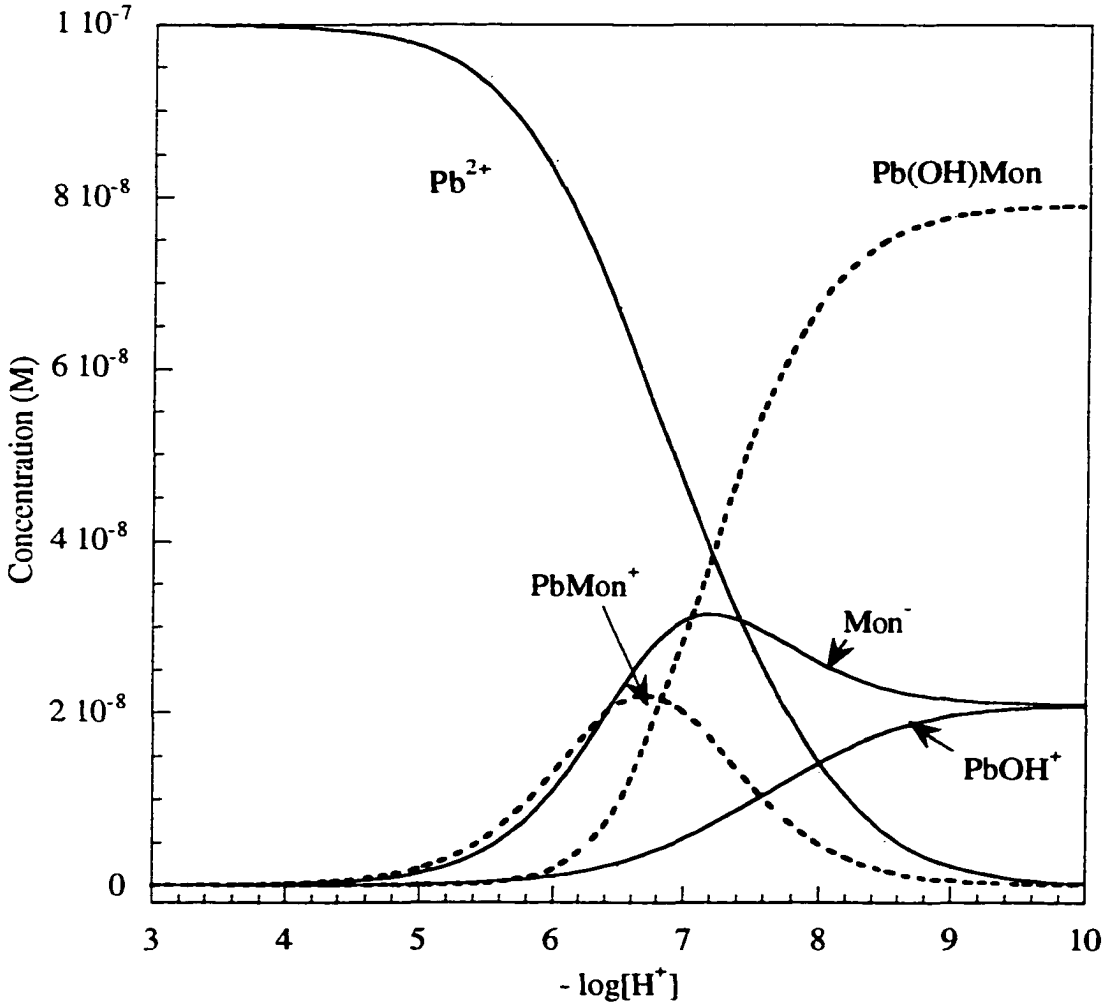

Figure V.1. Species distribution curves for monensin-lead(II) complexes in solution as a function of p[H] in 80% methanol-water, only species with monensin are shown. Species concentrations were calculated using the program Comics (ref. 30) for 0.1 μM monensin and 0.1 μM lead using the average values of the equilibrium constants listed in Tables III.10 and V.5. The concentration values were chosen to model the conditions used in the transport studies with liposomes (ref. 1).

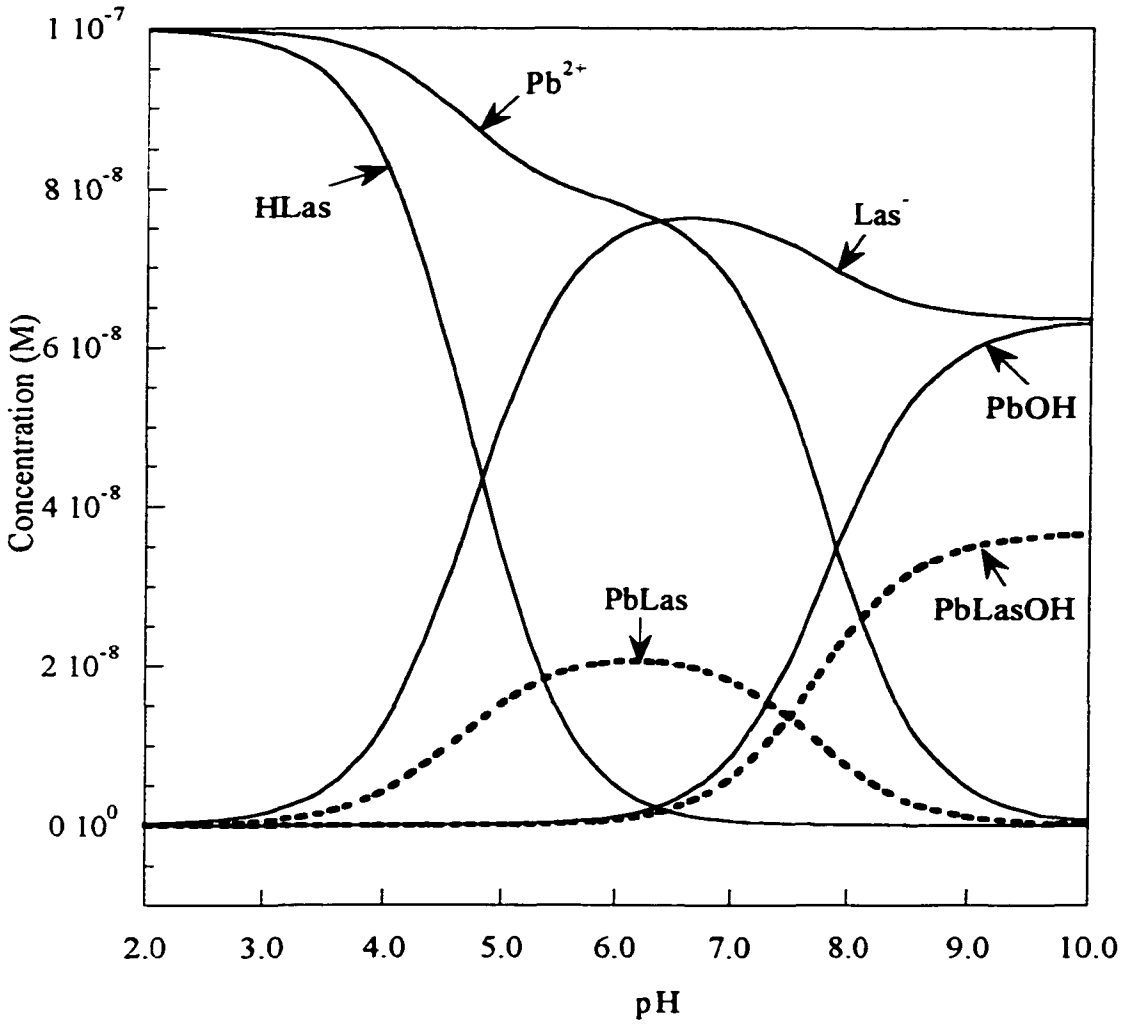

Figure V.2. Species distribution curves for lasalocid-lead(II) complexes in solution as a function of p[H] in 80% methanol-water, only species with lasalocid are shown. Species concentrations were calculated using the program Comics (ref. 30) for 0.1 μM lasalocid and 0.1 μM lead using the average values of the equilibrium constants listed in Tables IV.7 and V.5. The concentration values were chosen to model the conditions used in the transport studies with liposomes (ref. 2).

From the present work, it is clear that mixed ionophore-metal-hydroxide complexes can form with cations Zn^{2+} and Pb^{2+}. The fact that $pK_{a\ (MLOH)}$ values for the mixed complexes (as defined by eq V.14) are close to physiological pH, points to their formation in that pH range. Species distributions for the lead-lasalocid and lead-monensin systems (Figures V.1 and V.2) were calculated using the values of equilibrium constants obtained and ascertained that the ternary 1:1:1 ionophore-lead-hydroxide complexes are present in significant amounts at pH* above 7 in 80% methanol-water even at low lead and ionophore concentrations. If the formation constants for the hydroxy complexes in 80% methanol are similar to those for the membrane associated ionophore[8-10], then the transport of lead and zinc cations can take place through the mixed hydroxy species at the physiological pH. The tendency of these cations to form hydroxy complexes could explain their transport selectivity in comparison to calcium. In addition, more stable 1:1 lead-ionophore complexes in comparison with those of zinc or calcium, could contribute to the selectivity and better efficiency of lead transport.

The average experimental values of log β_{ML} for each complex having 1:1 ionophore-metal stoichiometry for lasalocid and monensin are listed in Table V.6 together with the published values for the ionophore antibiotic A23187 with same metal cations. In Figure V.3 the values of complexation constants for 1:1 ionophore-metal complexes are plotted against the ionic radius of divalent cations in question. The observed trends are similar for all three ionophores with the metals ions studied in this work. All ionophores form strong complexes with lead(II), whereas calcium complexes are the weakest. The magnitudes of binding constants for the complex formation between lead and all three ionophores are similar, with monensin complex slightly stronger that those of lasalocid and A23187. The trend of formation constants of ionophore-calcium

Table V.6. Comparison between values of equilibrium formation constants of complexes having 1:1 stoichiometry between antibiotics monensin, lasalocid and A23187 and metal cations obtained in 80% methanol-water[a]

Complex (ML)	L = monensin	L = lasalocid	L = A23187	Radius of M^{n+}, pm[f]
NaL	5.0	< 2	2.36[c]	102
CaL	3.10	< 2	4.50[d]	100
ZnL	3.74	2.59	6.79[d]	74
PbL	7.15[b]	6.55	6.49[e]	119

[a] Values obtained at 25 °C and ionic strength of 0.05 M (TEAP). [b] Composite value for both spectrophotometric and potentiometric methods. [c] From ref. 25. [d] From ref. 4. [e] From ref. 32. [f] The values of the effective ionic radii are listed for coordination number 6, from ref. 33.

complexes is A23187 > Monenesin > Lasalocid, and wider range of K_{CaL} values is observed. The zinc complex with A23187 is the strongest in comparison to those with the other two ionophores, and monensin forms the strongest complex with sodium in 80% methanol-water among the antibiotics studied.

Antibiotic A23187 forms equally strong complexes with lead and zinc. The lasalocid complexes with both sodium and calcium were the weakest in 80% methanol in comparison to the complexes of these cations with the other ionophores. This was as expected since the lasalocid was previously found to have higher stability for complexes of potassium and barium among alkali and alkaline-earth cations, respectively (Tables I.5 and I.6). Overall, the following trends in the values of formation constants of 1:1 ionophore-metal complexes are observed: for monensin, $Pb^{2+} >> Na^{+} >> Zn^{2+} > Ca^{2+}$; for lasalocid, $Pb^{2+} >> Zn^{2+} > Ca^{2+} \approx Na^{+}$; and for A23187, $Zn^{2+} \geq Pb^{2+} >> Ca^{2+} >> Na^{+}$. These trends in the stability of metal complexes seem to parallel those found for transport selectivities of divalent cations by monensin and lasalocid[1,2], and can account for the lead transport selectivity with respect to calcium[1,2] for all three compounds. On the other hand,

A23187 was found to transport zinc much better than lead(II)[2,34], and this can not be explained considering only the values of the 1:1 complex formation constants.

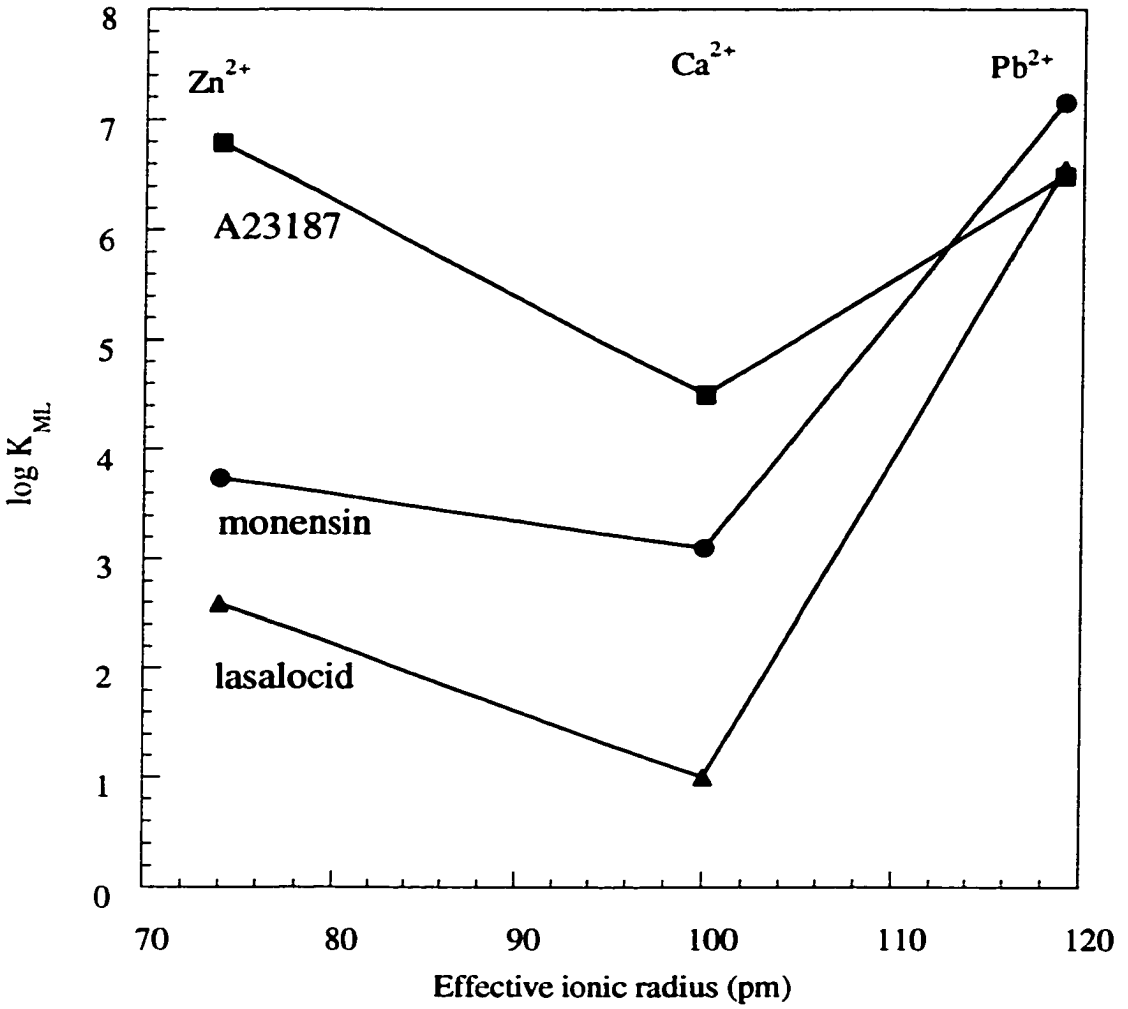

Figure V.3. Graph of log K_{ML} plotted versus the effective radius of metal cation (ref.33). The values for log K_{ML} in 80% methanol are listed in Table V.5.

A. A23187; B. monensin; C. lasalocid.

The radii used for the graph presented in Figure V.3 are for cations with coordination number six, which was chosen for the purpose of making comparisons. However, the divalent cations studied can have higher coordination numbers (8 or 10 for lead and calcium)[33]. This would result in an increase of their effective ionic radii and, as a result, less crowding of the ionophore ligands, especially in the monensin complexes. A higher coordination number would also require more ligand donor atoms to replace solvent molecule in the coordination sphere. The latter condition is more easily satisfied as the number of possible donor atoms increases going from A23187 to lasalocid to monensin. X-ray structures obtained for 2:1 A23187 complexes with calcium[35] showed that only three donor atoms from each ligand participated in metal coordination. On the other hand, NMR studies of 1:1 calcium-lasalocid complexes indicated that five donor oxygen atoms could participate in metal binding[36]. In addition, the X-ray structure of the 2:1 lasalocid-barium complex[35] showed coordination number eight for the cation; five of the coordination sites were occupied by oxygens from one lasalocid ligand, two – by oxygens from another lasalocid molecule and the eighth coordination site was occupied by the water molecule. The NMR studies of the complex having 1:1 monensin-calcium or monensin-manganese(II) stoichiometries in methanol suggested the involvement of only three donor oxygens of monensin[23], whereas the X-ray structure of monensin complex with sodium indicated six donor oxygen atoms in the ligand[35].

It has been shown from the X-ray data analysis that in lead(II) complexes the lone pair of electrons present on Pb^{2+} can affect the geometry of complex[38]. Both "holodirected" or "hemidirected" geometrical arrangements[a] of oxygen ligating atoms around the central metal cation were found. More complexes with holodirected geometry

[a] In a holodirected arrangement lead bonds to ligand coordinating atoms are equally distributed throught a 3-dimentional space around the cation. In a hemidirected geometry bonds to ligand atoms are directed through only part of the sphere, and there is an identifiable void in the distribution of bonds to the ligands. From ref. 38.

were found for higher coordination numbers of lead (6-8) indicating lesser influence of the lone pair of electrons on the spatial arrangement of the coordination bonds due to the ligand "crowding"[38]. This factor can also play a role in the transport process since the successful passage of metal cations through the membrane depends on the extent of their insulation from the lipophilic surroundings by the ionophore molecule.

V.D. NMR studies of ligand conformation and binding in lead complexes having 2:1 ionophore-lead stoichiometry.

Two different approaches were explored in an attempt to identify ligand donor atoms in the monensin and lasalocid molecules bound to lead(II). The first method consisted of calculating the differences in the values of ^{13}C chemical shift for each carbon between the complexed and free ionophore anion ($\Delta\delta^{13}C$) and comparing the resulting patterns from the various forms of free and complexed ionophores. The differences in the ^{13}C chemical shifts upon complexation of the free anion can result from changes in the environment of oxygen and neighboring carbon nuclei upon participation of the oxygens in lead-binding or hydrogen bonding (as a result, $\Delta\delta^{13}C$ is positive), the change in the molecular conformation ($\Delta\delta^{13}C$ can be negative or positive), or interactions with solvent molecules. The overall patterns of $\Delta\delta^{13}C$ obtained for the free acid form of the ionophores and for the lead-ionophore complexes were compared with those reported for the ionophore complexes with sodium and calcium.

The second method involved searching for the doublets or broadened peaks in the ^{13}C NMR spectra of complexes made with ^{207}Pb-enriched lead. Broadened lines could be caused by the efficient relaxation mechanism due to the chemical shielding anisotropy of ^{207}Pb nucleus which is manifested at higher magnetic fields, doublets could be resulting from the ^{13}C–^{207}Pb three or four-bond scalar coupling. Observation of these signals should identify the oxygen atoms, adjacent to these carbons and bound to lead. The latter approach was undertaken only for monensin complexes. Table V.7 summarizes the results obtained using both methods. The numbering schemes for monensin and lasalocid were presented in figures III.29 and IV.24, respectively.

The lead-monensin complex.

NMR data for the 2:1 monensin-lead complex were obtained in several solvents. The ^{1}H and ^{13}C spectra in 80% CD_3OD-D_2O solvent showed remarkable similarity to those obtained in pure CD_3OD. The carboxylic acid arm and the terminal pyran ring of the monensin ligand were most affected by the change in solvent polarity. Only one peak for each carbon from both monensin ligands was present in the ^{13}C NMR spectra of the 2:1 monensin-lead complex in methanol. Therefore, the chemical shifts were treated as the time-averaged value between the signals from carbons on the two ligands which undergo rapid exchange. The analysis of these data indicated that both monensin ligands could be bound to lead through a terminal hydroxyl group on the pyran ring. However, involvement of the carboxylate function in lead binding was not clear, probably due to the interference from the solvation processes involving the carboxylate group.

^{13}C NMR spectra obtained in chioroform at low temperature clearly showed that the ^{13}C chemical shifts for the two monensin ligands were different. This indicated that conformations or lead-binding patterns of the two ligands are dissimilar. The carboxyl group from only one of the monensin ligands (O1), the hydroxyl group from the terminal pyran ring (probably O11) and the ether oxygen O6 from both ligands were suggested to participate in the lead-binding. However, the results obtained were not unambiguous, especially those concerning the studies with ^{207}Pb-enriched lead. The latter indicated that binding patterns of both monensin ligands are similar and all oxygens (except O7) are bound to lead. This conclusion may be the result of generally broader peaks in the ^{13}C spectrum, decreased signal-to-noise ratio and inaccurate peak-shape assignments. One of the problems involves oxygens O4, O5 and O6. Oxygens O4 and O6 from the same ligand can not bind to the cation at the same time due to the conformational constraints imposed on monensin by the fused spiroketal rings. It is also unlikely that O4 and O5 bind at the same time because they are on the opposite ends of pyran ring A. Even so, it

is possible that one monensin uses oxygens O6 and O5, while the other ligand binds through O4. It is also possible that because binding to O4 was determined from the results of ^{207}Pb experiment which are more subject to errors, this oxygen may not be involved in the coordination to lead.

Table V.7. Positions of binding oxygens in monensin and lasalocid obtained with NMR spectroscopic methods.

	Oxygens identified as ligand donor atoms	
Method	in monensin	in lasalocid
By differences in ^{13}C chemical shifts		
in methanol	$O1_{1,2}$ or $O2_{1,2}$	$O1_{1,2}$ or $O2_{1,2}$
	$O6_{1,2}$	$O5_{1,2}$
	$O9_{1,2}$ or $O10_{1,2}$ or $O11_{1,2}$	$O6_{1,2}$
		$O8_{1,2}$
in chloroform	$O1_1$ or $O2_1$	
	$O5_1$	
	$O6_{1,2}$	
	$O7_2$	
	$O8_1$	
	$O9_{1,2}$ or $O10_{1,2}$, or $O11_{1,2}$	
By splitting/broadening of ^{13}C peaks	$O1_{1,2}$ or $O2_{1,2}$ or $O3_{1,2}$	
(with ^{207}Pb-enriched lead)	$O4_{1,2}$	
	$O5_{1,2}$	
	$O6_{1,2}$	
	$O8_{1,2}$	
	$O9_{1,2}$ or $O10_{1,2}$, or $O11_{1,2}$	

[a] Subscripts 1 and 2 identify the first and second ionophore molecules in a complex having 2:1 ionophore-lead stoichiometry.

The set of ^{13}C chemical shifts observed in chloroform for one of the monensin ligands (arbitrarily designated as molecule (2)) was very similar to that obtained for the free acid form of monensin. Several different possibilities can cause this result. First, monensin ligand (2) might adopt a closed conformation in chloroform, similar to that of the monensin free acid. The carboxylic group from the monensin ligand (2) could even be protonated, while monensin (2) is partially bound to lead. Second, the second monensin molecule could be completely separated from lead in a free acid form.

It was not possible to provide more evidence in the first case without accessing geminal proton coupling constants and comparing the molecular conformations through estimation of dihedral angles. This task was beyond the scope of the present work because the assignment of peaks in the ^{1}H NMR spectrum of the lead-monensin complex was not completed due to the heavy overlap of signals in some regions of the spectrum. However, in support of the hypotheses, the value for the chemical shift of the carboxylate carbon C1 was found to be similar in the second monensin ligand in the lead complex and in monensic acid. This indicated that the carboxylate group of the second monensin ligand can be protonated or can participate in strong hydrogen bonding with a water of crystallization or the terminal hydroxy group from the other monensin. The elemental analysis of the complex indicated the presence of one or two water molecules of hydration in the isolated compound. If this is the case, the following rearrangement can take place upon dissolving the complex in chloroform. If the oxygen from a water molecule is bound by lead and hydrogen-bonded to a carboxylate oxygen, then the water proton can be partially or completely transferred to the carboxylate of the monensin, which is schematically illustrated below

$$Pb(Mon)(Mon)\cdot H_2O \rightarrow PbOH\cdot(HMon)(Mon) \qquad (V.16)$$

HMon in the resulting complex can either be partially bound to lead or complete dissociation could occur.

One of the possible structures of the monensin-lead complex in chloroform is schematically shown in Figure V.4. The ligand arrangement provides better cation shielding and insulation in comparison with that suggested in the calcium complex[23]. In addition, and unlike binding suggested in calcium complex, at least four oxygen donor atoms from one or both of the monensin ligands can participate in cation binding assuming the lead coordination number is eight or higher.

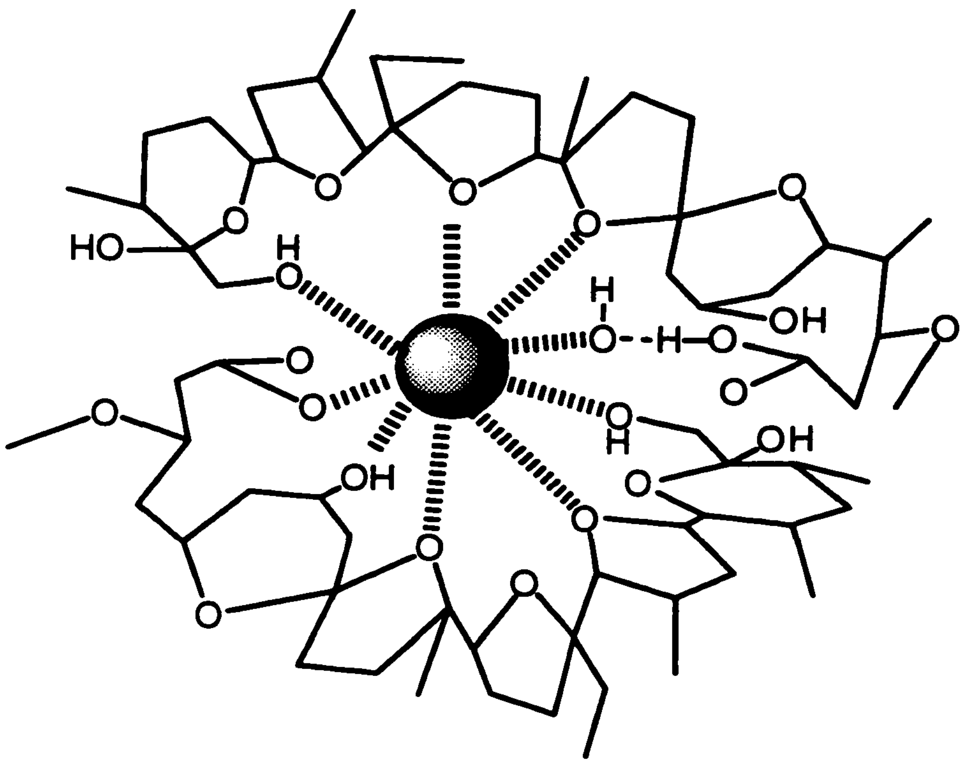

Figure V.4. Schematic diagram of possible monensin coordination in the lead(II) complex in chloroform based on ^{13}C chemical shift data from Table V.7.

Lead-lasalocid complex.

^{13}C NMR spectra of the 2:1 lasalocid-lead complex in methanol showed the presence of only one peak for the carbons from both ligands. Therefore, the chemical shift data can represent either the time-averaged values between the signals from carbons on the two ligands which undergo rapid exchange, or the signals from the two lasalocid ligands that have the same conformation and lead coordination patterns. It was not possible to distinguish between these two possibilities because the experimental data available did not allow an estimate of the ligand exchange rate.

The NMR data, although limited to methanol, indicated that coordination of lasalocid in the lead complex is similar to that proposed for the calcium complex[36a]. Cation binding involves a carboxylate group from one or both ligands and ether oxygens O5, O6, and O8 from both ligands. The schematic illustration of this binding arrangement is shown in Figure V.5. Ligand exchange, similar to that suggested for the calcium-lasalocid complex[36b], is possible and the diagram presents one of the instantaneous states of the complex.

Binding of the carboxylate

With respect to the nature of the carboxylate group binding in both monensin and lasalocid complexes, several modes can be possible: (a) monodentate binding of the carboxylate; (b) bidentate binding of the carboxylate; and (c) for lasalocid, a bidentate chelate formed by coordination of an oxygen from the carboxylate and the salicylic hydroxy oxygen. When calculations of ligand conformations and interatomic distances were performed for alkali metal – monensin complexes in methanol[39], only one oxygen from each carboxylic group was close enough to coordinate to the metal cation. This suggests that monensin prefers the monodentate coordination for the carboxylate group in

solution. The X-ray data of monensin complexes with the monovalent cations sodium and silver indicated that carboxylic acid group did not participate in metal coordination[35].

When lasalocid coordination with manganese(II) was studied in chloroform and dimethylformamide by ^{13}C NMR spin-relaxation[37], the results of calculations of carbon-metal distances indicated that monodentate binding by the carboxylate was most feasable. On the other hand, a binding mode involving the salicylic hydroxy group in a copper(II) complex of lasalocid was proposed in order to explain the results of the NMR study in chloroform[40]. However, only monodentate binding by the carboxylate was observed in the X-ray structures obtained for lasalocid complexes with sodium, silver(I) and barium[35]. In these structures the salicylate hydroxy-group was involved in a hydrogen bond to one of the carboxylate oxygens. Based on these results, a monodentate binding mode for carboxylate could be expected in the lead complex with lasalocid.

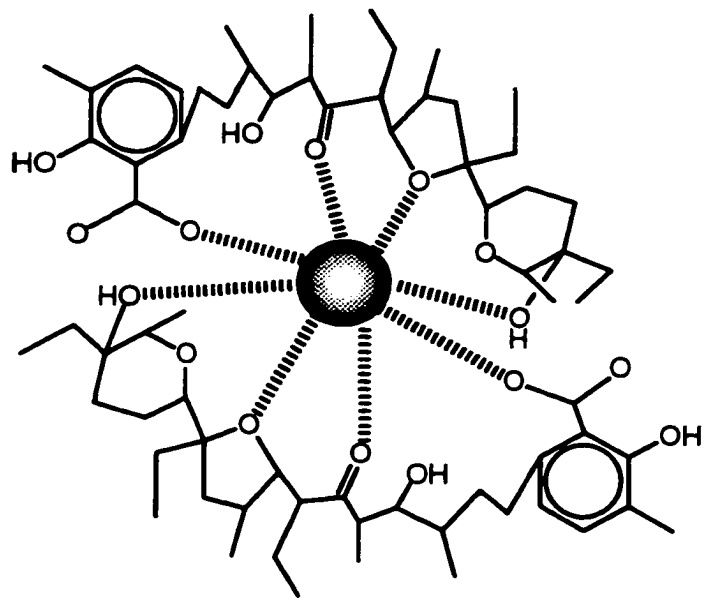

Figure V.5. Schematic illustration of possible lasalocid coordination in the lead(II) complex in methanol using information from Table V.7.

V.E. Discussion of the lead transport data with respect to the results of the present study.

The results of recent metal ion transport studies using several carboxylic acid ionophores indicated a remarkable selectivity for lead(II) in comparison with other divalent cations[27,28,34]. The transport rate data suggested that the transporting species have 1:1 monensin-lead stoichiometry and a mixture of both 1:1 and 2:1 lasalocid-lead stoichiometries.

Several factors can affect the selectivity and stoichiometry of transport. Among others, metal complexation and ionophore protonation equilibria play an important part in the transport process. "Cation transport with ionophores is the most efficient when the ionophore-cation association constant is within the intermediate range" of values, between 10^4 and 10^6, when 1:1 complexes are considered[10]. If the equilibrium constant values are lower, the transport rates can be diminished due to the limiting formation of transporting species. If the values are higher, the release of the metal cation following transport could be prevented, and the transport declines. The values of the formation constants for 1:1 metal-ionophore complexes were found in this work for lead(II), zinc, sodium and calcium. Those for lead complexes lie closer to the higher end of the optimal range mentioned above. The value of formation constant for the sodium-monensin complex is also within this range. However, the measured stability constants for calcium and zinc complexes were a factor of 10^3 to $10^{4.5}$ lower that those for lead and fall below the lower end of the optimal range. The relatively large values of the formation constants for 1:1 ionophore-lead complexes indicate that even low concentrations of lead would compete effectively with other divalent cations for the ionophore.

Because 1:1 complexes between lasalocid (or monensin) and lead(II) possess a positive charge, the selectivity of lead transport versus that of calcium can be justified if

the transport is electrogenic. In this case, the 1:1 ionophore-lead complexes would form preferentially to those of calcium or zinc due to the larger value of their formation constants. However, charged complexes are less favorable to cross the lipophilic membrane in comparison to neutral species. It has been shown that in the ionophores A23187 and ionomycin-mediated transport with Ca^{2+} charged species contributed less than 0.01% to the total transport[42].

The charged 1:1 lead-ionophore complex can be an intermediate reactant for the formation of 2:1 ionophore-lead or ternary 1:1:1 ionophore-lead-anion complexes. Such lead-ionophore-anion complexes with nitrate and chloride were identified in this work by mass-spectrometry. The potentiometric data obtained was consistent with the existence of ternary lead-ionophore-hydroxide complexes. The values of stability constants found for the formation of the mixed hydroxy species (defined in eqs V.1 and V.6) indicated that they could be present in significant concentrations at physiological pH. If the hydroxy complexes are transporting, the tendency of lead cation to form them in comparison to that of calcium could explain the transport selectivity. The existence of the ternary species points to the possibility of the electroneutral transport through complexes with 1:1 lead-ionophore stoichiometry.

On the other hand, electroneutral transport can also take place through the 2:1 ionophore-lead species. However, their concentration was found negligible in 80% methanol-water when both lead and ligand concentrations were low ($< 10^{-6}$) as shown in Figure V.1 for monensin and Figure V.2 for lasalocid. The second stepwise formation constant for a neutral 2:1 lasalocid-lead complex is relatively small (7×10^{2} M^{-1}). Because it is even smaller that that for the 2:1 monensin-lead complex (2.8×10^{3} M^{-1}), other factors should contribute to the proposed 2:1 lasalocid-lead transport stoichiometry. One of these may be the number of the effective ligand donor atoms. X-ray structures of lasalocid complexes with barium and sodium[35] showed that in the 2:1

ionophore-barium or in the binary 2:2 ionophore-sodium complexes both lasalocid ligands participated in metal coordination. The metal was bound with four or five oxygens from one lasalocid ligand and also with one or two oxygens from the second ligand. On the other hand, the X-ray structure of the monensin complex with sodium showed that six oxygens from the same ligand occupied available coordination sites with no solvent molecules present. Because lasalocid is smaller than monensin and has fewer potential donor atoms, two lasalocid ligands may be required in the complex to completely substitute all solvent molecules (8 or more) from the lead coordination sphere and to completely shield the cation from the lipophilic membrane interior during transport. Thus, the 2:1 lasalocid-lead complex could be necessary for the effective lead(II) transport.

Based on log K_H in 80% methanol it is predicted that more than 99% of lasalocid is present as a mono-anion at physiological pH. Therefore, no deprotonation step is required for this ligand to form a 2:1 neutral complex with lead in comparison with that for monensin. Still, if lasalocid is mostly deprotonated at physiological pH, the transport rate could be decreased due to the low concentration of the protonated form of the ionophore whose presence is required in order to shuttle the carrier back through the membrane upon the release of the metal (Figure I.4). Other monovalent counterions present in solution can assist in this antiport by forming neutral 1:1 lasalocid-metal complexes. Nevertheless, this lack of the protonated species could account for much smaller absolute rate found for the lead transport by lasalocid (65.7 nM/sec) in comparison with that by monensin (1,300 nM/sec)[2].

References.

1) Ivanova, O.G.; Erdahl, W.L.; Pfeiffer, D.R.; Taylor, R.W. *Abstracts of papers,* 219th National Meeting of the American Chemical Society, San Francisco, CA, March 25-30, 2000; American Chemical Society: Washington, DC, 2000; INOR 170.

2) Pfeiffer, D. R. Ohio State University, Columbus, OH; Taylor, R. W. University of Oklahoma, Norman, OK. Personal Communications, 1997-2000.

3) (a) Wang, K.; Gokel, G. *J. Org. Chem.* **1996**, 61, 4693-4697. (b) Blair, S. M.; Brodbelt, J. S.; Marchand, A. P.; Kumar, K. A.; Chong, H.-S. *Anal. Chem.* **2000**, 72, 2433-2445.

4) Wang, E.; Taylor, R. W.; Pfeiffer, D. R. *Biophys. J.* **1998**, 75, 1244-1254.

5) Martell, A. E.; Motekaitis R. J. *Determination and Use of Stability Constants*, 2nd ed., VCH Publishers, Inc.; N.Y., 1992.

6) Chapman, C. J.; Puri, A. K.; Taylor, R. W.; Pfeiffer, D.R. *Biochemistry* **1987**, 26, 5009-5018.

7) Fernandes, M. S.; Fromherz, P.J. *Phys. Chem.* **1977**, 81, 1755-1761.

8) Kauffman, R. F.; Taylor, R. W. Pfeiffer, D. R. *Biochemistry* **1982**, 21, 2426-2435.

9) Taylor, R. W.; Chapman, C. J.; Pfeiffer, D. R. *Biochemistry* **1985**, 24, 4852-4859.

10) Taylor, R. W., Pfeiffer, D. R.; Chapman, C. J.; Craig, M. E.; Thomas, T. P. *Pure and Appl.Chem.* **1993**, 65, 579-584.

11) Degani, H. *Biochim. Biophys. Acta* **1978**, 509, 364-369.

12) Rorabacher, D. B.; MacKellar, W. J.; Shu, F. R.; Bonavita, M. *Anal. Chem.* **1971**, 43, 561-573.

13) Bates, R. G.; Paablo, M.; Robinson, R. A. *J. Phys. Chem.* **1963**, 1833-1838.

14) Pointud, Y.; Pierzo, C.; Tissier, C.; Juillard, J. *J. Chim. Phys. Phys.-Chim. Biol.* **1985**, 82, 891-897.

15) Bolte, J.; Demuynck, C.; Jeminet, G.; Juillard, J.; Tissier, C. *Can. J. Chem.* **1982**, 60, 981-989

16) Tissier, C.; Juillard, J.; Boyd, D. W..; Albrecht-Gary, A. M. *J. Chim. Phys.* **1985**, 82, 899-906.

17) Craig, M. A. Ph.D. Thesis. University of Oklahoma, Norman, OK, USA, 1990.

18) Bacarella, A. L.; Grunwald, E.; Marshall, H. P.; Purlee, E. L. *J. Org. Chem.* **1955**, 20, 747-762.

19) Shedlovsky, T.; Kay, R. L. *J. Phys. Chem.*, **1956**, 60, 151-155.

20) Moreau, C. *Bull. Soc. Chim. Fr.* **1968**, 1, 31-35.

21) Mandal, A. K.; Lahiri, S. C. *J. Indian Chem. Soc.* **1977**, 54, 898-901.

22) De Ligny, C. L.; Luykx, P. F. M.; Rehbach, M.; Wieneke A. A. *Recl. Trav. Chim. Pays-Bas* **1960**, 79, 713-726 .

23) Hebrant, M.; Mimouni, M.; Tissier, M.; Juillard, J. *New J. Chem.* **1992**, 16, 999-1008

24) Mimouni, M.; Pointud, Y.; Juillard, J. *Bull. Soc. Chim. Fr.* **1994**, 131, 58-65.

25) Pointud, Y.; Juillard, J. *J. Chem. Soc., Faraday Trans. 1* **1988**, 84, 959-967.

26) Laubry, P., Tissier, C.; Mousset, G.; Juillard, J. *J. Chem. Soc., Faraday Trans. 1* **1988**, 84, 969-971.

27) Juillard, J.; Tissier, C, Jeminet, G. *J. Chem. Soc., Faraday Trans. 1* **1988**, 84, 951-958.

28) Amat, E.; Cox, B. G.; Rzeszotarska J.; Schneider, H. *J. Am. Chem. Soc.* **1988**, 110, 3368-3372.

29) Riddell, F. G.; Arumugam, S.; Cox, B. G. *Biochim. biophys. Acta* **1988**, 944, 279-284.

30) Perrin, D. D.; Sayce, I. G. *Talanta* **1967**, 14, 833-842.

31) Taylor, R. W.; Chapman, C. J.; Pfeiffer, D. R. *Biochemistry* **1985**, 24, 4852-4859.

32) Chapman, C. J.; Puri, A. K.; Taylor, R. W.; Pfeiffer, D.R. *Arch. Bichem. Biophys.* **1990**, 281, 44-57.

33) Richens, D.T. *The Chemistry of Aqua Ions*, John Wiley and Sons: New York, 1997.

34) Erdahl, W. L.; Chapman, C. J.; Taylor, R. W.; Pfeiffer, D. R. *J. Biol. Chem.* **2000**, 275, 7071-7079.

35) Duesler, E. N. and Paul, I. C. In *Polyether Antibiotics: Naturally Occuring Acid Ionophores, Volume 2: Chemistry*, Westley, J. W., Ed.; Marcel Dekker, Inc.: New York, 1983, pp. 170-178.

36) (a)Mimouni, M.; Malfreyt, P.; Lyazghi, R.; Palma, M.; Dauphin, G.; Pascal, Y.; Juillard, J. *J. Chem. Soc., Perkin Trans. 2*, **1995**, 1941-1947.; (b) Everett, G. W.; Parker, S. B.; Williams, R. J. P. *Biochemistry*, **1983**, 22, 6149-6155.

37) Hanna, D. A.; Yeh, C.; Shaw, J.; Everett, G. W. *Biochemistry*, **1983**, 22, 5619-5626.

38) Shimoni-Livny, L.; Glusker, J. P.; Bock, C. W. *Inorg. Chem.* **1998**, 1853-1867.

39) Martinek, T.; Riddell, F. G.; Wilson, C.; Weller, C. T. *J. Chem. Soc., Perkin Trans. 2*, **2000**, 35-41.

40) Lallemand, J. Y.; Rao. R.; Prange, T. *Nouv. J. Chim.* **1980**, 4, 315-319.

41) (a) Erdahl, W. L.; Chapman, C. J.; Taylor, R. W.; Pfeiffer, D. R. *Biophys. J.* **1994**, 66, 1678-1693. (b) Erdahl, W. L.; Chapman, C. J.; Taylor, R. W.; Pfeiffer, D. R. *Biophys. J.* **1995**, 69, 2350-2363.

Appendix I. Derivation of the equation used to fit UV-Vis data for the titration of lead with monensin.

In the expression for the conditional equilibrium binding constant

$$K' = \frac{[PbL]_i}{[HL]_i[Pb^{2+}]_i} \qquad \text{(A.I.1)}$$

the subscript "i"- stands for the concentration at equilibrium after each addition of the monensin ligand (L). Mass balance equation for the total metal concentration corrected for dilution can be written as:

$$[Pb^{2+}]_{tot} = [PbL]_i + [Pb^{2+}]_i \qquad \text{(A. I.2)}$$

Substituting $[Pb^{2+}]_i$ from (A.I.2) into (A.I.1):

$$K' = \frac{[PbL]_i}{[HL]_i([Pb^{2+}]_{tot} - [PbL]_i)} \quad \text{or} \quad [PbL]_i = \frac{K'[HL]_i[Pb^{2+}]_{tot}}{1 + [HL]_i K'} \qquad \text{(A.I.3)}$$

Substituting $[PbL]_i$ from (A.I.2) into (A.I.I):

$$K' = \frac{([Pb^{2+}]_{tot} - [Pb^{2+}]_i)}{[HL]_i[Pb^{2+}]_i} \quad \text{or} \quad [Pb^{2+}]_i = \frac{[Pb^{2+}]_{tot}}{1 + [HL]_i K'} \qquad \text{(A.I.4)}$$

The measured absorbance is the sum of absorbance of the metal ion and the absorbance of complex. Assuming that the absorbance from monensin is negligible and using a cell with a 1.00 cm light pathlength for measurements gives

$$Abs = \varepsilon_{Pb}[Pb^{2+}] + \varepsilon_{PbL}[PbL]$$

(A.I.5)

Substituting the equilibrium concentrations of $[PbL]_i$ from (A.I.3) and $[Pb^{2+}]_i$ from (A.I.4) into (A.I.5) yields

$$Abs_i = \frac{\varepsilon_{Pb}[Pb^{2+}]_{tot}}{1 + [HL]_i K'} + \varepsilon_{PbL}\frac{K'[HL]_i[Pb^{2+}]_{tot}}{1 + [HL]_i K'} \qquad \text{(A.I.6)}$$

Equation (A.I.6) can be rewritten employing the following relationships, initial $Abs_0 = \varepsilon_{Pb}[Pb^{2+}]_{tot}$ and final $Abs_\infty = \varepsilon_{PbL}[PbL]_{tot} = \varepsilon_{PbL}[Pb^{2+}]_{tot}$, as

$$Abs_i = \frac{Abs_0 + Abs_\infty K'[HL]_i}{1 + [HL]_i K'} \qquad \text{(A.I.7)}$$

Equation (A.I.7) can be modified to express absorbance differences using the following definitions,

$$\Delta Abs_i = Abs_i - Abs_0, \quad \Delta Abs_\infty = Abs_\infty - Abs_0 \qquad \text{(A.I.9)}$$

to give

$$\Delta Abs_i = \frac{\Delta Abs_\infty K'[HL]_i}{1 + [HL]_i K'} \qquad \text{(A.I.10)}$$